HEAT TRANSFER CHARACTERISTICS OF A ROTARY EVAPORATOR

By
SOMENATH CHATTERJEE
ENGG 01201304002

Bhabha Atomic Research Centre, Mumbai

A thesis submitted to the

Board of Studies in Engineering Sciences

In partial fulfillment of requirements

for the Degree of

DOCTOR OF PHILOSOPHY

of

HOMI BHABHA NATIONAL INSTITUTE

January 2019

Homi Bhabha National Institute

Recommendations of the Viva Voce Committee

As members of the Viva Voce Committee, we certify that we have read the dissertation prepared by Somenath Chatterjee entitled "Heat Transfer Characteristics of a Rotary Evaporator" and recommend that it may be accepted as fulfilling the thesis requirement for the award of Degree of Doctor of Philosophy.

Vijayan	24/1/2019
Chairman - Dr. P. K. Vijayan	Date:
	24.1.19
Guide / Convener - Dr. G. Sugilal	Date:
S. V. Prabhu	24/1/2019
Co-guide - Prof. S. V. Prabhu	Date:
	24/1/2019
Examiner - Prof. C. S. Mathpati	Date:
	24/1/19
Member 1- Dr. A. K. Nayak	Date:
Abijit Vaidya	24/1/19
Member 2- Dr. A. M. Vaidya	Date:
	24/1/19
Member 2- Prof. A. W. Patwardhan	Date:

Final approval and acceptance of this thesis is contingent upon the candidate's submission of the final copies of the thesis to HBNI.

I/We hereby certify that I/we have read this thesis prepared under my/our direction and recommend that it may be accepted as fulfilling the thesis requirement.

Date:

Place: Mumbai

S. V. Prabhu
Co-guide (if applicable)

24.1.19
Guide

STATEMENT BY AUTHOR

This dissertation has been submitted in partial fulfillment of requirements for an advanced degree at HomiBhabha National Institute (HBNI) and is deposited in the Library to be made available to borrowers under rules of the HBNI.

Brief quotations from this dissertation are allowable without special permission, provided that accurate acknowledgement of source is made. Requests for permission for extended quotation from or reproduction of this manuscript in whole or in part may be granted by the Competent Authority of HBNI when in his or her judgment the proposed use of the material is in the interests of scholarship. In all other instances, however, permission must be obtained from the author.

SOMENATH CHATTERJEE
(ENGG 01201304002)

DECLARATION

I, hereby declare that the investigation presented in the thesis has been carried out by me. The work is original and has not been submitted earlier as a whole or in part for a degree / diploma at this or any other Institution / University.

SOMENATH CHATTERJEE
(ENGG 01201304002)

List of Publications arising from the thesis

Journal

1. Chatterjee, S., Sugilal, G. and Prabhu, S.V., 2017. Flow transitions in a partially filled rotating inclined pipe with continuous flow. Experimental Thermal and Fluid Science, 83, pp.47-56.
2. Chatterjee, S., Sugilal, G. and Prabhu, S.V., 2018. Heat transfer in a partially filled rotating pipe with single phase flow. International Journal of Thermal Sciences, 125, pp.132-141.
3. Chatterjee, S., Sugilal, G. and Prabhu, S.V., 2018. Impact of inclination on single phase heat transfer in a partially filled rotating pipe. International Journal of Heat and Mass Transfer, 123, pp.867-878.

Conferences

1. Chatterjee, S., Sugilal, G. and Prabhu, S.V., 2016. Continuous flow in a partially filled circular duct. Proceedings of the 6th International and 43rd National Conference on Fluid Mechanics and Fluid Power, MNNITA, Allahabad, Uttar Pradesh.
2. Chatterjee, S., Sugilal, G. and Prabhu, S.V., 2017. Flow transition in continuous flow in a partially filled rotating circular duct. Innovative Solutions in Flow Measurement and Control – Oil, Water and Gas, FCRI, Palakkad, Kerala.

Under Review

1. "Heat transfer in a partially filled rotating evaporator", S Chatterjee, G Sugilal, SV Prabhu

SOMENATH CHATTERJEE
(ENGG 01201304002)

Dedicated to Teachers

ACKNOWLEDGEMENTS

I would like to express my deepest gratitude to my supervisors**Dr. G. Sugilal**and **Prof. S.V. Prabhu**, for their valuable guidance, patience, encouragement and the freedom given to me in carrying out research. Apart from the technical knowledge the discipline which I learned from my supervisors is indispensable to my growth as an engineer and as a person. I considered myself to be honoured and fortunate to be associated with them.

The help givenby Mechanical Engineering Department, Indian Institute of Technology Bombay in developing experimental facilities and technical support is gratefully acknowledged. I take this opportunity to especially thank Mr. Rahul Shirsat who has always been available for troubleshooting and customizing the experimental setup.

I would like to express my earnest gratitude to my Research Progress Committee members, Dr. P. K. Vijayan, Dr. A. K. Nayak, Dr. K. Velusami, Dr. A. M. Vaidya, Prof. J. C. Mandal, Prof. A. Sharma for their evaluation and critical advices which helped improving my work.

I would like to express thanks to Mr. Sashi Kumar, Mr.HanumanthaRao, Mr. Puneet Srivastava, Mr. Sunil Pawar, Mrs. Jyoti Jha,Mrs. RituparnaDatta for their valuable inputs during my work at Technology Development Division, Bhabha Atomic Research Centre.

I would like to thank my lab mates Mr Pramod K., Mr. Vinay R., Mr. Kishan K., Mr. Harshad S., Mr. Surfaraz H., Mr. Vimal P., Mr. Manish J., Mr. Mikhil, Mr.GajendraVarma, Dr. Ravish, Dr. Vijay H., Dr.Hardik K. and Prof. Pravin T. for sharing their problems and experiences over a cup of tea, sports and counter strike. I would like to thank my friends and fellow graduate students Mr. Ravi D., Mr. Ashish

S., Mr. Vinod B., Mr. Anuj S., Mr. Vineet V.,Mr. Ganesh K., Ms. Paridhi H., Ms. Parul G., Ms. Megha T., Mrs. Aruna S., Ms. Deepa K., Mr. Tribeni R., Dr. Abhishek T., Dr.Nitendra S. and Dr. Sunil K. for the many fruitful discussions and merry memories.

Special thanks goes to my father, Mr. Hari Prasanna Chatterjee, mother, Mrs. Moyna Chatterjee, brother, Mr. Jit Chatterjee, wife, Mrs. Priyanka Choudhury, my grand-parents and my dear friends Mr. Syed ArifHussain, Mr.SaralChandran and Mr. Amar Singh for their constant support, love and care.

ABSTRACT

Vitrification of high level radioactive liquid waste involves evaporation, drying, calcination and melting operations. All the above operations take place within a melter in a single stage vitrification operation. Substantial amount of the liquid feed can be concentrated by using a rotary evaporator before the high temperature glass melting operation. This will increase the output and operational life of the melter. A rotary evaporator is essentially a partially filled, inclined, heated pipe rotating about its azimuthal axis.

Rotation leads to transition of liquid flow pattern inside the partially filled pipe. The flow pattern transition will influence the heat transfer characteristics of the rotary evaporator. The current work explores fluid flow pattern transitions in a partially-filled, rotating inclined smooth pipe with liquid (water) flow. Different flow patterns are identified experimentally and reported. The effects of liquid flow rate, pipe inclination, diameter and length on the flow transitions are also investigated. A flow regime map is developed based on Reynolds number and Froude number to understand the parametric dependence responsible for fluid flow transitions.

The learning from the flow pattern transition experiments is extended to study single phase heat transfer in a partially-filled, rotating horizontal and inclined pipe with liquid (water) flow. Thermal imaging is used to capture the outer wall temperature of the partially filled rotating heated pipe. Local heat transfer coefficient along the length of the rotating pipe is calculated. Various parameters influencing the heat transfer rate i.e. wall heat flux, liquidflow rate, pipe inclination angle and rotation rate are identified and reported. It is observed that heat transfer rate is positively influenced by wall heat flux, flow rate and rotation rate. While heat transfer coefficient increases with the increase in wall heat flux, liquid volume flow rate and rotation rate, it decreases with increase in inclination angle. Empirical correlationsare developed based on dimensionless heat flux, flow Froude number, flow and rotation Reynolds number to predict the average Nusselt numbers.

Heat transfer with evaporation in a partially-filled, rotating pipe with water flowing through it is experimentally investigated. Uniform wall heat flux, water volume flow rate, rotation rate and pipe inclination angle are varied to study their influence on the heat transfer characteristics of a rotary evaporator. Two distinct temperature zones are identified based on the wall temperature distribution. Location of the onset of nucleate boiling is used to study the effect of various parameters on the rotary evaporator operation. With the increase in the pipe inclination angle and wall heat flux, the onset of nucleate boiling is achieved closer to the inlet of the rotary evaporator. Increasing liquid flow rate delays the onset of nucleate boiling for given wall heat flux and inclination angle. Rotation rate has no significant effect on the rotary evaporator operation in the subcooled boiling region.

The current study is focused on providing sufficient experimental data for the design of a partially filled rotary evaporator. This study highlights various influencing parameters which define the heat transfer characteristics of a partially filled rotating evaporator.

Table of Contents

Nomenclature

A	Area (m^2)
c	Constant (0-1)
C	Concentration (kg/m^3)
C_p	Heat capacity (J/kg K)
D	Inner diameter of pipe (m)
D_h	Hydraulic Diameter (m)
F	Filling fraction (0-1)
g	Acceleration due to gravity (m/s^2)
H	Liquid pool height (m)
$\bar{h}_0$	Mean thickness of viscous layer (m)
h	Heat transfer coefficient (W/m^2K)
h_1	Inside heat transfer coefficient (W/m^2 K)
h_2	Outside heat transfer coefficient (W/m^2 K)
k	Thermal conductivity (W/m K)
k_{ss}	Thermal conductivity of tube wall (W/m K)
L	Length (m)
$L_{h,turbulent}$	Hydraulic development length of fully filed turbulent pipe flow (m)
$\dot{m}$	Mass flow rate (kg/s)
Q	Volume (m^3)
$\bar{Q}$	Volume fraction (0-1)
$\dot{Q}$	Flow rate (m^3/s)

q''	Heat flux (W/m^2)
$\dot{q}$	Volumetric heat generation (W/m^3)
R	Pipe radius (m)
r	Distance of the liquid pool interface from the pipe center (m)
r_1	Inner radius of tube (m)
r_2	Outside radius of tube (m)
S	Wetted perimeter (m)
T	Temperature (ºC)
t	Time (s)
V	Superficial liquid velocity (m/s)
$\bar{W}$	Critical load per unit length of cylinder (kg/m)

Subscript

air	Bulk air
average	Average
b	Bulk water
crit	Critical rotation rate
loss	Liquid vaporization rate
f	Liquid
fg	Specific volume difference
g	Gas
i	Interface
in	Inlet
local	Local
out	Outlet

pool	Liquid pool cross sectional area in a stationary pipe (m^2)
TR	Transition
sat	Saturation
sens	Sensible
Solid	Solids
surface	Heat transfer surface area of the pipe (m^2)
W	Wall
x	X-axis direction

Greek Symbols

β	Angle between the pool interface and the pipe center (degrees)
β'	Thermal coefficient of thermal expansion (K^{-1})
γ	Dimensionless heat flux
ε	Emissivity
ξ	Heat losses due to exchange between the liquid and gaseous phases
θ	Inclination angle (degrees)
μ	Dynamic viscosity (Ns/m^2)
v	Kinematic viscosity (m^2/s)
ρ	Density (kg/m^3)
ψ	Camera angle (degrees)
τ	Residence time (sec)
ω, φ	Angular velocity (rad/sec)
ϑ	Angle between the centre of the pipe and a specific location on the liquid pool interface
σ	Surface tension (N/m)

Non Dimensional Numbers

Bo	Boiling number	$Bo = \frac{\pi q'' D^2}{4\dot{Q}\rho\lambda}$
Fr	Froude number	$Fr = \frac{16\dot{Q}^2}{\pi^2 g \sin\theta\, D^5}$
Fr_φ	Rotation Froude number	$Fr_\varphi = \frac{\omega^2 R}{g}$
Gr	Grashof number	$Gr = \frac{g\beta'(T_w - T_{b,air})D^3}{\mu^2}$
Nu	Nusselt number	$Nu = \frac{hD}{k}$
Re'_f	Flow Reynolds number in terms of hydraulic diameter	$Re'_f = \frac{D_h V}{v}$
Re_f	Flow Reynolds number	$Re_f = \frac{4\dot{Q}\rho}{\pi\mu D}$
Re_ϕ	Rotation Reynolds number	$Re_\phi = \frac{\rho\omega D^2}{\mu}$
γ	Dimensionless heat flux	$\gamma = \frac{\pi q'' D^2}{4\dot{Q}\rho C_p T_{in}}$
Λ	Ratio of viscous stress and gravity	$\Lambda = \frac{\omega\mu R}{\rho g \bar{h}_0^2}$

List of Figures

List of Tables

CHAPTER 1

INTRODUCTION

1.1 Motivation

Process industry has experienced major advancements in the last century. With the increasing environmental impact, the focus is shifting to better and sustainable technologies. Improving equipment performance, while reducing operational costs is a major area of thrust in today's industry. Various techniques are incorporated to enhance heat transfer in an existing setup. Simple geometrical changes such as baffles or flow destabilizers are easy and cost effective methods of improving heat transfer. Additionally, active techniques such as application of electric field, surface vibration or acoustic forces are also utilized where the surface geometry cannot be altered due to operational constrains. Active methods are costly compared to passive methods, but both serve the purpose of improving equipment efficiency.

Flow inside a pipe is a topic which is very widely studied both in classical fluid mechanics and heat transfer owing to its wide application base. Use of lobed walls, helical coils, twisted tapes inside the pipe offer major enhancement in heat transfer in a fully filled pipe. However, the enhancement using these passive techniques is limited by the fluid dynamics character. To further improve upon the optimum passive technique based design, active flow modification techniques are introduced into the system. Rotating a pipe serves one such purpose. The pipe rotation along different axis finds various industrial applications from the sophisticated pharmaceutical production process to an eye-catching rotating chocolate fountain in an ice cream parlour.

Nuclear process industry has been one of the major advancements of this century. However, the waste material produced by this industry is radioactive. This dictates that the disposal of the waste is performed keeping the highest standards of safety and containment in mind. Several countries have been working on various aspects of disposal of radioactive wastes. The most widely used method is containment of the waste products in a glass matrix and isolating them from the environment. The process of incorporating waste in a glass matrix is better known as vitrification.

Vitrification of high-level liquid waste produced from nuclear fuel reprocessing has been in operation for more than 20 years with three major objectives: durable containment of the long-lived fission products, minimization of the final waste volume and operability in industrial context [Lennemann (1978), Petitjean *et al.* (2006), Murray *et al.* (2009), Marsden *et al.* (2010), Fukasawa *et al.* (2014), Suzuki *et al.* (2018)]. The liquid waste is concentrated to 5-15% of its initial volume. The final step involves the solidification of the waste to make it immobile and stable. Lennemann (1978) highlights several approaches to the solidification of high-level liquid waste such as, the use of fluidized beds, stirred beds, rotary kilns, pots and spray chambers.

The reduction of the high-level waste volume is primarily achieved by evaporating part of the liquid waste. However, due to the radioactive nature of the waste, the process design has to be highly tolerant towards various corrosive materials, sedimentations and high operating temperatures. The evaporation operation is typically carried out in specially designed thermo siphon type evaporators. The high temperature operations involving corrosive materials reduce the operational life of these evaporators. Another major disadvantage is that since this is a batch operation, the cycle times are typically large. In order to proceed to a continuous type operation, multiple parallel evaporators are used, until the use of rotary calciner was started in France in the 1980's [Lennemann (1978)].

Rotary calciner satisfies the necessity of high volume reduction factor, solid and colloids handling capacity, easy maintenance and continuous operations. A basic rotary calciner contains four main sections i.e. the inlet section, heating and evaporation section, calcination section and outlet as shown in Fig. 1.1. The necessary rotation rate to the calciner is provided using an electric motor. The calciner can also be inclined at certain angles along the horizontal plane based on the operational requirements. The process involves simple evaporation of liquid waste inside a moderately slow rotating cylinder, which is heated using external heaters. The rotating motion uniformly distributes the liquid waste and a thin film is formed on the inner cylinder surface. The heat provided by the external heaters evaporates the thin film readily while further concentrating the liquid waste which eventually dries and calcines as it moves along the length of the calciner.

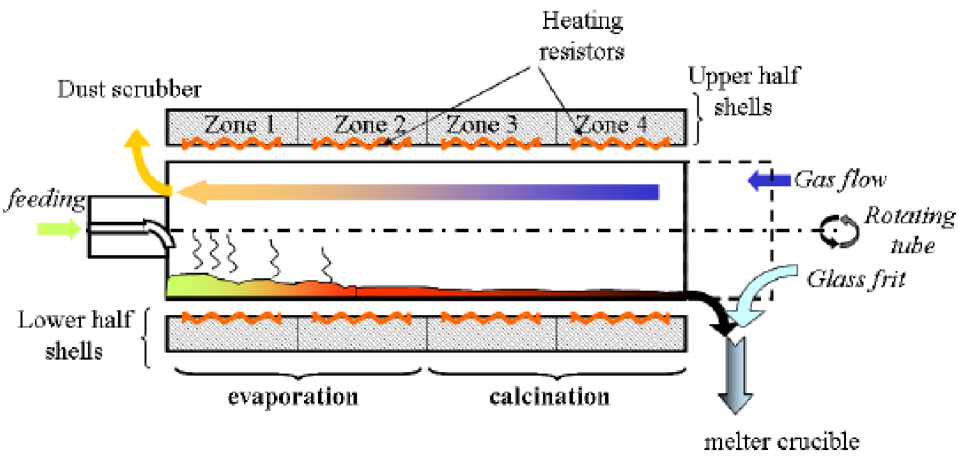

Fig. 1.1 Rotary Calciner [Petitjean *et al.* (2006)]

The present study is confined to the heating and evaporation section of a rotary calciner. Comparing the radius of the cylinder and the thickness of the liquid film wetting the rotating inner wall, a close resemblance to film-flow over a flat plate problem could be drawn. Film flow over a flat plate has been studied extensively in the literature. However, the rotating motion increases the complexities in the hydrodynamics and alters the phase interactions compared to that in flat plate evaporators. The heat transfer characteristics are further influenced by the fluid flow pattern, which is dependent on the speed of rotation and inclination angle. Effective scaling and sizing of this equipment requires the knowledge of correct heat transfer characteristics. Adequate data is not available in the literature which addresses the influence of various parameters on the heat transfer characteristics in a rotary evaporator. Hence, an in-depth study of the parameters influencing the heat transfer characteristic of a rotary evaporator is required and has been taken up for this research work.

1.2 Overview of Evaporators

Evaporators are simple devices which are used to vaporize liquid from a solution or emulsion by boiling off part of the feed solution. Evaporation process is generally used to concentrate a non-volatile solute from a solvent usually water. A typical evaporator consists of a heat exchanger to supply the heat required for boiling and a means to separate the vapour from the boiling liquid. Concentration by evaporation is generally stopped before the solute starts to precipitate which is better known as crystallization.

Evaporators are used in a wide variety of applications i.e. volume reduction for economical packaging and shipping, purifying products, concentration of a process stream, extracting higher value products from waste streams etc. [Lopez (2006), Patel and Mavani (2012), Ilmanen (2017) and Khetni (2018)]. The criteria based on which a specific evaporator is selected for a process depends on various factors such as operational capacity, product characteristics, operating cost, standard and purity of product required, site location and legal regulations. Standiford (2000), classified steam heated evaporators as natural circulation, forced convection and film type evaporators.

Batch evaporators are the simplest type of evaporators. However, these evaporators are not well suited for temperature sensitive materials due to the long residence time. In large batch type evaporators, the static head of the liquid also leads to increase in the boiling point of the liquid volume at the bottom, leading to extra energy costs [Lopez (2006)]. Batch evaporators are extensively used in vitrification of nuclear wastes. Natural circulation evaporators are the most commercially used evaporators [Standiford (2000)]. Depending on the configuration of the tubes, these are further classified as horizontal tube evaporators, short-tube vertical evaporator and long tube vertical evaporator or rising film evaporator. Natural circulation short-tube vertical evaporators as shown in Fig. 1.2, find wide spread application in the sugarcane industry [Lopez (2006)]. The same is not used in nuclear waste treatment due to the hazardous and corrosive nature of the process liquids.

Forced convection evaporators use a pump to circulate the process fluid through the heater. A schematic diagram of a generic forced convection evaporator is shown in Fig. 1.3. Forced convection evaporators generally operate at higher pressures and hence the process fluid does not boil in the heaters. The vapour generation only takes place in a flash chamber. These types of evaporators are very useful in large capacity continuous operations. The same is not used in nuclear waste treatment due to the corrosive nature of the process liquids leading to frequent equipment replacements and increasing operational costs.

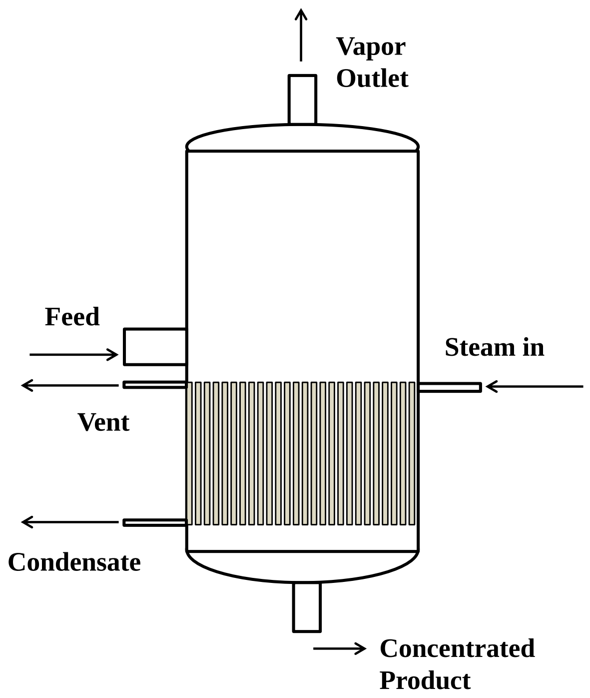

Fig. 1.2 Short tube vertical evaporator [Buflovak, P. K (2018)]

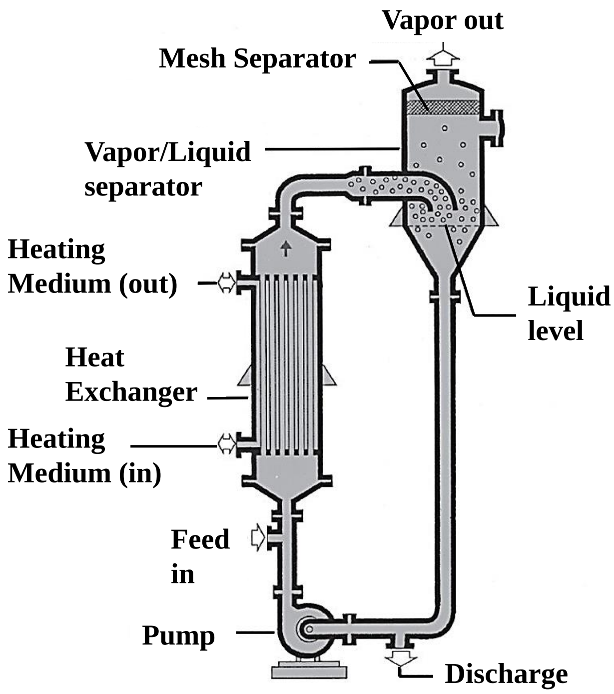

Fig. 1.3 Forced convection evaporator [Buflovak, P. K (2018)]

Film type evaporators use special flow distributers to form a uniform film of liquid on the heat transfer area. These evaporators have good heat transfer performance at low temperatures and small temperature differences. Film type evaporators are widely used for processing of citrus juice and production of fresh water from saline water [Lopez (2006)]. The schematic of a typical industrial falling film evaporator is shown in Fig. 1.4.

A variation of thin film evaporator is a wiper film evaporator or agitated thin film evaporator. The schematic of a typical industrial vertical wiped film evaporator is shown in Fig. 1.5. These evaporators use specialised mechanical wipers to distribute a uniform thin film on the heat transfer surface. The motion of the wiper distributing the liquid also improves the heat transfer in the system. These evaporators find use in specialized processes tackling high viscosity liquids, liquids with suspension, low volume flow rate operations and thermally unstable fluids, which require very small residence time inside evaporators [Mutzenburg (1965)]. Falling film and wiped film evaporators are not suitable for nuclear waste treatment as the process liquid may easily clog the flow distributers or damage the wipers due to its corrosive nature. This will lead to frequent maintenance schedule which poses a high health and environmental risk.

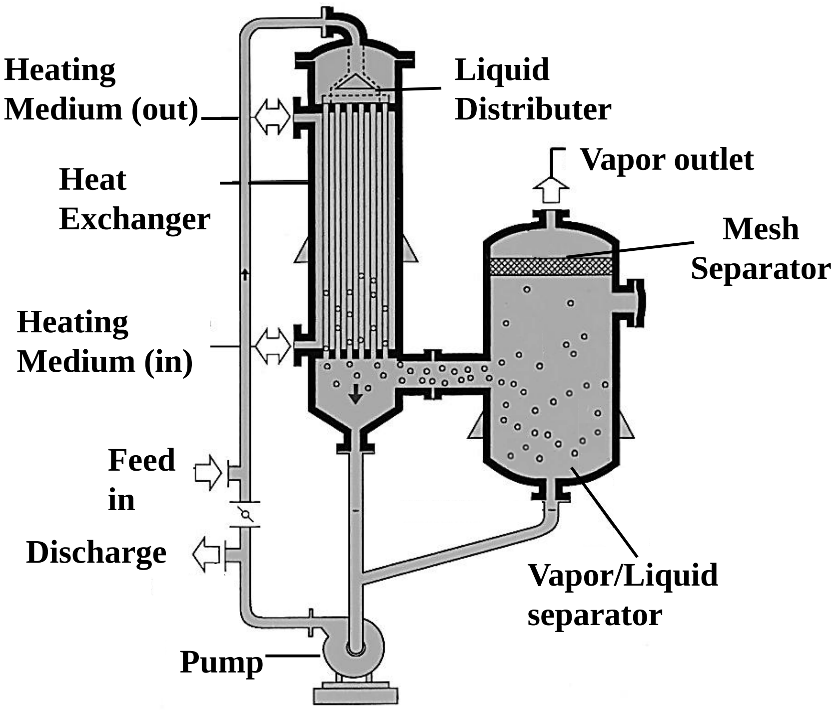

Fig. 1.4 Falling film evaporator [Buflovak, P. K (2018)]

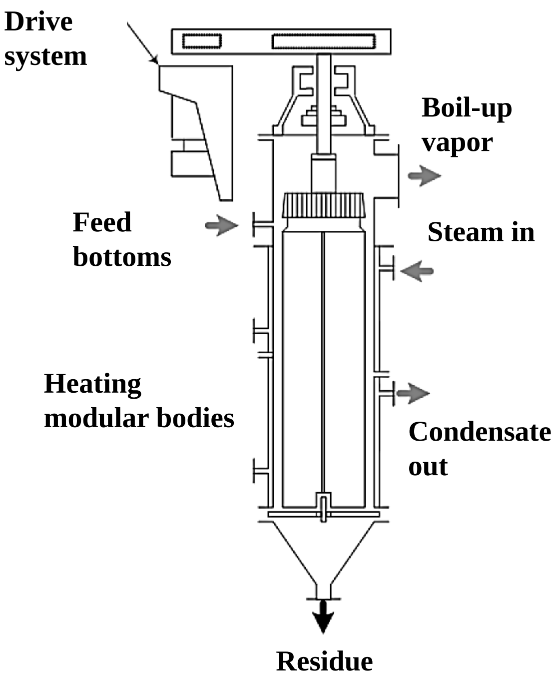

Fig. 1.5 Wiped film evaporator [Lopez (2006)]

Rotary evaporators are another variation of thin film evaporator. The thin film of liquid is achieved by rotating the evaporator wall. The liquid wets the heated rotating evaporator wall thus forming a thin film which can be evaporated. The schematic of a typical rotary evaporator will be similar to the schematic of a rotary calciner as shown in Fig. 1.1 without the calcination section. Rotary evaporators are mainly used in operation where minimum maintenance is required, while conserving similar effectiveness as that of wiped film evaporators. Rotary evaporator is essentially a horizontal or inclined tube rotating azimuthally. They have essentially no internal mechanical parts and the film is formed by the rotation of the pipe. Based on its application, the rotation speed varies from very slow to very fast, thus achieving the film thickness that is required for a specific application

1.3 Objectives of the present study

The present work is motivated by the need to understand the characteristics of the fluid flow and heat transfer in a partially filled rotating heated pipe. The fluid flow pattern transition inside an isothermal partially filled rotating pipe is experimentally visualised to understand the fluid mechanics involved. Further experiments on single phase and subcooled boiling heat transfer are performed to study the fundamental relationship between the fluid flow pattern inside the rotating tube and its influence on the heat transfer characteristics. The focus of the present study is towards the prediction of reasonably accurate heat transfer coefficient in partially filled rotating heated pipes. In this context, the flow visualisation experiments are carried out in acrylic pipes of varying dimensions to examine the effect of pipe dimensions on the fluid flow pattern. Further, the pipe inclination angle is varied along with the rotation rate to understand their effect on the heat transfer character of the rotating partially filled heated pipe. The objective of the present study can be categorized in to two sections: (1) Fundamental understanding, (2) Application towards prediction of heat transfer coefficient. Following are the objectives of the present study;

1.3.1 Fluid flow transitions in a partially filled rotating pipe

- Experimentally study on the influence of pipe diameter and pipe length on fluid flow pattern inside a partially filled rotating pipe
- Experimentally study on the influence of pipe rotation rate and pipe inclination angle on the fluid flow pattern inside a partially filled rotating pipe

1.3.2 Single phase heat transfer in a partially filled rotating horizontal rotating pipe

- Experimental investigation of the effect of wall heat flux, fluid flow rate and pipe rotation rate on the single phase heat transfer in a partially filled rotating heated pipe
- Experimental investigation of the local temperature variation along the longitudinal axis of a partially filled rotating heated pipe
- Development of empirical correlation to predict the average Nusselt number in a partially filled rotating heated pipe based on dimensionless parameters

1.3.3 Impact of inclination on single phase heat transfer in a partially filled rotating horizontal rotating pipe

- Experimental study of the effect of pipe inclination on the variation of local temperature and heat transfer coefficient in an inclined partially filled rotating heated pipe
- Experimental investigation of the influence of pipe inclination in combination with various input parameters i.e., wall heat flux, flow rate and rotation rate, on the heat transfer coefficient
- Development of empirical correlation to predict average Nusselt number in an inclined partially filled rotating heated pipe

1.3.4 Heat transfer in a partially filled rotating heated pipe with evaporation

- Experimental study of the local temperature variation along the longitudinal axis of a partially filled horizontal and inclined rotating evaporator

- Experimental investigation of the effect of pipe inclination, pipe rotation rate, fluid flow rate and wall heat flux on the subcooled boiling heat transfer coefficient in a partially filled rotating evaporator

1.4 Organization of the Report

This report presents the study carried out to understand the fluid flow and heat transfer characteristics and to accurately predict the heat transfer coefficient in partially filled rotating pipes with continuous inflow and outflow of liquid. The thesis is organized as follow:

Present Chapter introduces the various types of evaporators available in commercial industries and briefly highlights the importance of its use in hazardous environment where regular maintenance is difficult.

Second Chapter is a comprehensive review of the state of current knowledge on fluid flow and heat transfer in partially filled rotating systems.

Third Chapter consists of various experiments conducted to study the fluid flow pattern transitions inside a partially filled rotating pipe. The effect of pipe diameter, length, inclination, rotation rate and fluid flow rate on the fluid flow patterns inside a partially filled rotating pipe with continuous inflow and outflow of liquid is presented.

Fourth Chapter presents experimental results to highlight the influence of fluid flow pattern inside a partially filled horizontal rotating heated pipe on its single phase heat transfer coefficient. A correlation is presented to predict the Nusselt number in a partially filled horizontal rotating heated pipe with continuous inflow and outflow of liquid.

Fifth Chapter highlights the influence of pipe inclination angle on the single phase heat transfer performance of a partially filled rotating heated pipe. A correlation is presented to predict the Nusselt number in a partially filled inclined rotating heated pipe with continuous inflow and outflow of liquid.

Sixth Chapter presents the local wall temperature and heat transfer coefficient profiles of a partially filled rotating evaporator. The influence of various parameters i.e. fluid flow rate, pipe rotation rate, inclination angle and wall heat flux on the heat transfer characteristics of the rotating evaporator is reported.

Seventh Chapter concludes the present study with summary of outcomes from the work. The future scope in the domain of the present work is suggested.

CHAPTER 2

LITERATURE REVIEW

2.1 Introduction

The present section reviews the different studies reported in the literature exploring hydrodynamics and heat transfer in partially filled pipes. Published studies on various fluid flow patterns inside a partially filled rotating pipe are collectively reviewed. Studies highlighting single phase heat transfer inside a partially filled rotating heated pipe are mentioned. The literature on two-phase boiling heat transfer coefficient in horizontal straight tube and heat pipes is reviewed.

Various passive and active methods are used in the industry to improve the overall heat transfer in conventional equipment. Such methods help improve energy efficiency at relatively low costs. Rotating a partially filled duct to invoke flow pattern variations leading to the formation of thin liquid film on the rotating surface is one way of achieving a higher transfer area. Flow in a partially filled non rotating pipe has been studied by many researchers. Many researchers working in the field of multiphase flow and heat transfer have investigated the problem of estimating the height of the liquid pool in a partially filled pipe with flowing liquid [Mouza *et al.* (2003), Lioumbas *et al*. (2005,2007) and Kascheev and Podymova (2012)]. The knowledge of pool height inside a partially filled pipe under various inclination angles provides the researcher with an idea of how much of the pipe is filled with liquid (filling fraction), how much heating would be required to attain a certain output (temperature and quality) or what kind of rotation speed will be required to transition the flow pattern in a stationary pipe to annular or rimming flow patterns [Phillips (1960), Karweit and Corrsin (1975), Moffatt (1977), Orr and Scriven (1978), Johnson (1988), Melo (1993), Benjamin *et al*., (1993), Lin and Groll (1996), Thoroddsen and Mahadevan (1997), Boote and Thomas (1999), Baker *et al.* (2001), Tirumkudulu and Acrivos (2001), Wilson *et al.* (2002), Ashmore *et al.* (2003), Chen *et al.* (2007), Chicharro *et al.* (2011) and Benilov and Lapin (2013)].

The concept of using partially filled rotating pipes as heat pipes for heat transfer and cooling applications was proposed by Gray (1969). Heat pipes are effective heat transfer devices which use evaporation and condensation to transmit heat. Heat pipes conventionally are circular in shape with or without surface modifications for enhancing heat transfer characteristics. Krivosheev *et al.* (1979), Lin and Faghri (1996), Lin and Faghri (1997), Lin and Faghri (1999) experimentally and numerically studied the effect of pipe rotation on the heat transfer coefficient of heat pipes. The heat pipes are generally closed off at its end with a fixed volume of fluid inside them for operation.

Continuous flow inside a rotating circular duct has been experimentally studied by Barnea *et al.* (1972), Cowen *et al*. (1982) and Singaram *et al.* (2014). Rimming flow can be established in a partially filled rotating circular duct with continuous feed and recovery of liquid and referred to as ‘continuous mode’ in Singaram *et al*. (2014). Single phase heat transfer studies inside horizontal partially filled rotating pipes have been reported in the literature [Kuo *et al.* (1960), Pattenden (1964) and Beckman *et al.* (1998)]. The studies highlight the effect of fluid flow pattern on the convective heat transfer characteristics in a partially filled horizontal rotating pipe. However, all the heat transfer studies mentioned above focus on systems where there is no fluid phase transition.

Few researchers further developed the idea of using partially filled rotating heated pipes with continuous inflow and outflow of liquid for waste treatment applications [Petitjean *et al.* (2006) and Kascheev and Podymova (2012)]. A small inclination is incorporated in the rotary calciner design to assure unidirectional flow of fluids and solids under the influence of gravity. Petitjean *et al.* (2006) reported an improvement in the waste treatment processing operation using a rotating inclined heated pipe.

Available literature can be categorised based on whether the system is rotating or non-rotating. Rotating systems can been further classified as non-flowing (Batch) and flowing (Continuous) systems.

2.2 Free falling liquid layer in an inclined pipe

2.2.1 Laminar flow model

Mouza *et al.* (2003) investigated the effect of tube diameter, inclination angle and liquid properties on inception of flooding in a partially filled inclined pipe with or without co current gas flow. Water and kerosene is used as the working fluid. Three flow regions are identified based on the liquid and gas flow rates. Mouza *et al.* (2003) derived the average liquid velocity in the pool as shown in Eqn. (2.2). The height of the liquid pool is computed implicitly using Eqn. (2.1) and Eqn. (2.3)

$$H = R\,(1 - \cos\frac{\beta}{2}) \tag{2.1}$$

$$V_x = \frac{\rho g_x R^2}{4\mu}\left[1 - \left(\frac{r}{R}\right)^2 + 2\frac{\cos^2(\beta/2)}{\cos^2\vartheta}\ln\left(\frac{r}{R}\right)\right] \tag{2.2}$$

$$\dot{Q} = V_{x_{average}}(Area\ ACB) \tag{2.3}$$

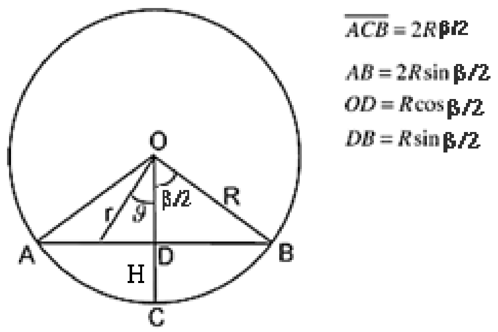

Fig. 2.1 Parameters for the definition of the flowing layer thickness [Mouza *et al.* (2003)]

where, $\beta/2$ is the angle subtended between the centre of the pipe and the liquid pool interface i.e. angle DOB, H is the height of the liquid pool, $\dot{Q}$ is the liquid volume flow rate, R is the radius of the pipe, ρ is the fluid density, μ is the fluid viscosity, r is the distance of the liquid pool interface from the pipe centre and ϑ is the angle between the centre of the pipe and a specific location on the liquid pool interface as shown in Fig. 2.1. A fairly good agreement is reported between the theory and the experimental pool height values.

Kascheev *et al.* (2012) used Navier-Stokes equation and assumed a parabolic relation between the height of the pool and the width i.e. line segments DC and AD or BD respectively as shown in Fig. 2.1. This assumption of parabolic relation in contrast to the use of geometrical interpretations inherited by Mouza *et al.* (2003) predicts the liquid pool height using a single equation as given by Eqn. (2.4).

$$H = 1.28\left(\frac{\dot{Q}\mu}{\sqrt{R}\rho g\sin\theta}\right)^{\frac{2}{7}} \tag{2.4}$$

where, H is the average height of the liquid pool, θ is the inclination angle of the duct, g is the acceleration due to gravity. A general coordinate system of a partially filled inclined pipe is shown in Fig. 2.2 where, D is the diameter of the pipe, β is the angle subtended by the pool interface with the centre of the cylindrical cross section, S_L is the wetted pool surface area, A is the cross sectional area of the liquid pool and S_i denotes the interface of the liquid pool.

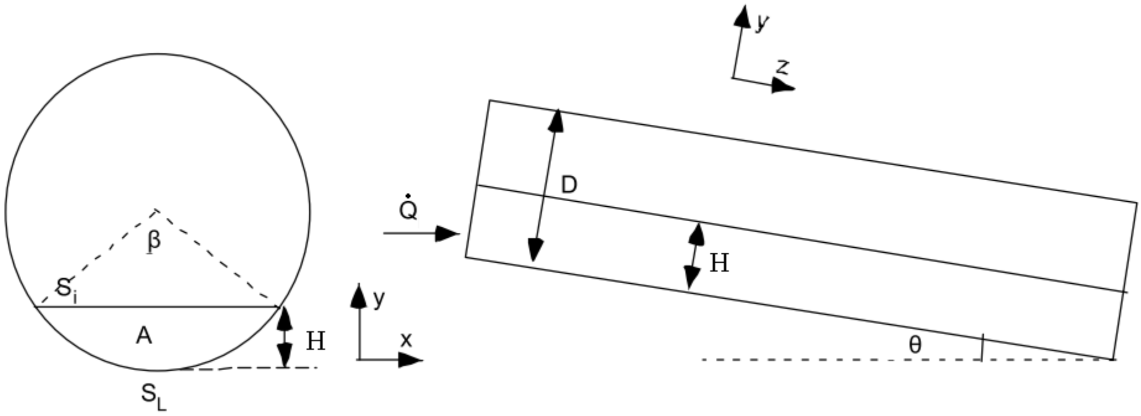

Fig. 2.2 Coordinate system [Lioumbas *et al.* (2005)]

Comparing the methods to predict the height of the liquid pool in a stationary inclined circular duct, Kascheev *et al.* (2012) method requires no prior knowledge of the angle the interface makes with the centre of the duct. Both the methods described above make use of assumptions where the flow is laminar. However, at certain flow rates the flow will transition into turbulent where the above methods might predict wrong results.

2.2.2 Turbulent flow model

Lioumbas *et al*. (2005) studied the transition of smooth stratified flow into wavy stratified flow for various inclination angles and pipe diameters. Four specific regions were identified based on the appearance of waves on the pool interface using visual methods. Liquid pool height and the interface fluctuations are measured using parallel wire conductance technique. It is reported that the first solitary waves appear at $Re_L = VD_h\rho/\mu$ = 2100-2300, where, Re_L is the flow Reynolds number based on superficial liquid velocity "V", hydraulic diameter "D_h". The flow Reynolds number range investigated in this study is between 180 – 2800. At low flow Reynolds numbers, small amplitude waves are observed on the liquid surface. As the liquid flow rate is increased, the interface turns smooth. At still higher flow rates, two-dimensional, large amplitude, long wavelength waves are observed. Based on the observations it is concluded that the appearance of the solitary waves in the interface at $Re_L \approx 2100$ for all inclination angles and tube diameters attributes to the transition from laminar to turbulent flow inside the liquid layer.

Lioumbas *et al*. (2005) used an analytical model to predict the average height of the liquid pool based on the transition Reynolds number "Re_{TR}" given by Eqn. (2.5)

$$Re_{TR} = 7598\left(\frac{\mu^2}{D^3\rho^2 g \sin\theta}\right)^{0.185} \tag{2.5}$$

Based on the transition flow Reynolds number the appropriate equation to predict the angle between the circular duct centre and the interface i.e. β is calculated for laminar or turbulent flow using Eqn. (2.7) and Eqn. (2.8) respectively. The pool height is calculated using Eqn. (2.6).

$$H = \frac{D}{2}(1 - \cos\frac{\beta}{2}) \tag{2.6}$$

$$\beta = 5.155\left(\frac{\dot{Q}\mu}{D^4\rho g \sin\theta}\right)^{0.142} \quad laminar\ flow \tag{2.7}$$

$$\beta = 2.480\left(\frac{\dot{Q}^{1.8}\mu^{0.2}}{D^{4.8}\rho^{0.2} g \sin\theta}\right)^{0.128} \quad turbulent\ flow \tag{2.8}$$

A very good agreement is reported between the theoretical predictions by Lioumbas *et al*. (2005) and the experimental data. The theoretical pool height predictions using Mouza *et al.* (2003) method, shows deviations at higher flow rates.

2.3 Fluid flow inside a rotating circular duct with no in flow or out flow of liquid "Batch mode"

Fluid flow pattern inside and outside a rotating cylinder is extensively reported in the literature [Phillips (1960), Balmer (1970), Karweit and Corrsin (1975), Moffatt (1977), Orr and Scriven

(1978), Johnson (1988), Melo (1993), Lin and Groll (1996), Thoroddsen and Mahadevan (1997), Hosoi and Mahadevan (1999), Baker *et al.* (2001), Tirumkudulu and Acrivos (2001), Wilson *et al.* (2002), Ashmore *et al.* (2003), Benilov *et al*. (2003), Benilov and O'Brien (2005), Chen *et al.* (2007), Chicharro *et al.* (2011) and Benilov and Lapin (2013)]. Most of the study mainly focuses on coating the inner surface of a circular duct. Coating process is used in many industries where thermosetting plastic is placed inside the mould and rotated, coating of fluorescent light bulbs etc. Various fluid flow patterns inside a partially filled rotating cylinder are shown in Fig. 2.3. As the duct rotation rate is increased the fluid flow pattern inside the rotating duct varies from pool flow to annular flow pattern where the complete volume of fluid is spread uniformly over the inner rotating wall. In between, pool flow and annular flow pattern there exists prominently two flow patterns namely, flat front and rimming flow pattern. Both in flat front and rimming flow pattern the fluid is distributed over the rotating wall but the film thickness is not uniform as shown in Annular flow pattern.

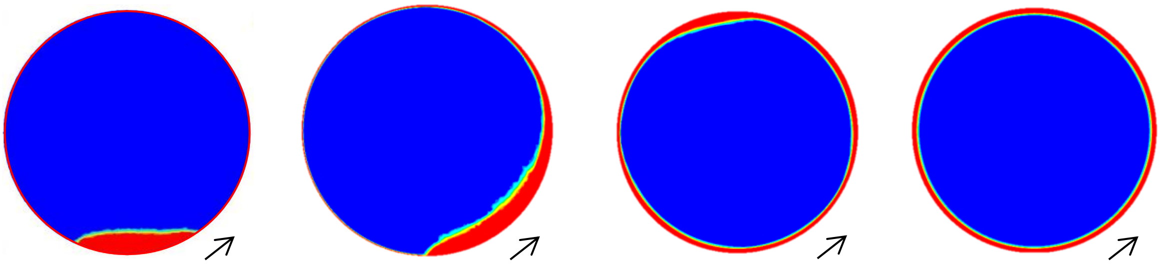

(A) Pool flow (B) Flat front (C) Rimming (D) Annular

Fig. 2.3 Fluid flow patterns in a partially filled rotating pipe

Phillips (1960) experimentally analysed rimming flow pattern and the collapse of homogenous film state to a flat front state in a horizontal rotating cylinder. The wave motion on the free surface of a rapidly rotating liquid is analysed assuming small perturbations to a rigid body rotation. The empty circular duct is rotated at a certain rotational speed and then water is added slowly to find the critical volume or filling fraction of water (which corresponds to a certain thickness of water layer) above which the homogenous film becomes unstable and collapsed suddenly. A criterion for the stability of the motion in terms of rotational Froude number "Fr_{ϕ}" is presented as given by Eqn. (2.9)

$$Fr_{\phi} = \frac{\omega^2 R}{g} > \frac{3}{c} \tag{2.9}$$

where, c varies between 0 and 1, R is the radius of the rotating pipe, cR is the radius of the liquid free surface and ω is the angular velocity of the rotating pipe. Phillips (1960) reported experimental results in the rotational Froude number range of 3 - 30.

However, it is also stated that in presence of large amplitude waves, instability and collapse of flow may be observed even if the value of rotational Froude number satisfies the criteria of stability as given by Eqn. (2.9). The necessary conditions for the validity of the stability criterion are that the film should not be very thin i.e. $(1 - c)$ should not be very small and that the system is characterized by a large rotational Reynolds number "Re_{ϕ}" i.e. inertial effects dominate the flow as given by Eqn. (2.10).

$$Re_{\phi} = \frac{\omega^2 R^2 \rho (1 - c)^2}{\mu} \gg 2 \tag{2.10}$$

Balmer (1970) experimentally studied free-surface flows in rapidly rotating partially-filled horizontal circular ducts using SAE-30 motor oil. Formation of fluids instabilities i.e. 'hygrocysts' or 'fluid cells' due to the centrifugal, viscous and gravitational forces is discussed in this study. It is concluded that surface tension "σ" is an important parameter in small tubes with high surface to volume ratio. However, surface tension did not play an important at 70% filling fraction as explored in the study.

Karweit and Corrsin (1975) experimentally studied the various flow patterns inside a rotating partially filled horizontal cylinder fitted with end plates. Formation of variation of fluid flow pattern such as pool flow and fluid finger pattern is reported. Parameters such as liquid volume filling fraction, pipe radius, lengths and rotation rates, fluid density, viscosity and surface tension are varied to study their effect on fluid flow pattern variations. The effect of surface tension and fluid viscosity on the fluid flow patterns inside the partially filled rotating duct is reported to be minimal.

Moffatt (1977) reported studies on the dynamics of a thin film of viscous fluid on the outer surface of a horizontal rotating roller. The fluid flow pattern is studied based on lubrication theory assumptions. An approach to a steady state solution as given by Eqn. (2.11)

$$\bar{W}_{crit} = 4.428\,\rho R \left(\frac{\mu \omega_{crit} R}{\rho g}\right)^{0.5} \tag{2.11}$$

where, $\bar{W}_{crit}$ is the critical load per unit length of the cylinder and ω_{crit} is the critical angular velocity. Hence, for a given load of liquid on the rotating cylinder if the angular velocity decreases below the critical angular velocity, part of the liquid on the rotating cylinder drops off to attain a new equilibrium. Furthermore, the appearance of flow instabilities with increasing rotation rates is reported. The instabilities evolve into a sequence of rings of liquid "lobes" around the cylinder exhibiting depth discontinuities.

Orr and Scriven (1978) used finite element method to study rimming flow pattern inside a partially filled rotating horizontal cylinder. A numerical scheme which can be used to locate the free surface is developed taking into account inertial, gravitational, pressure, viscous and capillary forces. It is claimed that more irregular free-surface flow domains of similar complexity can be simulated by the developed method.

Haji-Sheikh *et al.* (1984) experimentally reported the formation of a recirculation region, Small and large eddies in the liquid pool at the bottom of the partially filled horizontal pipe rotating at below the transition speed for annular flow. Johnson (1988) numerically investigated thin coating flows inside partially filled rotating circular ducts. The study investigates power law fluids with negligible inertia. Four distinct flow pattern configurations i.e. pool flow, two partial coating flow configurations and rimming flow inside a partially filled rotating pipe are derived with accurate transition solutions. One of the continuous film configurations involves varying film thickness i.e. the film is thicker on one portion compared to the other portion (Fig.

2.3(C)). The second continuous film configuration involves regions with rapid change in film thickness on the rising side of the cylinder i.e. where the rotating wall is ascending out of the liquid pool (Fig. 2.3(B)). The rapid change in thickness also leads to the development of recirculating zones inside the pool. Pool flow (Fig. 2.3(A)) is described as one of the partial film solutions. The second partial film solution involves partial coating of the ascending cylinder wall depending on the volume fraction of the fluids inside the rotating cylinder.

Melo (1993) studied experimentally the rimming flow of a viscous liquid (Silicone oil). The domain of the homogenous film state for different fill-fractions of liquid inside a horizontal rotating circular duct is reported. The pipe rotational speed is increased to attain the homogenous film state and then decreased slowly in small increments to observe the collapse of the homogenous film. The transition between the homogeneous film and the flat front state is reported to be discontinuous. As the rotation rate is decreased from a homogeneous film state, small local disturbances develop on the homogeneous film leading to its collapse at a specific critical rotational speed. The disturbances develop due to an excess amount of liquid travelling azimuthally at a localized spot. A phase diagram is presented based on the experimental observations showing the state of the film based on the area of the cross section of the cylinder occupied by the fluid and the rotation rate. A new dimensionless number which is a ratio of viscous stress and gravity as given by Eqn. (2.12) is defined to predict the flow transitions

$$\Lambda = \frac{\omega\mu R}{\rho g \bar{h}_0^2} = \frac{Fr_\phi}{Re_\phi}\left(\frac{R}{\bar{h}_0}\right) \tag{2.12}$$

where, $\bar{h}_0$ is the mean thickness of the viscous layer, $Re_\phi = \rho\omega R\bar{h}_0/\mu$ is the rotational Reynolds number and $Fr_\phi = \omega^2 R/g$ is the rotational Froude number. Depending on the amount of filling fraction the pattern of the bump is observed to be varying. For a small filling fraction (< 10 cm^2) the bump disappears gradually as the rotation rate is increased. While at moderate filling fractions ($10 - 14$ cm^2), the linear front becomes wavy along the length of the pipe. As the rotation rate is further increased, the fluid in the bump is dragged up by the raising wall of the rotating circular duct which generated disturbances on the film. At larger filling fractions (> 14 cm^2), the front did not disappear completely, but a homogeneous and flat front film state is observed to coexist at different sections of the rotating tube. The critical rotational speeds reported by Melo (1993) derived experimentally matched very well with the values predicted by Moffatt's lubrication analysis as reported by Moffatt (1977).

Melo (1993) also studied the dynamic stability of the homogeneous film similar to the studies performed by Phillips (1960). Artificially created disturbances in the form of liquid drops are released on the free surface of the film. Two phenomena are observed as a result of the disturbances. First, the disturbances are quickly absorbed by the flow. Secondly, the disturbance is either amplified or damped depending on the angular position of the initiation of the disturbance. Generally, a dampening of the disturbances is reported overall. However, if the rotation rate is reduced to an extent that the characteristics time of advection of the disturbance is larger than the characteristics time of amplification of the disturbance, then it may lead to amplification of the disturbance leading to instability in the homogeneous film. It is concluded that the amplification effect is not responsible for the instability of the homogeneous film as the stabilizing effects of surface tension, centrifugal force and radial component of gravity dominated the flow pattern.

Lin and Groll (1996) experimentally investigated the stability of annular flow in a heat pipes with cylindrical walls. A two-dimensional dynamic model describing rimming flow in the partially filled rotating pipe is used to analyse critical conditions for the collapse of annular flow in the rotating heat pipe. Flow visualisation experiments are conducted to compare theoretical results. A correlation based on rotational Froude number (3 - 15) and fluid loading parameter (0.01 – 0.5) i.e. $\bar{h}_0/R$ as given by Eqn. (2.13) is presented to predict the critical point of collapse of annular flow pattern

$$Fr_{\phi} = \frac{3}{\left(1 - \frac{\bar{h}_0}{R}\right)^2} \tag{2.13}$$

Thoroddsen and Mahadevan (1997) experimentally studied fluid flow patterns inside a partially filled rotating tube and developed a phase diagrams showing the flow modes that occur at different rotational speeds for different volume filling fractions. It is deduced that the flow phenomena observed exists due to the interaction of gravity, viscous, inertial and surface tension forces. At a critical angular velocity, the rising side is reported to become unstable and a sloshing action is observed on the free surface. The hydrodynamic behaviour of this sloshing is termed as "pendants". The instability caused is reported to be independent of both the volume filling fraction and the viscosity of the fluid. However, the onset of this instability is delayed when a more viscous fluid is used.

As the rotation rate is further increased, the viscous stress overcomes the gravity force acting on the fluid body and the pendants are pulled over the top of the circular duct. With further increasing rotation rate, flow instabilities appear on the liquid pool. These instabilities are strongly dependent on the filling fraction of the circular duct. At larger filling fractions (larger than 6.5%), strong instabilities such as "duck bills" are observed on the pool surface. At lower filling fractions (smaller than 6.5%), large amplitude stationary waves i.e. "shark tooth" is realised while at moderate filling fractions (~ 4.5%), appearance of "fish like" flow pattern is reported. It is pointed out that the rotational speed at which the fluid enters the homogenous film state (annular flow) is larger than the rotational speed at which the fluid leaves the homogenous film state (collapse). This hysteresis is more pronounced in the cases of higher filling fractions and smaller viscosities and similar work has been reported by Melo (1993), Baker *et al.* (2001), Lin and Groll (1992).

Hosoi and Mahadevan (1999) numerically investigated the axial instabilities of the free surface front in a partially filled rotating horizontal cylinder. A model based on classical lubrication theory is developed which includes the effects of gravity, capillarity, inertia and viscosity. Study reports numerical stability analysis to determine the onset of instabilities in the fluid flow pattern. It is reported that inertia plays an important role in the onset of the fluid instabilities. The model is further used to perform numerical simulations to capture three-dimensional flow patterns such as shark tooth as observed in the experiments reported by Thoroddsen and Mahadevan (1997). A phase diagram based on the ratio of viscous to gravity force and rotation Reynolds number is developed to identify steady and unsteady flow regimes at a fixed volume filling fraction and surface tension.

Baker *et al.* (2001) experimentally investigated the onset of annular flow, annular flow and its subsequent collapse inside a partially filled rotating horizontal cylinder of finite length under adiabatic condition. A correlation based on rotational Froude number (3 – 180) and fluid loading parameter (0.04 – 0.6) i.e. (Q_f/Q) as given by Eqn. (2.14) is developed to predict the critical flow transitions

$$Fr_{\phi} = C_1\left(1-\frac{Q_f}{Q}\right)^{C_2} \tag{2.14}$$

where, Q_f is the volume of fluid loaded inside the rotating pipe, Q is the volume of the rotating pipe, C_1 and C_2 are constants based on experimental results.

It is observed that the annular flow regime always initiates from the ends of the circular duct and gradually moves up the length of the circular duct as the rotation speed is increased, eventually transitioning to a complete annular regime. Once annular regime is achieved, the rotation rate is reduced till the annular regime collapses. The collapse of annular regime occurs at a much lower rotation rate compared to its initiation. The hysteresis associated with the realisation of annular flow and its subsequent collapse is confirmed by experiments and the same has been reported by Melo (1993), Lin and Groll (1992) and Thoroddsen and Mahadevan (1997). The correlation by Lin and Groll (1992) and the one derived by Baker *et al.* (2001) compared well with the experimental results. Lin and Groll (1992) and Baker *et al.* (2001) both explored the filling fraction range between 0.1-0.5.

Tirumkudulu and Acrivos (2001) used lubrication analysis to study the fluid film of a highly viscous liquid inside a partially filled rotating cylinder. Hydrostatic pressure term is added to the standard lubrication equation to study creeping flow conditions (negligible inertial effects). The addition of hydrostatic pressure term leads to the computation of the fluid film thickness profile along with the regions of sharp film thickness variations. A very good agreement with experimental observations and solution of the full two dimensional stokes equations is reported.

Wilson *et al.* (2002) used a combination of analytical and numerical techniques to develop highly accurate numerical solutions to determine the critical weight of fluid that can be supported on the inside or outside of a rotating horizontal cylinder. It is reported that the higher order terms dominate the solution for steady Stokes flow on a cylinder in order to determine the critical weights and the analysis is valid when Eqns. (2.15) and (2.16) hold true

$$\frac{\rho R^2 \omega}{\mu} \ll \left(\frac{\mu\omega}{\rho g R}\right)^{-1/3} \tag{2.15}$$

$$\frac{\sigma}{\rho g R^2} \ll \left(\frac{\mu\omega}{\rho g R}\right)^{5/6} \tag{2.16}$$

where, $\mu\omega/\rho g R$ is the aspect ratio of the liquid film as defined by Moffatt (1977). The critical weights computed in both coating and rimming flow is reported to exceed the values computed by Moffatt (1977).

Ashmore *et al.* (2003) used 2D numerical simulation to study the shape of the interface in a partially filled horizontal circular duct rotating about its axis when the liquid filling fraction i.e. the ratio of volume of liquid to the total volume of the duct is very low and when the rotational Reynolds number is small. Ashmore *et al.* (2003) included surface tension and curvature effect to study the fluid film profile inside a rotating partially filled circular duct when the ratio of gravitational force to viscous forces is large. This essentially implies that the majority of the liquid will be located at the bottom of the duct like a pool while a thin liquid film will coat the inner wall of the duct. It is concluded that when the ratio of gravity to viscous forces is large, and the ratio of viscous to surface tension stress is small, the effect of surface tension is found to be significant in determining the liquid pool profile i.e. the curvature of the liquid pool and the height of thin liquid film. An equation to compute the dimensionless film thickness is derived as given by Eqn. (2.17)

$$\bar{h}_0 = 0.798\frac{(\mu\omega R)^{2/3}}{{F_f}^{1/3}(\rho g)^{1/2}\sigma^{1/6}} \tag{2.17}$$

where, F_f is the filling fraction of the rotating duct. Equation (2.17) is valid when the ratio of gravity to viscous forces is large i.e. (≤ 5) and the ratio of gravity to surface tension stress is less than the filling fraction i.e. $(\ll 1)$.

Benilov *et al*. (2003) examined the fluid flow dynamics of a viscous fluid inside a horizontal rotating pipe. Based on lubrication approximation, an equation is derived to compute the steady state distribution of film around the cylinder. Benilov *et al*. (2003) used first order approximation to describe the initial stage of the flow instabilities as described by Balmer (1970). The model did not account for axial flow variations and surface tension.

Benilov and O'Brien (2005) numerically explored the stability of the liquid film inside a partially filled horizontal rotating pipe by incorporating higher order corrections for inertia, surface tension and hydrostatic pressure derivatives. It is concluded that inertia plays a pivotal role in inducing instability while hydrostatic pressure gradient did not influence stability. Surface tension is reported to be having a stabilizing effect on the instabilities. Finally, a stability criterion based on the balance of inertia and surface tension is reported. Based on the stability criterion it is observed that thinner films are more unstable compared to thicker films.

Chen *et al*. (2007) experimentally studied the establishment of uniform rimming flow for small liquid filling fractions in a partially filled horizontal rotating circular duct using two low viscosity glycerol and polyvinyl alcohol (PVA) solutions. At low rotation speeds a shark tooth pattern is observed as reported by Thoroddsen and Mahadevan (1997). With increasing rotational speed, the pattern transitions into uniform rimming flow. With decreasing volume fractions the shark tooth pattern disappeared and the liquid fingers are observed. It is reported that rimming flow pattern cannot be realised when the rotation speed is suddenly increased from zero to the known rimming speed value in a single step. Rather, a long liquid strip with fingers is formed which rotated with the circular duct. The number of rings increased with increasing fluid viscosity or reduced liquid filling fraction.

Below a certain critical volume filling fraction, the rotation speed for rimming flow is reported to be inversely proportional to the filling fraction i.e. much higher rotation rates are required to achieve rimming flow for slight decrease in filling fraction values. Below the critical volume filling fraction, surface tension and rotation speed did not have significant impact on the number and the width of the rings on the fluid surface. Above the critical filling fraction, achieving rimming flow pattern is reported to be difficult when the surface tension is reduced. It is concluded that surface tension plays a less significant role in the determination of the critical rotation speed. The effects of fluid inertia, viscous drag and gravity is demonstrated by means of the ratio of inertia force to gravity force and the ratio of volume of fluid to its viscous drag. Three distinct regions were identified based on volume fraction "$\bar{Q}$" as given by Eqn. (2.18)

$$\bar{Q} = \frac{2\pi R \bar{h}_0 L}{R^2 \left(\frac{\mu \omega_{crit} R}{\rho g}\right)^{1/2}} \tag{2.18}$$

where, L is the length of the cylinder, $\bar{h}_0$ is the coating thickness and ω_{crit} is the minimum rotation speed required to establish rimming flow regime.

In the region where the ratio of volume of fluid to its viscous drag is greater than 1, lower inertia force is required to achieve rimming flow. While in the region where the ratio of volume of fluid to its viscous drag is greater than 0.32, a considerably larger inertia force is required to achieve rimming flow regime.

Chicharro *et al*. (2011) experimentally studied flow pattern transition inside partially filled horizontal rotating pipe. The experiments are conducted with distilled water and at low filling fractions. Shadowgraph technique is used to observe the flow pattern transition and develop free surface projections. Four flow patterns namely finger, furrows, waterfall and smooth tooth are observed before the onset of annular flow regime. It is concluded that factors such as rotational inertia, surface tension, gravitation, viscous forces as well as geometric parameters such as filling fraction and circular duct radius have prominent influence on the flow pattern. It is also identified that correlation dimension can be used to characterize rimming flow patterns.

Benilov and Lapin (2013) examined instabilities in the thin film flow on the inside or outside of a rotating horizontal cylinder. The analysis is based on the full Navier–Stokes equation. It is reported that in the absence of surface tension, the instabilities grow in the top but decays in the lower portion of the cylinder. The instabilities grow when the disturbances are approximately three times larger than the film thickness. It is concluded that surface tension supress instabilities in cylinders of sufficiently small radius. Similar stabilizing effect of surface tension is reported by Benilov and O’Brien (2005).

2.4 Fluid flow inside a rotating circular duct with continuous in and out flow of liquid

Available experimental and theoretical studies on partially filled rotating circular duct mainly focus on confined flows (batch mode of operation) and are mainly restricted to highly viscous fluids. In many industrial processes, chemicals are processed by spreading them as a thin film over a surface for the transport processes. The mechanical devices that are used to spread and maintain the reactants in thin films are usually rotary devices because of the centrifugal force that can be used to spread the liquid over the solid surface. Some of the mechanical systems that are used to form a thin film include rotating circular duct (or drum), spinning disc reactor, etc.

Barnea *et al*. (1972) developed a mathematical model to compute the film thickness, total holdup and overall residence time of a liquid film inside a partially filled rotating tube. Annular flow pattern is studied in inclined pipes with continuous inflow and outflow of liquid based on laminar flow assumptions and neglecting end effects. It is concluded that with increasing rotation rate, the residence time of the annular film inside the pipe decreases. The mathematical model is reported to compare well with experimental results which can be used to predict the annular film thickness, residence time and the holdup of annular film inside a partially filled rotating horizontal or inclined pipe.

Cowen *et al*. (1982) studied single-phase rimming flow in continuous mode and the rotational speeds studied were above 1000 rotations per minute (rpm). Based on uniform annular thin film assumption equations to compute the average film thickness and average residence time of the fluid in the partially filled rotating pipe is given by Eqns. (2.19) and (2.20)

$$\bar{h}_o \approx 1.18\left(\frac{\mu \dot{Q} L}{\rho D^2 \omega^2}\right)^{1/4} \tag{2.19}$$

$$\tau = \frac{\pi D \bar{h}_0 L}{\dot{Q}} \tag{2.20}$$

Singaram *et al*. (2014) studied annular flow regime in a horizontal rotating circular duct with liquid flowing through the rotating circular duct. Flow transition and film thickness measurement are conducted using non-invasive optical techniques on low viscosity liquids. The annular flow film thickness along the length of the rotating horizontal pipe is measured. In a continuous mode of operation, the volume of liquid inside the circular duct is not readily known unlike in the case of batch flow, as the circular duct sheds more liquid at higher rotational speeds.

It is observed that the flow transition from pool flow regime to annular flow regime is highly sensitive to the rate at which the rotational speed is increased as also reported by Chen *et al*. (2007). Singaram *et al*. (2014) concluded that if the surface tension values of different fluids are similar, then the critical rotation speed for the flow transition to annular flow decreases with increasing fluid viscosity. Singaram *et al*. (2014) also validated an optical interferometry technique for liquid film thickness measurement in the annular flow regime. It is reported that the liquid film becomes more uniform in azimuthal direction with increase in rotational speed and also with increase in axial distance from where the liquid is introduced. The film thickness decreases along the axial length in the flow direction. It is also observed that the annular film thickness decreases with increasing rotational speeds and increases with flow rate for a given rotational speed.

Singaram *et al*. (2014) developed a two-dimensional steady-state theoretical model for annular flow and validated the model experimentally. The model is simplified using lubrication approximation and the reduced Navier-Stokes equations are analytically solved to obtain a velocity profile for the thin film in the axial flow direction. An expression to predict the annular film thickness of viscous fluids and water are given by Eqns. (2.21) and (2.22) respectively. Equation (2.21) is comparable to Eqn. (2.19) as reported by Cowen *et al*. (1982).

Viscous fluids
$$\bar{h}_o \approx 1.33\left(\frac{\mu\dot{Q}L}{\rho D^2\omega^2}\right)^{1/4} \tag{2.21}$$

Water
$$\bar{h}_o \approx \left(\frac{5.06}{R}\right)\left(\frac{\mu\dot{Q}L}{\rho\omega^2}\right)^{1/3} \tag{2.22}$$

2.5 Heat transfer in partially filled rotating circular duct

Single phase heat transfer studies inside horizontal partially filled rotating pipes have been reported in the literature. Kuo *et al.* (1960) experimentally investigated the effect of fluid flow pattern variation inside a rotating pipe with continuous in and outflow of liquid with heated walls. Various insert configurations such as paddles, annulus partially filled, annulus fully filled and partially filled pipe with no inserts are explored to understand their effect on the heat transfer characteristics of the system. It is reported that with increasing fluid flow rate and rotation rate, the heat transfer coefficient improves and the heat transfer coefficient is essentially independent of the wall to bulk fluid temperature difference. It is concluded that at any given rotational speed and fluid flow rate, the Nusselt number for a partially filled rotating pipe is equal to or slightly greater than the Nusselt number for the same rotating pipe when it is fully filled while the paddle inserts reduced the overall heat transfer coefficient.

Pattenden (1964) studied the effect of rotating a tube with separate fluids flowing on the inside and outside. The results highlight the fact that rotation rate has a greater influence on the heat transfer coefficient. Gray (1969) proposed the concept of rotating heat pipes and experimentally demonstrated the improvement in its heat transfer capacity over conventional heat pipes. Heat pipes are effective heat transfer devices which use evaporation and condensation to transmit heat. One of the most conventional heat pipe configurations is where the heat pipe is circular in shape with or without any axial taper which rotates about its own axis or revolves off-axis and the other one is in the shape of a disk. Krivosheev *et al.* (1979) experimentally studied the effect of pipe rotation on the wall temperature variation and heat transfer coefficient of heat pipes with and without wick inserts. At lower rotation rates (~ 1 RPM) the local azimuthal wall temperature monotonously increases as the wall rises out of the liquid pool at the bottom and subsequently falls as the wall submerges below the liquid pool leading to quenching. As the rotation rate is increased, the amplitude of the local azimuthal wall temperature variation decreases. Above 7 RPM, the azimuthal wall temperature variation is reported to be negligible. It is also reported that with increasing rotation rate, the average heat transfer coefficient inside a wickless rotating heat pipe improves. Addition of wicks improved heat transfer coefficient with increasing rotation rate when a heat transfer medium with low surface tension is used (e.g. Acetone).

Lin and Faghri (1997) studied the flow behaviour and heat transfer characteristics of a rotating horizontal heat pipe in stratified flow conditions. It is concluded that overall heat transfer in the condensation region decreases with increasing rotation rate as the flow transitions from a laminar to a turbulent film. In the range of turbulent liquid film, the heat transfer coefficient did not change with rotation rate increases. The study suggests that in the turbulent film flow regime, the effect of rotation rate on the heat transfer coefficient can be neglected. In the evaporator region, the effect of rotation rate and fill fraction in the stratified flow region is reported to be having minimum positive influence. The heat transfer coefficient in the laminar film region of the evaporator section of the heat pipe is reported to be a function of fluid thermal conductivity and the ratio of gravity to viscous force as given by Eqn. (2.23)

$$h = 16.63\frac{k_f}{R}\left(\frac{gR\rho_f}{\omega\mu_f}\right)^{0.177} \tag{2.23}$$

where, h is the heat transfer coefficient and k_f is the fluid thermal conductivity. Lin and Faghri (1999) concluded that the effect of rotation rate on the evaporator region of a heat pipe with groves is negligible. Rotating cylindrical heat pipes are used to cool electrical motors and cutting tools such as drill bits etc. However, the heat pipes are generally closed off at its end with a fixed volume of fluid inside them for operation.

Beckman *et al.* (1998) experimentally studied heat transfer in partially filled concentric rotating drum equipment with liquid in between. The fluids separated the rotating tube. It is reported that liquid viscosity did not affect the film heat transfer coefficient. It is concluded that in the experimental regime explored, conduction heat transfer dominates instead of forced convection mechanism. An empirical correlation based on Peclet number is devised to predict the experimental Nusselt number as given by Eqns. (2.24) and (2.25)

$$Nu = 0.148\, Pe^{0.6} \qquad Pe > 9\times 10^{5} \tag{2.24}$$

$$Nu = 8.5\times 10^{-4}\, Pe^{0.98} \qquad Pe < 9\times 10^{5} \tag{2.25}$$

where, C_p is the fluid heat capacity, k is the thermal conductivity of the fluid, $Pe = \pi\omega D^2\rho C_p/30k$ is the Peclet number and $Nu = hD/k$ is the Nusselt number.

Duffy and Wilson (2009) numerically investigated the flow of a fixed fluid mass on a uniformly heated or cooled rotating cylinder with temperature dependent fluid viscosity and large Biot number. It is reported that the solution for fluid velocity, pressure and temperature can be expressed in terms of fluid film thickness. The film thickness can be calculated from the isothermal flow condition where the fluid, wall and the surrounding temperature is equivalent.

Kascheev and Podymova (2012) developed a numerical model to evaluate the performance of a rotary calciner. The calciner consists of three stages namely sensible heating zone, evaporation zone and calcination zone respectively. The model can estimate the product temperature as shown by Eqn. (2.26), the residence time "τ_{sens}" required to heat the feed to the boiling temperature "T_{sat}" is given by Eqn. (2.27) and length of the sensible heating zone "L_{sens}" of a rotating calciner with 3° inclination angle and rotation rates of 30 RPM at various feed rates is given by Eqn. (2.28).

$$T = T_W - (T_W - T_{in})exp\left(-\frac{3\tau_{sens}k_f}{H^2\rho_f C_{p_f}(1+\xi)}\right) \tag{2.26}$$

$$\tau_{sens} = 0.55\frac{\rho_f C_{p_f}(1+\xi)}{k_f}\left(\frac{\dot{Q}}{\sqrt{R}}\frac{\mu_f}{g\,\rho_f \sin\Theta}\right)^{2/7} ln\left(\frac{T_W - T_{in}}{T_W - T_{sat}}\right) \tag{2.27}$$

$$L_{sens} = \frac{1}{6(1+0.5\omega)}\frac{\rho_f C_{p_f}(1+\xi)}{k_f}\left(\frac{\dot{Q}}{\sqrt{R}}\right)^{8/7}\left(\frac{\mu_f}{g\,\rho_f \sin\Theta}\right)^{1/7} ln\left(\frac{T_W - T_{in}}{T_W - T_{sat}}\right) \tag{2.28}$$

Where, T_W is the temperature of the rotating heated pipe, T_{in} is the inlet temperature of the feed, T_{sat} is the boiling temperature of the feed solution, H is the height of the liquid pool inside the rotary calciner which is evaluated using Eqn. (2.4) and ξ accounts for the heat losses due to exchange between the liquid and gaseous phases.

Similarly, the residence time of the feed in the evaporation section "τ_b" of the rotary calciner where $T_W > T_{sat}$ is given by Eqn. (2.29) and the length of the evaporator section is given by Eqn. (2.30)

$$\tau_b = 1.28 \frac{\lambda \rho_f (1+\xi_1)}{Z(T_W - T_{sat})^3} \left(\frac{\dot{Q}}{\sqrt{R}}\right)^{2/7} \left(\frac{\mu_f}{g\ \rho_f \sin\theta}\right)^{2/7} \left(1 - \left(\frac{C_{solid}}{\rho_{solid}}\right)^{2/3}\right) \tag{2.29}$$

$$L_b = \frac{0.125}{1+0.5\omega} \frac{\lambda \rho (1+\xi_1)}{Z(T_W - T_{sat})^3} \left(\frac{\dot{Q}}{\sqrt{R}}\right)^{6/7} \left(\frac{g \rho_f \sin\theta}{\mu_f}\right)^{2/7} \left(1 - 2M - \left(\frac{C_{solid}}{\rho_f}\right)^2 + 2\frac{M C_{solid}}{\rho_f} + 2M^2 ln \left\{\frac{1+M}{\left(\frac{C_{solid}}{\rho_f}\right) + M}\right\}\right) \tag{2.30}$$

where, $M = \{(\mu/\rho)_{solid} - (\mu/\rho)_f\}/(\mu/\rho)_f$, $Z \approx$ 9.6 W/(m^{2}K^3), λ is the latent heat of vaporization, ξ_1 accounts for the heat losses due to exchange between the material and gaseous phases, C_{solid} is the concentration of the solid particles, ρ_{solid} is the density of the solid particles, ρ_f is the feed liquid density, μ_f is the dynamic viscosity of the liquid phase and μ_{solid} is the dynamic viscosity of the suspension. A small inclination in incorporated in rotary evaporator design to assure unidirectional flow of fluids and solids under the influence of gravity. The various parameters investigated by different researchers have been tabulated in Table 2.1.

2.6 Literature summary and conclusions

It is observed from the available literature that majority of the studies in partially filled rotating pipes are focused on rimming flow pattern. A limited number of studies are reported in the regime of rimming flow that is established in a partially filled rotating pipe with continuous inflow and outflow of liquid "continuous mode" except for Barnea *et al*. (1972), a US patent by Cowen *et al.* (1982), and Singaram *et al*. (2014). There is no systematic experimental and theoretical study available on fluid flow pattern transitions that are established in a continuous mode partially filled rotating pipe. Furthermore, there is only one reported literature on the performance of a rotary calciner by Kascheev and Podymova (2012) which explores the applicability of continuous mode partially filled rotating pipes for heat transfer applications. There is no available study which explores the heat transfer behaviour of a partially filled rotating heated pipe in continuous mode.

This research work aims to study flow transitions inside a partially filled rotating pipe in continuous mode operation. The fluid dynamics study is further extended to understand the single phase and evaporating heat transfer characteristics of a partially filled rotating heated pipe. Infrared thermography technique is used to capture local wall temperature profile of the rotating heated pipe and develop empirical correlations to predict the heat transfer characteristics of partially filled rotating heated pipe equipment.

Table 2.1 Fluids used by different researchers and their physical properties

Literature	Type of Study	Fluid	Mode	Viscosity (Liquid) (25°C) kg/m s	Surface tension (Liquid) (25°C) N/m	Rotation rate RPM	Heat Transfer
Kuo *et al.* (1960)	Experimental	Water	Continuous	1.0×10^{-3}	72×10^{-3}	0 - 500	Yes
Phillips (1960)	Experimental and Numerical	Water	Batch	1.0×10^{-3}	72×10^{-3}		No
Pattenden (1964)	Experimental	Water	Continuous	1.0×10^{-3}	72×10^{-3}	500 – 3000	Yes
Gray (1969)	Experimental	Water	Batch	1.0×10^{-3}	72×10^{-3}	500 – 3000	Yes
Balmer (1970)	Experimental	SAE - 30	Batch	1.83×10^{-1}	36×10^{-3}		No
Barnea *et al*. (1972)	Experimental	Water Glycerine	Continuous	$1.0 – 29 \times 10^{-3}$		0 - 1050	No
Karweit and Corrsin (1975)	Experimental	Water	Batch	1.0×10^{-3}	72×10^{-3}	0 - 1750	No

Table 2.1 Fluids used by different researchers and their physical properties (cont.)

Literature	Type of Study	Fluid	Mode	Viscosity (Liquid) (25°C) kg/m s	Surface tension (Liquid) (25°C) N/m	Rotation rate RPM	Heat Transfer
Moffatt (1977)	Experimental and Numerical	Sucrose solution	Batch	8		8 - 100	No
Orr and Scriven (1978)	Numerical	Newtonian fluids	Batch				No
Krivosheev *et al.* (1979)	Experimental	Water	Batch	1.0×10^{-3}	72×10^{-3}	10 - 500	Yes
		Acetone		0.31×10^{-3}	24×10^{-3}		
Cowen (1982)	Experimental	Multiple fluid type	Continuous			0 - 3000	No
Johnson (1988)	Numerical	Newtonian and Power law fluids	Batch				No
Melo(1993)	Experimental and Numerical	Silicon oil	Batch	4.85×10^{-1}	21×10^{-3}	6 - 180	No
Lin and Groll (1996)	Experimental	Water	Batch	1.0×10^{-3}	72×10^{-3}	100 - 2000	No

Table 2.1 Fluids used by different researchers and their physical properties (cont.)

Literature	Type of Study	Fluid	Mode	Viscosity (Liquid) (25°C) kg/m s	Surface tension (Liquid) (25°C) N/m	Rotation rate RPM	Heat Transfer
Lin and Faghri (1997)	Experimental and Numerical	Water	Batch	1.0×10^{-3}	72×10^{-3}	0 – 3000	Yes
Thoroddsenand Mahadevan (1997)	Experimental	Mixture of glycerine and water	Batch	0.002 – 1.02	69×10^{-3}	0 - 1750	No
Beckman *et al.* (1998)	Experimental	LiCl solution	Continuous	$0.6 – 1.7 \times 10^{-3}$		0 - 350	Yes
Lin and Faghri (1999)	Numerical	Water	Batch	1.0×10^{-3}	72×10^{-3}	0 – 3000	Yes
Hosoi and Mahadevan (1999)	Numerical	Newtonian fluids	Batch	2.99 – 5.49	69×10^{-3}	120 - 192	No
Boote and Thomas (1999)	Experimental	Silicon oil	Batch	4.85×10^{-1}	21×10^{-3}	0 – 282	No
Baker *et al.* (2001)	Experimental	Water and methanol	Batch	1.0×10^{-3}	72×10^{-3}	300 - 2500	No

Table 2.1 Fluids used by different researchers and their physical properties (cont.)

Literature	Type of Study	Fluid	Mode	Viscosity (Liquid) (25°C) kg/m s	Surface tension (Liquid) (25°C) N/m	Rotation rate RPM	Heat Transfer
Tirumkudulu and Acrivos (2001)	Experimental and Numerical	Mixture of TritonX-100, ZnCl2, and water	Batch	4	31×10^{-3}	0 – 120	No
Wilson *et al.* (2002)	Numerical	Sucrose solution	Batch	8		8 - 100	No
Ashmore *et al.* (2003)	Experimental and Numerical	Newtonian fluids	Batch	1.0×10^{-3}	$12 - 75 \times 10^{-3}$	0 - 2500	No
Benilov *et al.* (2003)	Numerical	Newtonian fluids	Batch				No
Mouza *et al.* (2003)	Experimental	Air	Continuous	1.8×10^{-5}		0	No
		Water		1.0×10^{-3}	28×10^{-3}		
		Kerosene		1.4×10^{-3}	72×10^{-3}		
Lioumbas *et al.* (2005)	Experimental	Air and Water	Continuous	1.0×10^{-3}	72×10^{-3}	0	No

Table 2.1 Fluids used by different researchers and their physical properties (cont.)

Literature	Type of Study	Fluid	Mode	Viscosity (Liquid) (25°C) kg/m s	Surface tension (Liquid) (25°C) N/m	Rotation rate RPM	Heat Transfer
Benilov and O'Brien (2005)	Numerical	Newtonian fluids	Batch				No
Chen *et al.(*2007)	Experimental	Water, Glycerol, PVA	Batch	$1 – 28 \times 10^{-3}$	$20 - 72 \times 10^{-3}$		No
Duffy and Wilson (2009)	Numerical	Newtonian fluids	Batch				Yes
Chicharro *et al.* (2011)	Experimental	Water	Batch	1.0×10^{-3}	72×10^{-3}	3 - 312	No
Kascheev and Podymova (2012)	Numerical	Newtonian fluids	Continuous				Yes
Benilov and Lapin (2013)	Numerical	Glycerine	Batch	1.41	63×10^{-3}	300 - 1700	No
Singaram *et al.* (2014)	Experimental	Water and UCON fluid	Continuous	$1.0 – 30 \times 10^{-3}$	0.038 - 0.072	0 - 1000	No

CHAPTER 3

FLOW TRANSITIONS IN A PARTIALLY FILLED ROTATING INCLINED PIPE WITH CONTINUOUS FLOW

3.1 Introduction

Formation of a liquid thin film on the inner surface of a partially filled, rotating pipe is one way of enhancing heat and mass transfer. Equipment based on this special type of flow can be used for a variety of engineering applications such as coating, drying, cooling and evaporation/boiling [Kuo *et al.* (1960), Orr and Scriven (1978), Petitjean *et al.* (2006), Borisov *et al.* (2011), Chicharro *et al.* (2011) and Kascheev and Podymova (2012)]. Borisov *et al.* (2011), Kascheev and Podymova (2012) and Petitjean *et al.* (2006) describe the application of rotating inclined pipe in evaporation of hazardous waste. The rotating system is inclined at an angle and has a rotation rate of approximately 3-30 rpm and the flow rate is maintained at 10-25 LPH. The inclination angle improves the liquid flow velocity due to the effect of gravity. Kascheev and Podymova (2012) did not highlight the effect of flow pattern on the heat transfer. Kuo *et al.* (1960) highlights the influence of flow transition on heat transfer in a partially filled rotating pipe.

Free-surface flows in a partially filled, horizontally rotating pipe with no inflow and outflow of liquid (known as batch mode) are well documented in the literature [Phillips (1960), Karweit (1975), Moffat (1977), Orr and Scriven (1978), Melo (1993), Lin and Groll (1996), Thoroddsen and Mahadevan (1997), Boote and Thomas (1999), Baker *et al.* (2001), Tirumkudulu and Acrivos (2001), Ashmore *et al.* (2003), Chen *et al.* (2007), Chicharro *et al.* (2011) and Benilov and Lapin (2013)]. The liquid layer in a horizontal, partially filled, rotating pipe exhibits different hydrodynamic flow regimes based on its physical properties, filling fraction, aspect ratio of the pipe and its rotational speed [Karweit (1975), Thoroddsen and Mahadevan (1997) and Chicharro *et al.* (2011)]. Thoroddsen and Mahadevan (1997) carried out flow visualization studies by rotating a partially filled horizontal pipe in batch mode. When the horizontal pipe is stationary, the liquid inside the pipe resides at the bottom like a stationary pool (Fig. 3.1(A)). At very low rotational speeds, the liquid from the pool at the bottom of the pipe develops surface instabilities and wets the pipe inner wall (Fig. 3.1(B)). This flow regime is known as *pool flow*. As the rotational speed increases, the thin liquid film pulled out of the pool thickens. All the liquid at the bottom of the pipe is dragged up by the rotating wall to form a *rimming flow* (Fig. 3.1(C)) [Orr and Scriven (1978) and Singaram *et al.* (2014)]. *Rimming flow* with a uniform thin liquid film is termed as *annular flow* (Fig. 3.1(D)) as labelled by Singaram *et al.* (2014). In batch mode, the annular film thickness is essentially uniform along the length of the rotating pipe.

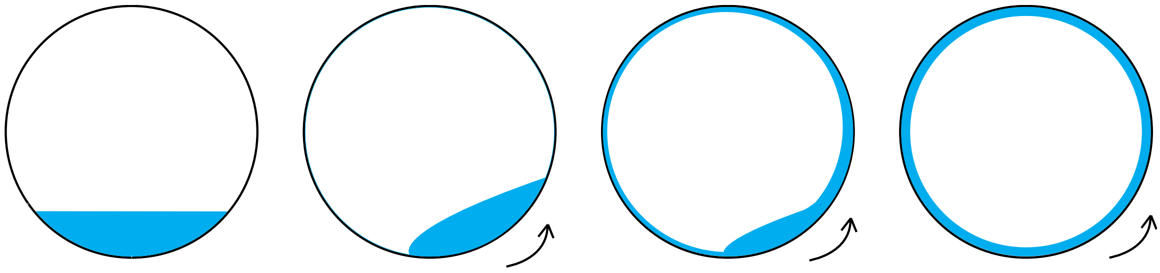

Fig. 3.1 Cross sectional view of liquid flow pattern in a partially filled pipe in batch mode, when the pipe is (a) stationary , (b) rotating at low speed with inner wall wetting to form pool flow, (c) rotating at moderate speed forming rimming flow, (d) rotating at a higher speed resulting in annular flow

Fluid flow in a partially filled, rotating pipe with continuous inflow and outflow of liquid (known as continuous mode) is available in the literature [Barnea *et al.* (1972), Cowen *et al.* (1982) and Singaram *et al.* (2014)]. All the flow patterns observed in batch mode (as shown in Fig.3.1) are also observed in continuous mode. However, the annular liquid film thickness varies along the length of the pipe in continuous mode. In addition, Singaram *et al.* (2014) observed that for a given liquid flow-rate, there exist three flow transition rotational speeds which correspond to *onset of annular flow*, *complete annular flow* and *collapse of annular flow*. *Onset of annular flow* is characterised by the appearance of *annular flow* at one end of the rotating pipe coexisting with *pool flow* pattern at the other end. On increasing the rotational speed, the liquid gets uniformly distributed along the inner surface of the cylinder forming the *complete annular flow*. After attaining the *complete annular flow*, rotational speed is reduced slowly to reach the third flow transition rotation speed at which the annular film collapses to *pool flow*. There exists a hysteresis between the appearance of the *annular flow* and the *collapse of annular flow*. This hysteresis phenomenon is widely reported in the open literature and is observed in both batch and continuous modes of operation [Moffat (1977), Lin and Groll (1996), Thoroddsen and Mahadevan (1997), Chicharro *et al.* (2011) and Singaram *et al.* (2014)]. Singaram *et al.* (2014) observed that the flow transition rotational speed for *onset of annular flow* is always higher than that for the *collapse of annular flow*. They also observed that the difference between these two flow transition speeds increases with increase in liquid flow rate.

Most of the reported experimental and analytical studies focus on *rimming flow* in partially filled, horizontal pipes rotating in batch mode [Phillips (1960), Karweit (1975), Moffat (1977), Orr and Scriven (1978), Melo (1993), Lin and Groll (1996), Thoroddsen and Mahadevan (1997), Boote and Thomas (1999), Baker *et al.* (2001), Tirumkudulu and Acrivos (2001), Ashmore *et al.* (2003), Chen *et al.* (2007), Chicharro *et al.* (2011) and Benilov and Lapin (2013)]. There are only a few studies reported on continuous systems [Kuo *et al.* (1960), Barnea *et al.* (1972), Cowen *et al.* (1982), Petitjean *et al.* (2006), Borisov *et al.* (2011), Kascheev and Podymova (2012) and Singaram *et al.* (2014)]. Most of these studies focus on *rimming* and *annular flow* regimes in rotating horizontal pipes [Barnea *et al.* (1972), Cowen *et al.* (1982) and Singaram *et al.* (2014)]. Limited information is available on flow transitions in a partially filled, inclined pipe rotating in continuous mode. The effect of inclination and aspect ratio of the pipe on the flow transition is not available in the open literature. In this research work, the main objective is to experimentally investigate the effect of inclination and aspect ratio on the flow transition in a partially filled smooth pipe rotating in continuous mode.

3.2 Description of the experimental setup

The schematic layout of the experimental set up is shown in Fig. 3.2. The test section is a Plexiglas pipe with a wall thickness of 3 mm. Three different pipe inside diameters (34, 44 and 54 mm) and four different pipe lengths (350, 500, 750 and 1000 mm) are used to study the effect of pipe aspect ratio on the flow transitions. The flow behaviour is governed by the boundary condition at the inner wall of the pipe. Therefore, the inside diameter of the pipe is used to accurately capture the rotational force transfer to the fluid surface via the solid wall.

The inner radius is used to compute Froude number as shown in Eqn. (3.5). The variation in pipe lengths is studied to understand the effect of liquid holdup on the flow transitions at steady state. A longer pipe will effectively hold a larger volume of liquid compared to a smaller one. The pipe lengths are considered based on flow development length of a fully filled pipe with fluid flow in the turbulent regime i.e. $L_{h,turbulent} = 10D$ [Incropera *et al.* (2007)]. For a 54, 44 and 34 mm ID pipe $L_{h,turbulent}$ is 540 mm, 440 mm and 340 mm respectively. Based on these values the pipe length was varied between 350 mm to 1000 mm keeping the ease of flow visualisation in mind. The flow rates investigated by Kascheev and Podymova (2012) are in the range of 10-25 LPH. In order to expand the flow regime a larger flow rate range of 10-60 LPH is investigated in this study. The rotation rate explored by Borisov *et al.* (2011), Kascheev and Podymova (2012) and Petitjean *et al.* (2006) in a rotary evaporator is limited to 3-30 rpm. Kuo *et al.* (1960) experimentally explored the effect of flow transition on heat transfer in a partially filled rotating pipe limited to ≈ 500 RPM. To cover the various different flow patterns in a partially filled smooth pipe, the rotation rate range is chosen within the range of 0-1200 RPM.

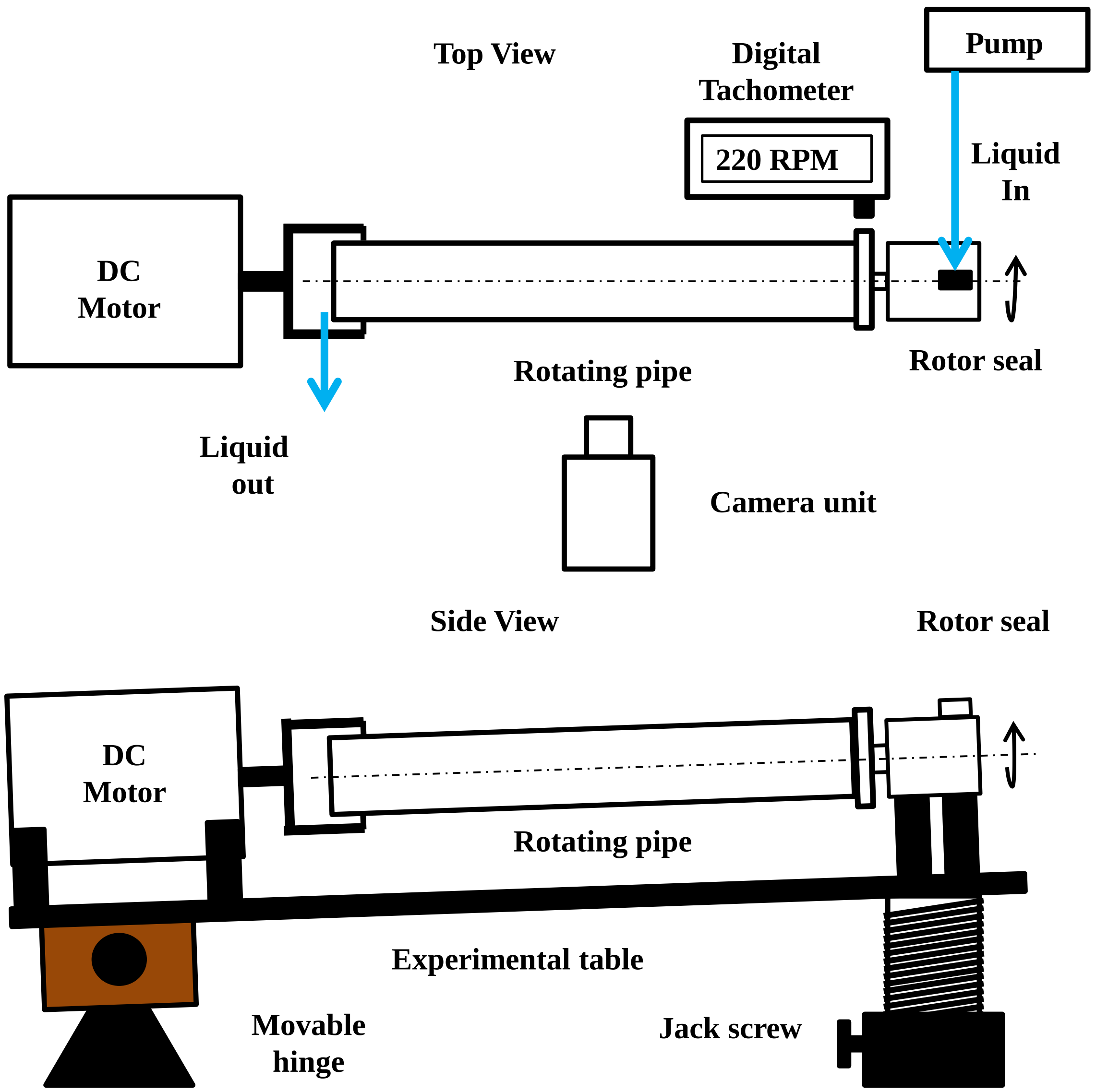

Fig. 3.2 Schematic diagram of the experimental setup

The liquid (water) enters into the rotating pipe through a rotor seal. The liquid flow rate can be varied between 10-60 ± 2.5×10^{-5} LPH using a Watson-Marlow 520DU peristaltic pump. The liquid exits the pipe at the other end through an opening between the coupling connecting the pipe outlet and an electric motor. Rotational speed of the DC motor can be varied between 0-1200 rpm using a variac. A Selec make RC2100 digital tachometer is used to measure the angular speed of the rotating pipe with an accuracy of 0.05% of full scale. The inclination angle of a typical rotary evaporator is generally 3˚ [Petitjean *et al.* (2006), Borisov *et al.* (2011) and Kascheev and Podymova (2012)].The whole experimental setup is mounted on a table with a hinge so that the pipe can be kept inclined at an angle between 0-5˚ from the horizontal plane using a screw jack assembly. The angle of inclination can be measured based on the change in the elevation using a vernier scale with a least count of 0.02 mm.

A digital SLR camera (Canon 550D) is used to record the liquid flow pattern inside the rotating pipe. The flow pattern can be captured from the side at three different viewing angles ψ, as shown in Fig. 3.3. For a fixed inclination angle (θ) of the pipe and a fixed flow rate ($\dot{Q}$), the rotational speed of the pipe is varied to obtain various flow transitions. The experiment is repeated for different liquid flow rates, inclination angles, pipe diameters and pipe lengths as shown in Table 3.1. The uncertainty of different parameters used in experimental measurement is shown in Table 3.2. Calculation methodology to compute the uncertainty in flow Reynolds number and rotational Froude number is described in Appendix B.1.

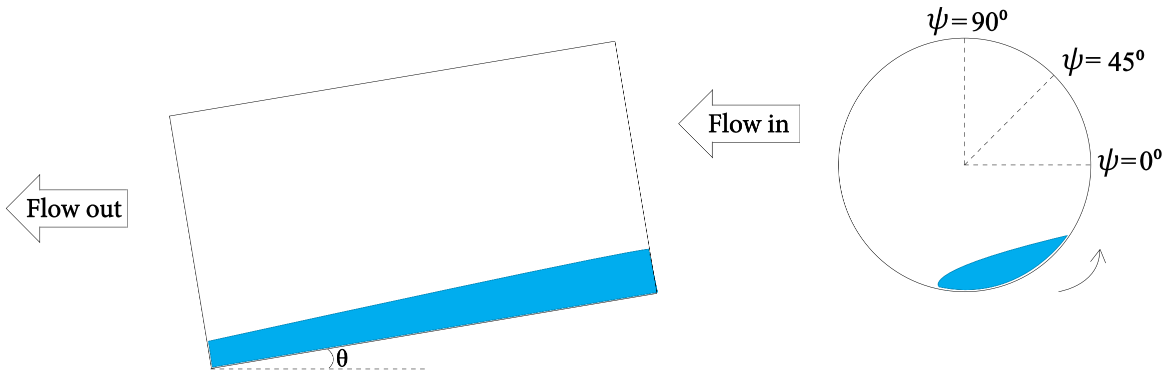

Fig. 3.3 Schematic of the camera viewing angles

The uncertainties in the geometrical parameters of the test section are obtained by measuring the values at different locations. Liquid holdups in a stationary pipe for various inlet flow rates and inclination angles are experimentally obtained based on catch and hold technique using a measuring cylinder with least count of 1 ml at room temperature. The liquid holdup thus obtained is used to compute the stationary pool cross sectional area (*A*) and wetted perimeter (*S*), which are required for data reduction (see Fig. 3.4).

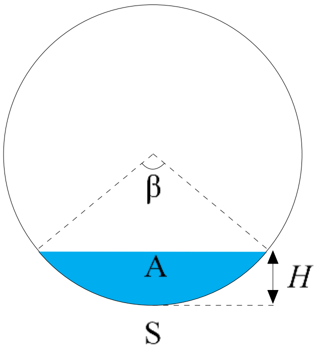

Fig. 3.4 Liquid holdup in a stationary pipe

Table 3.1 Experimental parameters

Pipe ID (mm)	Pipe Length (mm)	Inclination (degrees)	Water flow rate (ml/min)
34	350-1000	0° - 5°	100 - 1000
44	350-1000	0° - 5°	100 - 1000
54	350-1000	0° - 5°	100 - 1000

Table 3.2 Experimental uncertainties

Parameter	Relative uncertainty (%)
Pipe length	0.00285
Pool height	3.02
Holdup	2.90
Pipe diameter	0.04
Liquid flow rate	0.29
Rotation speed	0.15
Reynolds number	5.42
Rotational Froude number	0.21

3.3 Data reduction

Liquid holdups in a stationary pipe for various inlet flow rates and inclination angles are experimentally obtained. Assuming the pool height to be constant throughout the pipe length, the cross sectional area 'A' of the pool is calculated as Eqn. (3.1) where, R is the pipe radius (m) and H is the stationary liquid pool height as shown in Fig. 3.4 [Lioumbas *et al.* (2005)]. Derivation of Eqn. 3.4 is explained in Appendix C.1. Wetted perimeter is computed using Eqn. (3.2) where, β is the angle between the pool interface and the pipe centre (degrees) as shown in Fig. 3.4. Hydraulic diameter D_h is hence computed using Eqn. (3.3). Superficial flow velocity is calculated as given by Eqn. (3.4). Since hydraulic diameter and superficial flow velocity data is derived from stationary pipe experiments, they account for variation in flow rate, pipe inclination angles and diameters.

$$A = R^2 \cos^{-1}(1 - H/R) - (R - H)\sqrt{2RH - H^2} \tag{3.1}$$

$$S = R\beta \tag{3.2}$$

$$D_h = \left(\frac{4A}{S}\right) \tag{3.3}$$

$$V = \left(\frac{\dot{Q}}{A}\right) \tag{3.4}$$

The experimental results obtained for horizontal and inclined rotating smooth pipes at various flow rates and rotational speeds can be classified based on flow Reynolds number (Re'_f) and rotational Froude number (Fr_φ). Rotational Froude number, which is the ratio of rotational inertia to the gravitational force acting upon the liquid, can be defined as given by Eqn. (3.5).

$$Fr_\varphi = \frac{\omega^2 R}{g} \tag{3.5}$$

where, ω is the angular velocity (rad/s) and g is the acceleration due to gravity (m/s^2). The flow Reynolds number, which is the ratio of the inertial force in the axial direction to the viscous force, can be defined for the present problem as given in Eqn. (3.6).

$$Re'_f = \frac{D_h V}{v} \tag{3.6}$$

where, v is the kinematic viscosity (m^2/s), A and S are the cross sectional area and wetted perimeter, respectively, based on experimentally measured liquid holdup in a corresponding stationary pipe.

3.4 Results and discussion

Experiments are performed to study the flow transitions in an axially rotating, partially filled, inclined pipe in continuous mode. In order to compare the effect of angle of inclination, results of flow visualisation experiments are presented initially for a rotating horizontal pipe (see section 3.4.1) and subsequently for an inclined pipe (see section 3.4.2). Effect of pipe diameter and the length are discussed in section 3.4.3 and 3.4.4, respectively. Based on the experimental results, a flow transition map is presented in Section 3.4.5.

3.4.1 Flow transitions in a partially filled rotating horizontal pipe with continuous flow

Different flow patterns obtained for a water flow rate of 200 ml/min (12 LPH) through a rotating horizontal smooth pipe having an inside diameter of 54 mm and a length of 1000 mm are shown in Fig. 3.5. Figure 3.5(A) shows the *pool flow* pattern in a stationary pipe (also see Fig. 3.1(A)). At low rotation speed (0-15 RPM), a thin liquid film wets the inner surface of the pipe (also see Fig. 3.1(B)). The pool front remains stable along the length of the pipe. As the angular velocity is increased further, the pool front is pulled further in the direction of the rotation.

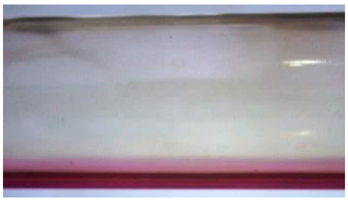

(A) Stratified pool
0 RPM

(B) Fluid pendants
50-107 RPM

(C) Smooth tooth profile
477 RPM

(D) Onset of annular flow
622 RPM

(E) Transition to annular flow
681 RPM

(F) Annular flow
681 RPM

(G) Collapse of annular flow
340 RPM

Fig. 3.5 Flow transitions in a partially filled horizontal pipe for a flow rate of 200 ml/min (12 LPH, $Re'_f = 498,\ Fr_\varphi = 0 - 14$). Pipe ID: 54 mm; Pipe length: 1000 mm. (Flow direction is from right to left. Images A, B, D-G are captured at ψ = 0º, Image C is captured at ψ = 90º)

At a higher rotation speed, the rising film becomes unstable and sloshing occurs due to which the pool starts moving to and fro [Thoroddsen and Mahadevan (1997)]. Fluid sloshing is observed in rotating horizontal pipes for inlet flow rates in the range of 200-1000 ml/min (12 - 60 LPH). As the rotational speed is increased further (50-107 RPM), flow instabilities termed as *pendants* are observed (Fig. 3.5(B)). When the rotational speed is increased to 477 RPM, *smooth tooth flow* pattern appears (Fig. 3.5(C)) [Chicharro *et al.* (2011)]. On increasing the rotational speed to 622 RPM, another flow transition initiates from the discharge end of the rotating pipe (Fig. 3.5(D)). The transition front moves upstream along the length of the pipe. This marks the *onset of annular flow*. The transition front stops moving midway along the length of the pipe and holds the same position for a certain range of rotational speed. At this point, two flow patterns - *rimming* and *annular* -coexist (the left half of Fig. 3.5(D) is *annular flow* and the right half is *rimming flow*).

As the rotational speed is increased to 681 RPM, a similar transition front originates from the inlet region (Fig. 3.5(E)). This transition front moves downstream along the length of the rotating pipe. The transition front pushes the previous transition front (shown in Fig. 3.5(D)) downstream along the length of the pipe. Eventually, the complete pipe flow pattern turns to *annular flow* pattern (Fig. 3.5(F)) at the same rotational speed for which the second transition front (Fig. 3.5(E)) appeared. As the rotational speed is gradually reduced, the *annular flow* pattern prevails through a certain range of rotational speed. At a particular rotational speed (340 RPM), the *annular flow* pattern collapses completely. The *collapse of annular flow* initiates from the inlet region of the rotating pipe and travels downstream (Fig. 3.5(G)).

The initial *onset of annular flow* (Fig. 3.5(D)) occurs at the discharge end due to the sudden decrease in liquid pool thickness at the pipe end. Hence, a comparatively smaller centrifugal force is required to achieve the flow transition at the outlet end. The current experimental observations reveal the presence of a second transition front evolving from the inlet section of the rotating pipe. Singaram *et al.* (2014) discusses the presence of only a single transition front i.e., *onset of annular flow* appearing from the outlet end of the pipe. This is due to the fact that the current experiments are conducted on significantly smaller diameter pipes compared to Singaram *et al.* (2014). Large diameter pipes ensure smaller liquid hold up at comparable flow rates. Hence, the experiments reported by Singaram *et al.* (2014) describe only the presence of *onset of annular flow* (shown in Fig. 3.5(D)) which transforms into complete *annular flow*. In the present experiment *onset of annular flow* does not translates into complete *annular flow*. As the rotational speed is increased from the point of realization of *onset of annular flow*, the increased centrifugal force available transforms the thicker flow in the inlet region into *annular*. This transition front (shown in Fig. 3.5(E)) travels downstream along the pipe length and transforms the flow pattern to complete *annular* (shown in Fig. 3.5(F)).

3.4.2 Flow transitions in a partially filled rotating inclined pipe with continuous flow

Flow transitions occurring in a rotating inclined smooth pipe with its longitudinal axis inclined at an angle of 2˚ to the horizontal are shown in Fig. 3.6. Unlike in a horizontal pipe, the *stratified pool* (Fig. 3.6(A)) in a stationary inclined pipe transforms into a *broken pool flow* (Fig. 3.6(B)) as the pipe starts rotating. For sufficiently low flow rates i.e. 100-400 ml/min (6 - 24 LPH), the pool flow breaks as the axial flow rate is unable to compensate the deviation of the liquid from its original path due to the rotational disturbances. As the rotational speed is increased gradually, the liquid at the bottom of the pipe reconstructs itself to form a continuous stable/wavy pool flow. At a higher rotational speed *pendant*, as shown in Fig. 3.6(C) appears.

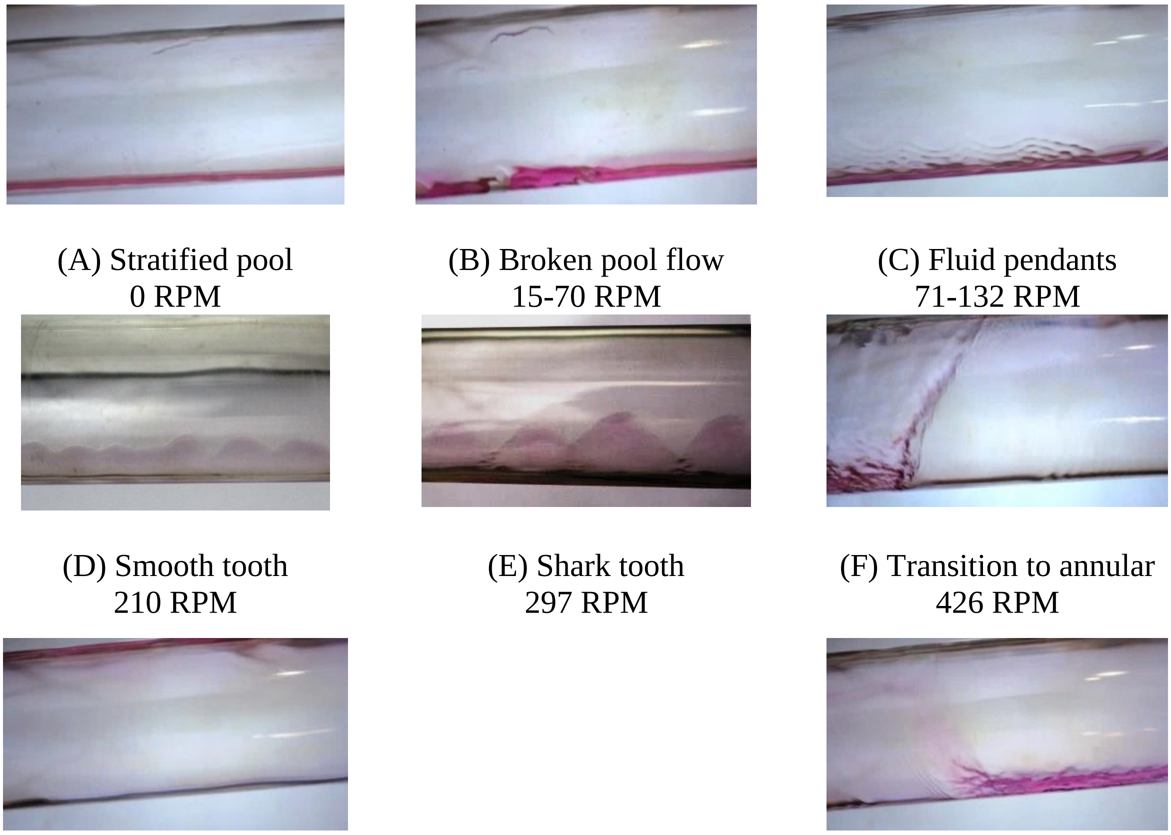

(A) Stratified pool
0 RPM

(B) Broken pool flow
15-70 RPM

(C) Fluid pendants
71-132 RPM

(D) Smooth tooth
210 RPM

(E) Shark tooth
297 RPM

(F) Transition to annular
426 RPM

(G) Annular flow
426 RPM

(H) Collapse of annular flow
372 RPM

Fig. 3.6 Flow transitions in a partially filled inclined pipe for a flow rate of 200 ml/min (12 LPH, $Re'_f = 852,\ Fr_\varphi = 0 - 5$). Pipe ID: 54 mm; Pipe length: 1000 mm; Inclination angle: 2°. (Flow direction is from right to left. Images A-C, F-H are captured at ψ = 0º, Images D and C are captured at ψ = 45º and 90º respectively.)

As the rotational speed is increased further, pendants disappear. On increasing the speed further, *smooth tooth* and *shark tooth* type flow patterns appear as shown in Fig. 3.6(D) and 3.6(E), respectively. Unlike horizontal pipes, inclined pipes do not exhibit a distinct *onset of annular flow*. Onset and transition to *annular flow* occurs at the same rotational speed (Figs. 3.6(F) and 3.6(G)). However, like in the horizontal pipe, the hysteresis phenomenon between the transition to *annular flow* (due to increasing rotation speed) and the *collapse of annular flow* (due to decreasing rotation speed) is observed in the inclined pipe (Figs. 3.6(G) and 3.6(H)).

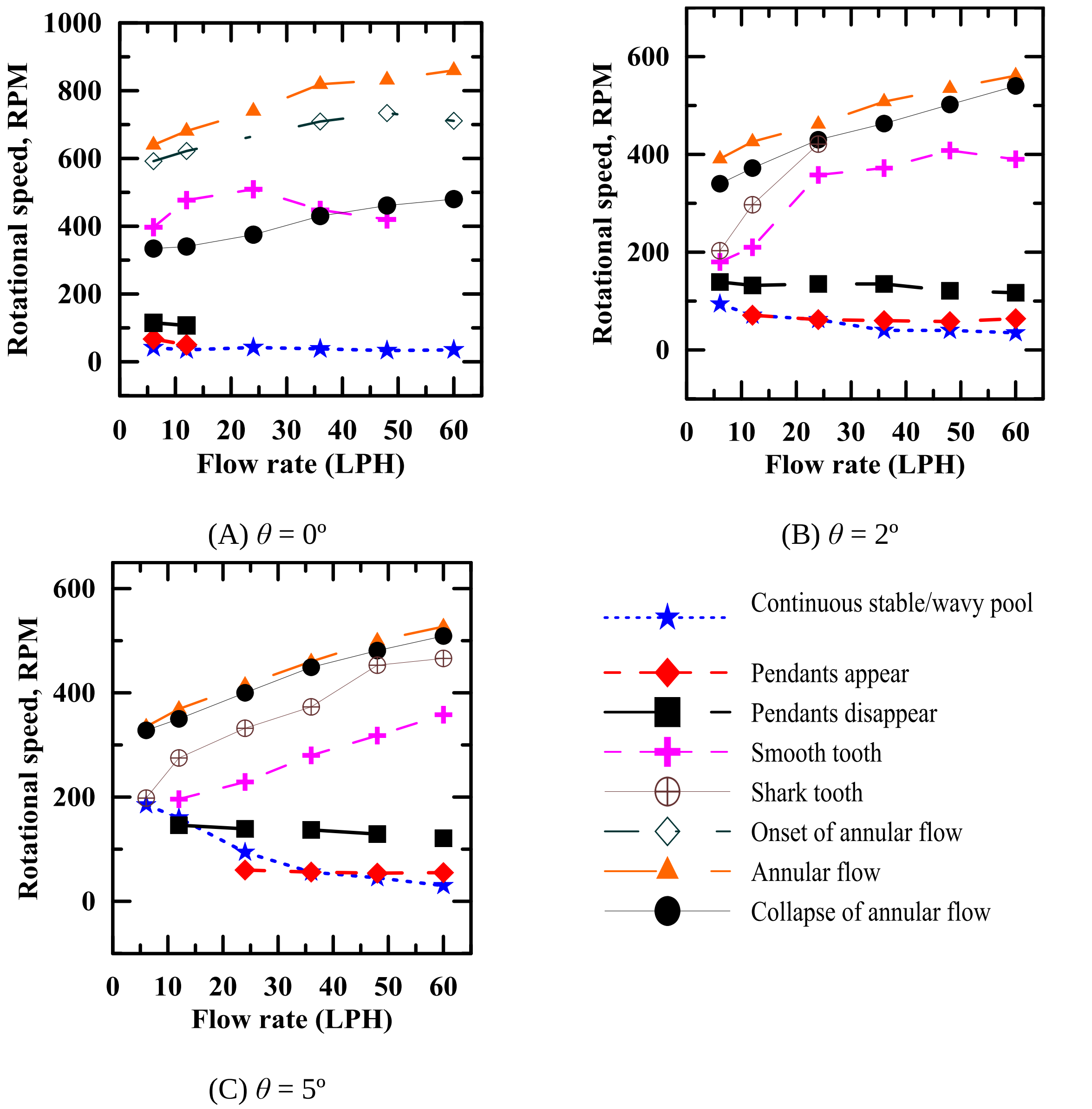

Fig. 3.7 Flow regime map for a rotating inclined pipe. ID: 54 mm; Pipe length: 1000 mm (A) $Re'_f = 258 - 1958,\ Fr_\varphi = 0.03 - 22$, (B) $Re'_f = 479 - 2908,\ Fr_\varphi = 0.03 - 9$, (C) $Re'_f = 547 - 3232,\ Fr_\varphi = 0.03 - 8$

A flow regime map is presented in Fig. 3.7 to compare the flow transitions occurring in a horizontal pipe with those in inclined pipes with two different angle of inclination. Fig. 3.7 clearly indicates the effect of angle of inclination on transitions to *annular flow* and *collapse of annular flow*. Pipe rotation speeds for these flow transitions systematically reduces as the angle of inclination increases (see Figs. 3.7(B) and 3.7(C)). In addition, the gap between the *annular flow* and *collapse of annular flow* reduces with increase in inclination. These effects are on account of the reduction in the liquid hold up in the pipe due to gravitational pull, which increases with angle of inclination. *Smooth tooth and Shark tooth* patterns are more prominently visible in inclined pipes. This shows a clear dependence of these flow patterns on the liquid hold up inside the rotating pipe. Different flow patterns appearing at various experimental conditions of flow rate inclination angle and rotation rate are presented in Appendix D Figs. D.1 - D.4.

3.4.3 Effect of pipe diameter on flow transitions in an inclined pipe with continuous flow

In order to investigate the effect of pipe diameter on flow transitions in a rotating inclined smooth pipe, flow visualization experiments are carried out using pipes of three different inside diameters (54, 44 and 34 mm).

Results obtained for pipes with an angle of inclination θ = 4º are presented in Fig. 3.8. In the 34 mm diameter pipe, *pendants* appear only for low flow rates i.e 100-400 ml/min (6-25 LPH) compared to the larger diameter pipes. Compared to the smaller diameter pipes, *smooth* and *shark tooth* patterns are observed in the 54 mm diameter pipe for a wider range of flow rate i.e. 100-830 ml/min (6-50 LPH). These effects are caused by the difference in the liquid hold up which is a function of the pipe diameter for a given flow rate of the liquid. Flow transition rotation speeds for *annular flow* and *collapse of annular flow* are also greatly affected by the diameter of the pipe. Figure 3.9 compares the effect of pipe diameter on the flow transition speeds for *annular flow* and *collapse of annular flow* for horizontal (θ = 0º) and inclined (θ = 3º) pipes. As the pipe diameter increases, the centrifugal force associated with the rotation increases at a specific rotational speed. Hence, for a larger diameter pipe, the flow transition occurs at a lower rotational speed compared to the smaller diameter pipes. Also, the liquid hold up in a larger diameter pipe for any particular flow rate and inclination is smaller than its corresponding lower diameter pipe.

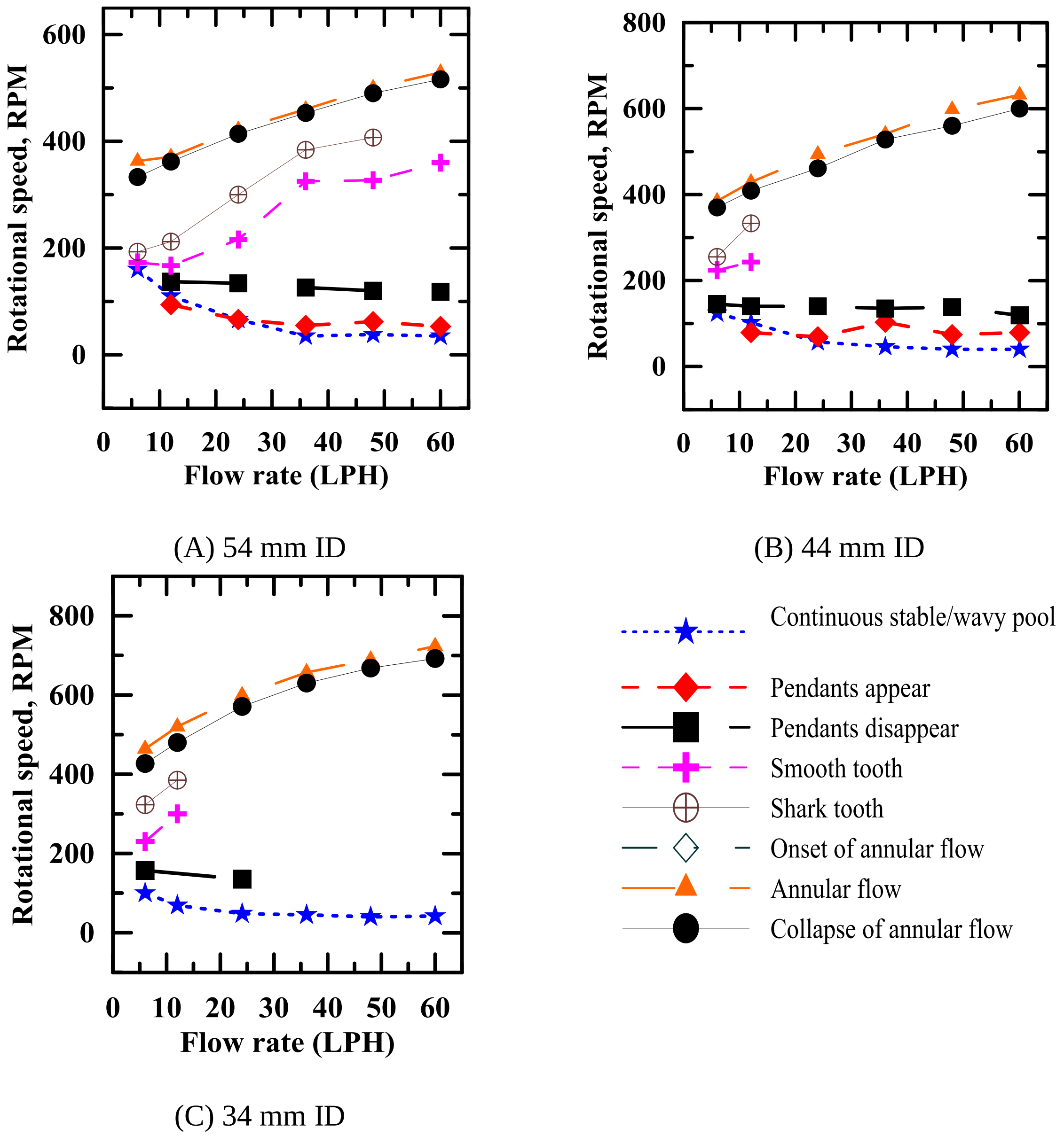

Fig. 3.8 Flow regime map for a rotating inclined pipe of different diameter. Pipe length: 1000 mm; angle of inclination: 4°

(A) $Re'_f = 533 - 3073,\ Fr_\varphi = 0.07 - 17$, (B) $Re'_f = 585 - 3429,\ Fr_\varphi = 0.09 - 24$, (C) $Re'_f = 638 - 3806,\ Fr_\varphi = 0.09 - 32$

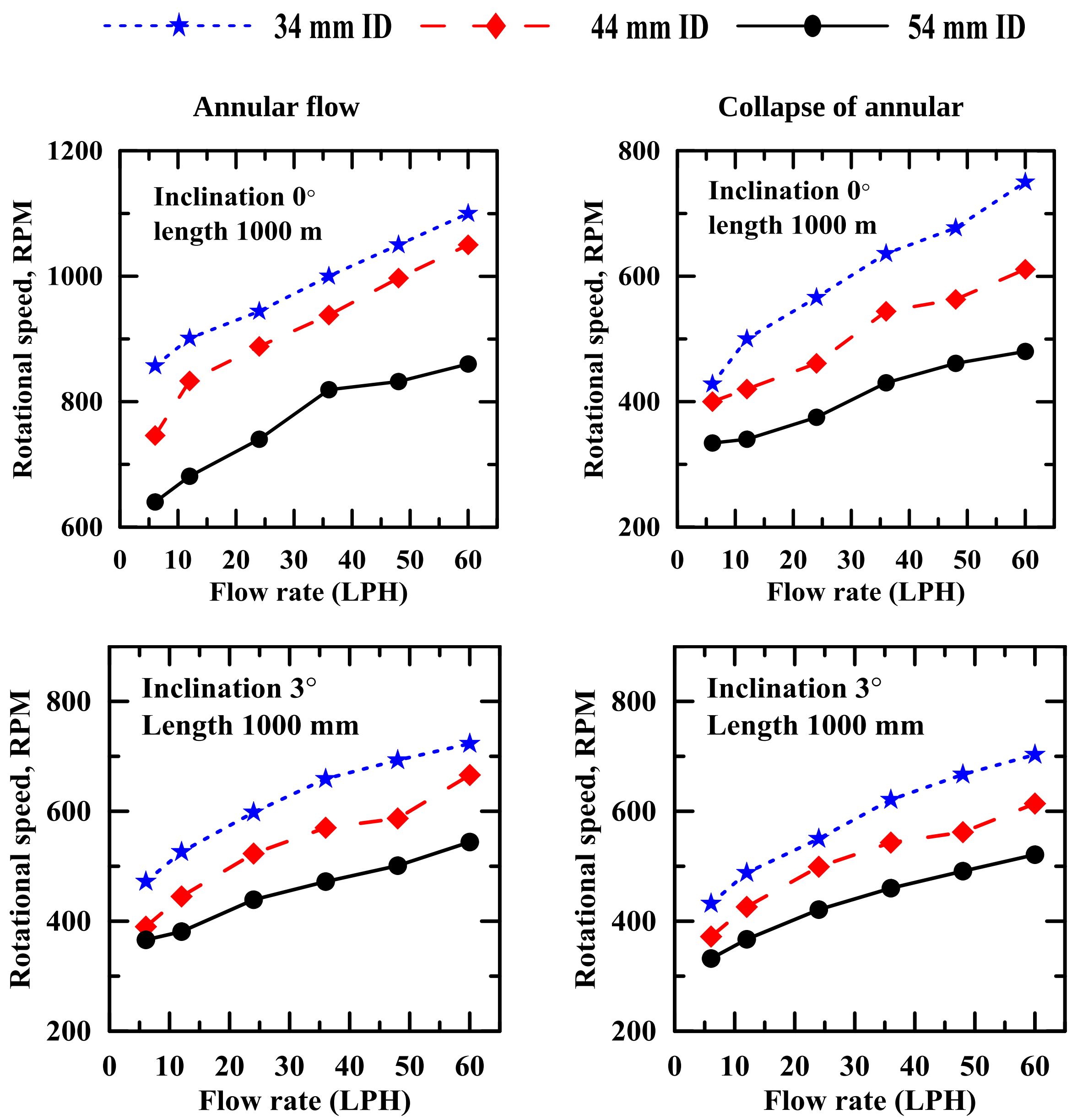

Fig. 3.9 Effect of pipe diameter on flow transitions in a horizontal (θ = 0º, $Re'_f = 258 - 2077,\ Fr_\varphi = 7 - 73$) and inclined pipe (θ = 3º, $Re'_f = 511 - 3607,\ Fr_\varphi = 7 - 31$). Pipe length: 1000 mm

3.4.4 Effect of pipe length on flow transitions in an inclined pipe with continuous flow

In order to study the effect of pipe length on flow transitions in a rotating inclined smooth pipe, flow visualization experiments are carried out using pipes of four different lengths (350, 500, 750 and 1000 mm). Figure 3.10 shows insignificant effect of pipe length on the flow transition speeds for *annular flow* and *collapse of annular flow* transitions for inclined pipes of two different diameters (34 and 54 mm) and two different angles of inclination (0.8º and 3º).

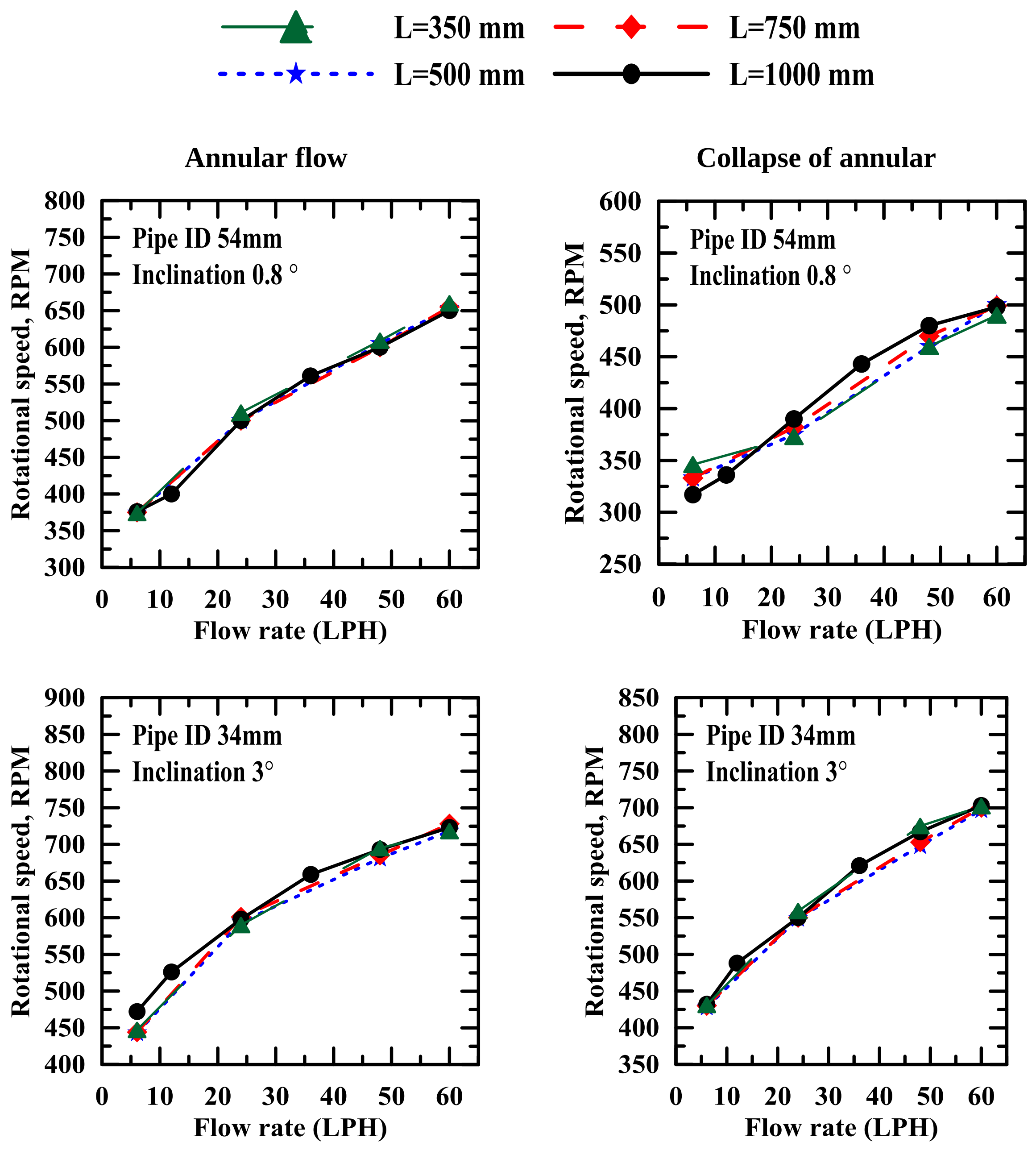

Fig. 3.10 Effect of pipe length on flow transition speeds for annular flow and collapse of annular flow (θ = 0.8º, $Re'_f = 399 - 2588$, $Fr_\varphi = 6 - 25$); (θ = 3º, $Re'_f = 637 - 3607$, $Fr_\varphi = 11 - 32$).

With 54 mm ID pipes inclined at an angle of 0.8°, the maximum deviations observed in the rotation speeds for transition to *annular flow* and the *collapse of annular flow* are is 1.4% and 4.8%, respectively. Reducing the pipe inner diameter to 34 mm ID and increasing the angle of to 3°, the maximum deviations in the rotation speeds for transition to *annular flow* and the *collapse of annular flow* are is 2.5% and 0.6%, respectively. Based on these observations, it can be concluded that varying the pipe length does not affect the flow transitions to annular flow and collapse of annular flow significantly. This is due to the fact that the flow transitions essentially occur due to the rotation of the pipe. As the wall is moving at a constant angular velocity throughout the pipe length, a thin layer of liquid is being pulled up by the raising wall, irrespective of the pipe length. This basically minimizes the effect of length of the pipe on the flow transition.

3.4.5 Flow regime map for rotating inclined pipe with continuous flow

Based on the flow visualization experimental results obtained for different pipe diameters (34, 44 and 54 mm), pipe lengths (350, 500, 750 and 1000 mm) and angle of inclinations (0º - 5º) a flow regime map is generated as shown in Fig. 3.11. In the present study, the angular velocity is much larger than the axial flow velocity and the main governing force is the rotation of the pipe. Therefore, the flow transitions occur essentially due to the interactions, between the inertial force due to the rotation and the gravitational force acting downwards, which can be characterised by the Rotational Froude number, Fr_{φ}. As the rotational speed is increased, the inertial forces due to the rotation acting on the liquid increases. Finally, when the centrifugal force is sufficiently large, the rimming flow becomes *annular flow* as seen in Fig. 3.11.

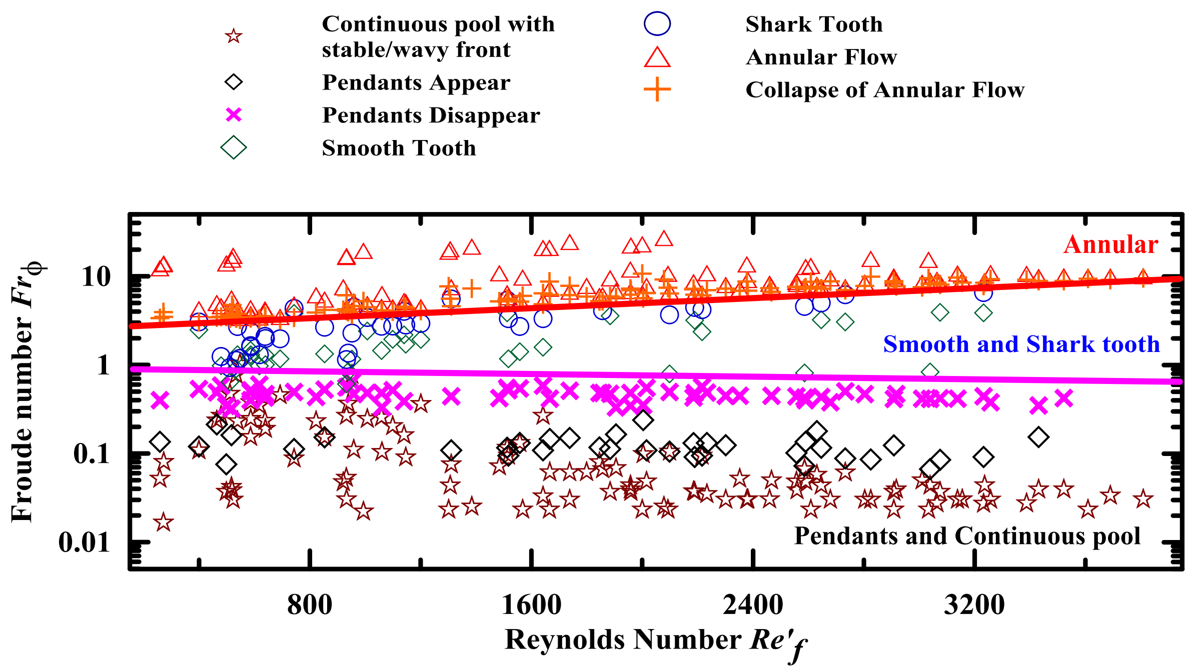

Fig. 3.11 Flow regime map for a partially filled rotating inclined pipe with continuous axial flow; Pipe ID 34 - 54 mm, Angle of inclination: 0°-5°

Continuous pool with stable/wavy front exists between $Fr_\varphi = 0.01 - 1$. Fluid *pendant* appears and disappears in the range of $Fr_\varphi = 0.06 - 0.8$. *Smooth* and *shark tooth* patterns are visible in the range of $Fr_\varphi = 0.9 - 6.65$. *Smooth tooth* and *shark tooth flow* patterns have an overlapping region. At higher flow Reynolds numbers, these flow profiles were not always visible in the transition region and hence not present in the flow regime map. As the rotational speed increases, *annular flow* pattern is realised. *Shark tooth* and *annular flow* patterns also have an overlapping region. Figure 3.11 shows that *annular flow* pattern exists when $Fr_\varphi > 2.4 + 2 \times 10^{-3} Re'_f$, which is valid for all inclination angles and pipe diameters explored in the present experimental study. *Collapse of annular flow* profile appears to be closely in coherence with the appearance of *annular flow* profile.

3.5 Conclusions

Flow transitions in a partially filled, rotating inclined smooth pipe with an axial liquid (water) flow are experimentally investigated. The effects of flow rate, pipe inclination, diameter and length on the flow transitions are reported. Rotation speeds for flow transitions to *annular flow* and *collapse of annular flow* systematically reduce as the angle of inclination is increased. The gap between the *annular flow* and *collapse of annular flow* also reduces with increase in inclination. These effects are on account of the reduction in the liquid hold up in the pipe due to gravitational pull, which increases with angle of inclination. For a larger diameter pipe, the flow transition occurs at a lower rotational speed. Flow transition in a rotating pipe is virtually independent of the pipe length.

A flow regime map is developed based on Reynolds number and Froude number. This work is expected to provide a basis for predicting flow transition rotational speeds for flow transitions in partially filled rotating pipes, which can be used for different industrial applications with fluid properties similar to water. Scientific investigations to study the effect of liquid properties will enhance further understanding of flow transitions in partially filled rotating pipes with axial liquid flows.

3.6 Contributions of the present work

The current work presents a detailed study of the fluid flow patterns inside a partially filled rotating pipe with continuous inflow and outflow of fluid. The effect of various parameters like pipe diameter, length, inclination angle, fluid flow rate and rotation rate on the fluid flow patterns inside the test section is addressed in this work. A flow regime map is developed to predict the flow transition rotational speeds for flow transitions.

CHAPTER 4

HEAT TRANSFER IN A PARTIALLY FILLED ROTATING PIPE WITH SINGLE PHASE FLOW

4.1 Introduction

The previous chapter explores the various flow transitions in a partially filled, rotating inclined smooth pipe with an axial liquid (water) flow. The effects of water volumetric flow rate, pipe inclination angle, rotation rate, diameter and length on the flow transitions are reported. Based on the previous studies, it is established that rotation and liquid hold up inside the partially filled rotating pipe with continuous in and outflow have significant effects on the character of the flow pattern. Liquid flow pattern will influence the heat transfer characteristics in a partially filled axially rotating channel. Such equipment is widely used in power industries, chemical engineering, aircraft engines etc. In general they are cylindrical in shape. However, channels with non-circular geometry are also used in industries. The rotation rate about the channel axis is a variable, and is in general, operated at a constant rate in industrial applications. Rotation has a substantial effect on the character of the flow pattern and heat transfer. The liquid holdup inside the rotating test section is modulated by varying the inlet flow rate, pipe inclination angle and the diameter of the pipe. Results reported in Section 3.4.3 highlight the fact that with increasing inclination angle, the influence of pipe diameter on the flow profile transition diminishes. Moreover, both increasing inclination angle and increasing pipe diameter lead to the reduction of the liquid holdup inside the partially filled rotating test section. Results described in Section 3.4.4 show that length of the test section does not have any influence on the flow pattern transitions. Hence, a single pipe diameter and length is used in the heat transfer studies.

Majority of the studies mentioned in the previous chapter were performed in rotating partially filled cylinders where the fluid volume is fixed and the pipe extremities are sealed. Singaram *et al.* (2014) and the studies reported in chapter 3 investigates the fluid flow transitions in a partially filled rotating horizontal pipe with continuous inflow and outflow of liquid. Singaram *et al.* (2014) reported a detailed study of the fluid film flow pattern along the length of the rotating pipe using optical interferometry technique. A correlation to determine the annular fluid film thickness along the length of the rotating horizontal pipes was reported.

Kuo *et al.* (1960), Pattenden (1964) and Beckman *et al.* (1998) experimentally studied heat transfer between fluids separated by a rotating tube. Kuo *et al.* (1960) studied the variation of heat transfer rate in a partially filled rotating pipe with and without inserts. It is reported that the average heat transfer in a partially filled pipe improves similar to a fully filled rotating pipe. The similarity is attributed to the continuous film that covers the surface of the pipe wall due to rotation. This improves the overall heat transfer area. Eventually the final mixing of the thin liquid film on the wall with the liquid pool at the bottom enhances heat transfer. Kuo *et al.* (1960) also identified change in flow pattern leading to change in heat transfer rate as the rotation rate is varied. It is indicated that under the investigated experimental domain, effect of free convection is of lesser importance compared to the rotation of the pipe. Kuo *et al.* (1960) experimentally explored heat transfer characteristics in a partially filled horizontal rotating pipe. Flow rates in the range of 12-240 LPH and rotation rates in the range of 10-500 RPM are used. Kuo *et al.* (1960) performed the experiment in a 650 mm long pipe with an outer diameter of 76.2 mm and wall thickness of 6.35 mm. The pipe was heated using external heaters and the inner wall temperature is measured using Patton-Feagan method (1941).

Pattenden (1964) reported exceptionally large overall heat transfer coefficients which are attributed to the flow instability caused by the rotating pipe. The range of experimental flow rate reported is limited to turbulent region. Pattenden (1964) concluded that the effect of axial flow rate is low compared to tube rotational speed. Beckman *et al.* (1998) concluded that in the experimental regime explored, conduction heat transfer dominates instead of forced convection mechanism.

Krivosheev *et al.* (1979) experimentally studied the effect of pipe rotation on heat transfer coefficient in a partially filled pipe with no inflow and outflow “heat pipes”. The influence of increasing pipe rotation rate on the reduction and subsequent dissolution of the azimuthal local wall temperature variation are highlighted. The heat transfer rate is reported to improve with the rotation rate. It is also reported that fluid property must be taken into account while designing rotating heat pipes with or without wicks. Kascheev and Podymova (2012) developed an analytical model based on constant wall temperature boundary condition for the various sections of an inclined rotary calciner. The developed analytical model provides an approximate estimate of the residence time of the materials in each zone, length of the calciner zones and the output product temperature based on the radius of the calciner, temperature of inner surface, inclination angle, liquid flow rate and thermodynamic property of the feed matter.

Petitjean *et al.* (2006) and Kascheev and Podymova (2012) describe the application of rotating inclined pipe in evaporation of hazardous waste. Kascheev and Podymova (2012) experimentally and analytically explored heat transfer in a partially filled rotating evaporator at 3 RPM with liquid flow rates in the range of 10-25 LPH. However, the effect of various experimental parameters is not discussed in detail.

Influence of flow transition on heat transfer in a partially filled rotating heated pipe and its application as a rotary evaporator is an interesting prospect. Experimental studies reported in the literature are based on thermocouple temperature averaged over the experimental geometry [Kuo *et al.* (1960), Pattenden, (1964), Krivosheev *et al.* (1979), Beckman *et al.* (1998), Petitjean *et al.* (2006) and Kascheev and Podymova (2012)]. Local temperature and heat transfer coefficient variation along the longitudinal axis of a partially filled rotating heated pipe is not reported in the literature. The current study is focused on providing adequate experimental data which can be used for designing a partially filled rotary pipe evaporator for radioactive waste management applications. Due to the corrosive and radioactive nature of the waste, the equipment is operated at lower rotation rates to improve its serviceability in a hazardous environment. It is reported that typical rotary calciner in nuclear waste management units operate at approximately 30 RPM with liquid flow rates in the range of 10-25 LPH [Petitjean *et al.* (2006) and Kascheev and Podymova (2012)]. Kuo (1960) reported single phase heat transfer studies in the range of 10-500 RPM and flow rate of 12-240 LPH. The present study highlights the effect of various parameters at low flow rates and moderate pipe rotation rates (10 – 309 RPM) and covers the following aspects:

- Local temperature variation along the longitudinal axis of a rotating heated pipe
- Effect of governing parameters i.e. heat flux (779-12522 W/m^2), flow rate (6-80 LPH) and rotation rate (10-309 RPM) on heat transfer coefficient in a partially filled horizontal rotating heated pipe

- Correlation to predict the average Nusselt number in a partially filled rotating heated pipe based on dimensionless parameters

This study is expected to provide insight into the heat transfer in a partially filled pipe rotating about its longitudinal axis with continuous inflow and outflow of water.

4.2 Experimental setup and procedure

The experimental setup (Fig. 4.1) consists of a Joule heated rotating SS-304 pipe, a feed water system, and associated controllers. Water, at a constant temperature, is pumped into the rotating test section using a Watson-Marlow 520DU peristaltic pump. The SS pipe has an inside diameter of 32.8 mm, 1.1 mm wall thickness and has a heating zone of 1000 mm. Joule heating is performed by passing electric current through the pipe to maintain constant heat flux. The current passes through the rotating setup using a pair of slip rings and carbon brush assembly. Power is supplied using a 415 V 2-phase primary, 0-40 V secondary 0-500 A, AC Transformer (Argo 15320/A- J.08) connected to a rheostat. The pipe rotation can be controlled between 10-350 RPM using a 5 HP DC motor and speed controller. A belt drive connects the motor to the rotating pipe using a set of pulleys.

Infrared imaging camera (Thermoteknix VisIR® 200) is used to capture the rotating pipe wall temperature. The thermal images captured have a resolution of approximately 1.9mm/pixel. For the infrared camera to convert the incident radiation to temperature, emissivity of the surface is to be separately determined and provided as an input to the camera. To compute the emissivity of the surface a target plate is used. The target plate used is a stainless steel sheet of SS 304, painted with high temperature paint – pyromark (2500 flat black). The dimension of the sheet is 55 mm × 55 mm, 0.2 mm thick. Uniform temperature across the target plate is achieved by direct electrical heating.

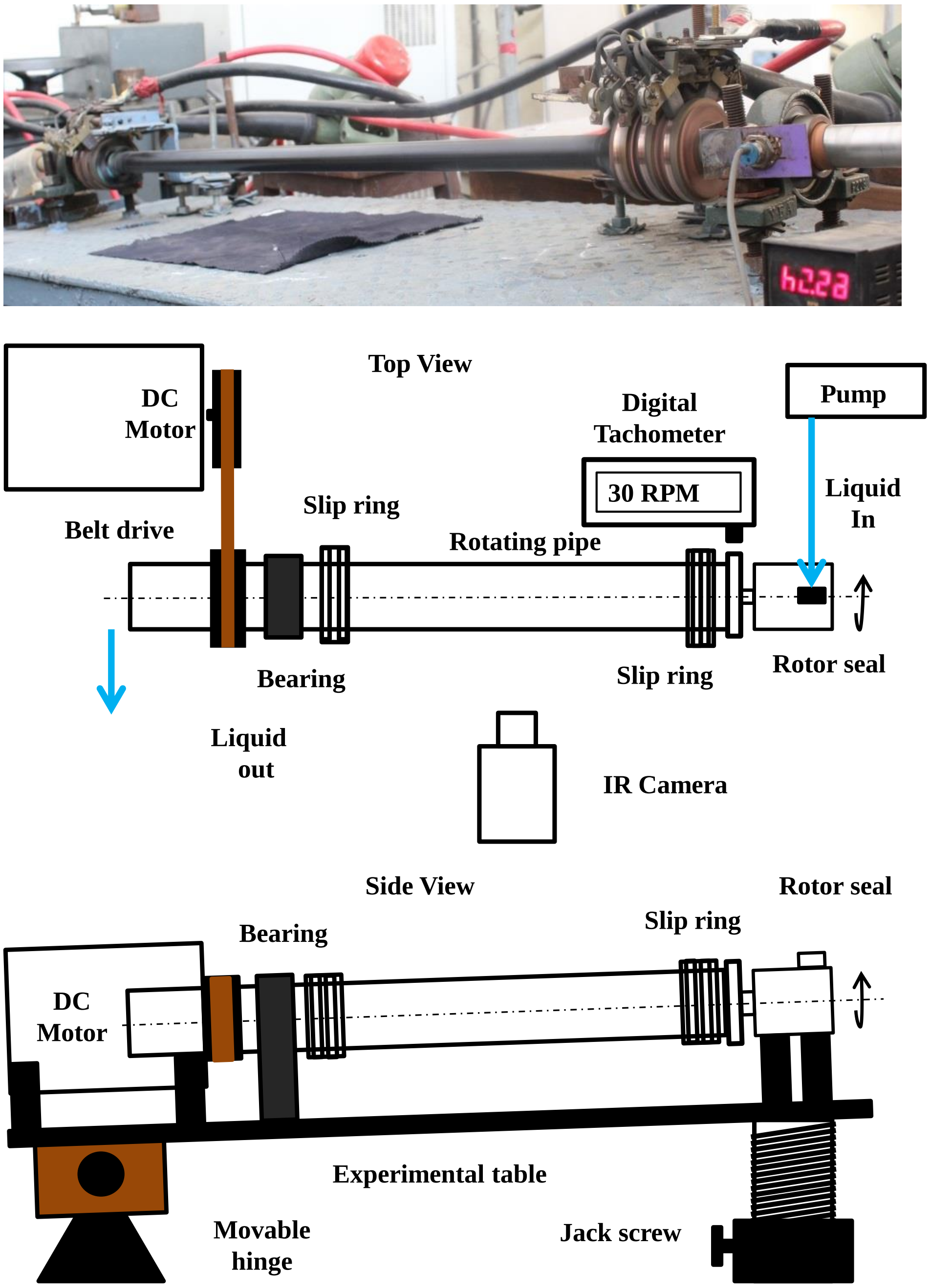

Fig. 4.1 Experimental setup for rotary evaporator

Four calibrated K-type thermocouples are spot welded onto the rear side of the target plate. Varying current supplied to the target plate controls the temperature of the plate. An enclosure is made to mitigate convective cooling of the plate. Thermal images are recorded at a set emissivity where the average image temperature matches the average thermocouple temperature. The thermal camera is set to capture images at emissivity, $\varepsilon = 0.69$. Details if calibration of various instruments used are given in Appendix A.

Liquid mass flow rate into the rotating pipe is set using a peristaltic pump. The rotation rate is set to a minimum rotational speed at which the local azimuthal temperature variation at any point along the length of the test section is negligible [Krivosheev *et al.* (1979)]. A specific heat flux is set by controlling the current (70-300 A) through the test section via the slip rings. The magnitude of current supplied is controlled using a regulator. For a particular experiment, the heat flux and flow rate are kept constant throughout the RPM range (10-309) explored. The flow is allowed to come to steady state. The thermal camera is used to capture 30 consecutive images with 3 seconds intervals. These images are used to average the temperature data in order to mitigate any signal noise that may have been captured. The temperature variation azimuthally along the rotating test section was found to be negligible once steady state is attained. The centre line temperature along the length of the rotating heated pipe is then extracted from the averaged thermal image to generate the outer wall temperature profile.

Figure 4.2(A) illustrates the 16 circumferential locations at a particular axial location of the rotating partially filled test section where the temperature is captured using the infrared camera. A typical circumferential wall temperature distribution at different lengths of the test section is shown in Fig. 4.2(B). The water flow rate is set at 200 ml/min (12 LPH), rotation rate and wall heat flux is maintained constant at 10 RPM and 3366 W/m^2 respectively. As shown in Fig. 4.2(B), the wall temperature variation along the circumference is negligible. Hence the central line temperature along the length of the rotating test should sufficiently represent the system temperature profile as a whole. The central line is indicated as a dotted line on the rotating test section schematic as shown in Fig.4.1 and corresponds to location 9 in Fig. 4.2(A).

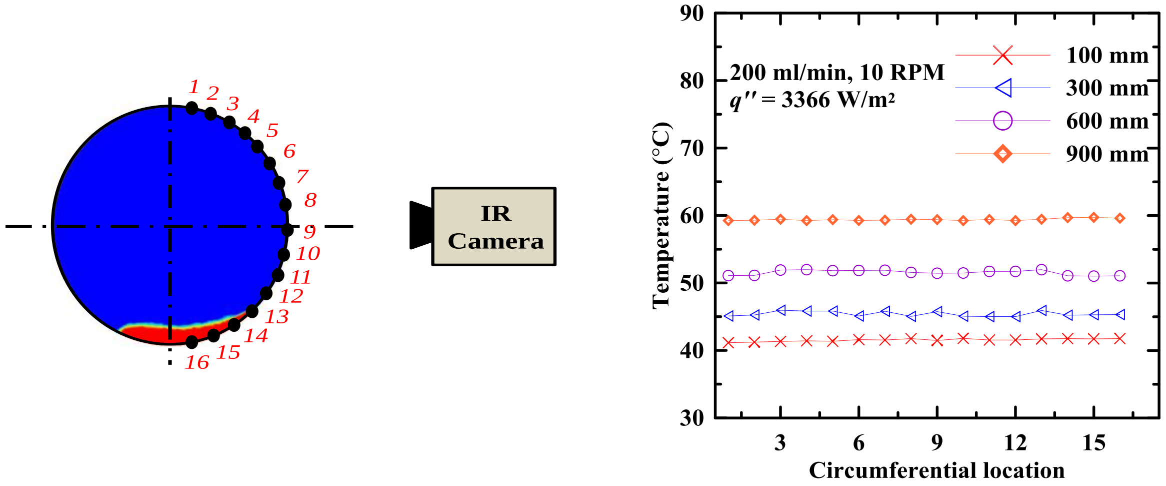

(A) Indication of local points for wall temperature measurement

(B) Circumferential temperature variation at different test section lengths

Fig. 4.2 Wall temperature variation along the circumference of a partially filled rotating heated pipe

The inner wall temperature is computed using the captured outer wall temperature images using one dimensional heat conduction equation under steady state conditions. Detailed description of the temperature correction methodology is documented in Baburajan *et al*. (2013). The maximum temperature variation across the wall thickness of the test section is analytically computed to be 0.25 ºC [Incropera (2006) and Baburajan *et al.* (2013)]. A sample calculation is explained in Appendix D.2.

The outlet flow rate is measured to ensure that there is no evaporation loss. The outlet water temperature is recorded using a 1 mm diameter K-type thermocouple strategically placed at the exit of the heating zone. The rotation rate is increased and the flow is allowed to come to steady state. At steady state all the data are recorded and the rotation rate is thus increased in steps till it reaches ~300 RPM. Once a complete set of data is available for a specific flow rate and heat flux input, either the flow rate or the power supplied is varied and the next set of experiment is performed. To ensure single phase operation, the heat flux is limited so that the outlet water temperature is below 70ºC.

4.3 Data Reduction

In order to process the experimental data, the following non-dimensional numbers, which are derived using Buckingham Pi theorem as explained in Appendix C.3, were used:

4.3.1 Flow Reynolds number

Flow Reynolds number is defined as the ratio of inertial force to the viscous force, as given in Eqn. (4.1)

$$Re_f = \frac{4\dot{Q}\rho}{\pi\mu D} \tag{4.1}$$

where, $\dot{Q}$ is the fluid volume flow rate. D is the inner diameter of the test section. ρ and μ are the density and dynamic viscosity of the liquid respectively. V is the superficial axial flow velocity of liquid in a stationary partially filled horizontal pipe as given by Eqn. (4.2).

$$V = \dot{Q}/A_{pool} \tag{4.2}$$

$$A_{pool} = R^2 \cos^{-1}(1 - H/R) - (R - H)\sqrt{2RH - H^2} \tag{4.3}$$

The experimental pool height measured at ambient condition for various volumetric flow rates in a stationary, partially filled pipe is tabulated in Table 4.1. The liquid pool height is calculated by experimentally measuring the liquid holdup inside the stationary pipe at a specific set of experimental condition i.e. liquid volume flow rate. An assumption of uniform pool height along the length of the pipe is made while calculating the pool height. Liquid hold up in the stationary horizontal circular pipe at various inlet flow rates are experimentally determined using catch and time technique. The inlet flow is disconnected and simultaneously all the liquid inside the partially filled pipe is collected at the exit using a measuring cylinder with a least count of 1 ml. The liquid hold-up values are used to derive the average height *H*, of the liquid pool in the circular duct. The experimental pool height measured in ambient condition at various flow rates are tabulated in Table 4.1

Table 4.1 Experimental pool height in a horizontal stationary pipe of ID 32.8 mm

Flow rate (ml/min)	Hold up (ml)	Pool height H (mm)
100	125	4.14
200	135	4.2
300	165	4.75
400	175	4.95
600	230	5.94
800	270	6.68
1350	400	9.01

The cross sectional area of the liquid pool (A_{pool}) developed as a result of the liquid flow through the partially filled stationary pipe is calculated geometrically using Eqn. (4.3) [Lioumbas et al. (2005)]. The derivation of Eqn. (4.3) is elaborated in Appendix C.1.

4.3.2 Rotation Reynolds number

Rotation Reynolds number is the ratio of rotational inertia to the viscous forces as given by Eqn. (4.4)

$$Re_{\phi} = \frac{\rho\omega D^2}{\mu} \tag{4.4}$$

where, ω is the angular velocity of the rotating pipe.

4.3.3 Prandtl number

Prandtl number is defined as the ratio of momentum diffusivity to thermal diffusivity. The dimensionless term is given by Eqn. (4.5)

$$Pr = \frac{C_p\,\mu}{k} \tag{4.5}$$

where, a Prandtl number value of 4.95 is used in the analysis.

4.3.4 Dimensionless heat flux

For an externally heated pipe with constant wall flux, a dimensionless heat flux can be defined as given by Eqn. (4.6)

$$\gamma = \frac{\pi q'' D^2}{4\dot{Q}\rho C_p T} \tag{4.6}$$

$$q" = \frac{\dot{m}C_p(T_{out} - T_{in})}{A_{surface}} \tag{4.7}$$

$$T_b = \frac{T_{out} + T_{in}}{2} \tag{4.8}$$

$$A_{surface} = \pi DL \tag{4.9}$$

where, $q"$ is the heat flux transferred to the liquid in the rotating pipe and $\dot{m}$ is the mass flow rate of liquid. Fluid properties such as heat capacity (C_p), density (ρ) and dynamic viscosity (μ) are calculated at average bulk temperature *i.e.*, T_b as given by Eqn. (4.8). The heat transfer area is $A_{surface}$ and is calculated as given by Eqn. (4.9) where, L is the length of the heating section. The experimental parameters studied and their corresponding dimensionless quantities are tabulated in Table 4.2.

4.3.5 Nusselt number

Nusselt number is given by Eqn. (4.10).

$$Nu_{local} = \frac{h_{local}D}{k_{local}} \tag{4.10}$$

where, h_{local} is experimental convective local heat transfer coefficient, k_{local} is the thermal conductivity of the bulk fluid along the length of the rotating pipe. The local heat transfer coefficient is calculated as given by Eqn. (4.11)

$$h_{local} = \frac{q"}{(T_{w,local} - T_{b,local})} \tag{4.11}$$

where, $q"$ is the heat flux, $T_{w,local}$ and $T_{b,local}$ are the local wall temperature and liquid bulk temperature respectively along the length of the rotating pipe, The local bulk temperature $T_{b,local}$ is calculated by linear interpolation between inlet T_{in} and outlet T_{out} liquid temperatures, assuming the flow is thermally fully developed.

4.3.6 Temperature dependent property data

Liquid properties i.e. thermal conductivity k_{local}, heat capacity C_p, density ρ, dynamic viscosity μ and surface tension σ are calculated based on temperature dependent polynomial fit on National Institute of Standards and Technology data at constant pressure with temperature increments. [NIST database (2016)]. The polynomials are listed below.

$$k = -1 \times 10^{-5} {T_b}^2 + 2.2 \times 10^{-3} T_b + 0.5594 \tag{4.12}$$

$$C_p = 4 \times 10^{-8} {T_b}^4 - 1 \times 10^{-5} {T_b}^3 + 1.1 \times 10^{-3} {T_b}^2 - 0.0471 T_b + 75.959 \tag{4.13}$$

$$\rho = 1 \times 10^{-5} {T_b}^3 - 5.6 \times 10^{-3} {T_b}^2 + 2.7 \times 10^{-3} T_b + 1000.2 \tag{4.14}$$

$$\mu = 3 \times 10^{-11} {T_b}^4 - 8 \times 10^{-9} {T_b}^3 + 9 \times 10^{-7} {T_b}^2 - 5 \times 10^{-5} T_b + 0.0017 \tag{4.15}$$

$$\sigma = 3 \times 10^{-14} {T_b}^4 + 2 \times 10^{-10} {T_b}^3 - 3 \times 10^{-7} {T_b}^2 - 3 \times 10^{-7} {T_b}^1 + 0.0756 \tag{4.16}$$

The uncertainty of different parameters used in the experimental measurement is shown in Table 4.3. Sample calculation methodology to compute the uncertainty in flow Reynolds number and heat transfer coefficient is described in Appendix B.2.

Table 4.2 Range of the experimental parameters covered in the present study

Flow rate (ml/min)	V (m/s)	T_b (°C)	q'' (W/m^2)	$Re_f = \frac{4\dot{Q}\rho}{\pi\mu D}$	RPM	$Re_\phi = \frac{\rho\omega D^2}{\mu}$	$\gamma = \frac{\pi q'' D^2}{4\dot{Q}\rho C_p T}$
100	2.95×10^{-2}	37	1243	87.3	10 - 304	1290 - 46555	5.50×10^{-3}
	2.95×10^{-2}	37.5	1115	88.5	18 - 305	2775 - 47293	4.61×10^{-3}
200	5.10×10^{-2}	36	1852	173.1	12 - 300	1873 - 45226	3.87×10^{-3}
	5.10×10^{-2}	40	3338	183.6	10 - 301	1025 - 49903	7.22×10^{-3}
	5.10×10^{-2}	32.5 - 34	908-1557	167.4	60	8580 - 8901	$1.89 – 3.24 \times 10^{-3}$
	5.10×10^{-2}	36.5 - 40	1552-4269	184.1	30	4543 - 5233	$3.09 - 8.55 \times 10^{-3}$
	5.10×10^{-2}	36.5 - 52	1487-5691	187.7	100	15143 - 17709	$2.93 - 11.3 \times 10^{-3}$
	5.10×10^{-2}	37.5 - 52.5	1583-5624	189.9	300	45955 - 53210	$3.07 - 11 \times 10^{-3}$
	5.10×10^{-2}	36.5	2289	174.4	18 - 308	2700 - 46990	4.96×10^{-3}
300	6.71×10^{-2}	38.5	3747	268.2	10 - 302	815 - 47321	5.22×10^{-3}
400	7.92×10^{-2}	37.5	4553	352.7	12 - 305	1780 - 47293	4.79×10^{-3}
	7.92×10^{-2}	29.5 - 34	779 - 2987	323.1	160	21806 - 23315	$0.83 – 3.22 \times 10^{-3}$
	7.92×10^{-2}	31.5 - 34.5	1168 - 2791	329.7	255	35764 - 37497	$1.21 – 2.91 \times 10^{-3}$
	7.92×10^{-2}	32 - 38	1686 - 5060	342.7	69	9754 - 10687	$1.78 – 5.37 \times 10^{-3}$
	7.92×10^{-2}	39	5052	359.1	30 - 300	4697 - 46792	5.23×10^{-3}
	7.92×10^{-2}	36	4591	346.1	14 - 305	2095 - 46227	5.08×10^{-3}
600	9.60×10^{-2}	35.5	5411	516.4	13 - 301	1942 - 45245	3.79×10^{-3}
	9.60×10^{-2}	41.5	9416	556.1	14 - 301	2349 - 48758	6.43×10^{-3}
	9.60×10^{-2}	31	2539	481.6	13 - 305	1812 - 42676	1.83×10^{-3}
	9.60×10^{-2}	35	4907	515.3	30 - 300	4446 - 45012	3.39×10^{-3}
	9.60×10^{-2}	36	6364	519.8	16 - 305	2477 - 46150	4.58×10^{-3}

Table 4.2 Range of the experimental parameters covered in the present study (cont.)

Flow rate (ml/min)	V (m/s)	T_b (°C)	q'' (W/m^2)	$Re_f = \frac{4\dot{Q}\rho}{\pi\mu D}$	RPM	$Re_\phi = \frac{\rho\omega D^2}{\mu}$	$\gamma = \frac{\pi q'' D^2}{4\dot{Q}\rho C_p T}$
800	1.06×10^{-1}	41.5	12522	742.3	15-309	2558 - 50104	6.37×10^{-3}
	1.06×10^{-1}	31-37	2466-8696	669.6	205	28579 - 31199	$1.30 – 4.61 \times 10^{-3}$
	1.06×10^{-1}	31	3450	642.8	13-302	1819 - 42369	1.87×10^{-3}
	1.06×10^{-1}	34-38	2467-7013	544.4	30	4450 - 4646	$1.75 – 3.38 \times 10^{-3}$
	1.06×10^{-1}	34-38.5	2727-7272	688.4	100	14991 - 15537	$2.31 – 3.50 \times 10^{-3}$
	1.06×10^{-1}	34-39	2077-7531	692.15	300	44508 - 47040	$0.98 – 3.57 \times 10^{-3}$
1342	1.19×10^{-1}	32	5176	1094.1	17-300	2515 - 42492	1.61×10^{-3}

Table 4.3 Experimental uncertainties

Parameter	Absolute uncertainty		
	Average	**Maximum**	**Minimum**
Time (s)	1	1	1
Flow rate (kg/s)	2.50×10^{-5}	2.50×10^{-5}	2.50×10^{-5}
Length (m)	2.00×10^{-5}	2.00×10^{-5}	2.00×10^{-5}
Pool height (m)	1.95×10^{-3}	2.10×10^{-3}	1.52×10^{-3}
Rotation rate (RPM)	0.25	2.5 (≥500RPM)	0.25
Temperature (°C)	0.5	0.5	0.5
Velocity (m/s)	1.73×10^{-4}	2.95×10^{-4}	8.86×10^{-5}
Heat transfer coefficient (W/m^{2}K)	39.83	70.89	28.16
Flow Reynolds number	1.33	1.48	1.30
Rotational Reynolds number	46.14	68.58	37.76
Dimensionless Heat flux	9.40×10^{-6}	5.22×10^{-5}	4×10^{-6}
Nusselt number	2.08	3.71	1.47

4.4 Results and discussion

Experiments are performed to study the effect of wall heat flux, fluid flow rate and pipe rotation rate on single-phase heat transfer in an axially rotating, partially filled pipe in continuous mode. In order to understand the effect of heat flux, flow rate and rotation rate on heat transfer each parameter is individually varied while the others are kept constant. Section 4.4.1 discusses the effect of heat flux variation on local heat transfer coefficient in a steady state partially filled rotating heated pipe. Section 4.4.2 highlights the effect of flow rate on local heat transfer coefficient. Section 4.4.3 presents the effect of rotation rate on the local heat transfer coefficient. Section 4.4.4 discusses the average heat transfer coefficient distribution as a result of various experimental conditions studied. Section 4.4.5 highlights the average Nusselt number distribution. Section 4.4.6 explains the formulation of correlations based on experimental data.

4.4.1 Effect of wall heat flux on local heat transfer coefficient

The liquid flow rate through the rotating pipe and the pipe rotation rate are kept constant and the wall heat flux is gradually increased to study its effect on the local heat transfer coefficient variation along the length of the rotating pipe. Fig. 4.3 shows the local wall and bulk water temperature profiles along the length of the partially filled rotating heated pipe.

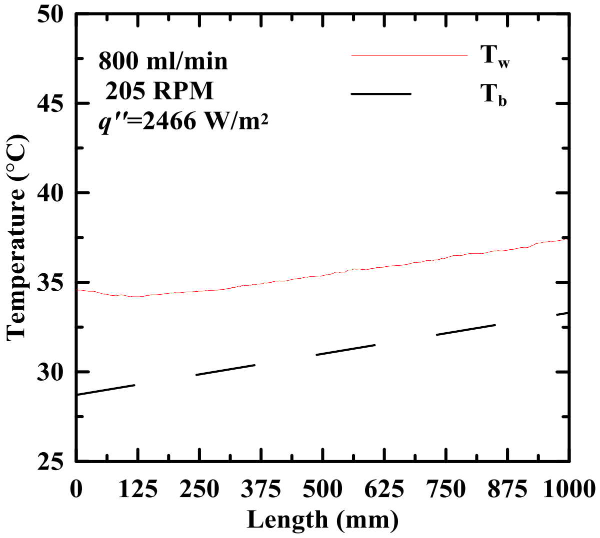

(A) q''=2466 W/m^2

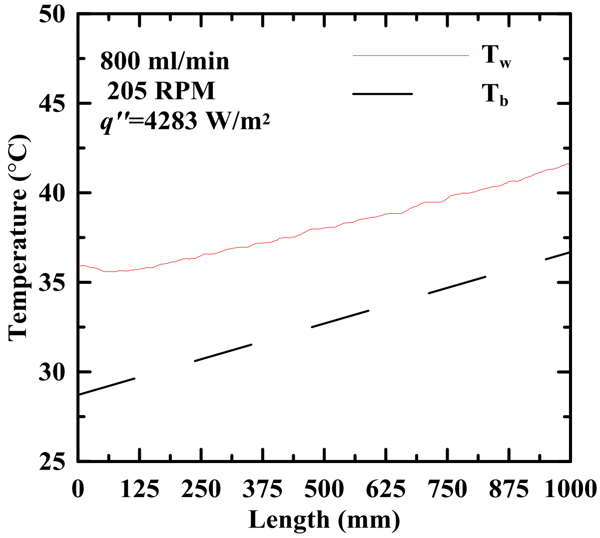

(B) q''=4283 W/m^2

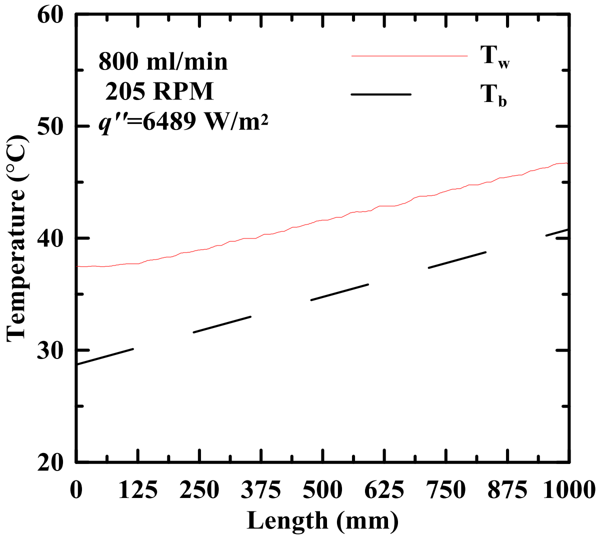

(C) q''=6489 W/m^2

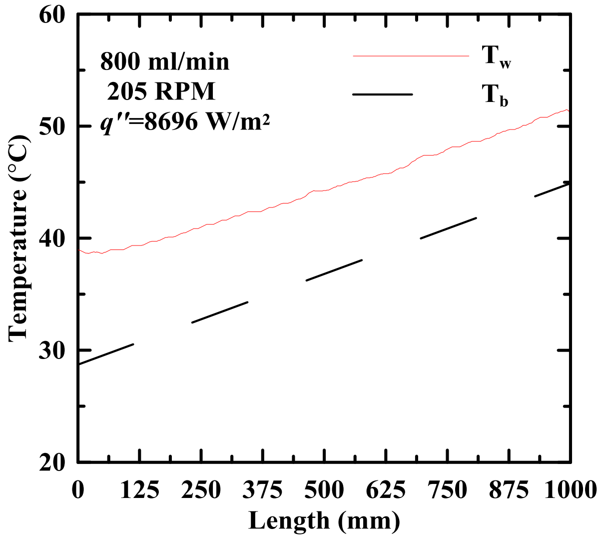

(D) q''=8696 W/m^2

Fig. 4.3 Wall and bulk temperature profiles along the length of the rotating pipe

The outlet water volume flow rate is measured at steady state to ensure there is no evaporation loss of liquid.

The variation of local heat transfer coefficient along the length of the rotating pipe is shown in Fig. 4.4 as a function of wall heat flux at a given liquid flow rate and pipe rotation speed. The increase in local heat transfer coefficient along the length of the partially filled rotating heated pipe at a particular heat flux input is due to the decrease in difference between the local wall and bulk temperatures. As the bulk fluid temperature increases, fluid physical property (viscosity, density and surface tension) decreases. Ashmore *et al.* (2003) developed a relation to compute the liquid film thickness wetting the rising wall using these fluid physical properties and pipe rotation rate. The relation highlights the fact that as the bulk fluid temperature increases, the film thickness wetting the rising wall decreases. As the film thickness decreases, the resistance to heat transfer decreases and improves the overall local heat transfer coefficient.

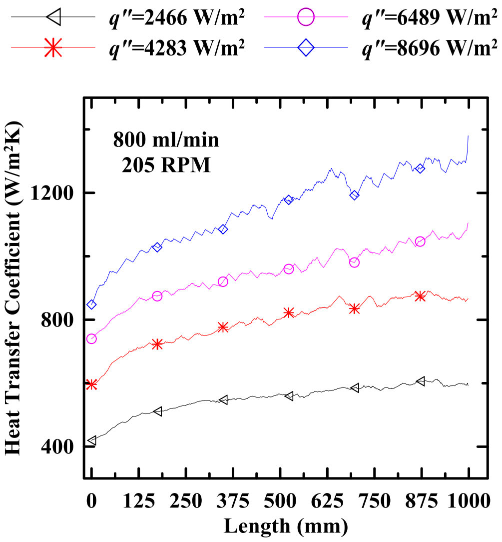

Fig. 4.4 Local heat transfer coefficient along the length of the rotating heated pipe with constant flow rate (48 LPH, Re_f = 669.6) and rotation rate (205 RPM, Re_ϕ = 28579-31199) and variable heat flux.

Kuo *et al.* (1960) carried out a similar experimental study using an externally heated 600 mm long rotating steel tube with an inner diameter of 76.2 mm and the flow Reynolds number was in the range of 60-530. Their experiments were carried out with constant wall temperature. They reported that average heat transfer coefficient remains constant in a partially filled rotating heated pipe at a constant flow rate, rotation rate and at variable heat fluxes. Based on the experimental observations they concluded that the flow phenomena is predominantly determined by the mass flow and pipe rotation and the influence of pure free convection is negligible. However, in the present study using a resistance heated rotating pipe, the heat transfer coefficient increases with increase in the wall heat flux as shown in Fig. 4.4. This suggests that the heat transfer coefficient is dependent on the heat flux in a partially filled rotating resistance heated pipe. The observed dependence of heat transfer coefficient on the heat flux can be explained in terms of the local temperatures of the wall, water and air as shown in Fig. 4.5.

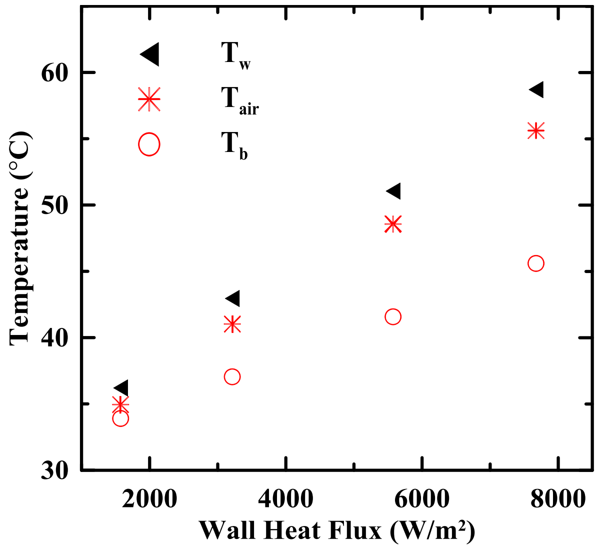

Fig. 4.5 Local temperatures of wall, water and air at 520 mm from the outlet of the rotating pipe (water flow rate: 400 ml/min (24 LPH, $Re_f = 342.7$), rotation rate: 60 RPM ($Re_\phi =$ 9754 - 10687)). Air relative humidity (70%)

The inner air temperature is measured using a K-type thermocouple which is placed axially along the centreline, 520 mm from the outlet of the partially filled rotating heated pipe. The flow rate is maintained at 400 ml/min (24 LPH) and the rotation rate is set at 60 RPM. The wall heat flux is increased from 2000-8000 W/m^2.

As seen in Fig. 4.5, local temperatures increase with increase in wall heat flux. Difference between the air temperature and water temperature also increases with increase in wall heat flux. Thus, the air gets heated by the wall and the hot air in turn transfers heat to the water through the free surface as shown in Fig. 4.6. Nusselt number correlation as given by Dropkin and Karmi (1956) estimates an increase in the wall to air core heat flux from 7–19 W/m^2 and the air core to the liquid interface heat flux from 6–61 W/m^2 as the wall heat flux increase from 1573–7673 W/m^2. The data used for this estimation is the Rotation Reynolds number for air i.e. $Re_{\phi,air} = 600.92$, Grashof number $Gr = g\beta'(T_w - T_{b,air})D^3/\mu^2 = 6416 - 14781$ at the wall and bulk air temperatures as shown in Fig. 4.5.

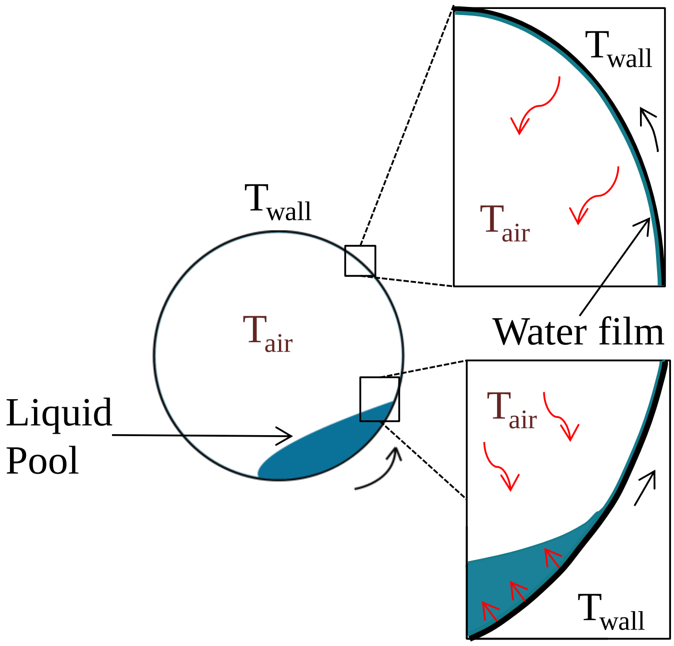

Fig. 4.6 Schematic representation of heat transfer inside the rotating pipe

The free surface heat transfer from hot air is expected to be responsible for the dependence of heat transfer coefficient on the heat flux. This effect was not dominant in the experiment conducted by Kuo *et al.* (1960) as they have used a relatively large pipe i.e. 76.2 mm outer diameter (6.35 mm wall thickness) and significantly larger liquid flow rates (13.24 – 242.09 LPH). Various experimental results highlighting the effect of heat flux on single phase heat transfer in a partially filled rotating pipe are shown in Appendix D, Figs. D.5 (A)-(F).

4.4.2 Effect of flow rate variation on local heat transfer coefficient

In this case, the heat flux and rotation rate is kept constant, while the flow rate through the rotating heated pipe is increased. The local heat transfer coefficient along the length of the partially filled rotating heated pipe is shown in Fig. 4.7. Both at lower rotation rate i.e. 100 RPM and higher rotation rate i.e. 300 RPM flow rate has a positive influence on the heat transfer rate as shown in Figs. 4.7A and 4.7B respectively [Kuo *et al.* (1960), Pattenden, (1964) and Beckman *et al.* (1998)].

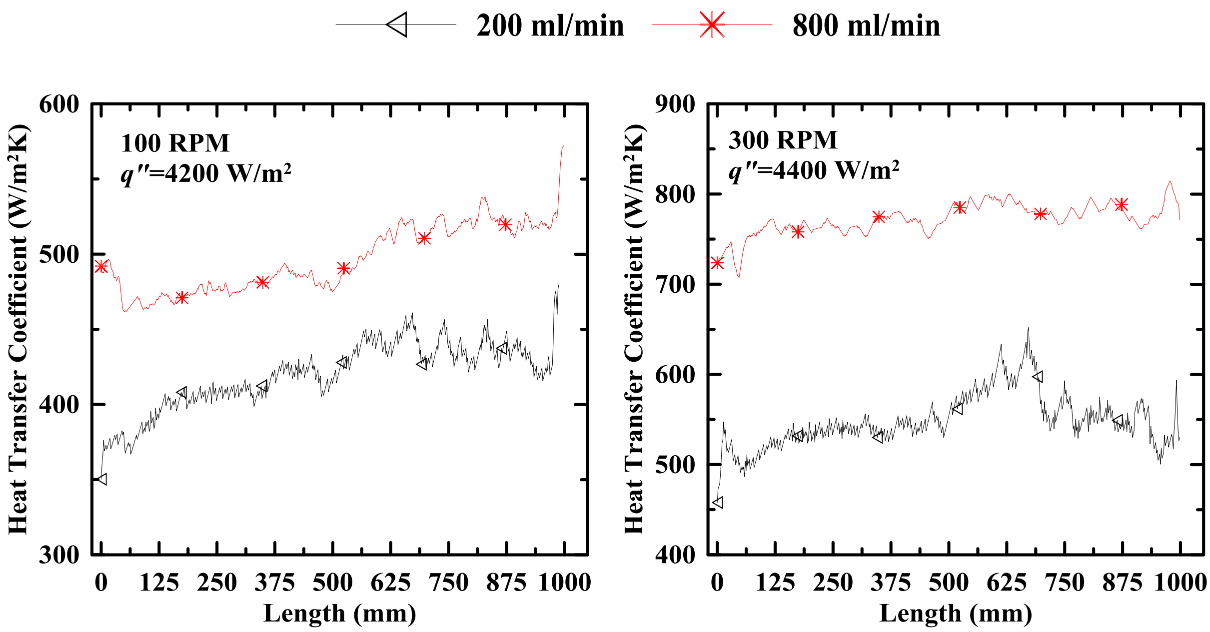

(A) 100 RPM, q''= 4200 W/m2 (B) 300 RPM, q''= 4400 W/m2

Fig. 4.7 Local heat transfer coefficient along the length of the rotating heated pipe for different liquid flow rates (12 LPH, Re_f = 193) (48 LPH, Re_f = 687) and rotation rate (100 RPM, Re_ϕ = 14991-16844) (300 RPM, Re_ϕ = 45279-51553)

In both the cases the rotation rate and heat flux are kept constant individually for different flow rates 200 (12 LPH) and 800 ml/min (48 LPH). The improvement in the local heat transfer coefficient along the length of the partially filled rotating heated pipe with increase in flow rate is evident as shown in Figs. 4.7(A)-(B) [Kuo *et al.* (1960), Pattenden (1964) and Beckman *et al.* (1998)]. Fig. 4.7 also shows that the heat transfer coefficient enhances due to increase in flow rate which is further enhanced by the RPM. This shows that the recirculating flow inside the liquid pool is influenced by the pool height which is a function of inlet flow rate and pipe dimension [Haji-Sheikh *et al.* (1984)]. Fig. 4.7(B) has higher heat transfer coefficient compared to Fig. 4.7(A) due to the higher rotation rate as discussed in the following section. The effect of flow rate on single phase heat transfer in a partially filled rotating pipe is shown in Appendix D, Figs. D.6 (A)-(D).

4.4.3 Effect of pipe rotation rate on local heat transfer coefficient

In this case, for a constant heat flux and specific flow rate, the rotation rate is varied. The rotation rate is gradually increased (14-301 RPM) and its effect on local heat transfer coefficient along the length of the partially filled rotating heated pipe is plotted in Fig. 4.8.

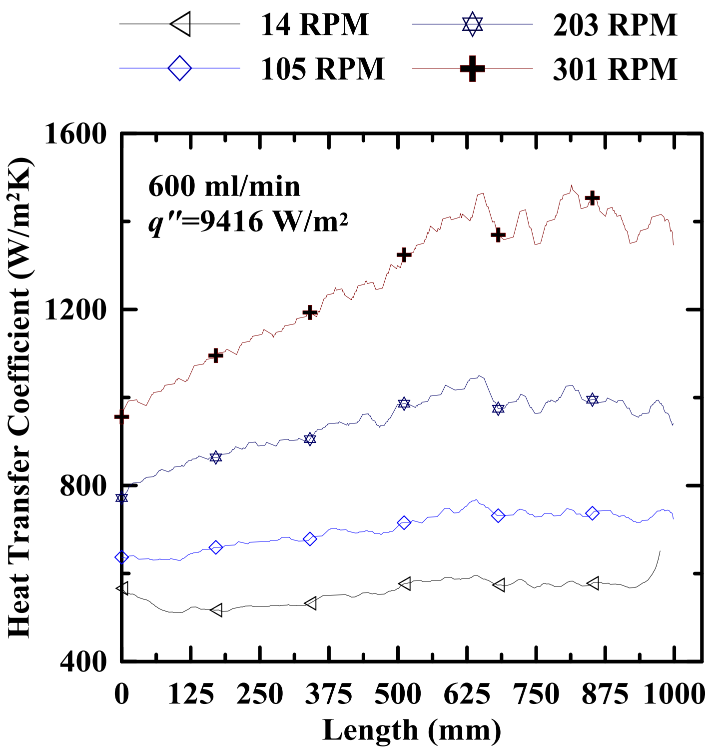

Fig. 4.8 Local heat transfer coefficient along the length of a partially filled rotating heated pipe at a constant flow rate (600 ml/min, 36 RPM, $Re_f = 556$) and heat flux (9416 W/m2) and variable rotation rates ($Re_\phi = 2349$-48758)

It is seen that the heat transfer coefficient improves as the rotation rate is increased. Better spreading of the liquid along the rotating wall as a result of increasing rotation rate improves heat transfer [Kuo *et al.* (1960)]. At lower rotation rates i.e. 10-100 RPM, there exists a liquid pool at the bottom *i.e.*, pool flow regime. As the rotation rate increases i.e. 200-300 RPM, the flow pattern inside the partially filled rotating heated pipe varies i.e. smooth tooth profile

[Phillips (1960), Karweit (1975), Moffat (1977), Thoroddsen and Mahadevan (1997), Chicharro *et al.* (2011) and Singaram *et al.* (2014)]. The change in flow pattern alters the mixing rates and subsequently influences the heat transfer coefficient. At 301 RPM, the local heat transfer coefficient data in Fig. 4.8 indicates sharper slope change compared to data at lower rotation rates. This can be attributed to flow transition from pool flow to pendent as discussed in chapter 3.

Similarly in Fig. 4.7(A) and 4.7(B), at comparable wall heat flux (i.e. 4200 and 4400 W/m^2) and 200 ml/min flow rate as the rotation rate is increased from 100 RPM to 300 RPM, the local heat transfer coefficient increases. The same is also true for 800 ml/min flow rate as shown in Fig. 4.7(A) and 4.7(B). The results highlight the predominant effect of rotation rate on the improvement of heat transfer coefficient. The effect of pipe rotation on single phase heat transfer in a partially filled rotating pipe is shown in Appendix D, Figs. D.7 (A)-(F).

4.4.4 Average heat transfer coefficient

At a constant flow rate and rotation rate as the wall heat flux is increased, the temperature difference i.e. T_w-T_{in} increases as shown in Fig. 4.9(A) and 4.9(B). The flow rate is maintained at 600 ml/min (36 LPH) and 800 ml/min (48 LPH) for all the experiments plotted in Fig. 4.9(A) and Fig 4.9(B) respectively. The curves are plotted as a function of pipe rotation speed for different wall heat fluxes. Fig. 4.9 illustrates that for a given heat flux, the average heat transfer coefficient increases with pipe rotation speed while the temperature difference decreases.

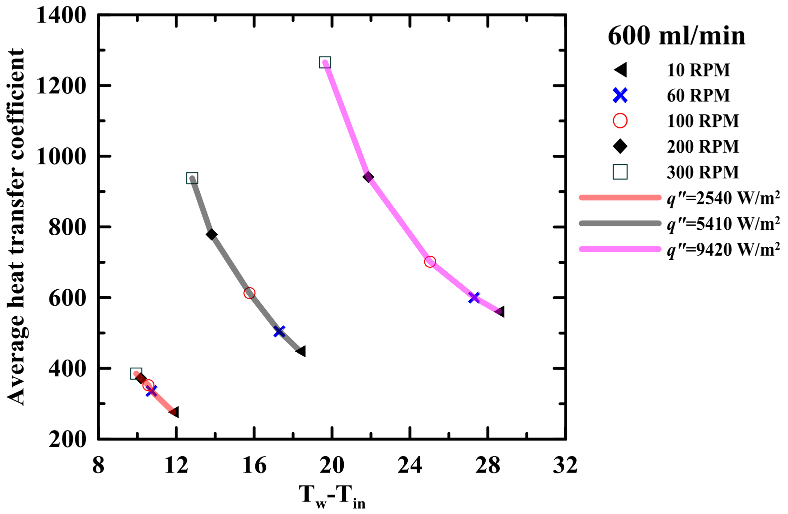

(A) 600 ml/min (36 RPM, $Re_f = 556$)

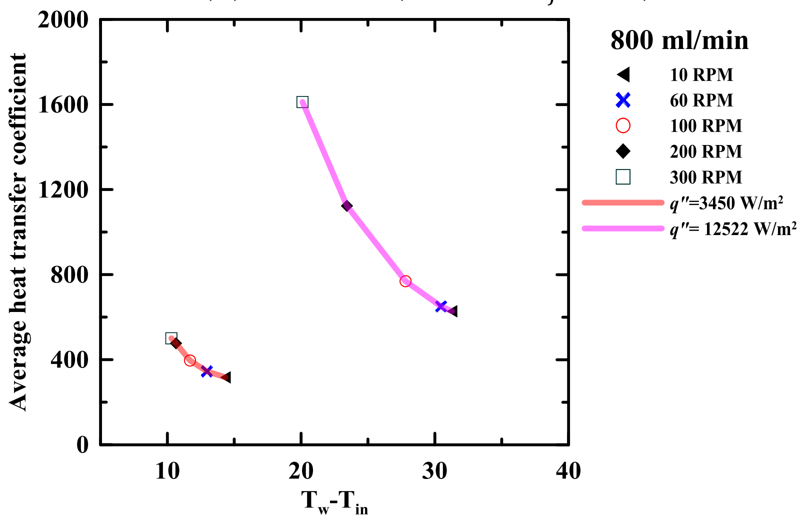

(B) 800 ml/min (48 RPM, $Re_f = 687$)

Fig. 4.9 Average heat transfer coefficient variation with heat flux

On the contrary, for a given rotation speed both the average heat transfer coefficient and the temperature difference increase with wall heat flux. However, the rate of increase in heat transfer coefficient decreases with wall heat flux for a given rotation speed. Thus, Fig. 4.9 illustrates that pipe rotation speed has a stronger impact on the heat transfer coefficient compared to the wall heat flux.

4.4.5 Average Nusselt number

The variation of average Nusselt number at various dimensionless heat fluxes for different flow and rotation Reynolds numbers is shown in Fig. 4.10. With increasing rotation Reynolds number, Nusselt number improves except for flow Reynolds number 87.36 and 88.51. For these low values of Reynolds numbers, the Nusselt number is not influenced by the rotation Reynolds number on account of the relatively smaller size of the liquid pool. Even at low rotation rates, the small liquid pool spreads on rotating wall easily. Spreading of the liquid decreases the pool height. The reduction in pool height restricts the mixing potential inside the liquid pool of the partially filled rotating heated pipe. The reduction of mixing thus restricts improvement of heat transfer coefficient even as the rotation rate increases [Kuo *et al.* (1960)].

For the higher flow Reynolds numbers, as the rotation Reynolds number increases, a significant amount of liquid remains in the pool. The fluid churning inside the liquid pool improves heat transfer to improve the Nusselt number. With increasing rotation Reynolds number, the rate of increase (slope) in Nusselt number also varies. This is on account of the change in fluid flow pattern [Kuo *et al.* (1960), Phillips (1960), Karweit (1975), Moffat (1977), Thoroddsen and Mahadevan (1997), Chicharro *et al.* (2011) and Singaram *et al.* (2014)]. The change in flow pattern alters the heat transfer phenomena and hence the Nusselt numbers. As the rotation Reynolds number is increased, the slope of average Nusselt number shifts at approximately $Re_{\phi} \approx 10^4$ for all the flow Reynolds numbers except for 87.36 and 88.51. The second change in average Nusselt number slope is observed between $Re_{\phi} \approx 2 \times 10^4 - 3 \times 10^4$. The change in slope indicates shift is fluid flow pattern due to rotation which in turn leads to the improvement of heat transfer. Rotation Reynolds number effectively captures the flow pattern shift for different flow rates at different rotation rate. Similar results are also discussed in Kuo *et al.* (1960).

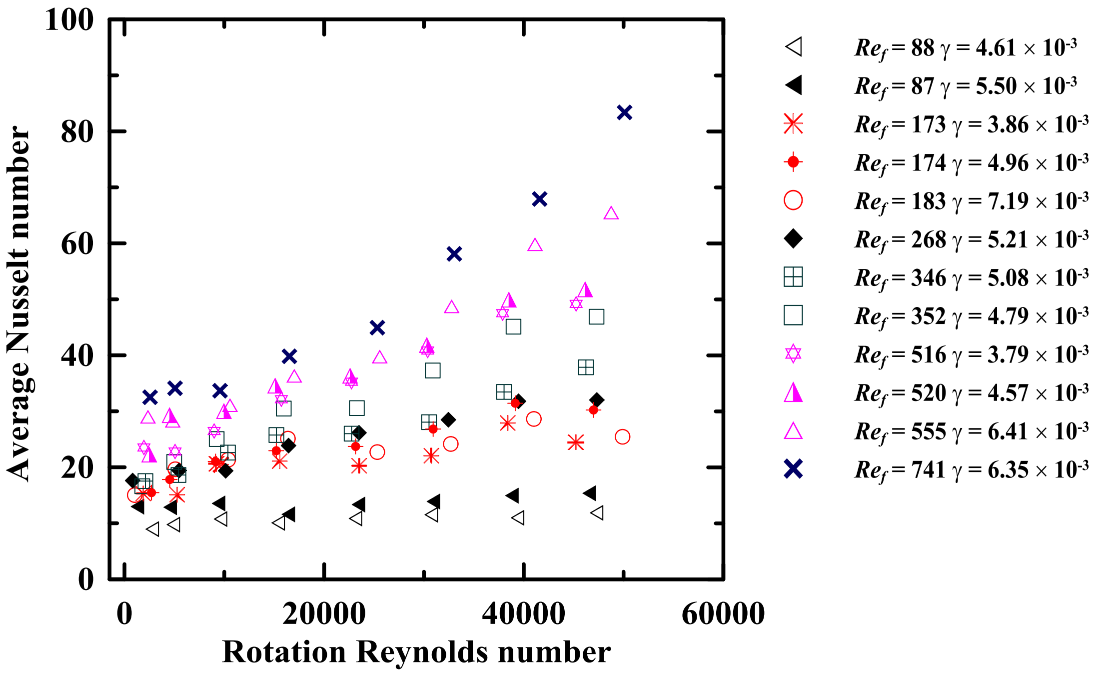

Fig. 4.10 Average Nusselt number variation

Beckman *et al.* (1998) reported an empirical correlation to predict the experimental Nusselt number as given by Eqns. (2.24) and (2.25) in the literature review. The same correlation is used to compute Nusselt number and is compared with experimental data as shown in Fig. 4.11. Although the trend of increasing Nusselt number with increasing rotation Reynolds number is captured, the correlation under-predicts the results. Also, as highlighted in Section 4.4.1, the effect of heat flux on the heat transfer coefficient is not reported by Kuo *et al.* (1960). The above comparison highlights the need for this study which systematically explores the effect of rotation rate, liquid flow rate and wall heat flux on the heat transfer characteristics of a partially filled rotating heated pipe with continuous inflow and outflow of liquid.

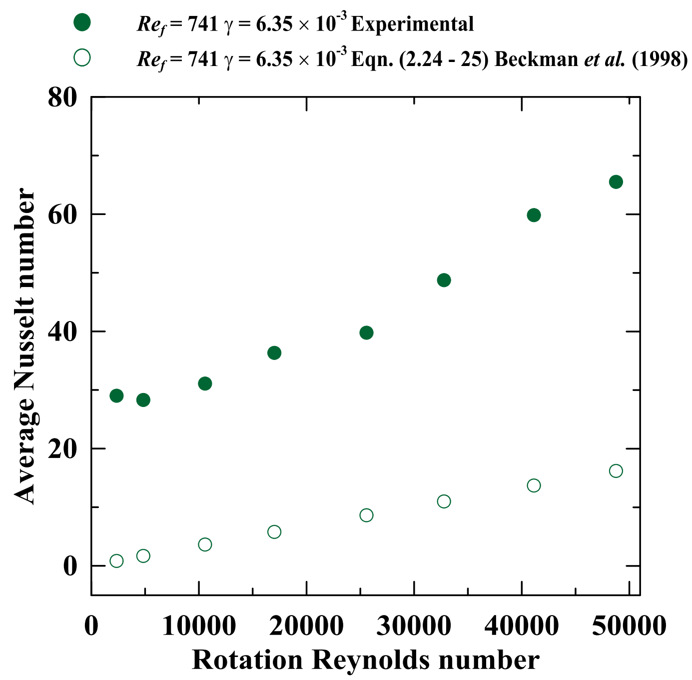

Figure 4.11. Comparison of experimental Nusselt number with Beckman *et al.* (1998) correlation

4.4.6 Correlation

A correlation to predict the average Nusselt number for the thermally fully developed flow in a horizontal partially filled rotating heated pipe is derived based on the experimental results. The correlation predicts within a maximum deviation of 30% and average deviation of 15% from the experimental data. The correlation predicts average Nusselt number as a function of flow Reynolds number (Re_f), rotation Reynolds number (Re_ϕ) and dimensionless heat flux (γ) as given by Eqn. (4.17). Flow Reynolds number is defined as the ratio of inertial force to the viscous force. Rotation Reynolds number, is the ratio of rotational inertia to the viscous forces. Dimensionless heat flux is defined as the ratio of thermal energy supplied to the thermal energy available at inlet. A comparison between the present experimental values and the correlation is presented in Fig. 4.12.

$$Nu_{Horizontal} = 1.72\, Re_f^{\;0.52} Re_\phi^{\;0.18} \gamma^{0.39} \tag{4.17}$$

Flow and rotational Reynolds numbers capture the effect of axial flow and rotational forces acting on the fluid body. Dimensionless heat flux captures the effect of wall heat flux on the heat transfer coefficient. The correlation emphasises the fact that all the contributing parameters positively influence the heat transfer characteristics of the partially filled rotating heated pipe. The above correlation is valid for the experimental conditions explored in this study *i.e.*, flow Reynolds number (87.1-1098.3), rotation Reynolds number (815-53210) and dimensionless heat flux (1.22×10^{-3}-1.12×10^{-2}).

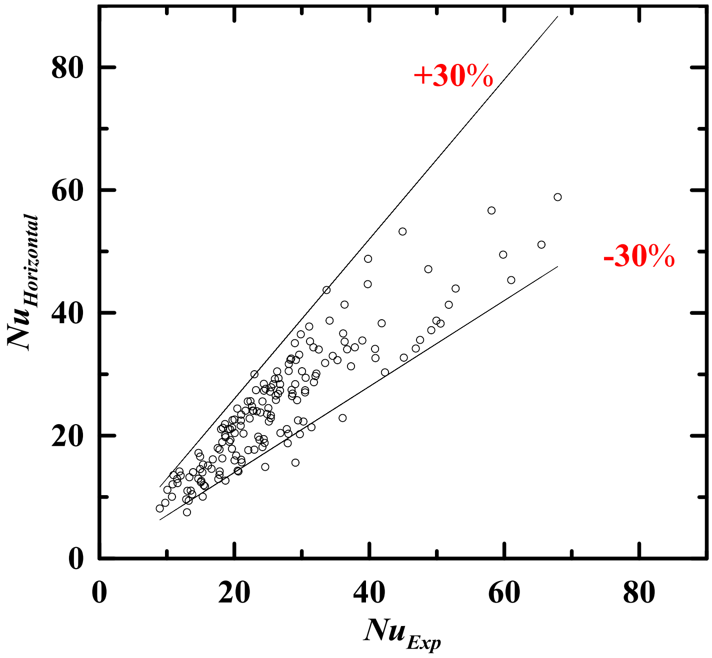

Fig. 4.12 Comparison of present correlation with experimental results

4.5 Conclusions

Single phase heat transfer in a partially filled horizontal rotating heated pipe with continuous liquid flow has been experimentally investigated. Flow rate is varied between 100~1350 ml/min (6 – 81 LPH). The rotation rate is varied between 10-309 RPM. Heat flux to the system is varied without triggering phase change of water. Local heat transfer coefficient along the length of a partially filled rotating horizontal pipe is reported.

- At a constant liquid flow rate and pipe rotation rate, increase in local heat transfer coefficient in the partially filled rotating heated pipe is observed as the wall heat flux is increased. A secondary heat transfer from the inner air to water through the free surface interface contributes to the improvement in heat transfer coefficient as the wall heat flux is increased.
- Heat transfer coefficient in the partially filled rotating heated pipe improves with increasing liquid flow rate.
- As the rotation rate is varied for a constant wall heat flux and water flow rate, the flow pattern inside the partially filled rotating pipe changes. Increasing the rotation rate at a constant flow rate and heat flux improves the heat transfer coefficient in the partially filled rotating heated pipe. The recirculating region the liquid pool improves the heat transfer coefficient as the rotation is increased.
- Effects of parameters influencing the heat transfer in a partially filled rotating heated pipe are quantified and a correlation to predict the average variation of Nusselt number is developed. The correlation is able to predict within 15% of the average experimental values.

4.6 Contributions of the present work

The current work presents a detailed study of the heat transfer process inside a partially filled rotating heated pipe. The effect of various parameters like heat flux, flow rate and rotation rate is addressed in this work exclusively using local and average data sets. Correlation is provided to predict the average variation in Nusselt at particular flow rates, rotation rates and wall heat flux in a partially filled rotating heated pipe.

CHAPTER 5

IMPACT OF INCLINATION ON SINGLE PHASE HEAT TRANSFER IN A PARTIALLY FILLED ROTATING PIPE

5.1 Introduction

Chapter 3 highlights the effect of various parameters i.e. liquid flow rate, pipe rotation rate, pipe inclination angle and pipe dimensions on the fluid flow pattern. Chapter 4 further discusses the effect of liquid flow rate, pipe rotation rate and wall heat flux on the heat transfer characteristics of a rotating horizontal heated pipe. Results discussed in the previous chapters establish the fact that single phase heat transfer in a partially filled horizontal rotating heated pipe is enhanced by rotation rate, wall heat flux and fluid flow rate. Kuo *et al.* (1960), Pattenden (1964) and Beckman *et al* (1998) have also experimentally studied the heat transfer characteristics in partially filled rotating pipes as well as fluids separated by a rotating tube. Pattenden (1964) reported that the axial flow rate has lower influence on the heat transfer compared to the rotation rate. Beckman *et al.* (1998) reported that the conduction heat transfer plays a pivotal role compared to the forced convection in the experimental domain explored. However, results discussed in chapter 4 highlights the influence of convective heat transfer and liquid flow rate towards the enhancement of the heat transfer coefficient in the partially filled horizontal rotating heated pipe. Difference in the heat transfer behaviour can be attributed to the difference in the experimental geometry between the current study and the geometries studied by Pattenden (1964) and Beckman *et al* (1998). Kuo *et al.* (1960) experimentally studied the heat transfer characteristics in a partially filled horizontal rotating pipe of dimensions 0.65 m long and 76.2 mm outer diameter. It is reported that the variation in the flow pattern as a result of pipe rotation leads to the enhancement in heat transfer. Similar results are discussed in chapter 4.

Kascheev and Podymova (2012) and Petitjean *et al.* (2006) explored the industrial usability of a rotating inclined pipe with 3° inclination angle for waste processing operations. Kascheev and Podymova (2012) derived a mathematical model to estimate the output product temperature, residence time and length of the heating zones of a partially filled rotating calciner. The rotation rate is maintained at 30 RPM with liquid volume flow rates of 10-25 litres per hour (LPH).

The influence of flow transition on heat transfer in a partially filled rotating heated pipe and its application as a rotary evaporator for nuclear liquid waste management is a motivating prospect. Open literature indicates that rotary evaporator for nuclear liquid waste management employs a small inclination angle in its design [Kascheev and Podymova (2012) and Petitjean *et al.* (2006)]. However, the effect of inclination on the local variation in temperature and heat transfer coefficient in a partially filled rotating heated pipe has not yet been reported in the literature to the best of the authors' knowledge. The current study is focused on providing sufficient experimental data for the design of a partially filled rotary evaporator for nuclear liquid waste management applications. The present study focuses on the following aspects:

- Variation in liquid pool height in an inclined partially filled stationary pipe
- Effect of pipe inclination on the variation of local temperature and heat transfer coefficient
- Influence of the angle of inclination in combination with various input parameters *i.e.*, wall heat flux, flow rate and rotation rate, on the heat transfer coefficient
- Correlation to predict average Nusselt number in an inclined partially filled rotating heated pipe

5.2 Experimental setup and procedure

The detailed description of the experimental setup as shown in Fig. 5.1 is presented in Section 4.2. The inclination angle (the angle subtended by the pipe with the horizontal plane) of the setup can be varied between 0°- 6° downward using the screw jack assembly at the inlet side as shown in Fig. 5.1.

The volumetric flow rate of water, pipe rotation rate and inclination angle is set initially. The rotation rate is set to a minimum rotational speed at which the local azimuthal temperature variation at any point along the length of the test section is negligible [Krivosheev *et al.* (1979)]. A specific wall heat flux is applied to the rotating partially filled test section. The system is allowed to come to steady state by waiting for 5 minutes after the input parameters are altered. At steady state, 30 infrared images of the rotating test section are captured with a three second interval. The images are averaged to mitigate signal noise. The azimuthal temperature along the length of the test section is checked. Upon confirmation of uniform temperature distribution circumferentially at any length on the test section, the central line outer wall temperature along the length of the inclined rotating pipe is processed further for analysis.

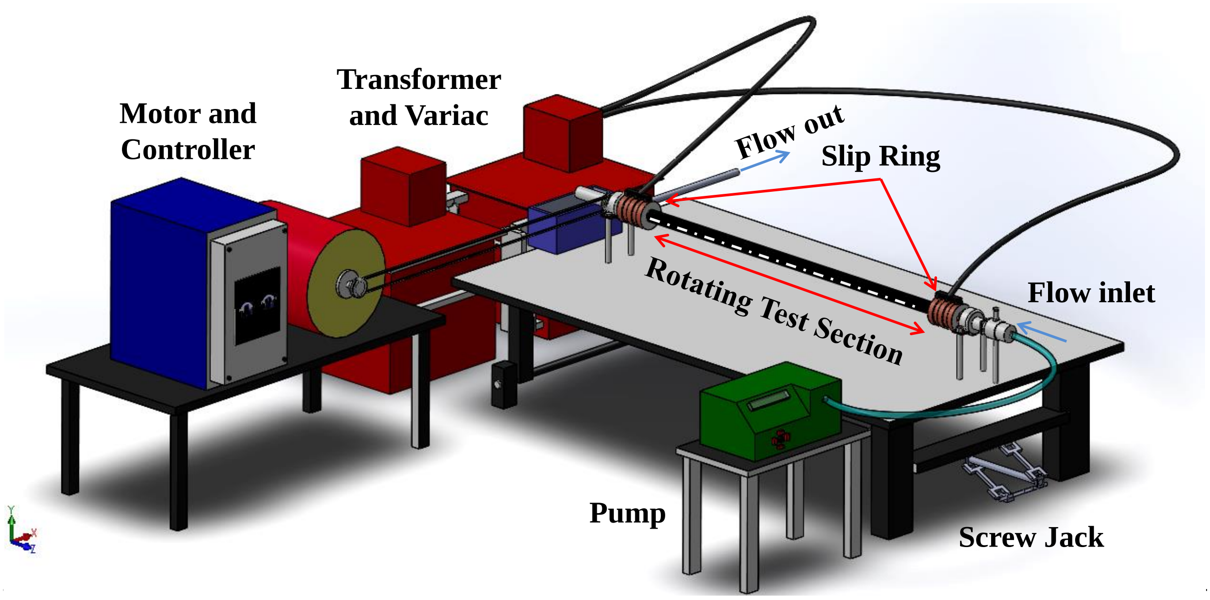

Fig. 5.1 Schematic of the experimental setup

Figure 5.2(A) illustrates the 16 circumferential locations at a particular axial location of the rotating partially filled test section where the temperature is captured using the infrared camera. A typical circumferential wall temperature distribution at different lengths of the test section is shown in Fig. 5.2(B). The water flow rate is set at 100 ml/min (6 LPH), rotation rate and wall heat flux is maintained constant at 13 RPM and 1223 W/m^2 respectively and the test section is inclined at an angle of 3°. As shown in Fig. 5.2(B), the wall temperature variation along the circumference is negligible. Hence the central line temperature along the length of the rotating test should sufficiently represent the system temperature profile as a whole. The central line is indicated as a dotted white line on the rotating test section schematic as shown in Fig.5.1 and corresponds to location 9 in Fig. 5.2(A).

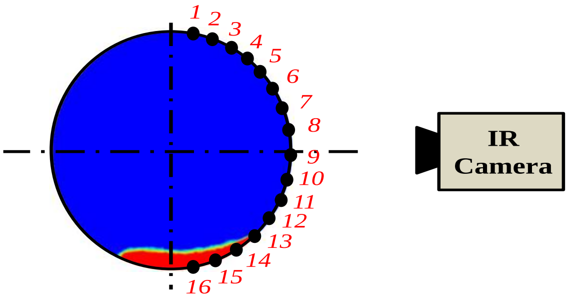

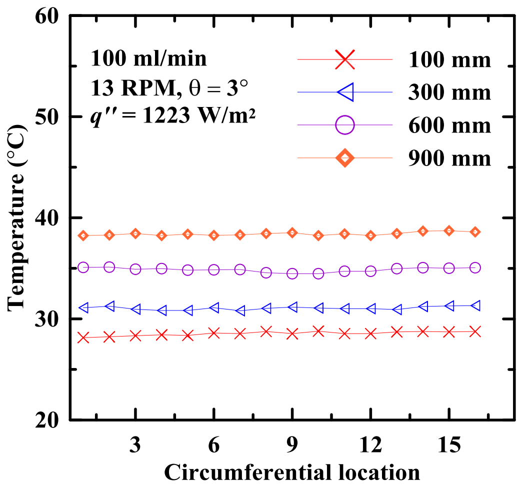

(A) Indication of local points for wall temperature measurement

(B) Circumferential temperature variation at different test section lengths

Fig. 5.2 Wall temperature variation along the circumference of a partially filled rotating heated pipe

One dimensional conduction equation is used to compute the inner wall temperature using the averaged external wall temperature data along the length of the inclined rotating pipe [Incropera (2006)]. Sample calculation is explained in Appendix C.2. The outlet water volume flow rate is measured to ensure that there is no evaporation loss and the maximum outlet water temperature is limited to approximately 70°C. Once the experimental data at a constant volumetric flow rate, inclination and wall heat flux are recorded at a particular rotation rate, the rotation rate is increased in steps. Further different sets of experiments are conducted to individually study the influence of inclination angle (3° and 6°), volumetric flow rate (100-830 ml/min) (6 – 50 LPH), wall heat flux (1405-10784 W/m^2) and rotation rate (10-300 RPM) on the heat transfer coefficient.

5.3 Data Reduction

Dimensionless numbers derived using Buckingham Pi theorem from the parameters governing the problem is used to analyse the data as listed in Section 4.3. The derivation of the same is shown in Appendix C.3. The dimensionless number which accounts for the effect of pipe inclination is described below.

5.3.1 Flow Froude number

Flow Froude number is defined as the ratio of flow inertia to the gravity force, as given in Eqn. (5.1)

$$Fr = \frac{16\dot{Q}^2}{\pi^2 g \sin\theta \, D^5} \tag{5.1}$$

where, $\dot{Q}$ is the fluid volume flow rate, D is the inner diameter of the test section, $g \sin\theta$ is the gravitational acceleration force acting on the fluid body in an inclined partially filled pipe. θ is the inclination angle of the test section.

The uncertainty of different parameters used in the experimental measurement is shown in Table 5.2. The uncertainty is calculated using multivariate propagation of error formula [Navidi (2008)]. Sample calculation methodology to compute the uncertainty in flow Reynolds number and heat transfer coefficient is described in Appendix B.3.

Table 5.1 Range of the experimental parameters covered in the present study

Flow rate (ml/min)	θ (deg)	V (m/s)	T_b (°C)	q'' (W/m^2)	RPM	$Re_f = \frac{4\dot{Q}\rho}{\pi\mu D}$	$Re_\phi = \frac{\rho\omega D^2}{\mu}$	$Fr = \frac{16\dot{Q}^2}{\pi^2 g \sin\theta\, D^5}$	$\gamma = \frac{\pi q'' D^2}{4\dot{Q}\rho C_p T_{in}}$
200	0	0.05	36.18	1880	60	173	9659	-	3.92×10^{-3}
100	3	0.198	35.91	1405	13 - 307	86	2015 - 46545	1.67×10^{-4}	6.73×10^{-3}
200	3	0.294	35.24	2436	11 - 307	171	1683 - 45689	8.41×10^{-4}	5.67×10^{-3}
400	3	0.437	34.91	5348	11 - 304	340	1613 - 45415	3.37×10^{-3}	6.52×10^{-3}
600	3	0.555	35.65	7247	12 - 310	516	1864 - 46913	7.57×10^{-3}	5.52×10^{-3}
200	3	0.305	40.89	2378 - 5777	30	183	4753	8.41×10^{-3}	$5.74 – 14.05 \times 10^{-3}$
200	3	0.308	43.09	2748 - 6209	100	187	16212	8.41×10^{-3}	$6.37 – 14.44 \times 10^{-3}$
200	3	0.308	42.94	2652 - 5821	200	187	32476	8.41×10^{-3}	$5.87 – 12.95 \times 10^{-3}$
200	3	0.309	43.66	2522 - 5981	300	188	49020	8.41×10^{-3}	$5.49 - 13.1 \times 10^{-3}$
830	3	0.644	29.65	2831 - 10114	30	649	4098	1.45×10^{-2}	$1.7 – 6.09 \times 10^{-3}$
830	3	0.649	30.67	2965 - 10784	100	660	13892	1.45×10^{-2}	$1.75 – 6.37 \times 10^{-3}$
830	3	0.655	32.05	3233 - 10509	200	675	28431	1.45×10^{-2}	$1.75 – 5.98 \times 10^{-3}$
830	3	0.656	32.21	3237 - 10239	300	677	42768	1.45×10^{-2}	$1.8 – 5.72 \times 10^{-3}$
200	3	0.309	45.29	5865	34 - 305	192	5589 - 50615	8.41×10^{-3}	15.3×10^{-3}
400	3	0.432	33.17	5257	30 - 308	331	4344 - 44600	3.37×10^{-3}	6.83×10^{-3}
600	3	0.533	29.65	5434	34 - 301	469	4608 - 41225	7.57×10^{-3}	4.8×10^{-3}
100	6	0.249	36.46	1155	13 - 304	87	2051 - 46635	7.57×10^{-3}	5.11×10^{-3}
200	6	0.367	35.26	2055	18 - 311	171	2668 - 46879	4.96×10^{-4}	4.53×10^{-3}
400	6	0.554	37.18	4812	18 - 300	351	2734 - 46282	1.98×10^{-3}	5.19×10^{-3}
600	6	0.69	35.06	6197	12 - 300	511	1784 - 44879	4.46×10^{-3}	4.6×10^{-3}
200	6	0.358	42.63	1320 - 5007	30	186	4873	4.96×10^{-4}	$2.59 – 9.89 \times 10^{-3}$
200	6	0.392	43.54	1789 - 5402	100	188	16374	4.96×10^{-4}	$3.58 – 10.91 \times 10^{-3}$

Table 5.1 Range of the experimental parameters covered in the present study (cont.)

Flow rate (ml/min)	θ (deg)	V (m/s)	T_b (°C)	q'' (W/m^2)	RPM	$Re_f = \frac{4\dot{Q}\rho}{\pi\mu D}$	$Re_\phi = \frac{\rho\omega D^2}{\mu}$	$Fr = \frac{16\dot{Q}^2}{\pi^2 g \sin\theta\, D^5}$	$\gamma = \frac{\pi q'' D^2}{4\dot{Q}\rho C_p T_{in}}$
200	6	0.391	42.76	1607 - 5420	200	186	32482	4.96×10^{-4}	$3.26 – 11.46 \times 10^{-3}$
200	6	0.391	43.21	1740 - 5253	300	187	48976	4.96×10^{-4}	$3.53 – 10.67 \times 10^{-3}$
830	6	0.828	34.10	2356 - 8011	38	697	5588	8.55×10^{-3}	$1.15 – 3.91 \times 10^{-3}$
830	6	0.829	34.14	2490 - 8011	100	697	14713	8.55×10^{-3}	$1.21 – 3.91 \times 10^{-3}$
830	6	0.828	33.99	2558 - 8482	217	696	31849	8.55×10^{-3}	$1.26 – 4.16 \times 10^{-3}$
830	6	0.826	33.66	2423 - 7271	308	692	44994	8.55×10^{-3}	$1.2 – 3.6 \times 10^{-3}$
200	6	0.388	46.44	5200	30 - 300	194	5016 - 50587	4.96×10^{-4}	11.77×10^{-3}
400	6	0.553	37	5364	30 - 300	350	4601 - 46154	1.97×10^{-3}	6.05×10^{-3}
600	6	0.685	33.75	5232	30 - 300	501	4372 - 44191	4.46×10^{-3}	3.89×10^{-3}

Table 5.2 Experimental uncertainties

Parameter	Absolute uncertainty		
	Average	Maximum	Minimum
Time (s)	1	1	1
Flow rate (kg/s)	2.50×10^{-05}	2.50×10^{-05}	2.50×10^{-05}
Length (m)	2.00×10^{-05}	2.00×10^{-05}	2.00×10^{-05}
Inclination angle (degree)	0.5	0.5	0.5
Pool height (m)	1.90×10^{-04}	1.95×10^{-04}	1.51×10^{-04}
Rotation rate (RPM)	0.25	2.5 (≥500RPM)	0.25
Temperature (°C)	0.5	0.5	0.5
Wall heat flux (W/m^2)	137.47	282.73	33.86
Heat transfer coefficient (W/m^{2}K)	29.56	24.82	30.92
Flow Reynolds number	1.31	1.50	1.17
Flow Froude number	2.03×10^{-05}	3.99×10^{-05}	6.34×10^{-06}
Rotational Reynolds number	46.87	68.54	37.77
Dimensionless heat flux	1.84×10^{-05}	8.46×10^{-05}	9.22×10^{-06}
Nusselt number	1.54	1.61	1.3

5.4 Results and discussion

Experiments are performed to study the effect of pipe inclination on the single-phase heat transfer in an axially rotating, partially filled pipe with continuous in and outflow of liquid. The wall heat flux, fluid volume flow rate, pipe inclination angle and pipe rotation rate are varied to investigate the effect on the local heat transfer. Section 5.4.1 discusses the effect of inclination angle on the liquid pool height inside a partially filled stationary pipe. Section 5.4.2 and section 5.4.3, respectively, discuss the effect of inclination angle and heat flux variation on the local heat transfer coefficient. Effect of volume flow rate and rotation rate on the heat transfer coefficient is presented in Sections 5.4.4 and 5.4.5 respectively. Section 5.4.6 gives average Nusselt number distribution. Section 5.4.7 presents a correlation for average Nusselt number as a function of dimensionless flow rate, rotation Reynolds number, flow Froude number and dimensionless heat flux.

5.4.1 Effect of inclination on the liquid pool height in a partially filled stationary pipe

The height of the liquid pool in a partially filled stationary circular duct is experimentally investigated. The pool height measured at ambient condition for various volumetric flow rates and pipe inclination angle is tabulated in Table 5.3. The liquid pool height is calculated by experimentally measuring the liquid holdup inside the stationary pipe at a specific set of experimental condition i.e. liquid volume flow rate and pipe inclination angle using catch and time technique. An assumption of uniform pool height along the length of the pipe is made while calculating the pool height. The inlet flow is disconnected and the liquid inside the partially filled test section is collected at the exit using a measuring cylinder with a least count of 1 ml.

Table 5.3 Experimental pool height in a stationary pipe of ID 32.8 mm

Flow rate (ml/min)	Inclination angle	Pool height (mm) (*H*) 0°	3°	6°
100		3.89	1.28	1.10
200		4.30	1.55	1.22
400		5.12	1.90	1.67
600		5.94	2.28	2.00
830		6.88	2.64	2.32

The effect of inclination angle on the average liquid pool height inside a 32.8 mm ID stationary circular duct is shown in Fig. 5.3.

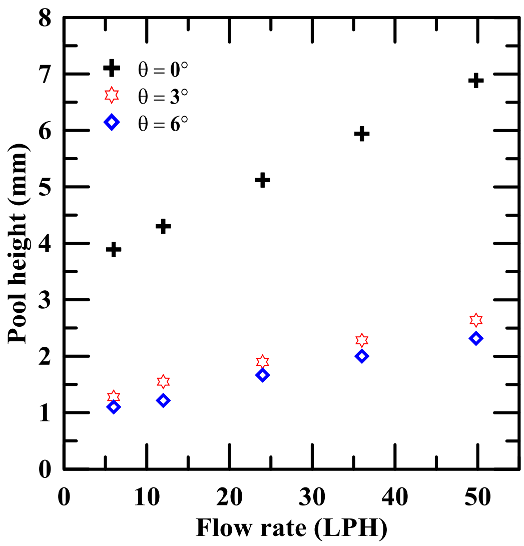

Fig. 5.3 Effect of inclination angle on average pool height for a 35 mm OD partially filled stationary circular duct

With the increase in the volumetric flow rate, the liquid hold up increases leading to an increase in average pool height. As the inclination angle is increased, the axial velocity of the flow increases due to an increase in the axial gravitational component on the fluid element. Increased flow velocity reduces the liquid residence time inside the partially filled pipe. The reduction in pool height with increasing inclination angle is visualised using a Plexiglas tube with 32.8 mm internal diameter as shown in Fig. 5.4. The liquid volume flow rate is maintained at 830 ml/min (50 LPH) while the inclination is varied from 0° to 6°. Figure 5.4 shows a clear reduction in the liquid pool height. The flow pattern in the inclined pipe is comparatively wavy. Lower liquid hold up leads to a lower mean liquid pool height inside the pipe. As shown in Fig. 5.3, a change in the inclination angle from horizontal to 3° leads to 63% reduction in average pool height. When the inclination angle is increased from 3° to 6°, the pool height reduction is 14%. Thus, Fig. 5.3 highlights the influence of pipe inclination on the pool height with increasing inclination angle.

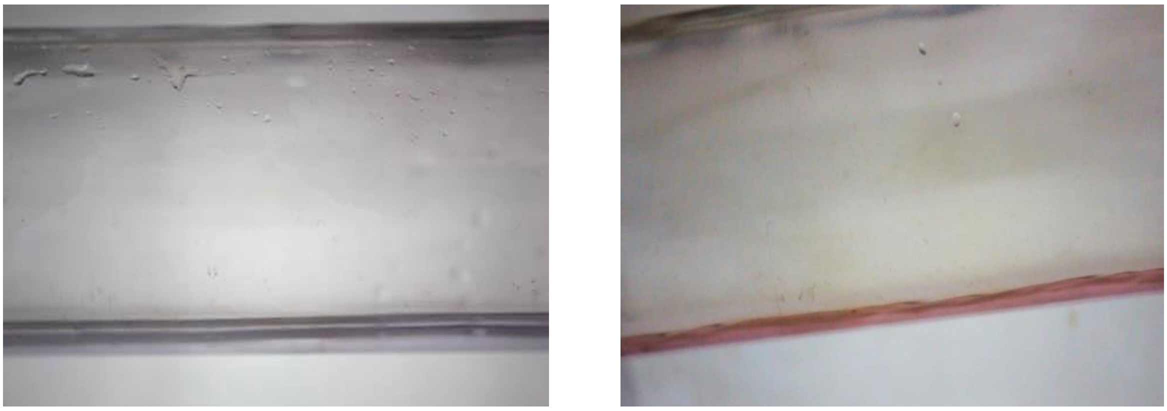

(A) 830 ml/min, 0 RPM, θ = 0° (B) 830 ml/min, 0 RPM, θ = 6°

Fig. 5.4 Effect of inclination on the liquid pool height in a partially filled stationary pipe with constant flow rate of 830 ml/min (50 LPH, Re_f = 650). (Flow direction is from right to left)

5.4.2 Effect of pipe inclination on local heat transfer coefficient

The pipe rotation rate, wall heat flux and the liquid volume flow rate through the rotating pipe are kept constant and the pipe inclination angle is gradually increased to study its effect on the variation of local heat transfer coefficient. The local wall and bulk water temperature profiles along the length of the partially filled rotating heated pipe are shown in Fig. 5.5. Based on the temperature profiles, the system can be defined as thermally fully developed.

The variation of the respective local heat transfer coefficient along the length of the test section corresponding to the local temperature profiles shown in Figs. 5.5(A)-(C) is presented in Fig. 5.6(A) as a function of pipe inclination angle at constant liquid flow rate, wall heat flux and pipe rotation rate. The variations of the local heat transfer coefficient along the length of the test section corresponding to the local temperature profiles shown in Figs. 5.5(D) and 5.5(E) are presented in Fig. 5.6(B) as a function of pipe inclination angle at constant liquid flow rate, wall heat flux and pipe rotation rate. As the local wall and bulk temperature difference reduces, the local heat transfer coefficient increases for a given wall heat flux input. Based on the experimental observations, it may be concluded that with increase in inclination angle, the overall heat transfer coefficient decreases. As shown Fig. 5.3, the liquid pool height in a partially filled stationary pipe decreases with the inclination angle. In a rotating pipe, as the pool height decreases it leads to reduction in the pool mixing and thereby, reduction in convective heat transfer.

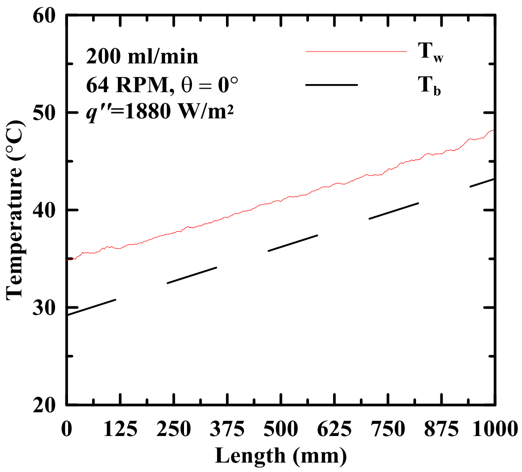

(A) $q'' = 1880$ W/m^2, $\theta = 0°$

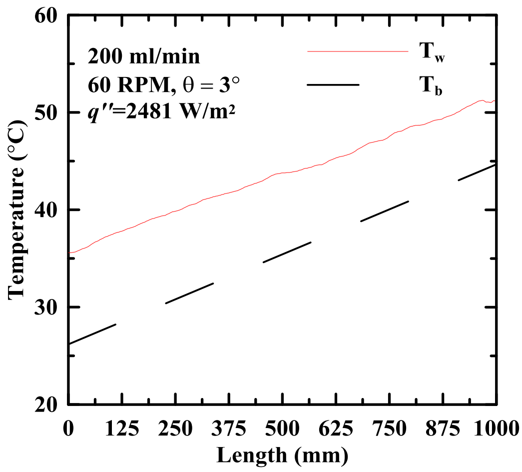

(B) $q'' = 2481$ W/m^2, $\theta = 3°$

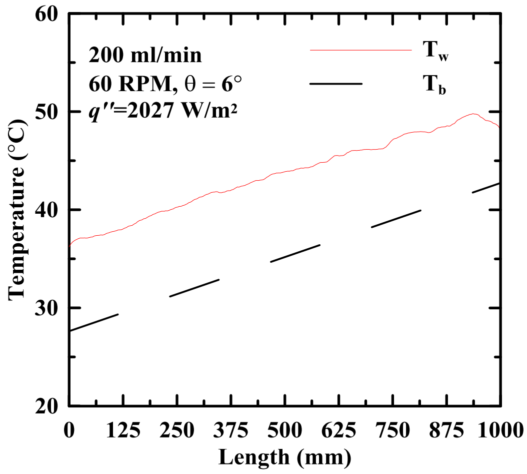

(C) $q'' = 2027$ W/m^2, $\theta = 6°$

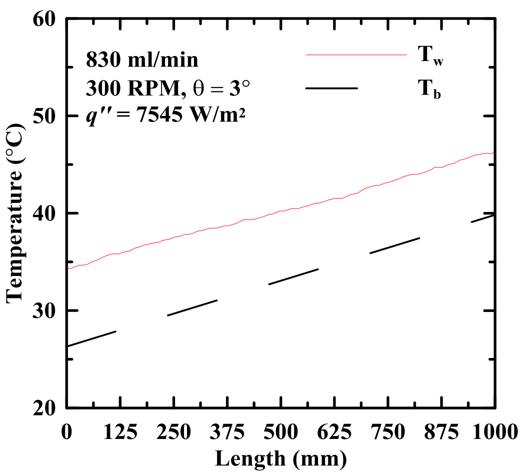

(D) $q'' = 7545$ W/m^2, $\theta = 3°$

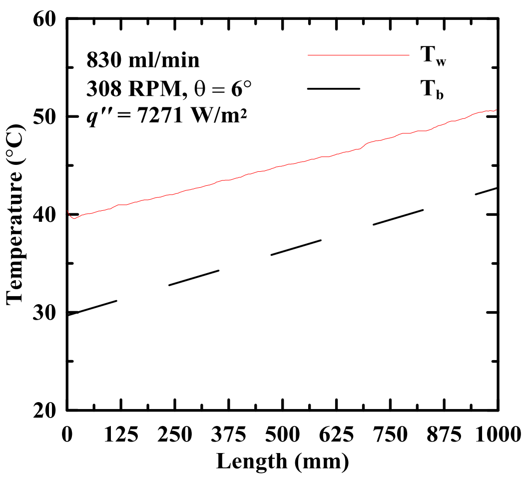

(E) $q'' = 7271$ W/m^2, $\theta = 6°$

Fig. 5.5 Effect of inclination angle on local wall temperature (T_W) and bulk temperature (T_b)

The results suggest that better heat transfer coefficient is achieved in a horizontal partially filled rotating heated pipe. The following sections discuss the effect of various parameters on inclined systems. Various experimental results highlighting the effect of pipe inclination on single phase heat transfer in a partially filled rotating pipe are shown in Appendix D, Figs. D.8 (A)-(F).

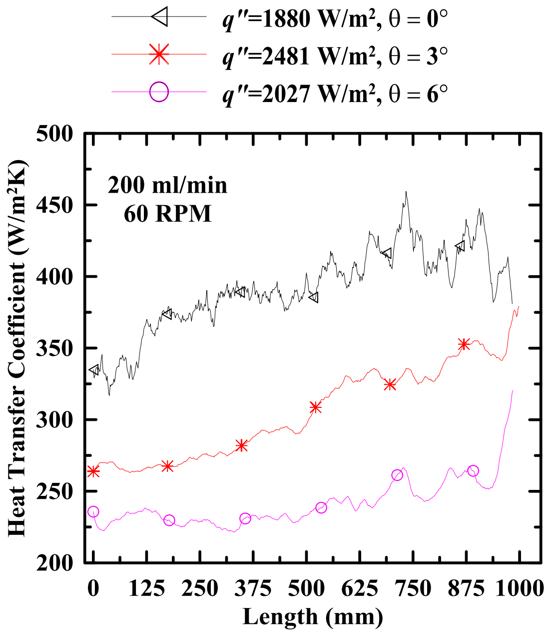

(A) 12 LPH, 60 RPM
($Re_f = 172, Re_\phi \sim 9659$)

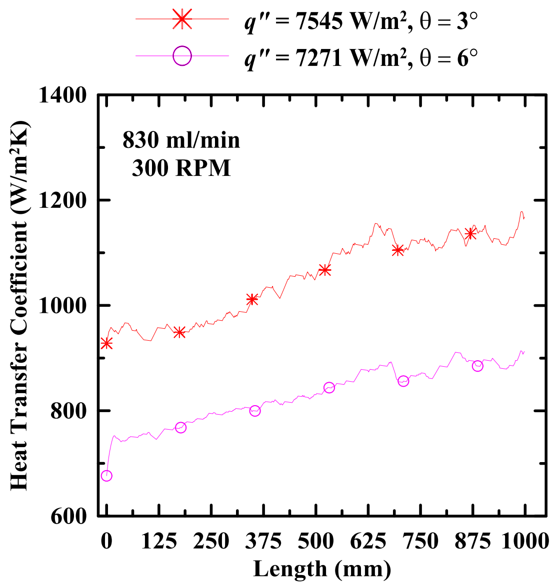

(B) 50 LPH, 300 RPM
($Re_f = 684, Re_\phi \sim 42856$)

Fig. 5.6 Local heat transfer coefficient along the length of the rotating inclined heated pipe

5.4.3 Effect of wall heat flux on the local heat transfer coefficient

Volumetric flow rate and the pipe rotation rate are kept constant and the wall heat flux is gradually increased to study the effect of uniform wall heat flux on the local heat transfer coefficient. Figure 5.7 shows the variation in local heat transfer coefficient along the length of the inclined rotating pipe as the wall heat flux is varied.

Kuo *et al*. (1960) reported constant average heat transfer coefficient in a horizontal partially filled rotating heated pipe where the liquid volume flow rate and rotation rate are kept constant while the wall heat flux is varied. However, in the present study, the local heat transfer coefficient increases with the increasing wall heat flux as shown in Fig. 5.7(A) and 5.7(B). This suggests that the heat transfer coefficient is dependent on the heat flux in a partially filled rotating resistance heated pipe. With increasing wall heat flux, the local air core temperature increases. The air gets heated by the rotating wall similar to the water in the pool. The hot air transfers heat to the liquid pool through the air-water free surface. The same is described in chapter 4, section 4.4.1. This phenomenon is expected to be the main factor which influences heat transfer coefficient as the wall heat flux is increased. As discussed in the previous section, it can be observed that increasing inclination angle leads to a decrease in heat transfer coefficient as shown in Fig. 5.7.

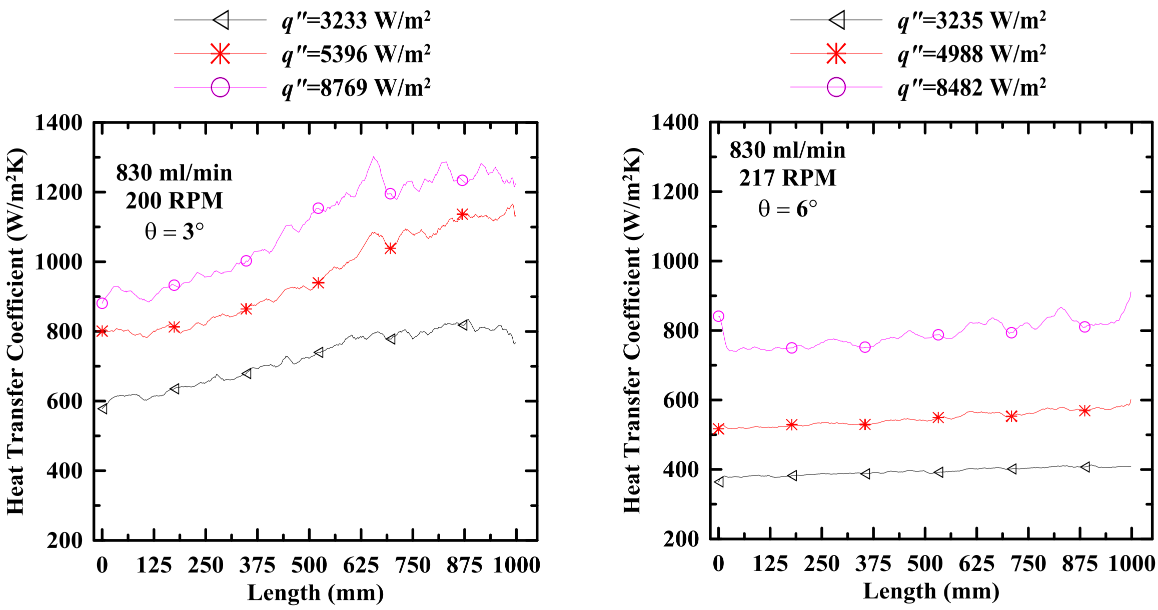

(A) 200 RPM, θ=3° (B) 217 RPM, θ = 6°

Fig. 5.7 Local heat transfer coefficient along the length of the inclined rotating heated pipe with constant flow rate of 830 ml/min (50 LPH, Re_f = 680) and rotation rate (~200 RPM, Re_ϕ~ 32482) and variable wall heat flux

Similar effect is not reported by Kuo *et al.* (1960) as the experiments were conducted using a relatively larger i.e. 650 mm long, outer diameter of 76.2 mm and wall thickness of 6.35 mm pipe with significantly greater flow rates (13.24-242.09 LPH). Various experimental results highlighting the effect of heat flux on single phase heat transfer in a partially filled rotating pipe are shown in Appendix D, Figs. D.9 (A)-(F).

5.4.4 Effect of volumetric flow rate variation on local heat transfer coefficient

In this study, the wall heat flux and rotation rate are kept constant, while the volume flow rate is increased. Fig. 5.8 shows the local heat transfer coefficient along the length of the partially filled inclined rotating heated pipe. Both at 3° and 6° inclination angle, volume flow rate has a positive influence on the heat transfer rate as shown in Fig. 5.8. Figure 5.8(A) represents the effect of flow rate for a 3° inclined system, while Fig. 5.8(B) represents the same for a 6° inclined system. In both the cases the wall heat flux and the rotation rate are kept constant independently for different volume flow rates 200 (12 LPH) and 600 ml/min (36 LPH). The improvement in the local heat transfer coefficient along the length of the partially filled rotating heated pipe with increase in the volumetric flow rate is evident regardless of the inclination angle as shown in Figs. 5.8(A) and 5.8(B).

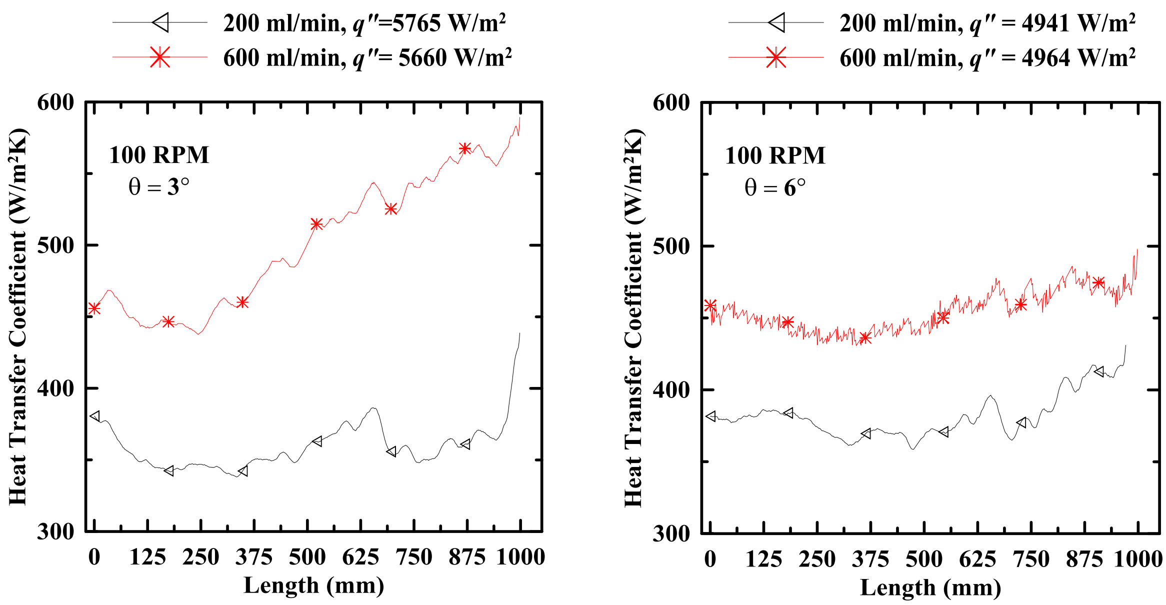

(A) 100 RPM, θ = 3° (B) 100 RPM, θ = 6°

Fig. 5.8 Local heat transfer coefficient for different liquid flow rates

Pool height directly influences the recirculating region inside the liquid pool [Haji-Sheikh *et al.* (1984)]. As discussed in the earlier section, the pool height is a function of inlet volumetric flow rate, pipe dimension and inclination. Similar improvement in heat transfer coefficient with increasing liquid flow rate in a horizontal partially filled heated rotating pipe is reported by Kuo *et al.* (1960) and discussed in chapter 4, section 4.4.2. The effect of liquid volume flow rate on single phase heat transfer in a partially filled inclined rotating pipe is shown in Appendix D, Figs. D.10 (A)-(D).

5.4.5 Effect of pipe rotation rate on local heat transfer coefficient

The volume flow rate through the rotating test section is maintained constant at a particular inclination angle and wall heat flux. The rotation rate of the test section is varied stepwise between 10-300 RPM. Figure 5.9 illustrates shows the cross sectional view of the liquid flow pattern inside a partially filled rotating pipe for different rotation rates.

In a partially filled pipe as the rotation rate is varied, the flow pattern changes as depicted in Fig. 5.9 and Fig. 5.10. At lower rotation rates (10-60 RPM), pool flow regime prevails where a liquid pool exists at the bottom of the pipe [Singaram *et al.* (2014), Chapter 3, section 3.4.1].

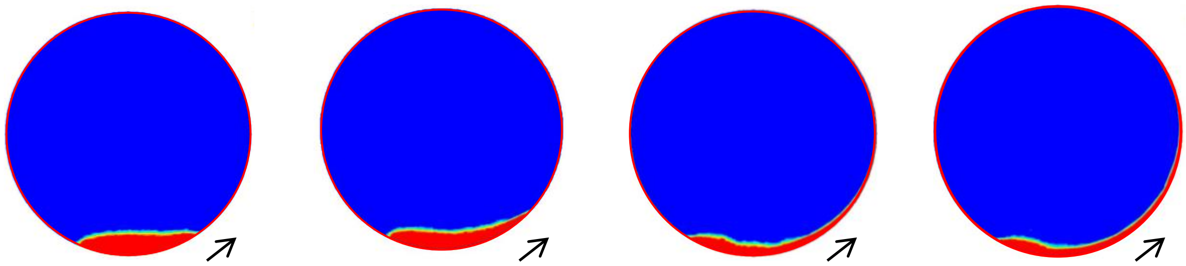

(A) 60 RPM (B) 100 RPM (C) 200 RPM (D) 350 RPM

Fig. 5.9 Cross sectional view of the liquid flow pattern inside a partially filled rotating pipe

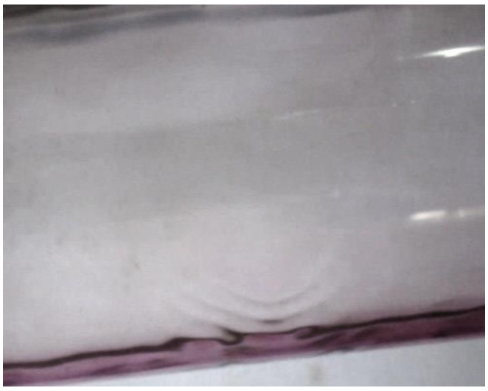

(A) Fluid Pendant (110 RPM) (B**)** Smooth Tooth (250 RPM)

(C) Shark Tooth (295 RPM) (D) Rimming Flow (350 RPM)

Fig. 5.10 Different liquid flow patterns in a partially filled rotating inclined pipe
32.8 mm ID, 24 LPH (Re_f = 340), θ = 3°

Figures 5.10(A)-(C) show that with increasing rotation rate (100-300 RPM) the flow pattern varies from pendant to shark tooth [Phillips (1960), Karweit (1975), Moffat (1977), Thoroddsen and Mahadevan (1997), Chicharro *et al.* (2011), Singaram *et al.* (2014), Chapter 3, section 3.4.1]. Figure 5.9(D) and Fig. 5.10(D) shows the rimming flow inside a partially filled rotating pipe. Change in the flow pattern influences the mixing rates and the heat transfer coefficient. Various flow patterns are tabulated in Appendix D, Figs. D.1-D.4.

With increasing rotation rate, the local heat transfer coefficient along the length of the partially filled rotating heated pipe is plotted in Figs. 5.11(A) and (B). As the rotation rate increases, the heat transfer coefficient improves. The effect of pipe rotation on single phase heat transfer in a partially filled inclined rotating pipe is shown in Appendix D, Figs. D.11 (A)-(F).

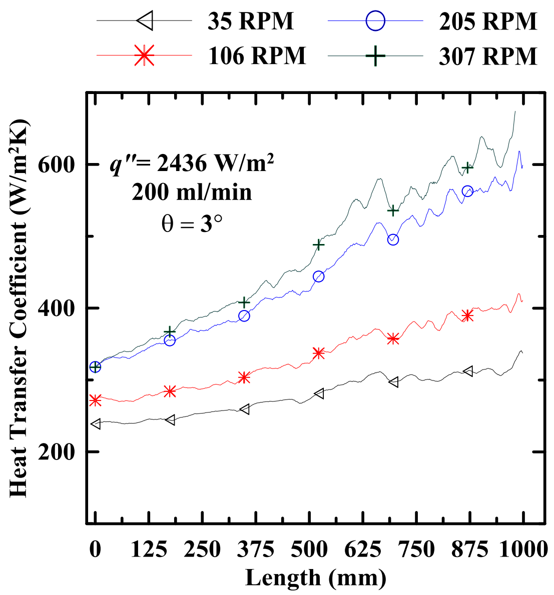

(A) 12 LPH, θ=3°, q''=2440 W/m^2
(Re_f = 171)

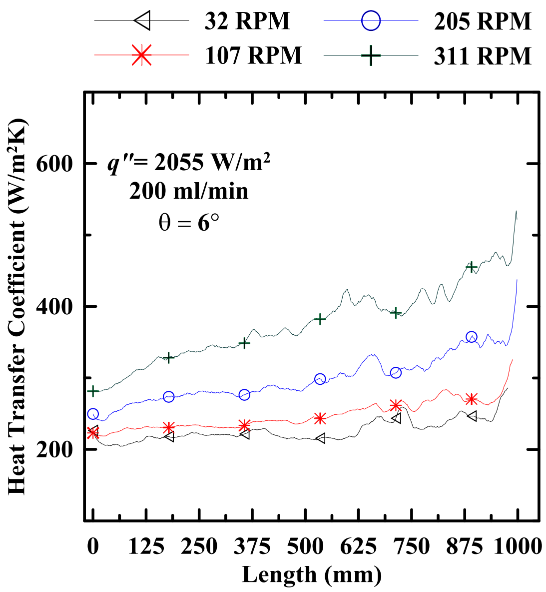

(B) 12 LPH, θ = 6°, q''=2055 W/m^2
(Re_f = 170)

Fig. 5.11 Effect of rotation rate on local heat transfer coefficient for a partially filled inclined rotating heated pipe (12 LPH, heat flux ~ 2200 W/m^2)

5.4.6 Average Nusselt number

Variation of average Nusselt number for various dimensionless heat fluxes, flow Reynolds number and rotation Reynolds numbers is shown in Fig. 5.12. For a given angle of inclination and non-dimensional heat flux, the average Nusselt number increases with rotation Reynolds number except for low flow Reynolds number ($Re_f < 100$). This is because of the relatively small liquid pool height corresponding to low flow Reynolds numbers. Reduced pool height limits the convective heat transfer potential inside the liquid pool of the partially filled inclined rotating heated pipe.

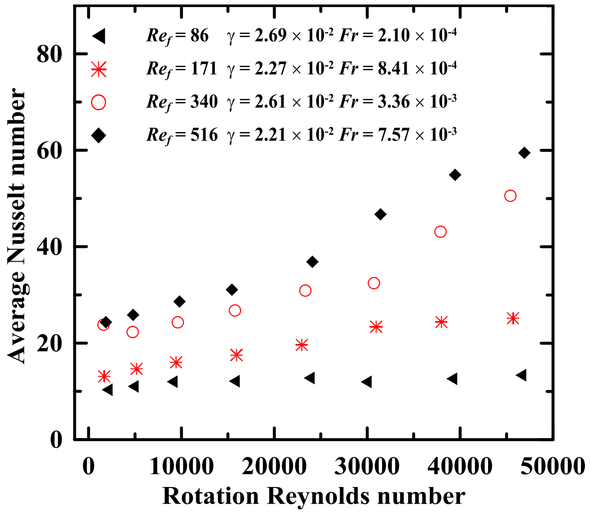

(A) θ= 3°

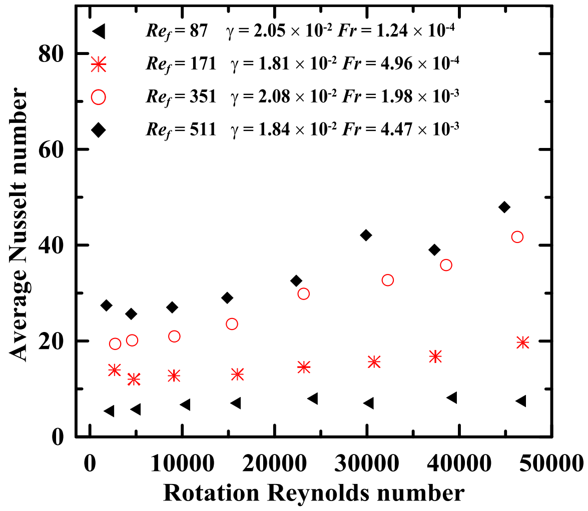

(B) θ = 6°

Fig. 5.12 Average Nusselt number variation

As the flow Reynolds number increases a significant amount of liquid remains in the pool even at higher rotation Reynolds numbers. The fluid agitating inside the liquid pool of the partially filled rotating pipe improves Nusselt number. For a given flow Reynolds number, the flow Froude number decreases as the inclination angle of the test section increases. With increasing inclination angle, the flow velocity increases due to the additional gravitational forces acting on the fluid body. This leads to a decrease in liquid pool height. The decrease in pool height adversely affects the Nusselt number as shown in Figs. 5.12(A) and 5.12(B). However, at a particular inclination angle as the liquid volume flow rate ($\dot{Q}$) increases, both the flow Reynolds number and Froude number increase as shown exclusively in Fig. 5.11. Thus, improvement in flow Reynolds number and Froude number is expected to enhance the heat transfer as it gives raise to thicker liquid pool flow inside the pipe. As the rotation Reynolds number increases, the slope of Nusselt number alters due to the variation in fluid flow pattern as shown in Figs. 5.9 and 5.10 [Phillips (1960), Karweit (1975), Moffat (1977), Thoroddsen and Mahadevan (1997), Chicharro *et al.* (2011), Singaram *et al.* (2014)].

5.4.7 Correlation for average Nusselt numbers

Based on the experimental results, a correlation to predict the average Nusselt number in an inclined partially filled rotating heated pipe with thermally fully developed flow is developed based on the flow Froude number and horizontal Nusselt number (Eqn. (4.17)) as given by Eqn.5.2. The correlation predicts within an average deviation is 16% from the experimental data. A total of 153 data points have been used to derive the correlation. A comparison between the present experimental values and the correlation is presented in Fig. (5.13).

$$Nu_{Inclined}/Nu_{horizontal} = 1.05\ Fr^{0.11} \tag{5.2}$$

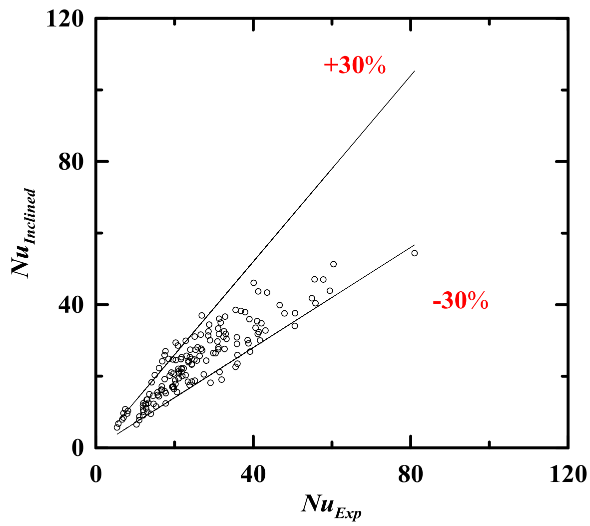

Fig. 5.13 Comparison of correlation with experimental results

The effect of rotational forces and axial flow are captured by the rotational and flow Reynolds numbers. Flow Froude number captures the effect of inclination angle on the axial flow. The effect of wall heat flux on the heat transfer coefficient is captured by dimensionless heat flux. The above correlation is valid for the experimental conditions explored in this study *i.e.*, flow Reynolds number (84.67-730.13), Froude number (1.24×10^{-4}-1.45×10^{-2}), angle of inclination (θ = 3°- 6°), rotation Reynolds number (1613-51615) and dimensionless heat flux (4.61×10^{-3}- 6.39×10^{-2}).

5.5 Conclusions

Experimental investigation of single phase heat transfer characteristics in a partially filled inclined rotating heated pipe with continuous axial liquid flow is reported in this study. Flow rate range of 100-830 ml/min (6 – 50 LPH) and rotation rate range of 10-300 RPM are investigated while the inclination angle is varied from 0°-6°. Wall heat flux (1405-10784 W/m^2) is varied within the bounds of single phase flow operation. Local heat transfer coefficient along the length of a partially filled inclined rotating pipe is reported.

- With increasing inclination angle a decrease in local heat transfer coefficient in a partially filled inclined rotating heated pipe is observed. The liquid volumetric flow rate, rotation rate and wall heat flux are maintained constant. The decrease in the heat transfer coefficient is attributed to the decrease in liquid pool height inside the rotating pipe with increasing inclination angle
- Local heat transfer coefficient improves with increasing wall heat flux at a constant liquid volume flow rate, pipe rotation rate and inclination angle. Secondary heat transfer from the air core to the liquid free surface leads to an enhancement in heat transfer coefficient as the wall heat flux is increased.
- With increasing liquid volume flow rate the heat transfer coefficient improves. The improvement is related to an increase in liquid pool height inside the partially filled rotating pipe. The increase in pool height provides larger mixing volume and enhances heat transfer
- At a constant volume flow rate, wall heat flux and inclination, as the rotation rate is increased, the heat transfer coefficient improves. The improvement is attributed to the

variation in the liquid flow pattern, which enhances mixing and ultimately heat transfer.

- A correlation based on the governing dimensionless numbers is developed to predict the average Nusselt number within 15% average deviation from the experimental values.
- Based on the experimental results, it is recommended to operate partially filled rotating pipe heat transfer equipment in nearly horizontal configuration for maximum heat transfer within the experimental domain of this study.

5.6 Contributions of the present work

The current work reports a comprehensive study of the various phenomena influencing heat transfer process inside a partially filled inclined rotating heated pipe. The influence of pipe inclination on the heat transfer coefficient with variations in input parameters such as wall heat flux, flow and rotation rates are discussed using local and average data sets. Correlation is derived to predict the average Nusselt number at particular wall heat flux, flow and rotation rates at various inclinations investigated in this study. It is recommended to operate partially filled rotating pipe heat transfer equipment in nearly horizontal configuration to achieve maximum heat transfer.

CHAPTER 6

HEAT TRANSFER IN A PARTIALLY FILLED ROTARY EVAPORATOR

6.1 Introduction

Chapters 4 and 5 highlight the effect of liquid volume flow rate, rotation rate, wall heat flux and inclination angle on the single phase heat transfer characteristics of a partially filled rotating heated pipe. Kuo *et al.* (1960) experimentally investigated the effect of fluid flow transition on the heat transfer characteristics in a partially filled horizontal rotating pipe. Pattenden (1964) highlighted the fact that rotation rate has a greater influence on the heat transfer inside a rotating heated pipe. Studies reported in Chapters 4 and 5 demonstrate that increasing fluid flow rate, rotation rate and wall heat flux enhances the heat transfer while increasing inclination angle deteriorates the heat transfer a partially filled horizontal rotating heated pipe.

All the heat transfer studies discussed previously focus on systems where there is no fluid phase transition. Heat transfer involving phase transition in a fully filled pipe is a widely investigated topic. Collier (1981) developed a flow boiling map correlating flow quality and heat transfer coefficient at various wall heat fluxes. The curve identifies four heat transfer regimes *i.e.*, single phase, subcooled, nucleate and convective boiling. Kandlikar (1991) developed a new flow boiling map representing heat transfer coefficient of fluids and variation in slope in the subcooled boiling region. Kandlikar (1991) segregated the subcooled boiling region into three sections as partial subcooled, fully subcooled and net vapour generation. Kandlikar (1998) derived a single correlation for complete range of subcooled boiling regime. Chen (1966), Shah (1976), Gungor and Winterton (1986), Liu and Winterton (1991), Baburajan *et al.* (2013), Yan *et al*. (2015) developed single correlations to predict the heat transfer coefficient profile in the complete subcooled boiling range. Hardik *et al.* (2016) compared the available correlations with experimental results and concluded that the Shah's (1976) correlation for subcooled flow boiling and Kandlikar's (1998) correlation for fully developed subcooled flow boiling heat transfer coefficient matches reasonably well with the experimental results. Sato and Matsumura (1964) analytically developed a model to predict the incipience of nucleation in water flowing through a rectangular duct. The model is compared with experimental data from Bergles and Rohsenow (1964). Davis and Anderson (1966) developed a mechanistic model based on the heated surface cavity radius. The model is compared with the experimental data presented by Bergles and Rohsenow (1964) and the predictions by the model proposed by Sato and Matsumura (1964). It is reported that the simple model proposed by Sato and Matsumura (1964) and Davis and Anderson (1966) can sufficiently predict the incipience of nucleate boiling in forced convection duct flows for simple design purposes. Marsh and Mudawar (1989) further proposed a mechanistic model to predict the inception of nucleate boiling in vertical turbulent falling films. The model includes an empirical multiplier along with the model proposed by Sato and Matsumura (1964) that accounts for the flow turbulence and interfacial waves.

Gray (1969) proposed the concept of rotating heat pipes and experimentally demonstrated the improvement in its heat transfer capacity over conventional heat pipes. Heat pipes are effective heat transfer devices which use evaporation and condensation to transmit heat. One of the most conventional heat pipe configurations is where the heat pipe is circular in shape with or without any axial taper which rotates about its own axis or revolves off-axis and the other one is in the shape of a disk. Krivosheev *et al.* (1979) experimentally studied the effect of pipe rotation on the heat transfer coefficient of heat pipes with and without wicks. The influence of increasing pipe rotation rate on the reduction and dissolution of the azimuthal local wall temperature variation is highlighted. It is reported that with increasing rotation rate, the heat transfer coefficient improves. Lin and Faghri (1999) concluded that the effect of rotation rate on the evaporator region of a heat pipe is negligible. Rotating cylindrical heat pipes are used to cool electrical motors and cutting tools such as drill bits etc. However the heat pipes are generally closed off at its end with a fixed volume of fluid inside them for operation.

Kascheev and Podymova (2012) developed a numerical model to evaluate the performance of a rotary calciner. The calciner consists of three stages namely sensible heating zone, evaporation zone and calcination zone respectively. The model can estimate the product temperature, residence time and length of the different heating zones of a rotating calciner with 3° inclination angle and rotation rates of 3 RPM at various feed rates. A small inclination in incorporated in rotary evaporator design to ensure unidirectional flow of fluids and solids under the influence of gravity. Petitjean *et al.* (2006) reported an improvement in waste treatment processing operation using a rotating inclined pipe. The rotation rate is maintained between 20 - 30 RPM with liquid volume flow rates up to 90 litres per hour.

Though a large literature database is available for multiphase heat transfer in a fully filled pipe, very limited study is reported on heat transfer with phase transition inside a partially filled rotating pipe with continuous inflow and outflow of liquid. The influence of rotation rate, heat flux, pipe inclination angle and fluid flow rate on heat transfer in a partially filled rotating heated pipe and its application as a rotary evaporator for liquid waste management is prospective areas of practical interest. The effect of rotation rate, heat flux, pipe inclination angle and fluid flow rate on the local variation in temperature and heat transfer coefficient in a partially filled rotating evaporator has not yet been reported in the literature to the best of the authors' knowledge. Experiments are performed to study the effect of liquid volume flow rate, rotation rate, inclination angle and heat flux on the subcooled boiling heat transfer characteristics of a partially filled rotating evaporator. The present study focuses on the following aspects:

- Local temperature variation along the longitudinal axis of a rotating heated pipe
- Effect of parameters namely heat flux, liquid volume flow rate, rotation rate and inclination angle on the temperature profile and heat transfer coefficient

The current study is focused on providing sufficient experimental data for the design of a partially filled rotary evaporator. This study highlights the various influencing parameters which define the heat transfer characteristics of a partially filled rotating evaporator.

6.2 Experimental setup and procedure

The detailed description of the experimental setup as shown in Fig. 6.1 is presented in Section 4.2. The table inclination can be varied between 0° - 6° using a screw jack assembly on the inlet side. The saturation temperature of water at atmospheric conditions is experimentally measured at 99.9 °C in a pool boiling setup.

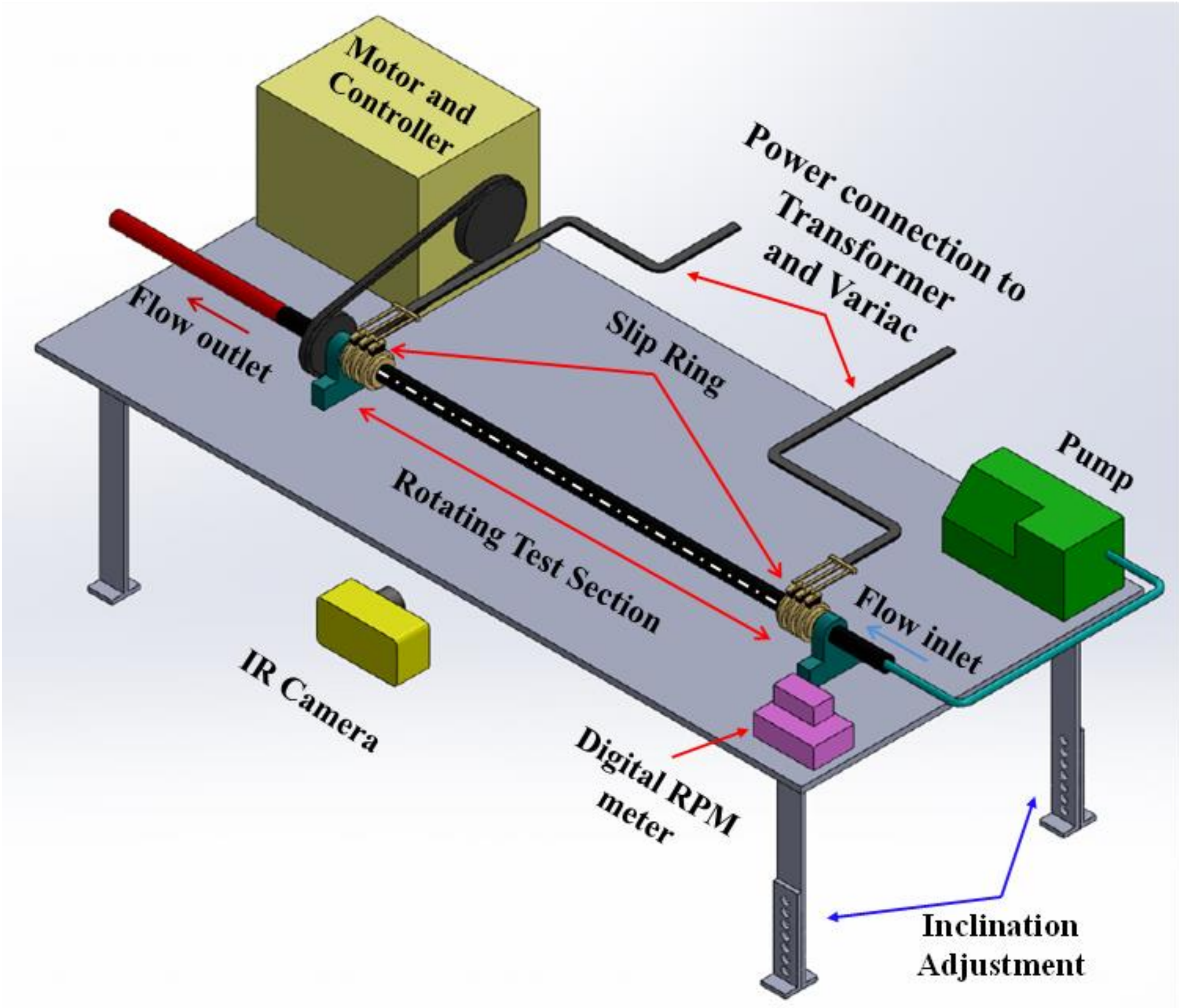

Fig. 6.1 Experimental setup

Water volume flow rate is adjusted to a set value for a given rotation rate and angle of inclination of the test section. The wall heat flux is fixed at a constant value. The rotation rate is set to a minimum rotational speed at which the local azimuthal temperature variation at any point along the length of the test section is negligible [Krivosheev *et al.* (1979)]. The system is allowed to come to steady state by waiting for 5 minutes. At steady state, 30 thermal images are captured of the rotating test section with 3 second interval. To moderate any signal noise, the images are averaged and a single averaged wall temperature image is used for heat transfer calculation. The wall temperature variation azimuthally along the length of the pipe is checked. As the azimuthal outer wall temperature variation at any particular location throughout the length of the test section is negligible, the centre line wall temperature along the length of the test section is used for further analysis (centre line is marked in the side view of the experimental setup as shown in Fig. 6.1). The inner wall temperature is computed from the wall heat flux and the outer wall temperature using one dimensional conduction equation [Incropera (2006)]. Sample calculation is explained in Appendix C.2.

The experimental results are computed based on the following assumptions:

- The wall heat flux is distributed uniformly
- The bulk fluid temperature rise is linear as long as the outlet fluid temperature is below saturation temperature

The outlet water flow rate is measured to quantify the evaporation rate ($\dot{m}_{loss}$). Once the experimental data at a constant flow rate, inclination and wall heat flux are recorded at a particular rotation rate, the rotation rate is stepwise increased. Further, different sets of experiments are conducted to individually study the influence of inclination angle (0° - 6°), flow rate (100 - 400 ml/min) (6 – 24 LPH), wall heat flux (3348 - 21200 W/m^2) and rotation rate (10 – 300 RPM) on heat transfer characteristics of the rotary evaporator.

6.3 Data Reduction

Dimensionless numbers derived using Buckingham Pi theorem from the parameters governing the problem is used to analyse the data as listed in Section 4.3. The derivation of the same is shown in Appendix C.3.

6.3.1 Local heat transfer coefficient

For an externally heated pipe the wall heat flux is defined as given by Eqn. (6.1)

$$q" = \frac{\dot{m}C_p(T_{out} - T_{in}) + \dot{m}_{loss}\lambda}{A_{surface}} \tag{6.1}$$

$$A_{surface} = \pi DL \tag{6.2}$$

$$T_b = \frac{T_{out} + T_{in}}{2} \tag{6.3}$$

where, C_p is the fluid heat capacity, $\dot{m}$ is the total mass flow rate of the fluid entering the rotary evaporator, $\dot{m}_{loss}$ is the mass of fluid evaporated, λ (2257 kJ/kg) is the latent heat of vaporization of water at atmospheric pressure and $A_{surface}$ is the total heat transfer area of the test section as shown by Eqn. (6.2). T_{in} and T_{out} are the inlet and outlet fluid temperatures respectively. Fluid properties such as heat capacity, density, viscosity is calculated at average fluid bulk temperature. The fluid bulk temperature is calculated as given by Eqn. (6.3). The experimental parameters studied, and their corresponding dimensionless quantities are tabulated in Table 6.1. Considering the outlet bulk fluid temperature is below saturation temperature (99.9 °C), the local bulk temperature $T_{b,local}$ is calculated by linear interpolation between inlet T_{in} and outlet T_{out} liquid temperatures.

The local heat transfer coefficient is given by Eqn. (6.4).

$$h_{local} = \frac{q"}{(T_{w,local} - T_{b,local})} \tag{6.4}$$

where, h_{local} is the apparent convective local heat transfer coefficient, $T_{w,local}$ and $T_{b,local}$ are the local wall temperature and liquid bulk temperature respectively. Apparent heat transfer coefficient is computed based on the assumption that the local bulk fluid temperature linearly increases along the length of the rotating test section. All heat transfer coefficient data reported in this study represent apparent experimental heat transfer coefficients.

6.3.2 Boiling number

Boiling number is defined as the ratio of energy supplied to the energy required in order to convert all the fluid into vapour as given by Eqn. (6.5)

$$Bo = \frac{\pi q" D^2}{4\dot{Q}\rho\lambda} \tag{6.5}$$

where, $\dot{Q}$ is the fluid volume flow rate, D is the inner diameter of the test section and $q"$ is the heat flux transferred to the liquid in the rotating pipe. The latent heat of vaporization (λ) of water is 2257 kJ/kg and the saturation temperature (T_{sat}) of water at atmospheric pressure is 99.9 °C. The uncertainty of different parameters used in the experimental measurement is shown in Table 6.2. The uncertainty is calculated using multivariate propagation of error formula [Navidi (2008)]. Sample calculation methodology to compute the uncertainty in flow Reynolds number and heat transfer coefficient is described in Appendix B.4.

Table 6.1 Range of the experimental parameters covered in the present study

Flow rate (ml/min)	θ (deg)	T_{in} (°C)	T_{out} (°C)	q'' (W/m^2)	Liquid loss (ml/min)	$Re_f = \frac{4\rho\dot{Q}}{\pi\mu D}$	RPM	$Bo = \frac{\pi q'' D^2}{4\dot{Q}\rho\lambda}$
100	0	28.47	85.24	3785	0*	104	15-303	8.64×10^{-4}
100	0	26.78	95.46	8155	10	106	15-302	1.87×10^{-3}
100	0	28.23	97.93	10005	15	106	11-306	2.29×10^{-3}
200	0	30.16	94.25	12111	10	213	16-302	1.39×10^{-3}
200	0	27.75	95.22	10208	4	212	14-300	1.18×10^{-3}
200	0	28.71	99.05	14273	14	213	12-302	1.63×10^{-3}
300	0	27.99	92.81	12949	0*	317	14-297	9.87×10^{-4}
300	0	29.19	98.69	17439	10	320	14-299	1.33×10^{-3}
400	0	28.23	89.64	16368	0*	421	12-303	9.35×10^{-4}
400	0	30.64	99.17	21794	10	428	12-297	1.25×10^{-3}
100	3	22.56	77.25	3657	0*	100	11-304	8.32×10^{-4}
100	3	21.96	86.39	6279	5.5	103	10-302	1.43×10^{-3}
100	3	23.77	96.67	8440	10	105	10-311	1.93×10^{-3}
100	3	26.42	99.77	13156	23	106	14-304	3.01×10^{-3}
200	3	21.72	84.88	8436	0*	205	11-301	9.61×10^{-4}
200	3	21.11	91.09	11133	5	208	11-301	1.27×10^{-3}
200	3	21.11	97.63	13782	10	211	10-302	1.58×10^{-3}
300	3	23.89	85.90	13855	4	310	11-309	1.05×10^{-3}
300	3	24.97	92.84	15270	5	316	15-308	1.16×10^{-3}
300	3	26.54	97.63	17639	9.6	319	10-301	1.35×10^{-3}

* Single phase experiments (For comparison)

Table 6.1 Range of the experimental parameters covered in the present study (cont.)

Flow rate (ml/min)	θ (deg)	T_{in} (°C)	T_{out} (°C)	q'' (W/m^2)	Liquid loss (ml/min)	$Re_f = \frac{4\rho\dot{Q}}{\pi\mu D}$	RPM	$Bo = \frac{\pi q'' D^2}{4\dot{Q}\rho\lambda}$
400	3	24.61	94.28	18566	0*	422	10-309	1.06×10^{-3}
400	3	24.61	97.57	21220	5	424	10-302	1.21×10^{-3}
100	6	29.43	79.60	3348	0*	103	16-310	7.63×10^{-4}
100	6	28.47	83.88	3696	0*	104	18-297	8.43×10^{-4}
100	6	26.78	88.4	5905	5	104	17-304	1.35×10^{-3}
100	6	27.38	97.66	6466	5	106	14-300	1.48×10^{-3}
100	6	28.23	99.89	8341	10	107	17-300	1.91×10^{-3}
200	6	30.04	77.70	6365	0*	205	16-299	7.25×10^{-4}
200	6	29.56	86.78	7628	0*	210	17-313	8.71×10^{-4}
200	6	27.75	95.16	9869	2.5	212	17-314	1.13×10^{-3}
300	6	29.92	90.21	12047	0*	317	20-310	9.18×10^{-4}
300	6	28.71	93.02	14636	5	318	18-309	1.12×10^{-3}
300	6	29.02	97	16574	9	320	20-310	1.27×10^{-3}
400	6	28.35	86.11	15406	0*	418	20-307	8.79×10^{-4}
400	6	26.06	91.87	19335	5	421	20-303	1.10×10^{-3}
400	6	27.99	95.31	20833	8	425	17-310	1.19×10^{-3}

* Single phase experiments (For comparison)

Table 6.2 Experimental uncertainties

Parameter	Absolute uncertainty		
	Average	Maximum	Minimum
Time (s)	1	1	1
Flow rate (kg/s)	2.50×10^{-05}	2.50×10^{-05}	2.50×10^{-05}
Length (m)	2.00×10^{-05}	2.00×10^{-05}	2.00×10^{-05}
Inclination angle (degree)	0.5	0.5	0.5
Pool height (m)	1.50×10^{-03}	2.23×10^{-03}	1.04×10^{-03}
Rotation rate (RPM)	0.25	2.5 (≥500RPM)	0.25
Temperature (°C)	1	1	1
Wall heat flux (W/m^2)	181.93	281.96	82.40
Heat transfer coefficient (W/m^2K)	12.52	56.28	10.68
Flow Reynolds number	1.61	1.64	1.52
Rotational Reynolds number	56.74	101.90	46.71
Boiling number	6.51×10^{-06}	1.08×10^{-05}	4.75×10^{-06}

6.4 Results and discussion

Experiments are performed to study the effect of wall heat flux, liquid volume flow rate, pipe rotation rate and inclination on the heat transfer characteristics of an axially rotating, partially filled evaporator in a continuous mode. Section 6.4.1 gives the effect of inclination on the liquid pool height inside a partially filled stationary pipe. Section 6.4.2 discusses the effect of inclination angle on the local wall and bulk temperature profile. Section 6.4.3 presents the effect of wall heat flux variation on the wall and bulk temperature profiles. Section 6.4.4 investigates the effect of liquid volume flow rate on the evaporator temperature profile. Section 6.4.5 investigates the effect of rotation rate on the evaporators local temperature and heat transfer coefficient. Section 6.4.6 presents a correlation to predict the outlet liquid flow fraction.

6.4.1 Effect of inclination on the liquid pool height in a partially filled stationary pipe

The height of the liquid pool in a partially filled circular duct is experimentally investigated. The liquid pool height in a stationary partially filled pipe is measured experimentally using catch and time technique at various inclination angles explored in this study. The same procedure is followed as explained in Section 5.4.1.

The experimental pool height measured at ambient condition for various flow rates is tabulated in Table 6.3.

Table 6.3 Experimental pool height in a stationary pipe of ID 32.8 mm

Flow rate (ml/min)	Inclination angle	Pool height (mm) 0°	3°	6°
100		3.89	1.28	1.10
200		4.30	1.55	1.22
300		4.71	1.68	1.44
400		5.94	2.28	2.00

The effect of inclination angle on the average liquid pool height inside a 32.8 mm ID stationary circular duct is shown in Fig. 6.2.

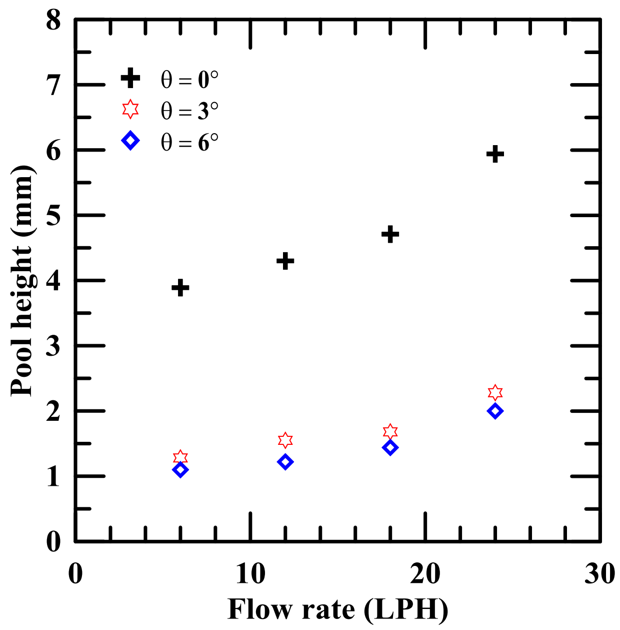

Fig. 6.2 Effect of inclination angle on average pool height for a 35 mm OD partially filled stationary circular duct

With the increase in the liquid flow rate, the liquid hold up inside the partially filled stationary pipe increases. This leads to an increase in the average pool height. Increasing the inclination angle leads to an increase in the axial velocity of the fluid flow. The increase in the flow velocity reduces the liquid residence time inside the partially filled pipe. As a result of the reduction in the liquid residence time, the liquid hold up inside the test section decreases. This leads to a reduction in the liquid pool height inside the partially filled stationary pipe. The same is visualised using a 32.8 mm internal diameter Plexiglas tube as shown in Fig. 6.3. The liquid volume flow rate is maintained at 300 ml/min (18 LPH) while the inclination is varied from 0° to 6°. Figure 6.3 shows a clear reduction in the liquid pool height. The flow pattern in the inclined pipe is comparatively wavy.

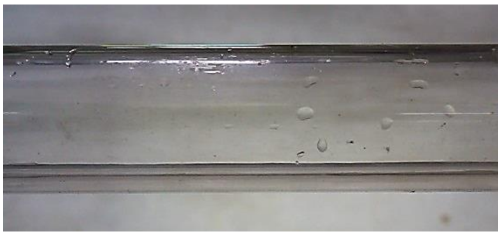

(A) 300 ml/min, 0 RPM, θ = 0°

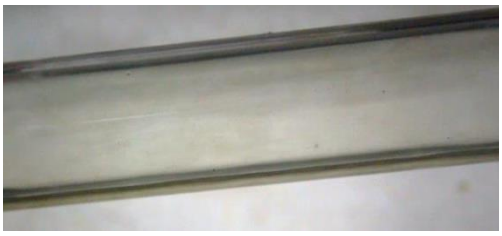

(B) 300 ml/min, 0 RPM, θ = 6°

Fig. 6.3 Effect of inclination in the liquid pool height in a partially filled stationary pipe with constant flow rate (300 ml/min, 18 LPH, $Re_f = 315$)

6.4.2 Local temperature distribution and heat transfer coefficient at variable inclination angles

The pipe rotation rate, wall heat flux and the liquid volume flow rate through the test section are kept constant. The pipe inclination angle is gradually increased to study its effect on the variation on the evaporator temperature profiles. The wall and bulk fluid temperature profile of a typical single phase partially filled rotating horizontal heated pipe is shown in Fig. 6.4(A). The corresponding local heat transfer coefficient is shown in Fig. 6.5. As the wall heat flux to the heated rotating pipe is increased, the temperature profile gets modified as shown in Fig. 6.4(B). The temperature profile shows two distinct zones Zone I, where the wall temperature increases rapidly with length and Zone II, where the wall temperature is nearly constant. The wall temperature starts rising in Zone I and saturates at an average value of 101.48 °C in Zone II as shown in Fig. 6.4(B).

The fluid viscosity decreases along the length of the rotating test section with increasing bulk fluid temperature. The decrease in fluid viscosity leads to the reduction of the liquid film thickness wetting the rotating wall [Ashmore *et al.* (2003)]. At high heat flux, the decrease in the film thickness leads to the break-up of the liquid film wetting the rotating wall thus forming dry sections. Fujita and Ueda (1978) highlighted the fact that at high wall heat fluxes, falling liquid films become distorted leading to their break down (local or permanent dry patch). The breakdown is a result of the distortion of the local force balance between the surface tension and the thin film dynamic pressure. Dry areas lead to the loss of heat transfer area and a drop in local heat transfer coefficient. The drop in local heat transfer coefficient triggers the rise in local wall temperature.

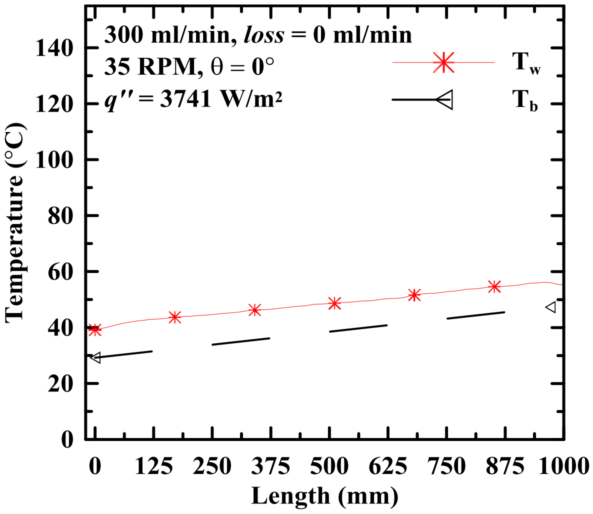

(A) $q'' = 3741$ W/m^2, $\theta = 0°$

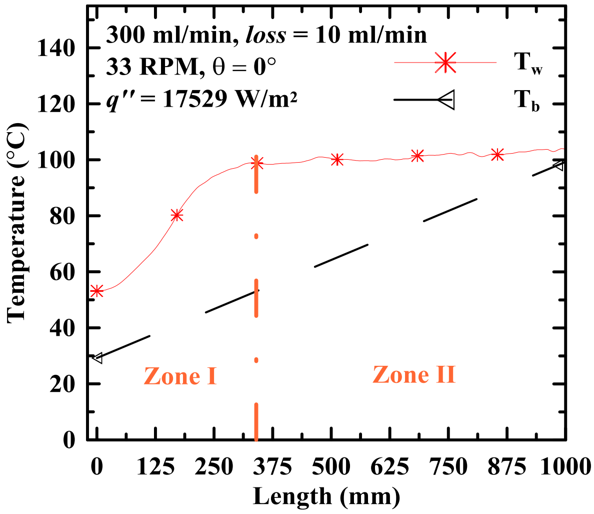

(B) $q'' = 17529$ W/m^2, $\theta = 0°$

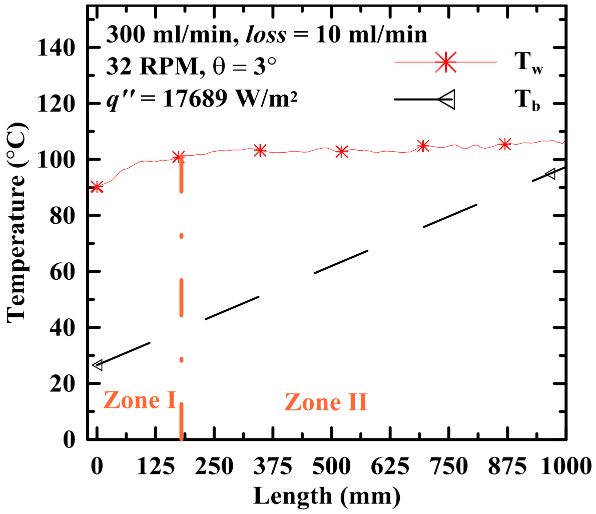

(C) $q'' = 17689$ W/m^2, $\theta = 3°$

Fig. 6.4 Wall and bulk temperature profiles along the length of the rotating evaporator

Under current experimental conditions, any dry area that may be formed is not visible in the thermal images. This is attributed to the fact that the wall is rotating. All the dry section will be wet as soon as the particular section submerges in the liquid pool at the bottom. With increasing rotation rate, the time interval where a particular section of wall remains dry will further reduce. Hence, we continue to assume that the heat flux is uniformly distributed along the surface area of the rotating test section. The rise in wall temperature in Zone I (Fig. 6.4(B)) is due to the formation of local dry sections leading to the loss of heat transfer area to water [Fujita and Ueda (1978)]. Similar developing region is not observed in single phase experiments at lower heat flux as shown in Fig. 6.4(A) or the studies reported in Chapters 4 and 5. This leads to a drop in the local heat transfer coefficient as shown in Fig. 6.5.

The inclination angle of the rotating pipe is increased from horizontal to 3°, while the fluid flow rate, rotation rate and wall heat flux is maintained constant. The wall temperature starts rising in Zone I and saturates at an average value of 103.78°C in Zone II as shown in Fig. 6.4(C). The corresponding local heat transfer coefficient is shown in Fig. 6.5.

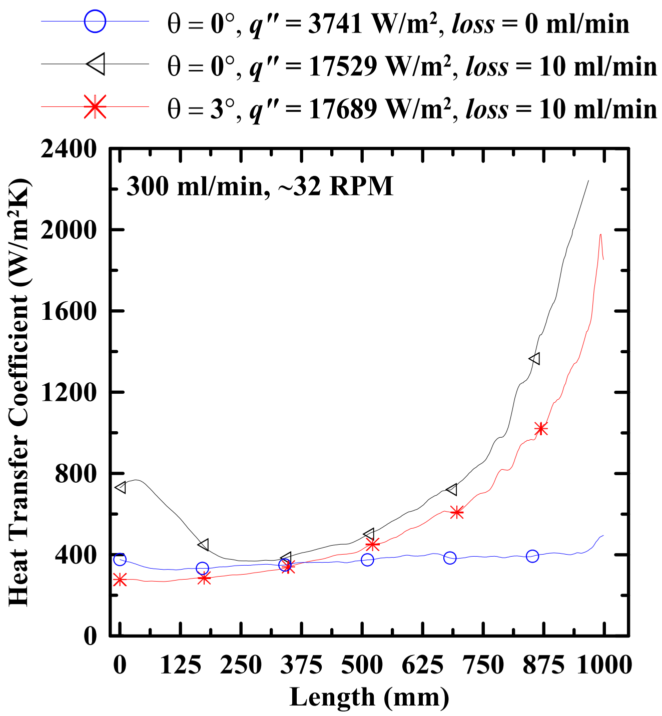

Fig. 6.5 Local heat transfer coefficient variation along the length of the rotating evaporator ~30 RPM, 300 ml/min (18 LPH, $Re_f = 315$)

A theoretical model developed by Davis and Anderson (1966) as given by Eqn. (6.6) to compute the wall temperature for the incipience of nucleate boiling in forced convection flow is used to estimate the wall temperature at which nucleation is initiated under current experimental conditions.

$$T_{Wi} = T_{sat} + \sqrt{\frac{8q"\sigma T_{sat} v_{fg}}{k\lambda}} \tag{6.6}$$

where, T_{Wi} is the wall temperature at the incipience of nucleation, v_{fg} is the specific volume difference $(v_g - v_f)$, v_f is the specific volume of water at the local bulk temperature and v_g is the specific volume of steam at saturation temperature (T_{sat}).

When the evaporator is set at horizontal configuration, Eqn. (6.6) estimates the incipience of nucleate boiling at 100.97 °C. The local wall temperature rises above 101 °C at approximately 470 mm from the inlet of the test section in Zone II as shown in Fig. 6.4(B). With the incipience of nucleation, the local heat transfer coefficient rises as shown in Fig. 6.5. Similarly, the incipience of nucleation is computed at 101 °C using Eqn. (6.6) when the test section is inclined at 3 degrees. The local wall temperature rises above this point at approximately 180 mm from the inlet of the test section i.e. in Zone II as shown in Fig. 6.4 (C). Beyond this point, the local heat transfer coefficient rises due to nucleation as shown in Fig. 6.5.

At the inlet, as the wall heat flux increases (3741 – 17529 W/m^2) at 0° inclination, the heat transfer coefficient increases [Section 4.4.1 and 5.4.3]. As the inclination angle is increased from 0° to 3° at a constant wall heat flux (~17609 W/m^2), the heat transfer coefficient at the inlet decreases due to the drop in liquid pool height [Sections 5.4.2 and 6.4.1]. The rate of liquid loss remained constant at 10 ml/min (0.6 LPH) for both horizontal and 3° inclined case at relatively constant wall heat flux.

The inclination angle of the partially filled rotating test section is varied from horizontal to 6°. The flow rate is maintained at 200 ml/min (12 LPH) and the rotation rate is set at approximately 260 RPM. The variation of local wall temperature and local heat transfer coefficient at 200 ml/min (12 LPH) and average wall heat flux 10878 W/m^2 is shown in Figs. 6.6(A), 6.6(B) and 6.7 respectively.

When the test section is inclined at 0°, the wall temperature increases steadily (Zone I) and becomes constant at approximately 104.38 °C (Zone II) as shown in Fig. 6.6(A). The experimental wall temperature increases above 100.96 °C at a distance of 680 mm from the inlet of the test section. Based on the theoretical estimates computed using Eqn. (6.6), nucleation is realised at the approximately 680 mm (Zone II Fig. 6.6(A)) from the inlet of the rotating partially filled evaporator leading to the increasing local heat transfer coefficient as shown in Fig. 6.7. As shown in Fig. 6.7, before the onset of nucleation, there exist two slopes in the heat transfer coefficient curve. The slope changes at approximately 570 mm from the inlet of the evaporator.

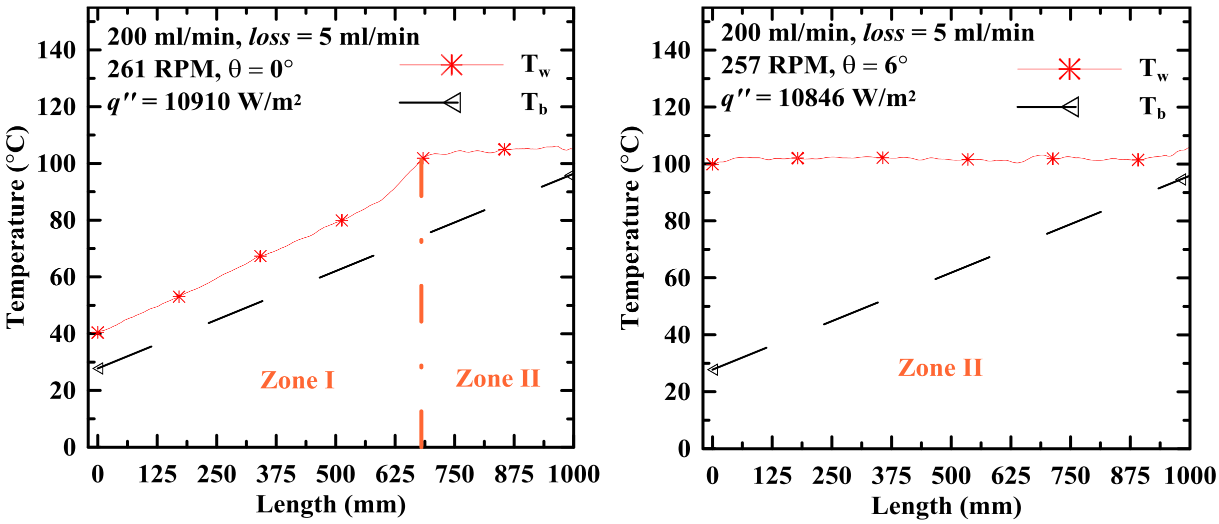

(A) $q'' = 10910$ W/m^2, $\theta = 0°$ (B) $q'' = 10846$ W/m^2, $\theta = 6°$

Fig. 6.6 Wall and bulk temperature profiles along the length of the rotating evaporator at a constant heat flux, rotation rate and variable inclination angle (12 LPH, $Re_f = 210$)

Shmerler and Mudawwar (1988a, 1988b) reported that the thermal developing length in sensible heating of vertical falling films is negligible compared to evaporative heating of vertical falling films. The loss of heat from the water-air interface by evaporative mass transfer increases the thermal development length. From 0 mm to 570 mm, the drop in heat transfer coefficient is attributed to the loss of heat as a result of interface mass transfer [Shmerler and Mudawwar (1988b)]. Post 570 mm till the point where the onset of nucleation is realised, the drop is attributed to the loss of heat transfer area due to the formation of local dry sections [Fujita and Ueda (1978)]. As a result of this drop in local heat transfer coefficients, the local wall temperature raises as shown in Zone I, Fig. 6.6 (A)

At 6° inclination angle the liquid pool at the bottom is smaller in comparison to the horizontal case (Section 6.4.1). This leads to the reduction in heat transfer coefficient at the inlet and hence the wall temperature at the inlet is comparatively higher at a higher inclination angle as shown in Fig. 6.6(B). The wall temperature remains constant at approximately 101.95 °C throughout the length of the rotating partially filled inclined evaporator (Zone II). The local wall temperature for incipience of nucleation is estimated to be 100.75 °C using Eqn. (6.6). Hence, it can be stated that onset of nucleation is realised at the inlet of the rotating test section leading to the steady rise in the local heat transfer coefficient a shown in Fig. 6.7.

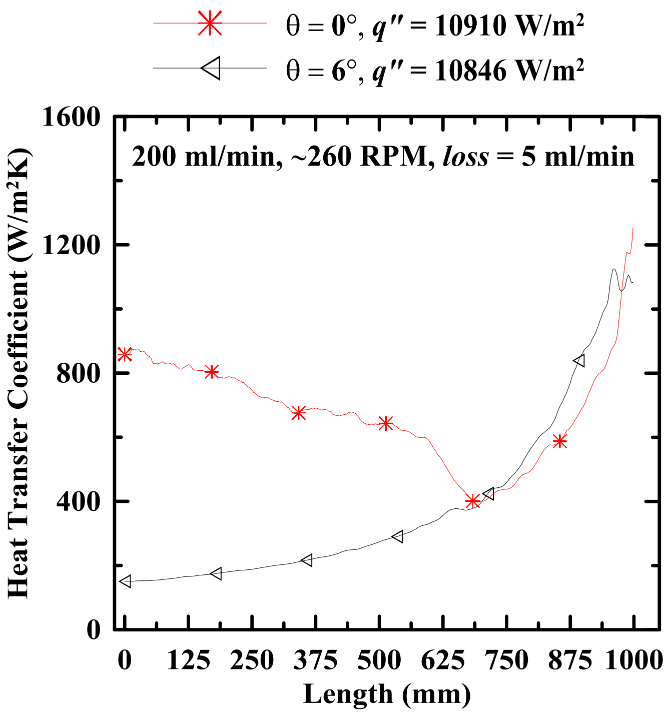

Fig. 6.7 Local heat transfer coefficient variation along the length of the rotating evaporator at a constant heat flux (~10878 W/m^2), rotation rate (~260 RPM) and variable inclination angle (12 LPH, $Re_f = 210$)

The loss of liquid remained the same at 5 ml/min (0.3 LPH) for both horizontal and 6° inclined case. As the surface area of the water-air interface does not change appreciably with the variation in the inclination angles, the rate of liquid loss remains constant at comparable wall heat flux. Table 6.4 shows similar results where various experimental conditions i.e. liquid flow rate, pipe rotation rate, wall heat flux are maintained constant while the inclination angle is varied.

It is evident from the temperature profiles as shown in Figs. 6.4(B), 6.4(C), 6.6(A) and 6.6(B) that with increasing inclination angle, it is easier to achieve an early constant wall temperature zone (Zone II) at the same flow rate, rotation rate and wall heat flux. The results suggest that a rotating partially filled evaporator should incorporate some degree of inclination for easier and effective operation i.e. to ensure unidirectional flow of fluids. In the following sections, Zone I and Zone II are mentioned, but not marked in the graphs. Various experimental results highlighting the effect of pipe inclination on heat transfer in a partially filled rotating evaporator are shown in Appendix D, Figs. D.12 (A)-(F).

Table 6.4 Loss of liquid at various inclination angles

Inclination (Degrees)	Flow rate (ml/min)	Re_f	RPM	q'' (W/m^2)	Liquid loss (ml/min)	Bo	Water T_{in}	Water T_{out}
0	100	105	104	8159	10	1.87×10^{-3}	26.5	95.5
3	100	105	102	8380	10	1.92×10^{-3}	23.5	95.5
3	200	207	163	10984	5	1.25×10^{-3}	21	90
6	200	213	148	11295	5	1.29×10^{-3}	27.5	99
0	200	212	261	10910	5	1.25×10^{-3}	27.5	96
6	200	212	257	10846	5	1.24×10^{-3}	29.5	88
3	200	209	301	11402	5	1.30×10^{-3}	21	93
6	200	213	314	11167	5	1.28×10^{-3}	27.5	98
0	200	213	12	12879	10	1.48×10^{-3}	28.5	98.5
3	200	211	10	13790	10	1.58×10^{-3}	21	97.5
0	200	213	32	12879	10	1.48×10^{-3}	28.5	98.5
3	200	211	30	13822	10	1.58×10^{-3}	21	98
0	300	321	33	17529	10	1.34×10^{-3}	29	99
3	300	319	32	17689	10	1.35×10^{-3}	26.56	97
0	300	321	61	17385	10	1.33×10^{-3}	29	98.5
3	300	318	60	17496	10	1.33×10^{-3}	26.5	96
0	300	320	100	17337	10	1.32×10^{-3}	29	98
3	300	319	103	17593	10	1.34×10^{-3}	26.5	96.5
0	300	321	151	17529.	10	1.34×10^{-3}	29	99
3	300	319	152	17785	10	1.36×10^{-3}	26.5	97.5
0	300	321	205	17578	10	1.34×10^{-3}	29	99
3	300	319	204	17785	10	1.36×10^{-3}	26.5	97.5
6	300	320	209	17368	10	1.33×10^{-3}	29	98
0	300	321	255	17578	10	1.34×10^{-3}	29	99.5
6	300	321	259	17609	10	1.35×10^{-3}	29	99.5
0	300	320	299	17289	10	1.32×10^{-3}	29	98
3	300	320	301	18074	10	1.38×10^{-3}	26.5	99
6	300	321	310	17561	10	1.34×10^{-3}	29	99
3	400	422	10	20289	5	1.16×10^{-3}	24.5	94
6	400	424	17	19192	5	1.10×10^{-3}	28	93.5
3	400	425	60	21380	5	1.22×10^{-3}	24.5	98.5
6	400	424	64	19449	5	1.11×10^{-3}	28	94.5
0	400	428	100	21914	10	1.26×10^{-3}	30.5	99.5
6	400	424	106	21240	10	1.22×10^{-3}	28	94.5
0	400	428	153	21914	10	1.26×10^{-3}	30.5	99.5
6	400	425	155	21690	10	1.24×10^{-3}	28	96
0	400	428	197	21914	10	1.26×10^{-3}	30.5	99.5
6	400	427	211	22524	10	1.29×10^{-3}	28	99.5
0	400	428	259	21914	10	1.26×10^{-3}	30.5	99.5
6	400	426	260	21947	10	1.26×10^{-3}	28	97
0	400	428	297	21914	10	1.26×10^{-3}	30.5	99.5
6	400	425	310	21690	10	1.24×10^{-3}	28	96

6.4.3 Effect of wall heat flux on the local temperature distribution and heat transfer coefficient

Water volume flow rate, pipe inclination angle and the rotation rate is kept constant while the wall heat flux is gradually increased to study its effect on the local temperature profiles. The variation in local wall and bulk fluid temperatures along the length of the rotating test section with increasing wall heat flux is shown in Figs. 6.8(A) and 6.8(B). In Figs. 6.8(A)-(B), the solid line represents the wall temperature and the dashed line represents the bulk fluid temperature profile.

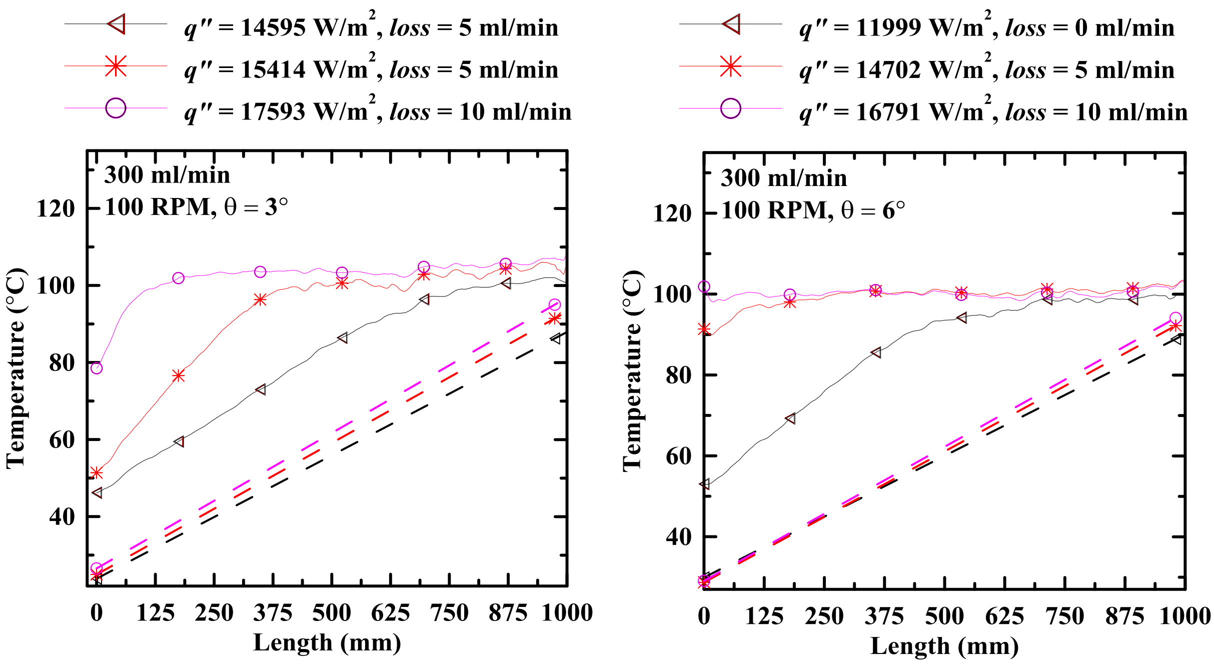

(A) 100 RPM, θ=3° (B) 100 RPM, θ=6°

Fig. 6.8 Local wall and bulk temperatures along the length of the inclined rotating heated pipe with constant flow rate (300 ml/min, 18 LPH, $Re_f = 316$) and rotation rate (~100 RPM) and variable wall heat flux

The effect of increasing wall heat flux on the wall and the bulk fluid temperatures, where a volume flow rate of 300 ml/min (18 LPH) is maintained through the test section rotating at 100 RPM, at an inclination of 3° is illustrated by Fig. 6.8(A). At a wall heat flux of 14595 W/m^2, the wall temperature increases (Zone I) and reaches a constant value of 101.09 °C

(Zone II). The incipience of nucleation is computed to be at 100.85 °C using Eqn. (6.6). The local wall temperature reaches 100.93 °C at 920 mm from the inlet of the test section where the incipience of nucleation is realised.

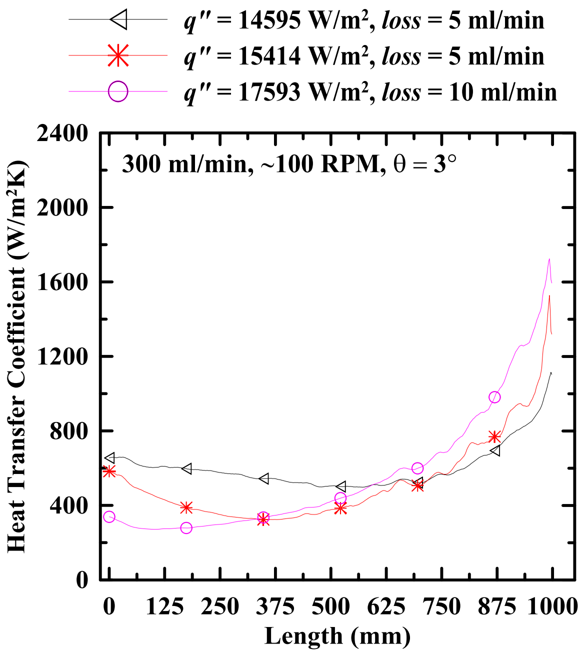

(A) Local heat transfer coefficient
~100 RPM, θ = 3°

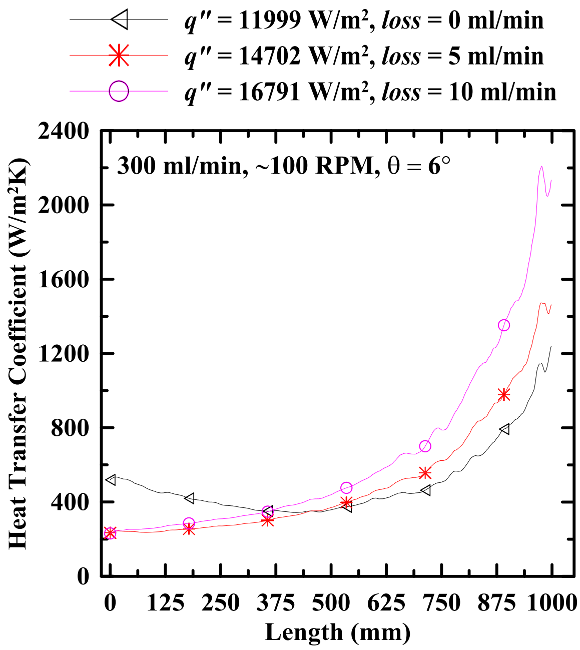

(B) Local heat transfer coefficient
~100 RPM, θ = 6°

Fig. 6.9 Local heat transfer coefficient variation along the length of the inclined rotating evaporator with constant flow rate (300 ml/min, 18 LPH, $Re_f = 318$) and rotation rate (~100 RPM) and variable wall heat flux

As the wall heat flux is increased to 15414 W/m^2, the wall temperature rises (Zone I) and becomes constant at an average 102.25 °C (Zone II) as shown in Fig. 6.8(A). Nucleation is realised when the local wall temperature rises above 101 °C at a distance of 550 mm from the inlet of the test section (Zone II). The wall temperature for incipience of nucleation as computed by Eqn. (6.6) is 100.88 °C. At a higher wall heat flux i.e. at 17593 W/m^2, the wall temperature rises (Zone I) and reaches a constant average value of 103.98 °C (Zone II) as shown in Fig. 6.8(A). The local wall temperature reaches above 101.1 °C i.e. greater than 101 °C as computed by Eqn. (6.6) and the onset of nucleate boiling occurs within 160 mm from the inlet (Zone II).

The corresponding local variation of the heat transfer coefficient is shown in Figs. 6.9(A). As the wall heat flux increases from 14595 W/m^2, 15414 W/m^2 and 17593 W/m^2, the rate of rise in wall temperature per unit length increases respectively as shown in Fig. 6.8(A). At a wall heat flux of 14595 W/m^2, the local heat transfer coefficient first starts rising at 750 mm from the inlet due to the turbulence in the interfacial waves [Shmerler and Mudawwar (1988a)]. It further rises (slope change) at approximately 920 mm from the inlet as nucleation is realised as shown in Fig. 6.9(A). At higher heat fluxes i.e. 15414 W/m^2 and 17593 W/m^2 the rise in local heat transfer coefficient is due to the onset of nucleation. With early onset of nucleation, the local heat transfer coefficient at exit is highest for the highest wall heat flux.

As shown in Fig. 6.9(A), before the onset of nucleation, there exists a thermal developing length where the local heat transfer coefficient monotonously decreases. At a comparatively lower heat flux the drop in local heat transfer coefficient is due to the loss of heat as a result of interface mass transfer [Shmerler and Mudawwar (1988b)]. With increasing heat flux, the drop in local heat transfer coefficient is comparatively steeper as shown in Fig. 6.9(A). This is due to the formation of local dry sections leading to the loss of heat transfer area to water [Fujita and Ueda (1978)]. Also as the wall heat flux is increased, the rate of liquid loss increases from 5 ml/min to 10 ml/min (0.3- 0.6 LPH).

At a higher inclination angle i.e. 6 degrees, the liquid pool at the bottom is smaller (Fig. 6.2). Reduction in the liquid pool height decreases the heat transfer potential by secondary flows inside the recirculating region of the liquid pool [Section 5.4.2, Haji-Sheikh *et al.* (1984)]. As a result of the decrease in the heat transfer, wall temperatures are higher at the inlet at comparable heat fluxes as shown in Fig. 6.8(B).

At a wall heat flux of 11999 W/m^2, the wall temperature increases in Zone I and becomes constant at an average 100 °C (Zone II). The incipience of nucleation is estimated at 100.84 °C using Eqn. (6.6). Hence, nucleation is not realised at the wall heat flux of 11999 W/m^2.

Owing to the smaller pool leading to a drop in heat transfer potential and no liquid loss due to phase change, the initial drop in the local heat transfer coefficient (Zone I) as shown in Fig. 6.9(B) is attributed to the formation of local dry sections leading to the loss of heat transfer area to water [Fujita and Ueda (1978)]. This leads to the rise in the wall temperature (Zone I) as shown in Fig. 6.8(B). Further downstream, the subsequent increase in the local heat transfer coefficient as shown in Fig. 6.9(B) is due to the turbulence in the interfacial waves [Shmerler and Mudawwar (1988a)]. As the wall heat flux is increased to 14702 W/m^2, the wall temperature increases in Zone I and reaches saturation at an average 101.36 °C (Zone II) as shown in Fig. 6.8(B). The incipience of nucleation is only realised above 100.85 °C as computed by Eqn. (6.6) at a distance of 470 mm from the inlet of the test section (Zone II). As nucleation is realised, the local heat transfer coefficient rises as shown in Fig. 6.9(B).

Increasing the wall heat flux to 16791 W/m^2, the wall temperature at the inlet is measured at 101.86 °C i.e. greater than 101 °C as computed by Eqn. (6.6). Onset of nucleation is realised at the inlet and the local heat transfer coefficient increases as shown in Fig. 6.9(B). The overall wall temperature throughout the length of the rotating evaporator remains constant at approximately 100.75 °C (Zone II). Along the length of the rotating test section, the wall temperature occasionally falls below the temperature where incipience of nucleation is predicted. Chun and Seban (1971) reported similar observations while studying evaporating liquid films where, once nucleation is initiated, nucleation continued at lower superheats.

At 6 degree inclination, the rate of liquid loss increases from 0 ml/min to 10 ml/min (0 – 0.6 LPH) between the lowest and the highest wall heat fluxes. A higher local heat transfer coefficient is achieved at the exit at a higher wall heat flux and inclination angle as shown in Figs. 6.9(A) and 6.9(B). Considering Figs. 6.8(A) and 6.8(B), it is clear that with increasing wall heat flux, the slope of the bulk fluid temperature profile marginally varies from one another. This variation is due to an increase in heat transfer from the inner air core to the fluid as the wall heat flux is increased [Section 4.4.1]. Loss of liquid due to phase change is realised while the bulk fluid temperature at the exit is still below saturation temperature of water i.e. 99.9°C. Since the fluid volume is low, the vapour generated easily escapes before the subcooled bulk fluid may condense it. In industrial applications where volume reduction of temperature sensitive fluid is required, rotating evaporator setups may find possible application. Lowering the system pressure may further enhance evaporator performance [Lopez (2006)]. Various experimental results highlighting the effect of wall heat flux on heat transfer in a partially filled rotating evaporator is shown are Appendix D Figs. D.13 (A)-(D).

6.4.4 Effect of fluid flow rate on the local temperature distribution and heat transfer coefficient

The pipe inclination angle, rotation rate and the wall heat flux are kept constant. The water volume flow rate through the evaporator is increased and the variation in the wall, bulk fluid temperature and the local heat transfer coefficient profiles are reported. The local wall and bulk water temperature variation along the length of the rotary evaporator are reported in Figs. 6.10(A) and 6.10(C). The solid line represents the wall temperature and the dashed line represents the bulk fluid temperature profile.

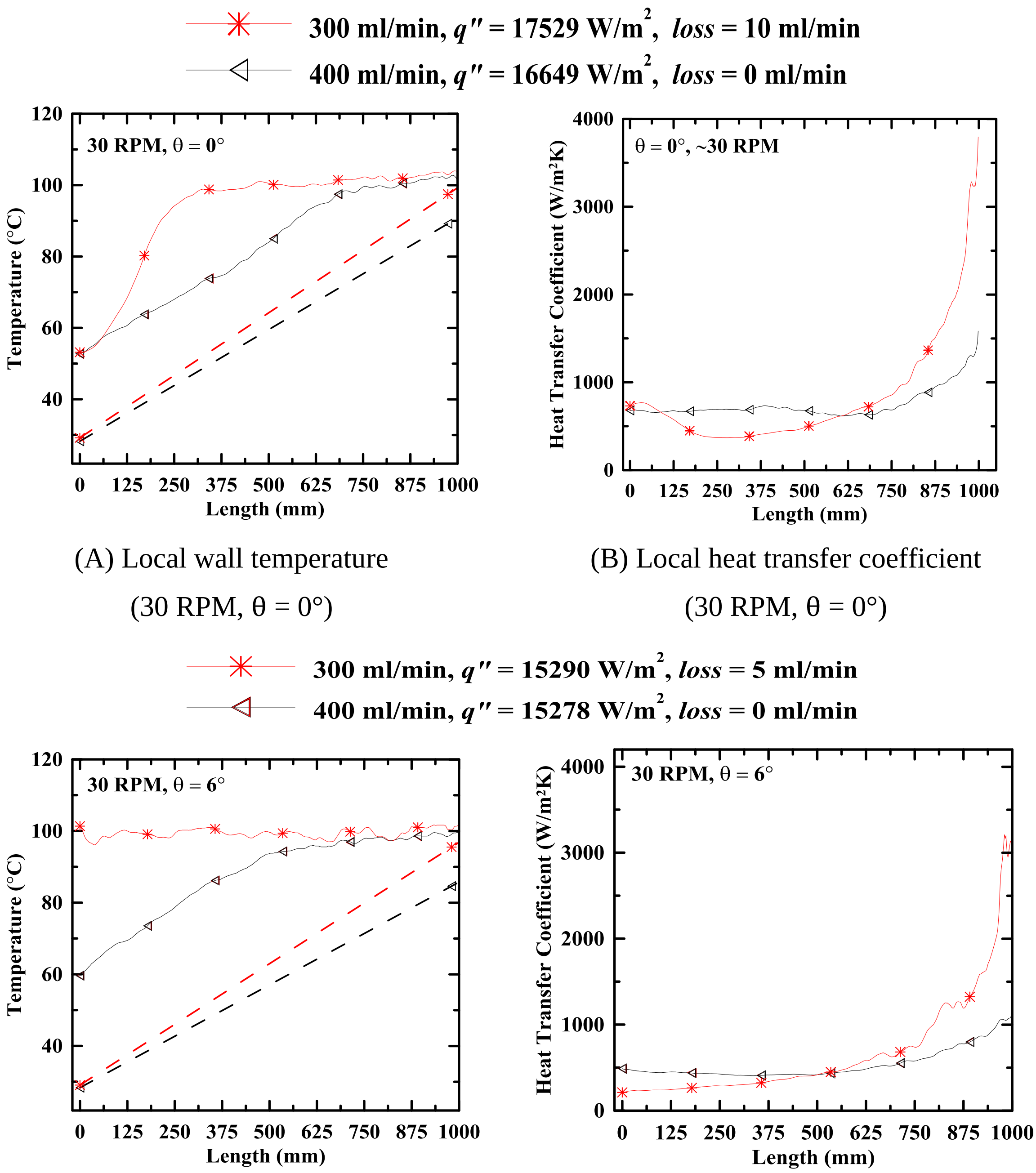

(A) Local wall temperature

(30 RPM, θ = 0°)

(B) Local heat transfer coefficient

(30 RPM, θ = 0°)

(C) Local wall temperature

(30 RPM, θ = 6°)

(D) Local heat transfer coefficient

(30 RPM, θ = 6°)

Fig. 6.10 Local wall temperature profile variation at a constant heat flux, rotation rate, pipe inclination and variable volume flow rates

The volume flow rate of water is varied from 300 ml/min to 400 ml/min (18 – 24 LPH) in the rotary evaporator inclined at 0° while maintaining a rotation rate of 30 RPM and comparable wall heat flux. A clear difference in the temperature profiles is visible as shown in Fig. 6.10A. At 300 ml/min (18 LPH), and 17529 W/m^2 wall heat flux, the wall temperature rises

(Zone I) and saturates at an average temperature of 101.48 °C (Zone II). The incipience of nucleation is computed at 100.97°C using Eqn. (6.6), and hence, nucleation is realised at approximately 450 mm from the inlet of the rotary evaporator (Zone II). Before nucleation is realised, the rise in the wall temperature (Zone I) is attributed to the formation of local dry sections leading to the loss of heat transfer area to water [Fujita and Ueda (1978)]. This leads to the initial drop in the local heat transfer coefficient as shown in Fig. 6.10(B). The heat transfer coefficient further increases with the initiation of nucleation. Liquid loss rate of 10 ml/min (0.6 LPH) is measure at 300 ml/min (18 LPH) flow rate. As the water flow rate is increased to 400 ml/min (24 LPH), the liquid pool height inside the test section increases (Fig. 6.2). The increase in pool height improves convective heat transfer and hence leads to the cooling of the evaporator wall [Sections 4.4.2, 5.4.1 and 5.4.4]. Nucleation is not achieved at 400 ml/min (24 LPH) flow rate and the system remains in single phase with no loss of liquid due to phase change.

At 6 degrees inclination, 30 RPM and an average wall heat flux of 15284 W/m^2, the flow rate is increased from 300 to 400 ml/min (18 – 24 LPH). At 300 ml/min (18 LPH), the wall temperature at the inlet reaches 101.3 °C as shown in Fig. 6.10(C). The wall temperature is higher than the incipience of nucleation temperature i.e. 100.9 °C as computed by Eqn. (6.6). Hence, onset of nucleation is realised at the inlet. The wall temperature remains constant above 100 °C (Zone II). However, fluctuations are present where the wall temperature drops below the incipience of nucleation temperature as shown in Fig. 6.10(C). Chun and Seban (1971) reported experimental studies concluding that once nucleation is initiated, nucleation continues at lower superheats. The local heat transfer coefficient increases as shown in Fig. 6.10(D) as a result of onset of nucleate boiling.

At 400 ml/min (24 LPH), the liquid pool height at the bottom of the rotating pipe increases (Fig. 6.2). A larger liquid pool enhances heat transfer inside the pool by secondary mixing in the recirculating region [Sections 4.4.2, 5.4.1 and 5.4.4]. The excess fluid in the pool absorbs the heat supplied as sensible heat and cools the wall. Hence, the wall temperature stays below saturation temperature of water i.e. 99.9 °C at the current experimental condition as shown in Fig. 6.10(C). This leads to a comparatively lower heat transfer coefficient at the exit as shown in Fig. 6.10(D). The rate of liquid loss due to phase change decreases with increasing flow rate i.e. from 5 ml/min to 0 ml/min (0.3 – 0 LPH). At a higher volume flow rate, the excess bulk fluid absorbs the majority of the supplied energy as sensible heat. Hence as the flow rate is increased, the loss of liquid reduces under similar operating conditions. Various experimental results highlighting the effect of fluid volume flow rate on heat transfer in a partially filled rotating evaporator are shown in Appendix D, Figs. D.14 (A)-(D).

6.4.5 Effect of pipe rotation rate on the local temperature distribution and heat transfer coefficient

The wall heat flux, liquid volume flow rate and inclination angle is maintained constant while the pipe rotation rate is varied. The local wall, bulk fluid temperature and the local heat transfer coefficient along the length of the partially filled rotating evaporator are plotted in Figs. 6.11(A) and 6.12(B) respectively.

The wall temperature profile changes with increasing rotation rate as shown in Fig. 6.11(A). Increasing rotation rate, improves the intensity of the secondary flows inside the recirculating region of the liquid pool thus improving heat transfer [Kuo *et al.* (1960), Haji-Sheikh *et al.* (1984), Sections 4.4.3 and 5.4.5]. Hence, the wall temperatures in Zone I are higher at lower rotation rates as shown in Fig. 6.10(A). Furthermore, the wall temperature increases (Zone I) and reaches saturation (Zone II) further downstream with increasing rotation rate.

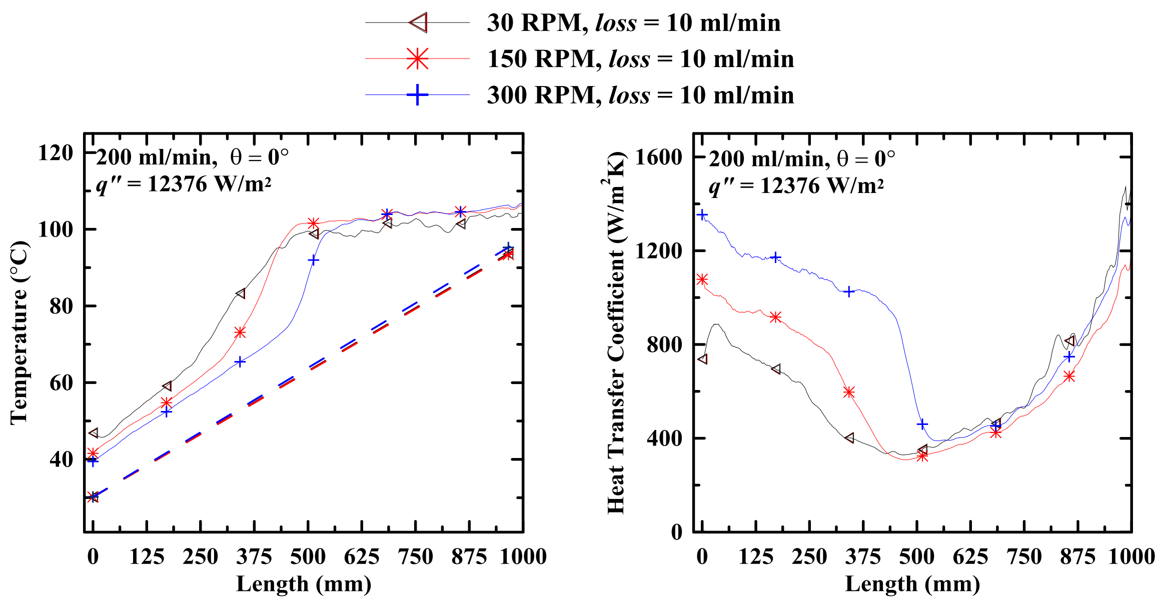

(A) Temperature profile

200 ml/min, θ = 0°, $q'' = 12376$ W/m^2

(B) Heat transfer coefficient

200 ml/min, θ = 0°, q″ = 12376 W/m2

Fig. 6.11 Local temperature and heat transfer coefficient variation in a partially filled horizontal rotating evaporator at a constant flow rate, wall heat flux and variable rotation rates (12 LPH, $Re_f = 212$)

The wall temperature reaches saturation (Zone II) at an average temperature of 100.97 °C, 103.53 °C and 104.12 °C at a distance of approximately 471 mm, 488 mm and 574 mm from the inlet of the rotating test section as the rotation rate is increased from 30 RPM, 150 RPM and 300 RPM respectively. With increasing rotation rate, the liquid inside the rotating partially filled test section is spread across the inner wall leading to various flow patterns. The liquid film thickness on the rotating wall increases with increasing rotation rate [Ashmore *et al.* (2003)]. The increase in film thickness leads to a marginal increase in local resistance to heat transfer. Hence, with increasing rotation rate, the wall temperature saturates at a marginally higher temperature.

The wall temperature for the incipience of nucleation is computed to be 100.7-100.8 °C using Eqn. (6.6). The onset of nucleation is realised at 530 mm, 500 mm and 575 mm (Zone II) from the inlet of the test section as the rotation rate is varied from 30 to 300 RPM. After the onset of nucleate boiling, the heat transfer coefficient increases for all the rotation rates at the same rate as shown in Fig. 6.11(B). This is due to the fact that heat transfer in the subcooled boiling region is primarily due to nucleation which is not significantly influenced by the rotation rate.

At the inlet, the local heat transfer coefficient increases with increasing rotation rate as shown in Fig. 6.11(B) [Kuo *et al.* (1960), Sections 4.4.3 and 5.4.5]. The local heat transfer coefficient decreases along the length of the test section before the onset of nucleation. The decreasing local heat transfer coefficient can be divided into two sections depending on their slope. The change in the slope of the decreasing local heat transfer coefficient appears at approximately 240 mm, 300 mm and 450 mm at 30 RPM, 150 RPM and 300 RPM respectively as shown in Fig. 6.11(B). The initial drop in heat transfer coefficient is due to the loss of heat as a result of interface mass transfer [Shmerler and Mudawwar (1988b)]. Further, the heat transfer coefficient drop per unit length increases with the formation of local dry sections leading to the loss of heat transfer area to water [Fujita and Ueda (1978)]. The increasing rotation rate delays the appearance of local dry sections and hence the drop in local heat transfer coefficient associated to this effect appears further downstream.

The loss of liquid due to phase change remained constant at 10 ml/min (0.6 LPH), throughout the range of rotation rates explored. Hence, the effect of rotation rate on the heat transfer coefficient post onset of nucleate boiling is negligible. Also, the rotation rate did not influence the rate of liquid loss.

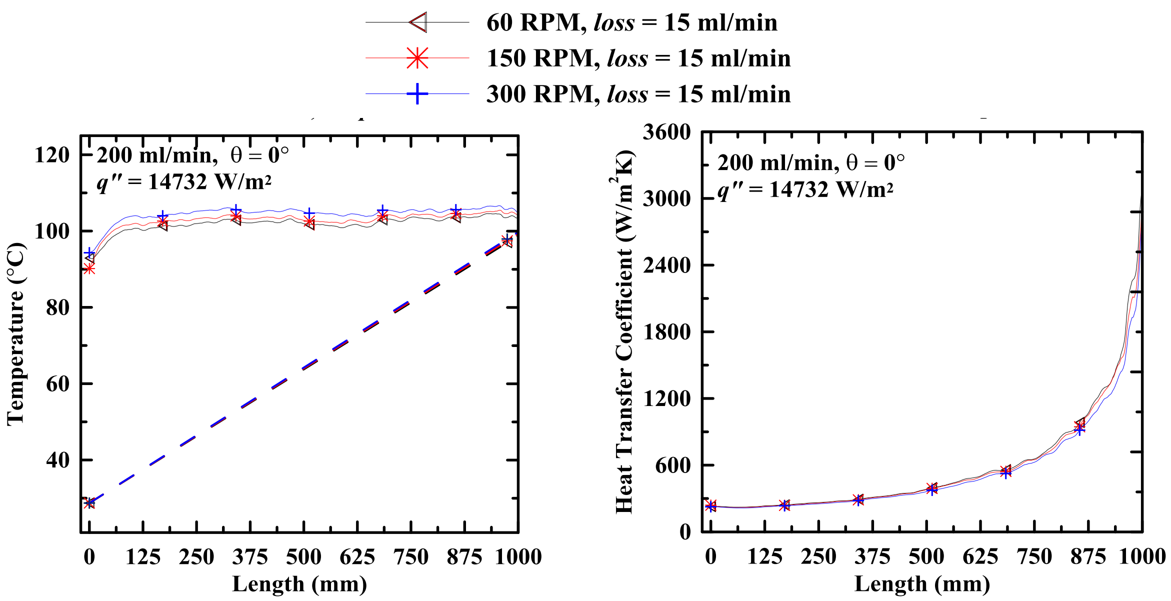

(A) Temperature profile

200 ml/min, θ = 0°, q'' = 14732 W/m^2

(B) Heat transfer coefficient

200 ml/min, θ = 0°, q'' = 14732 W/m^2

Fig. 6.12 Local temperature and heat transfer coefficient variation in a partially filled horizontal rotating evaporator at a constant flow rate, wall heat flux and variable rotation rates (12 LPH, Re_f = 213)

The wall heat flux is increased to 14732 W/m^2 while the other parameters i.e. volume flow rate of water and the pipe inclination angle is maintained constant at 200 ml/min (12 LPH) and 0° respectively. The rotation rate is increased gradually from 60 to 300. The local wall, bulk fluid temperature and the local heat transfer coefficient along the length of the partially filled rotating evaporator are plotted in Figs. 6.12(A) and 6.12(B) respectively. With increasing rotation rate, the wall temperatures at all the rotation rates reach average temperatures of 102.36 °C, 103.35 °C and 104.92 °C i.e. above the saturation temperature of water (99.9°C) within the first 50 mm from the inlet of the rotating test section (Zone II). The liquid film thickness on the rotating wall comparatively increases with increasing rotation rate [Ashmore *et al.* (2003)]. The increase in film thickness leads to a relative increase in local resistance to heat transfer. Hence, with increasing rotation rate, the wall temperature saturates at a marginally higher temperature.

Onset of nucleation is estimated to be achieved at wall temperatures above 100.8–100.9 °C using Eqn. (6.6). Post the onset of nucleation point, the heat transfer coefficient for all the rotation rate increases at the same rate as shown in Fig. 6.12(B). The loss of liquid remains constant at 15 ml/min (0.9 LPH) throughout the rotation rate range explored. Thus as stated before, the effect of rotation rate on the heat transfer coefficient post onset of nucleate boiling is negligible.

The results effectively signify that in a rotary evaporator, a minimum rotation rate, just enough to maintain a constant wet film across the inner wall is sufficient at different operating conditions (Inclination, liquid volume flow rate and wall heat flux). Lin and Faghri (1999) experimentally demonstrated that rotation rate has negligible enhancement effect on the heat transfer characteristics in the evaporation section of a rotating heat pipe. Various experimental results highlighting the effect of rotation rate on heat transfer in a partially filled rotating evaporator are shown in Appendix D Figs. D.15 (A)-(D).

6.4.6 Correlation for outlet liquid fraction

Based on the results discussed in the previous section, the variation in the rate of liquid loss depends on the wall heat flux supplied and the liquid volume flow rate. The outlet liquid fraction is defined as given by Eqn. (6.7)

$$\dot{Q}_{Outfrac} = \frac{\dot{Q}_{in} - \dot{Q}_{loss}}{\dot{Q}_{in}} \tag{6.7}$$

where, the experimental range varies between 1 to 0.75. A correlation to predict the outlet liquid fraction ($\dot{Q}_{Outfrac}$) based on the experimental boiling numbers (Bo) in a partially filled rotating evaporator is developed as given by Eqn. (6.8). The correlation predicts within an average deviation is 5% from the experimental data. A total of 305 data points have been used to derive the correlation. A comparison between the present experimental values and the correlation is presented in Fig. 6.13.

$$\dot{Q}_{Outfrac} = -16493 \times Bo^2 - 48.05 \times Bo + 1.056 \tag{6.8}$$

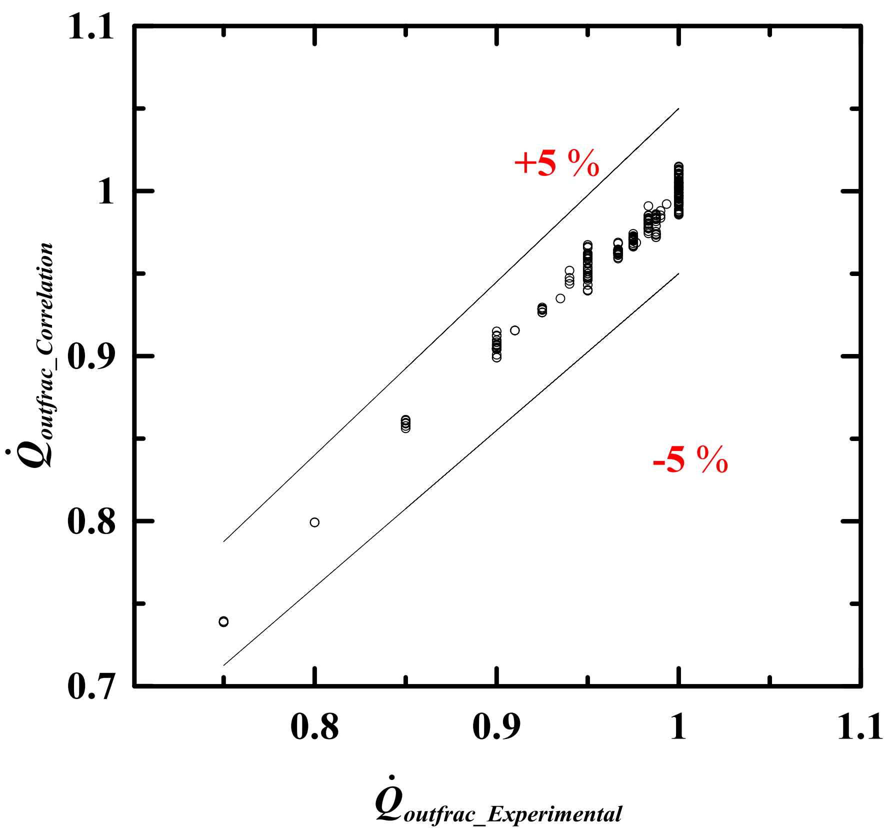

Fig. 6.13 Comparison of correlation with experimental results

6.5 Conclusions

Experimental investigation of heat transfer characteristics in a partially filled rotating evaporator with continuous liquid flow is reported in this study. Flow rate range of 100-400 ml/min (6 – 24 LPH), rotation rate range of 10-300 RPM, wall heat flux range of 3203-22524 W/m^2 are investigated, while the inclination angle is varied from 0° and 6°. Local heat transfer coefficient along the length of a partially filled rotating evaporator is reported.

- At a given set of operating conditions, as the inclination angle increases, pool holdup reduces and in turn reduces the heat transfer. Thus, the zone of constant temperature region increases in length with inclination angle.
- Heat transfer decreases due to the reduction in the wall-liquid contact area as a result of the film break up at high heat flux. Decrease in fluid viscosity with increase in temperature leads to the thinning of the liquid film. At high heat flux, the decrease in the film thickness leads to the break-up of the liquid film wetting the rotating wall thus forming dry sections. The breakup of the thin film as a result of imbalance in the film dynamic pressure and surface tension leads to the formation of local dry patches, thus reducing the heat transfer area to water and the consequent rise in wall temperature. Local heat transfer coefficient also reduces as a result of loss of heat from the water air interface as a result of mass transfer.
- With increasing wall heat flux, a higher wall temperature is realised. The wall temperature reaches saturation temperature earlier i.e. onset of nucleate boiling is realised closer to the inlet. Once saturation temperature is realised, wall temperature variation with heat flux is negligible as majority of the energy supplied is consumed as heat of vaporisation by water thus increasing overall loss of liquid and heat transfer coefficient at the exit
- Increasing the liquid volume flow rate at a constant rotation rate, inclination angle and wall heat flux leads to an increase in the liquid pool height inside the rotating evaporator. This leads to an increase in wall cooling effectively supressing the onset of nucleation.
- At constant volume flow rate, wall heat flux and inclination angle as the rotation rate is increased; the recirculating region inside the pool enhances heat transfer and cools

the wall further. This leads to a delay in the rise in wall temperature and a longer Zone I.

- At constant volume flow rate, wall heat flux and inclination angle as the rotation is increased, the flow pattern inside the rotating test section changes. The fluid increasingly spreads along the inner wall with increasing rotation rate. Hence, the liquid film thickness on the rotating wall increases. The increase in the film thickness increases the resistance to the heat transfer. Hence, a comparatively higher wall temperature is realised in Zone II with increasing rotation rate.
- Once the onset of nucleation is realised, heat transfer is primarily governed by the nucleation. After the onset of nucleate boiling, rotation rate has negligible influence on the heat transfer coefficient.
- Rate of liquid loss is not influenced substantially by the inclination angle and the rotation rate. A correlation based on Boiling number is developed to predict the overall outlet liquid fraction based on experimental values.
- Based on the experimental results, it is recommended to operate a partially filled rotary evaporator with some degree of inclination. The inclination will ensure unidirectional flow of fluid and earlier onset of nucleation. A minimum rotation rate should be maintained to ensure wetting of the inner wall at operational wall heat fluxes. Rate of liquid loss is directly dependent on the fluid volume flow rate and the applied wall heat flux. The same should be modulated based on volume reduction requirements at the exit.
- It is recommended that multi-zone heating be used such that initial low temperature zone can utilize the pipe inner surface more effectively. As the heat transfer area

reduces subsequently due to dry patches, heating can be improved employing higher heat flux/wall temperature leading to efficient volume reduction at boiling condition.

6.6 Contributions of the present work

The current work reports a comprehensive study of the various factors influencing heat transfer process inside a partially filled rotating evaporator. The influence of pipe inclination, liquid volume flow rate, rotation rate, wall heat flux on the behaviour of a partially filled rotating evaporator are discussed using local data sets. Correlation is derived to predict the average outflow liquid fraction at particular wall heat flux and liquid volume flow rate. It is recommended to operate partially filled rotating evaporators with some degree of inclination, minimum rotation rate to maintain a wet film on the inner wall and a high wall heat flux depending upon the application.

CHAPTER 7

CONCLUSIONS AND SCOPE FOR FUTURE WORK

7.1 Conclusions

Fluid flow and heat transfer inside a partially filled rotating system with continuous inflow and out of liquid is studied. To understand the effect of various parameters i.e. fluid flow rate, pipe rotation rate, pipe inclination, pipe diameter and pipe length, detailed experimental flow visualisation studies are conducted. Experiments are performed to study the effect of pipe rotation rate, inclination angle, liquid volumetric flow rate and wall heat flux in single phase and two phase flow inside a partially filled rotating heated pipe. Water is used as the flow medium and the experiments are conducted at atmospheric pressure. The wall temperature is measured using infra-red thermal imaging technique with an image resolution of 1.9mm/pixel. Wall temperature is measured in axial direction.

Influence of flow transition on single phase and evaporative heat transfer in a partially filled rotating heated pipe is studied experimentally and reported in Chapters 4, 5 and 6. There are no available correlations in the literature to predict the heat transfer characteristics of a partially filled rotating heated pipe with continuous inflow and outflow of fluid. Hence, correlations are developed to predict single phase Nusselt number and the outlet liquid fraction in a partially filled rotary evaporative operating in continuous mode.

7.2 Flow transitions in a partially filled rotating inclined pipe with continuous flow

Flow transitions in a partially filled, rotating inclined smooth pipe with axial liquid (water) flow is experimentally investigated. The effects of flow rate, pipe inclination, diameter and length on the flow transitions are reported in Chapter 3.

(1) Rotational speeds for flow transitions to *annular flow* and *collapse of annular flow* systematically reduce as the angle of inclination is increased.

(2) The gap between the *annular flow* and *collapse of annular flow* also reduces with increase in inclination. These effects are on account of the reduction in the liquid hold up in the pipe due to gravitational pull, which increases with angle of inclination.

(3) For a larger diameter pipe, the flow transition occurs at a lower rotational speed.

(4) Flow transition in a rotating pipe is virtually independent of the pipe length.

(5) A flow regime map is developed based on flow Reynolds number and rotation Froude number.

7.3 Heat transfer in a partially filled rotating pipe with single phase flow

Single phase heat transfer in a partially filled horizontal rotating heated pipe with continuous axial liquid flow has been experimentally investigated. Flow rate is varied between 100~1350 ml/min (6 – 81 LPH) (Horizontal) and 100~830 ml/min (6 – 50 LPH) (Inclined). The rotation rate has been varied between 10-309 RPM while the inclination angle is varied from 0°-6°. Heat flux to the system has been varied without triggering phase change of water. Local heat transfer coefficient along the length of a partially filled rotating horizontal and inclined pipe is reported in Chapters 4 and 5 respectively.

(1) Increasing wall heat flux improves the local heat transfer coefficient in the partially filled rotating heated pipe at a constant liquid flow rate and pipe rotation rate.

(2) A secondary heat transfer from the inner air to water through the free surface interface contributes to the improvement in heat transfer coefficient as the wall heat flux is increased.

(3) Heat transfer coefficient in the partially filled rotating heated pipe improves with increasing liquid flow rate. The improvement is related to an increase in liquid pool height inside the partially filled rotating pipe. The increase in pool height provides larger mixing volume and enhances heat transfer.

(4) As the rotation rate is varied for a constant wall heat flux and water flow rate, the flow pattern inside the partially filled rotating pipe changes. Increasing the rotation rate at a constant flow rate and heat flux improves the heat transfer coefficient in the partially filled rotating heated pipe. The secondary flow inside the recirculating region of the liquid pool improves the heat transfer coefficient as the rotation is increased.

(5) With increasing inclination angle a decrease in local heat transfer coefficient in a partially filled inclined rotating heated pipe is observed. The liquid volumetric flow rate, rotation rate and wall heat flux are maintained constant. The decrease in the heat transfer coefficient is attributed to the decrease in liquid pool height inside the rotating pipe with increasing inclination angle.

(6) A correlation based on the governing dimensionless numbers is developed to predict the average Nusselt number within 15% average deviation from the experimental values.

(7) Based on the experimental results, it is recommended to operate partially filled rotating pipe heat transfer equipment in nearly horizontal configuration for maximum heat transfer within the experimental domain of this study.

7.4 Heat transfer in a partially filled rotary evaporator

Experimental investigation of heat transfer characteristics in a partially filled rotating evaporator with continuous axial liquid flow is reported in this study. Flow rate range of 100-400 ml/min (6 – 24 LPH), rotation rate range of 10-300 RPM, wall heat flux (3203-22524 W/m^2) are investigated, while the inclination angle is varied from 0° and 6°. Local heat transfer coefficient along the length of a partially filled rotating evaporator is reported in Chapter 6.

(1) With increasing inclination angle, the liquid pool holdup inside the rotary evaporator reduces thus reducing the heat transfer. This leads to a longer constant temperature region.

(2) At comparatively higher heat fluxes, imbalance in the film dynamic pressure and surface tension leads to the break-up of the thin liquid film wetting the rotating wall thus forming dry sections. Formation of dry patches effectively reduces local heat transfer area to water. This leads to the rise in wall temperature. Local heat transfer coefficient also reduces as a result of loss of heat from the water air interface as a result of mass transfer.

(3) A higher wall temperature is realised at a higher wall heat flux. The wall temperature reaches saturation and an early onset of nucleate boiling is realised closer to the inlet with increasing wall heat flux. Once saturation temperature is realised, wall temperature variation with heat flux is negligible as majority of the energy supplied is consumed as heat of vaporisation by water. Higher wall heat flux leads to higher overall evaporation rates and heat transfer coefficient at the exit.

(4) Increasing the liquid volume flow rate at constant rotation rate, inclination angle and wall heat flux leads to an increase in the liquid pool height inside the rotating evaporator. Increased liquid holdup inside the rotary evaporator improves wall cooling and effectively supressing the onset of nucleation.

(5) At a constant volume flow rate, wall heat flux and inclination angle as the rotation rate is increased; the secondary flows inside the pool enhance heat transfer and cools down the wall. This leads to a delay in the rise in wall temperature and onset of nucleation.

(6) With increasing rotation rate, the flow pattern inside the rotating test section changes. The liquid film thickness on the rotating wall increases with increasing rotation rate. The increase in the film thickness increases the resistance to the heat transfer. Hence, the wall temperature saturates at a comparatively higher temperature at a higher rotation rate.

(7) Once the onset of nucleation is realised, heat transfer is primarily governed by the nucleation. After the onset of nucleate boiling, rotation rate has negligible influence on the heat transfer coefficient.

(8) Evaporation rate is not influenced substantially by the inclination angle and the rotation rate. A correlation based on Boiling number is developed to predict the overall outlet liquid fraction based on experimental values.

(9) Based on the experimental results, it is recommended to operate a partially filled rotary evaporator with some degree of inclination. The inclination will ensure unidirectional flow of fluid and earlier onset of nucleation. A minimum rotation rate should be maintained to ensure wetting of the inner wall at operational wall heat fluxes. Evaporation rate is directly dependent on the fluid volume flow rate and the

applied wall heat flux. The same should be modulated based on evaporation requirement at the exit.

(10) It is recommended that multi-zone heating be used such that, initial low temperature zone can utilize the pipe inner surface more effectively. As the heat transfer area reduces subsequently (local dry up), heating can be improved employing higher heat flux/wall temperature leading to efficient evaporation at boiling condition.

7.5 Contributions of the present work

Following are the key contribution of the present work;

(1) The study presents a comprehensive literature review on fluid mechanics, single phase and evaporative heat transfer coefficients in partially filled rotating systems.

(2) The work presents a flow regime map which can be used to assess the flow patterns inside partially filled rotating pipes where visualisation is not a possibility. This work is expected to provide a basis for predicting critical rotational speeds for flow transitions in partially filled rotating pipes, which can be used for different industrial applications.

(3) The work presents a technique to measure the local wall temperature through infrared thermal imaging technique. The technique helps to calculate local heat transfer coefficient.

(4) Local temperature and heat transfer coefficient distribution presented in this study would serve as benchmark data for validation of numerical results.

(5) The present work helps to understand the effect of wall heat flux, fluid flow rate, inclination angle and rotation rate on single phase and evaporative heat transfer in a partially filled rotating system operating in continuous mode. The data is useful in designing rotary evaporation systems for industrial application.

(6) Correlations are developed to accurately calculate single phase Nusselt numbers in partially filled rotating heated pipes with continuous inflow and outflow of water.

(7) Simple correlation is derived based on experimental result to accurately compute evaporation rates at the exit of a partially filled rotary evaporator.

7.6 Suggested correlations from the present work

Following are the correlations suggested to predict the critical flow transitions, single phase Nusselt numbers and outlet fluid flow fraction in horizontal and inclined partially filled rotating pipe systems with continuous inflow and outflow of liquid.

(1) Critical rotational Froude number for flow transitions in partially filled rotating horizontal and inclined pipes with continuous inflow and outflow of fluid

Flow pattern	Fr_φ
Continuous pool with stable/wavy front	0.01 – 1
Fluid pendant	0.06 – 0.8
Smooth and Shark tooth	0.9 – 6.65
Annular	$Fr_\varphi > 2.4 + 2 \times 10^{-3} Re'_f$

The range is valid for all inclination angles and pipe diameters explored in the present experimental study i.e. $Re'_f = D_h V/\nu$ = 258 – 3803 and $Fr_\varphi = \omega^2 R/g$ = 0.01 – 27.14.

(2) Single phase Nusselt number in horizontal partially filled rotating heated pipe with continuous inflow and outflow of water

$$Nu_{Horizontal} = 1.72\, {Re_\phi}^{0.18} \gamma^{0.39} {Re_f}^{0.52}$$

The above correlation is valid for the experimental conditions explored in this study i.e. $Re_f = 4\dot{Q}\rho/\pi\mu D =$ 87 – 1098, $Pr = C_p\mu/k \approx$ 4.93, $Re_\phi = \rho\omega D^2/\mu =$ 815 – 53210, $\gamma = \pi D^2 q''/4\rho\dot{Q}C_p T_{in}$ = 1.22 × 10^{-3} – 1.12 × 10^{-2} and $Nu = hD/k$ = 8 – 67..

(3) Single phase Nusselt number in inclined partially filled rotating heated pipe with continuous inflow and outflow of water

$$Nu_{Inclined}/Nu_{Horizontal} = 1.05Fr^{0.11}$$

The above correlation is valid for the experimental conditions explored in this study i.e. $Re_f = 4\dot{Q}\rho/\pi\mu D = 84 – 730$, $Pr = C_p\mu/k \approx 4.95$, $Fr = 16\,\dot{Q}^2/\pi^2 g \sin\theta\, D^5 = 1.24 \times 10^{-4} – 1.45 \times 10^{-2}$, $Re_\phi = \rho\omega D^2/\mu = 1613 – 51615$, $\gamma = \pi D^2 q''/4\rho\dot{Q}C_pT_{in} = 4.61 \times 10^{-3} – 6.39 \times 10^{-2}$ and $Nu = hD/k = 5 – 81$.

(4) Outlet liquid fraction at the exit of a partially filled rotating evaporator with continuous inflow and outflow of water

$$\dot{Q}_{Outfrac} = -16493 \times Bo^2 - 48.05 \times Bo + 1.056$$

The above correlation is valid for the experimental conditions explored in this study i.e. $Re_f = 4\dot{Q}\rho/\pi\mu D = 81 – 336$, $Bo = \pi q"D^2/4\dot{Q}\rho\lambda = 0.7 \times 10^{-3} – 3.17 \times 10^{-3}$, $Pr = C_p\mu/k = 3.69 – 6.79$, $\dot{Q}_{Outfrac} = (\dot{Q}_{in} - \dot{Q}_{loss})/\dot{Q}_{in} = 1 – 0.75$ and $Re_\phi = \rho\omega D^2/\mu = 1934 – 53909$.

7.7 Scope for future work

Partially filled rotating heating systems may find applications in industries treating thermally unstable compounds which require very small residence time inside a heater. Furthermore, since this system can handle liquid with suspension, it can be used for waste management operation. The following aspects may be considered for future work;

(1) Since the amount of evaporation achieved is only about 10-15% of the incoming liquid, experimental study at higher wall fluxes can be performed using multi-zone heating along with local bulk fluid temperature measurements.

(2) Liquid film thickness measurement in continuous systems is only reported for isothermal conditions by Singaram *et al.* (2014). Further experimental

investigation of film thickness variation and breakup inside a partially filled rotating continuous system may be taken up as a future study for deriving empirical correlations to predict the liquid film thickness in non-isothermal partially filled rotating continuous systems.

(3) Comprehensive 3D numerical study can be performed to study the underlying flow physics and heat transfer phenomena in greater detail. Available local experimental data may be used for validating the model.

(4) The current study may be extended to operations at reduced pressure. Reactive fluids and fluids with suspension may also be included in the study.

(5) The evaporator may be further extended to a calciner for treating slurry and solids.

APPENDIX A

CALIBRATION OF INSTRUMENTS

In the experimental study, a number of measuring instruments are used to determine heat transfer coefficient and fluid flow through the test sections. These include thermocouples and Infra-red thermal camera. Additionally, AC voltage and current meters are used to measure the heat input. All the measuring devices are calibrated inside the lab and their uncertainties are determined.

A.1 Calibration of thermocouples

The K-type (Chromel-Alumel) thermocouples are calibrated with respect to standard thermometer. All thermocouples and thermometer immersed in oil bath at same level. The oil bath equipped with a thermostat is used to control the rate of heat supplied to oil bath. The calibration process is started by adjusting the thermostat to a specific temperature. The bath is left for approximately 15 minutes to reach steady state temperature. Reading of thermocouples and thermometer is recorded. Then, the thermostat set to a new point and the procedure is repeated. The reading of thermometer is recorded in degree Centigrade (°C). The thermocouples are connected to a data logger. The electrical wiring diagram of thermocouple circuit is shown in Fig. A.1(A). Reading of the thermocouple is measured from voltmeter in voltage. The calibration curve for thermocouple is shown in Fig. A.2.

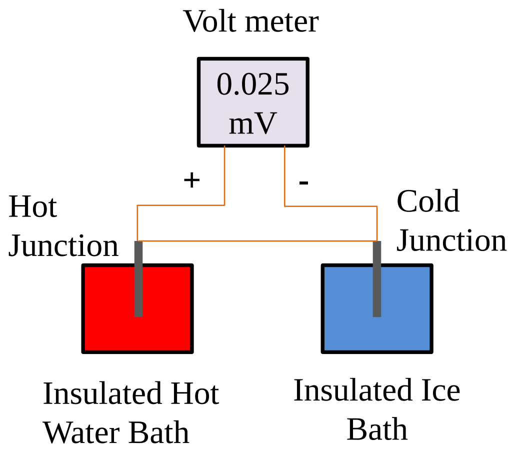

(A) Electrical wiring diagram of thermocouple

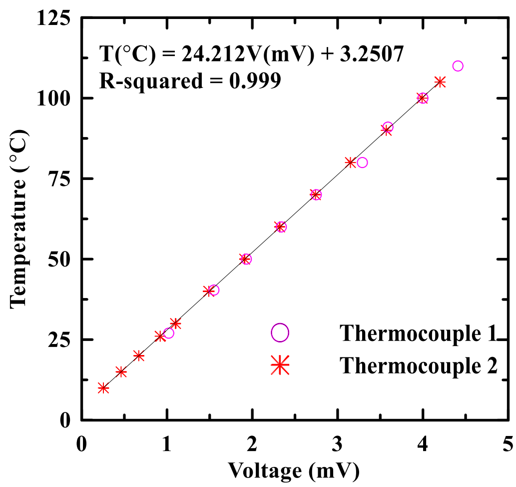

(B) Thermocouple calibration chart

Fig. A.1 Thermocouple calibration

A.2 Calibration of IR thermal camera

Thermal infrared camera reads the temperature of the plate depending on the emissivity value of the surface of the plate. Therefore, it is necessary to calibrate the emissivity of the surface. This is done by constructing a 50mm × 50mm × 8mm copper solid cube. Copper has high Peclet number and hence behaves as a lumped body. Four thermocouples are drilled 10 mm inside copper cube at four edges (50mm × 8mm) of cube. Front surface (50mm × 50mm) is painted with high temperature black board paint to achieve uniform emissivity all over the surface. The back surface (50mm × 50mm) is heated by supplying electric current in Nichrome tape. The Nichrome has high resistance hence heat is generated through Joule heating. The fiberglass tape is kept between copper cube and Nichrome tape. DC power supply is used to supply constant current in Nichrome tape. The cube is insulated from the five sides and one side with black paint is kept open to the atmosphere. Initially, low current is passed and then increases in small amount. The temperature of the copper cube is observed through thermocouples. Once, the temperature reaches steady state, thermal images of the free surface is captured through a thermal camera. Ten thermal images are captured at the interval of 1 min between two images. The emissivity input to the images is then adjusted till the temperature read by the image is the same as that read by the average of thermocouples. The temperature read by all four thermocouples are within the difference of less than 0.5 ºC. This procedure is repeated for different temperatures of the exposed surface till it reaches 110 ºC. The emissivity is found to be 0.69. The calibration curve for thermal camera is shown in Fig. A.2.

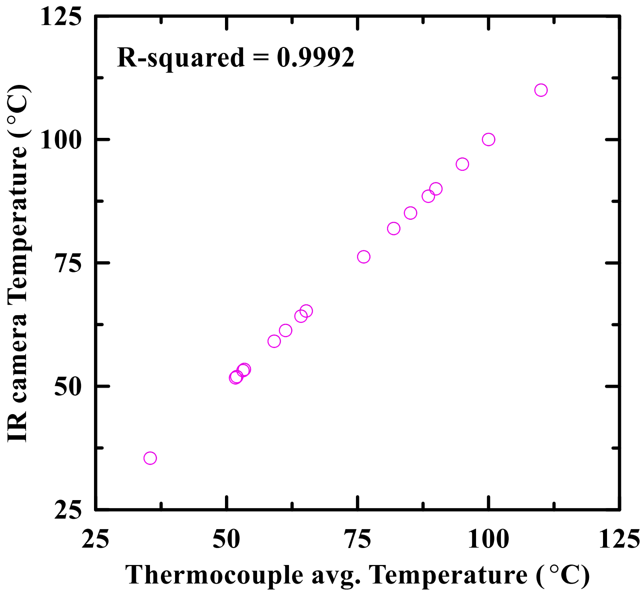

Fig. A.2 Calibration of Infra-red thermal camera

APPENDIX B

EXPERIMENTAL UNCERTAINTIES

B.1 Parameters in Chapter 3

The calculation methodology to calculate the uncertainty in flow Reynolds number is provided below

Reynolds number is calculated as

$$Re_f = \frac{D_h V}{\nu} \tag{B.1.1}$$

Absolute uncertainty in Reynolds number σ_{Re_f} is calculated using multivariate propagation of error formula [Navidi 2008].

$$\sigma_{Re_f} = \sqrt{\left(\frac{\partial Re_f}{\partial V}\right)^2 {\sigma_V}^2 + \left(\frac{\partial Re_f}{\partial D_h}\right)^2 {\sigma_{D_h}}^2} \tag{B.1.2}$$

where, σ_V is the uncertainty in velocity measurement, σ_{D_h} is the uncertainty in hydraulic diameter calculation, v is the kinematic viscosity of water.

The partial derivative of Reynolds number Re_f based on velocity '*V*' and hydraulic diameter 'D_h' is therefore

$$\frac{\partial Re_f}{\partial V} = \frac{D_h}{v} \tag{B.1.3}$$

$$\frac{\partial Re_f}{\partial D_h} = \frac{V}{v} \tag{B.1.4}$$

The absolute uncertainty in flow velocity $V = \dot{Q}/A_{pool}$ is calculated as

$$\sigma_V = \sqrt{\left(\frac{1}{A_{pool}}\right)^2 \sigma_{\dot{Q}}{}^2 + \left(\frac{-\dot{Q}}{A_{pool}{}^2}\right)^2 \sigma_{A_{pool}}{}^2} = 0.00682 \text{ m/s} \tag{B.1.5}$$

where, $\overline{A_{pool}} = 42.5\ mm^2$ is the average pool cross sectional area, $\dot{Q} = 8.611$ ml/sec is the average volume flow rate, $\sigma_{\dot{Q}}$ =1.5 ml/min is the least count of the peristaltic pump and $\sigma_{A_{pool}} =$ 1.42 mm^2 $^{\text{is}}$ the uncertainty in pool cross sectional area measurement based on stationary pipe liquid holdup experimental data.

The absolute uncertainty in hydraulic diameter $D_h = 4A_{pool}/R\beta$ is calculated as

$$\sigma_{D_h} = \sqrt{\left(\frac{\partial D_h}{\partial A_{pool}}\right)^2 \sigma_{A_{pool}}{}^2 + \left(\frac{\partial D_h}{\partial R}\right)^2 \sigma_R{}^2 + \left(\frac{\partial D_h}{\partial \beta}\right)^2 \sigma_\beta{}^2} \tag{B.1.6}$$

$$= \sqrt{\left(\frac{4}{R\beta}\right)^2 \sigma_{A_{pool}}{}^2 + \left(\frac{-4A_{pool}}{R^2\beta}\right)^2 \sigma_R{}^2 + \left(\frac{-4A_{pool}}{R\beta^2}\right)^2 \sigma_\beta{}^2} = 0.27 \text{ mm}$$

where, $R = 22$ mm is the average inner radius of the pipe and $\beta = 0.9793°$ is the average angle subtended by liquid pool interface with the centre of the pipe, $\sigma_\beta = 0.3377°$ is the uncertainty in the measurement of the angle subtended by the pool interface "β", $\sigma_R = 0.02$ mm i.e. the least count of the length measurement equipment "Vernier scale".

$$\frac{\partial Re_f}{\partial V} = \frac{D_h}{v} = 7719.23 \text{ s/m}, \ \frac{\partial Re_f}{\partial D_h} = \frac{V}{v} = 301700.93 \text{ m}^{-1}$$

$$\nu = 8.922 \text{ m}^2/\text{s}$$

The absolute uncertainty in Reynolds number is therefore

$$\sigma_{Re_f} = 96.66$$

Average of all the Reynolds number explored in this study is 1783.76

Relative uncertainty in Reynolds number

$$Re_f = \frac{96.66}{1783.76} \times 100 = 5.4192 \text{ \%}$$

Uncertainty in rotational Froude number is provided below

Rotational Froude number is calculated as

$$Fr_\varphi = \frac{\omega^2 R}{g} \tag{B.1.7}$$

Absolute uncertainty in rotational Froude number σ_{Fr_φ} is calculated using multivariate propagation of error formula [Navidi 2008].

$$\sigma_{Fr_\varphi} = \sqrt{\left(\frac{\partial Fr_\varphi}{\partial R}\right)^2 \sigma_R{}^2 + \left(\frac{\partial Fr_\varphi}{\partial \omega}\right)^2 \sigma_\omega{}^2} \tag{B.1.8}$$

where, $\sigma_R = 0.02$ mm is the uncertainty in length measurement, $\sigma_\omega = 0.0522$ rad/sec is the uncertainty in rotation measurement

The partial derivative of rotation Froude number Fr_φ based on radius 'R' and rotation rate 'ω' is therefore

$$\frac{\partial Fr_\varphi}{\partial R} = \frac{\omega^2}{g} = 117.34 \text{ m}^{-1}, \ \frac{\partial Fr_\varphi}{\partial \omega} = \frac{2\omega R}{g} = 0.1552 \text{ s}$$

The absolute uncertainty in rotation Froude number is therefore

$$\sigma_{Fr_\varphi} = 0.0082$$

Average of all the rotational Froude number explored in this study is 3.828

Relative uncertainty in Reynolds number

$$Re_f = \frac{0.0082}{3.828} \times 100 = 0.21 \text{ \%}$$

B.2 Parameters in Chapter 4

A sample calculation methodology to compute experimental uncertainty is provided below

Uncertainty in flow Reynolds number is calculated as

$$Re_f = \frac{4\dot{Q}\rho}{\pi\mu D} \tag{B.2.1}$$

Absolute uncertainty in Reynolds number σ_{Re_f} is calculated using multivariate propagation of error formula [Navidi 2008].

$$\sigma_{Re_f} = \sqrt{\left(\frac{\partial Re_f}{\partial \dot{Q}}\right)^2 \sigma_{\dot{Q}}{}^2 + \left(\frac{\partial Re_f}{\partial D}\right)^2 \sigma_D{}^2} \tag{B.2.2}$$

where, $\sigma_{\dot{Q}}$ is the uncertainty in flow measurement, μ is the kinematic viscosity of water.

The partial derivative of Reynolds number $\mathrm{Re_f}$ based on volume flow rate '$\dot{Q}$' is therefore

$$\frac{\partial Re_f}{\partial \dot{Q}} = \frac{4}{\pi v D} \tag{B.2.3}$$

$$\frac{\partial Re_f}{\partial D} = -\frac{4\dot{Q}}{\pi v D^2} \tag{B.2.4}$$

where, $\dot{Q} = 8.92 \times 10^{-6}$ m^3/sec is the average volume flow rate, $\sigma_{\dot{Q}}$ =1.5 ml/min is the least count of the peristaltic pump, $\sigma_D = 0.02$ mm i.e. the least count of the length measurement equipment "Vernier scale". The kinematic viscosity is calculated as $v = 7.46 \times\ 10^{-7}$ m^2/s.

$$\frac{\partial Re_f}{\partial \dot{Q}} = \frac{4}{\pi v D} = 5.2 \times\ 10^7 \text{ s/m}^3 \tag{B.2.5}$$

$$\frac{\partial \mathrm{Re_f}}{\partial \mathrm{D}} = -\frac{4\dot{Q}}{\pi v D^2} = -14161.78 \text{ m}^{-1} \tag{B.2.6}$$

The absolute uncertainty in average Reynolds number is therefore

$$\sigma_{Re_f} = 1.33$$

Average of all the Reynolds number explored in this study is 434.06

Average relative uncertainty in Reynolds number

$$Re_f = \frac{1.33}{434.06} \times 100 = 0.306\ \%$$

Uncertainty in heat transfer coefficient is calculated as

$$h = \frac{q"}{(T_w - T_b)} \tag{B.2.7}$$

Absolute uncertainty in heat transfer coefficient σ_h is calculated using multivariate propagation of error formula [Navidi 2008].

$$\sigma_h = \sqrt{\left(\frac{\partial h}{\partial q"}\right)^2 {\sigma_{q"}}^2 + \left(\frac{\partial h}{\partial (T_w - T_b)}\right)^2 {\sigma_T}^2} \tag{B.2.8}$$

where, $\sigma_{q"}$ is the uncertainty in heat flux measurement, σ_T is the uncertainty in temperature measurement

The partial derivative of heat transfer coefficient h based on wall heat flux $q"$ and temperature difference $T_w - T_b$ is therefore

$$\frac{\partial h}{\partial q"} = \frac{1}{(T_w - T_b)} = \frac{1}{8.06} \tag{B.2.9}$$

$$\frac{\partial h}{\partial (T_w - T_b)} = -\frac{q"}{(T_w - T_b)^2} = -\frac{4287.09}{8.06} \tag{B.2.10}$$

Heat flux is calculated as

$$q" = \frac{\dot{m} C_p (T_{out} - T_{in})}{A_{surface}} \tag{B.2.11}$$

The absolute uncertainty in heat flux is calculated as

$$\sigma_{q"} = \sqrt{\left(\frac{C_p (T_{out} - T_{in})}{A_{surface}}\right)^2 {\sigma_{\dot{m}}}^2 + \left(\frac{\dot{m} C_p}{A_{surface}}\right)^2 {\sigma_T}^2} = 180.64\ \mathrm{W/m^2} \tag{B.2.12}$$

where, $A_{surface} = 0.103$ m^2 is the average heat transfer are, $C_p = 4183.11$ J/ Kg K is the average heat capacity of water in the experimental conditions, $\sigma_{\dot{m}} = 2.48 \times 10^{-5}$ kg/s is the least count of the peristaltic pump and $\sigma_T = 0.5$ °C is the uncertainty in temperature measurements

The absolute uncertainty in average heat transfer coefficient is therefore

$$\sigma_h = \sqrt{\left(\frac{1}{8.06}\right)^2 (180.64)^2 + \left(-\frac{4287.09}{8.06}\right)^2 (0.5)^2} = 39.83 \text{ W/m}^2 \text{ K} \tag{B.2.13}$$

Average of the entire heat transfer coefficient reported in this study is 504.51 W/m^2 K

Average relative uncertainty in heat transfer coefficient

$$h = \frac{39.83}{504.51} \times 100 = 7.89\ \%$$

B.3 Parameters in Chapter 5

A sample calculation methodology to compute experimental uncertainty is provided below

Uncertainty in flow Reynolds number is calculated as

$$Re_f = \frac{4\dot{Q}\rho}{\pi\mu D} \tag{B.3.1}$$

Absolute uncertainty in Reynolds number σ_{Re_f} is calculated using multivariate propagation of error formula [Navidi 2008]

$$\sigma_{Re_f} = \sqrt{\left(\frac{\partial Re_f}{\partial \dot{Q}}\right)^2 {\sigma_{\dot{Q}}}^2 + \left(\frac{\partial Re_f}{\partial D}\right)^2 {\sigma_D}^2} \tag{B.3.2}$$

where, $\sigma_{\dot{Q}}$ is the uncertainty in flow measurement, μ is the kinematic viscosity of water.

The partial derivative of Reynolds number Re_f based on volume flow rate '$\dot{Q}$' is therefore

$$\frac{\partial Re_f}{\partial \dot{Q}} = \frac{4}{\pi v D} \tag{B.3.3}$$

$$\frac{\partial Re_f}{\partial D} = -\frac{4\dot{Q}}{\pi v D^2} \tag{B.3.4}$$

where, $\dot{Q} = 6.75 \times 10^{-6}$ m^3/sec is the average volume flow rate, $\sigma_{\dot{Q}}$ =1.5 ml/min is the least count of the peristaltic pump, $\sigma_D = 0.02$ mm i.e. the least count of the length measurement equipment "Vernier scale". The kinematic viscosity is calculated as $v = 7.47 \times\ 10^{-7}$ m^2/s.

$$\frac{\partial Re_f}{\partial \dot{Q}} = \frac{4}{\pi v D} = 5.20 \times\ 10^7 \text{ s/m}^3 \tag{B.3.5}$$

$$\frac{\partial Re_f}{\partial D} = -\frac{4\dot{Q}}{\pi v D^2} = -10699.99 \text{ m}^{-1} \tag{B.3.6}$$

The absolute uncertainty in average Reynolds number is therefore

$$\sigma_{Re_f} = 1.31$$

Average of all the Reynolds number explored in this study is 356.03

Average relative uncertainty in Reynolds number

$$Re_f = \frac{1.31}{356.03} \times 100 = 0.37\ \%$$

Uncertainty in heat transfer coefficient is calculated as

$$h = \frac{q"}{(T_w - T_b)} \tag{B.3.7}$$

Absolute uncertainty in heat transfer coefficient σ_h is calculated using multivariate propagation of error formula [Navidi 2008]

$$\sigma_h = \sqrt{\left(\frac{\partial h}{\partial q"}\right)^2 \sigma_{q"}{}^2 + \left(\frac{\partial h}{\partial (T_w - T_b)}\right)^2 \sigma_T{}^2} \tag{B.3.8}$$

where, $\sigma_{q"}$ is the uncertainty in heat flux measurement, σ_T is the uncertainty in temperature measurement

The partial derivative of heat transfer coefficient h based on wall heat flux $q"$ and temperature difference $T_w - T_b$ is therefore

$$\frac{\partial h}{\partial q"} = \frac{1}{(T_w - T_b)} = \frac{1}{9.32} \tag{B.3.9}$$

$$\frac{\partial h}{\partial (T_w - T_b)} = -\frac{q"}{(T_w - T_b)^2} = -\frac{4459.54}{9.32} \tag{B.3.10}$$

Heat flux is calculated as

$$q" = \frac{\dot{m}C_p(T_{out} - T_{in})}{A_{surface}} \tag{B.3.11}$$

The absolute uncertainty in heat flux is calculated as

$$\sigma_{q"} = \sqrt{\left(\frac{C_p(T_{out}-T_{in})}{A_{surface}}\right)^2 \sigma_{\dot{m}}{}^2 + \left(\frac{\dot{m}C_p}{A_{surface}}\right)^2 \sigma_T{}^2} = 137.47 \text{ W/m}^2 \tag{B.3.12}$$

where, $A_{surface}$ = *0.103 m*^{2} is the average heat transfer are, C_p = 4183.23 J/ Kg K is the average heat capacity of water in the experimental conditions, $\sigma_{\dot{m}} = 2.48 \times 10^{-5}$ kg/s is the least count of the peristaltic pump and $\sigma_T = 0.5$ °C is the uncertainty in temperature measurements

The absolute uncertainty in average heat transfer coefficient is therefore

$$\sigma_h = \sqrt{\left(\frac{1}{9.32}\right)^2 (137.47)^2 + \left(-\frac{4459.54}{9.32}\right)^2 (0.5)^2} = 29.56 \text{ W/m}^2 \text{ K} \tag{B.3.13}$$

Average of all the heat transfer coefficient explored in this study is 494.83 W/m^2 K

Average relative uncertainty in Reynolds number

$$h = \frac{29.56}{494.83} \times 100 = 5.97 \%$$

B.4 Parameters in Chapter 6

A sample calculation methodology to compute experimental uncertainty is provided below

Uncertainty in flow Reynolds number is calculated as

$$Re_f = \frac{4\dot{Q}\rho}{\pi\mu D} \tag{B.4.1}$$

Absolute uncertainty in Reynolds number σ_{Re_f} is calculated using multivariate propagation of error formula [Navidi 2008]

$$\sigma_{Re_f} = \sqrt{\left(\frac{\partial Re_f}{\partial \dot{Q}}\right)^2 \sigma_{\dot{Q}}{}^2 + \left(\frac{\partial Re_f}{\partial D}\right)^2 \sigma_D{}^2} \tag{B.4.2}$$

where, $\sigma_{\dot{Q}}$ is the uncertainty in flow measurement, μ is the kinematic viscosity of water.

The partial derivative of Reynolds number Re_f based on volume flow rate '$\dot{Q}$' is therefore

$$\frac{\partial Re_f}{\partial \dot{Q}} = \frac{4}{\pi v D} \tag{B.4.3}$$

$$\frac{\partial Re_f}{\partial D} = -\frac{4\dot{Q}}{\pi v D^2} \tag{B.4.4}$$

where, $\dot{Q} = 4.17 \times 10^{-6}$ m^3/sec is the average volume flow rate, $\sigma_{\dot{Q}}$ =1.5 ml/min is the least count of the peristaltic pump, $\sigma_D = 0.02$ mm i.e. the least count of the length measurement equipment "Vernier scale". The kinematic viscosity is calculated as $v = 6.04 \times 10^{-7}$ m^2/s.

$$\frac{\partial Re_f}{\partial \dot{Q}} = \frac{4}{\pi v D} = 6.43 \times 10^7 \text{ s/m}^3 \tag{B.4.5}$$

$$\frac{\partial Re_f}{\partial D} = -\frac{4\dot{Q}}{\pi v D^2} = -8169.67 \text{ m}^{-1} \tag{B.4.6}$$

The absolute uncertainty in average Reynolds number is therefore

$$\sigma_{Re_f} = 1.61$$

Average of all the Reynolds number explored in this study is 239.27

Average relative uncertainty in Reynolds number

$$Re_f = \frac{1.61}{239.27} \times 100 = 0.67 \text{ \%}$$

Uncertainty in heat transfer coefficient is calculated as

$$h = \frac{q"}{(T_w - T_b)} \tag{B.4.7}$$

Absolute uncertainty in heat transfer coefficient σ_h is calculated using multivariate propagation of error formula [Navidi 2008]

$$\sigma_h = \sqrt{\left(\frac{\partial h}{\partial q"}\right)^2 \sigma_{q"}{}^2 + \left(\frac{\partial h}{\partial (T_w - T_b)}\right)^2 \sigma_T{}^2} \tag{B.4.8}$$

where, $\sigma_{q"}$ is the uncertainty in heat flux measurement, σ_T is the uncertainty in temperature measurement

The partial derivative of heat transfer coefficient h based on wall heat flux $q"$ and temperature difference $T_w - T_b$ is therefore

$$\frac{\partial h}{\partial q"} = \frac{1}{(T_w - T_b)} = 0.03 \tag{B.4.9}$$

$$\frac{\partial h}{\partial (T_w - T_b)} = -\frac{q"}{(T_w - T_b)^2} = -11.21 \tag{B.4.10}$$

Heat flux is calculated as

$$q" = \frac{\dot{m} C_p (T_{out} - T_{in})}{A_{surface}} \tag{B.4.11}$$

The absolute uncertainty in heat flux is calculated as

$$\sigma_{q"} = \sqrt{\left(\frac{C_p (T_{out} - T_{in})}{A_{surface}}\right)^2 \sigma_{\dot{m}}{}^2 + \left(\frac{\dot{m} C_p}{A_{surface}}\right)^2 \sigma_T{}^2} = 181.93 \text{ W/m}^2 \tag{B.4.12}$$

where, $A_{surface} = 0.103$ m^2 is the average heat transfer are, C_p = 4191.68 J/ Kg K is the average heat capacity of water in the experimental conditions, $\sigma_{\dot{m}} = 2.49 \times 10^{-5}$ kg/s is the least count of the peristaltic pump and $\sigma_T = 0.5$ °C is the uncertainty in temperature measurements

The absolute uncertainty in average heat transfer coefficient is therefore

$$\sigma_h = \sqrt{\left(\frac{1}{9.32}\right)^2 (137.47)^2 + \left(-\frac{4459.54}{9.32}\right)^2 (0.5)^2} = 12.52 \text{ W/m}^2 \text{ K} \tag{B.4.13}$$

Average of all the heat transfer coefficient explored in this study is 502.90 W/m^2 K

Average relative uncertainty in Reynolds number

$$h = \frac{12.52}{502.90} \times 100 = 2.48\ \%$$

APPENDIX C

CALCULATION METHODOLOGY

C.1 Cross sectional area of the liquid pool

The calculation methodology to calculate the cross sectional area of the liquid pool (blue) as shown in Fig. C.1.1 is similar to computing the area of a portion of a disk (blue) whose upper bound is circular (arc i.e. "*S*") and lower bond is a chord (liquid pool free surface).

If R is the radius of the pipe, H is the height of the arced portion, a is the length of the chord (liquid pool free surface) and the chord (pool surface) makes a central angle β then the distance of the pool surface from the centre of the pipe cross section is

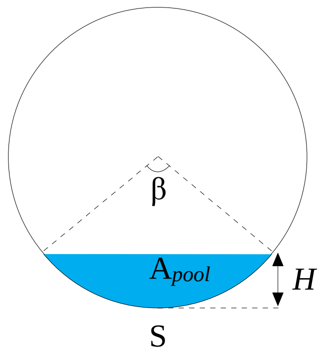

Fig. C.1.1 Liquid holdup in a stationary pipe

$$r = R\cos\left(\frac{\beta}{2}\right) \tag{C.1.1}$$

$$r = \frac{1}{2}a\cot\left(\frac{\beta}{2}\right) = \frac{1}{2}\sqrt{4R^2 - a^2} \tag{C.1.2}$$

The wetted perimeter *S* is the arc length given by Eqn. (C.1.3)

$$S = R\beta \tag{C.1.3}$$

i.e.

$$\beta = 2\cos^{-1}\left(\frac{r}{R}\right) = 2\sin^{-1}\left(\frac{a}{2R}\right) \tag{C.1.4}$$

The length of the chord is

$$a = 2R\sin\left(\frac{\beta}{2}\right) = 2\sqrt{R^2 - r^2} = 2\sqrt{H(2R - H)} \tag{C.1.5}$$

The area of the section inside the liquid pool is given by the area of the circular sector minus the area of the triangular portion i.e. centre of the pipe cross section and the pool interface.

$$A_{pool} = A_{circular\ sector} - A_{triangle} \tag{C.1.6}$$

$$A_{pool} = \frac{1}{2}R^2\beta - \frac{1}{2}ar = R^2\cos^{-1}\left(\frac{r}{R}\right) - r\sqrt{R^2 - r^2} \tag{C.1.7}$$

$$A_{pool} = R^2\cos^{-1}\left(1 - \frac{H}{R}\right) - (R - H)\sqrt{2RH - H^2} \tag{C.1.8}$$

C.2 One dimensional, steady state solution to the heat conduction in cylindrical walls

One dimensional, steady state solution to the heat conduction in cylindrical walls with uniform heat generation with suggested heat transfer coefficient and ambient temperatures is used to predict the radial wall temperature variation in the partially filled rotating test section [Incropera, 2006].

The energy balance for the tube inside wall is given by

$$h_1\left(T_{\infty,1} - T_{s,1}\right) = \frac{\dot{q} r_1}{2} - \frac{k_{ss}\left[\left(T_{s,2} - T_{s,1}\right) + \left(\dot{q} {r_2}^2/4k_{ss}\right)\left(1 - ({r_1}^2/{r_2}^2)\right)\right]}{r_1 ln(r_2/r_1)} \tag{C.2.1}$$

The energy balance for the tube the outside tube is given by

$$h_2\left(T_{\infty,2} - T_{s,2}\right) = \frac{\dot{q} r_2}{2} - \frac{k_{ss}\left[\left(T_{s,2} - T_{s,1}\right) + \left(\dot{q} {r_2}^2/4k_{ss}\right)\left(1 - ({r_1}^2/{r_2}^2)\right)\right]}{r_2 ln(r_2/r_1)} \tag{C.2.2}$$

where, r_1 and r_2 is the inside and outside tube radius; $T_{s,1}$, $T_{s,2}$ is the tube inside and outside wall temperature; $T_{\infty,1}$, $T_{\infty,2}$ are the inside and outside bulk fluid temperatures; h_1, h_2 are inside and outside heat transfer coefficient; k_{ss} is the thermal conductivity of the tube wall and $\dot{q}$ is the heat generation rate.

Table C.2.**1** Wall Temperature difference for various boundary conditions with internal heat generation (Flow rate = 400 ml/min, 160 RPM) (Chapter 4)

***q"* (W/m²)**	**ΔT (°C)** (***h₂*** = 10 W/m² K)	**ΔT (°C)** (***h₂*** = 50 W/m² K)
1169	0.06	0.05
1558	0.09	0.07
2403	0.14	0.11
2987	0.17	0.14

Table C.2.2 Wall Temperature difference for various boundary conditions with internal heat generation (Flow rate = 200 ml/min, Inclination = 3°) (Chapter 5)

q" **(W/m²)**	**ΔT (°C)** (***h₂*** = 10 W/m² K)	**ΔT (°C)** (***h₂*** = 50 W/m² K)
2378	0.13	0.09
3770	0.21	0.14
4903	0.28	0.19
5777	0.33	0.23

Table C.2.3 Wall Temperature difference for various boundary conditions with internal heat generation (Flow rate = 400 ml/min, Inclination = 6°) (Chapter 6)

q" **(W/m²)**	**ΔT (°C)** (***h₂*** = 10 W/m² K)	**ΔT (°C)** (***h₂*** = 50 W/m² K)
15342	0.91	0.75
18808	1.15	0.98
21240	1.26	1.07

The wall temperature difference predicted using Eqns. (C.2.1) and (C.2.2) for the different convective boundaries are tabulated in Table C.2.1-2.3. The inside wall temperature is estimated assuming the outside heat transfer coefficient is 10 W/m^2 K.

C.3 Dimensionless numbers

Based on Buckingham Pi theorem

Variables = h, $\dot{Q}$, ρ, μ, C_p, k, T, q'', D, ω, A_{pool}, $g sin\theta$, λ

Variables = n = 13

where, h is the heat transfer coefficient (W/m^{2}K), D is the diameter of the pipe (m), ω is the angular velocity (rad/sec), ρ is the fluid density (kg/m^3), μ is the kinematic viscosity of the fluid (kg/m s), C_p is the heat capacity of the fluid (J/ Kg K), q'' is the input heat flux (W/m^2), g sin θ is gravitational component for an inclined pipe (m/s^2), $\dot{Q}$ is the volumetric flow rate of fluid (m^3/s), k is the fluid thermal conductivity (W/m K), T is the inlet fluid temperature (K), $A_{pool}$is the liquid pool cross sectional area (m^2) and λ is the latent heat of vaporisation (J/Kg)

The repeating variables are selected as $\dot{Q}$, ρ, T, D

Repeating variables = j = 4

Possible Pi groups = $n - j$ = 12 – 4 = 9

$$\prod_1 = \frac{hD^6T}{\dot{Q}^3\rho} \qquad \prod_2 = \frac{\mu D}{\dot{Q}\rho} \qquad \prod_3 = \frac{\omega D^3}{\dot{Q}} \qquad \prod_4 = \frac{q"D^6}{\rho \dot{Q}^3}$$

$$\prod_5 = \frac{C_pTD^4}{\dot{Q}^2} \qquad \prod_6 = \frac{kTD^5}{\rho \dot{Q}^3} \qquad \prod_7 = \frac{g \sin\theta \, D^5}{\dot{Q}^2} \qquad \prod_8 = \frac{A_{pool}}{D^2}$$

$$\prod_9 = \frac{\lambda D^4}{\dot{Q}^2}$$

Combining Pi terms

$$\prod_1 / \prod_6 = \frac{hD}{k} = Nu \tag{C.3.1}$$

$$\prod_4 / \prod_5 = \frac{q''D^2}{\dot{Q}\rho C_p T} = \gamma \tag{C.3.2}$$

$$1/\prod_2 = \frac{\dot{Q}\rho}{\mu D} = Re_f \tag{C.3.3}$$

$$\prod_3 / \prod_2 = \frac{\rho \omega D^2}{\mu} = Re_\omega \tag{C.3.4}$$

$$1 / \prod_7 = \frac{\dot{Q}^2}{g \sin\theta \, D^5} = Fr \tag{C.3.5}$$

$$\prod_4 / \prod_9 = \frac{q'' D^2}{\dot{Q} \rho \lambda} = Bo \tag{C.3.6}$$

APPENDIX D

EXPERIMENTAL RESULTS

D.1 Stratified pool

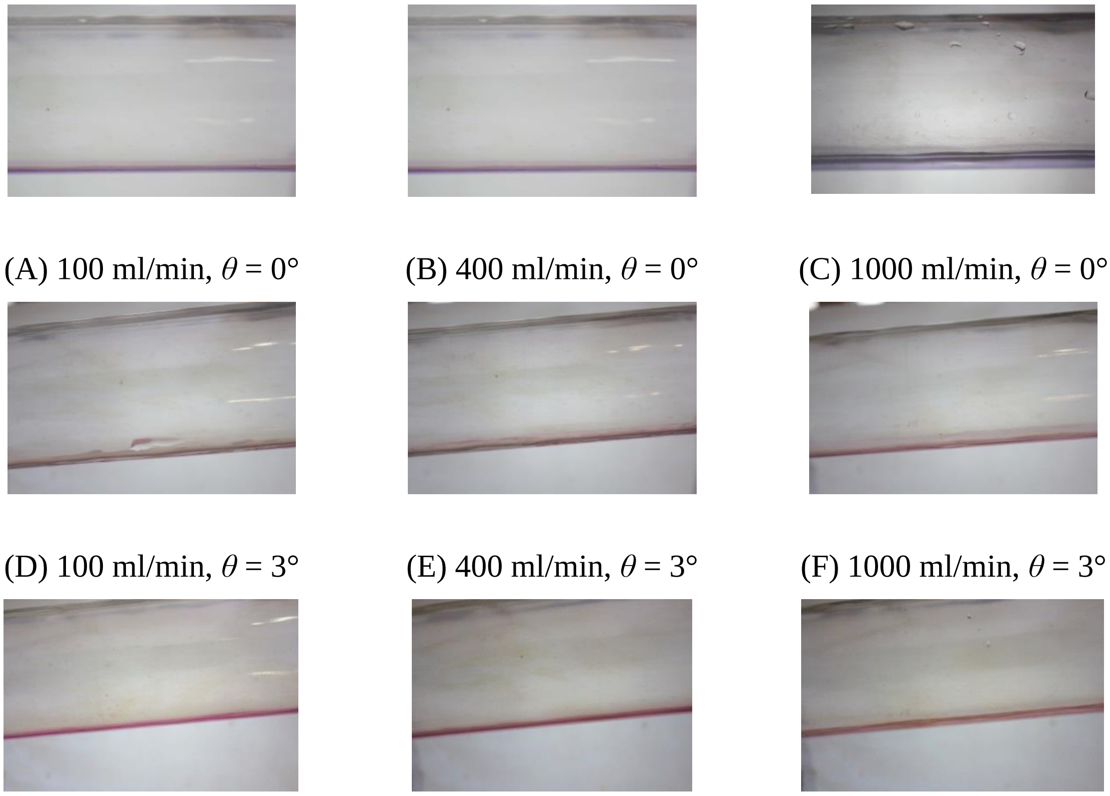

(A) 100 ml/min, θ = 0° (B) 400 ml/min, θ = 0° (C) 1000 ml/min, θ = 0°

(D) 100 ml/min, θ = 3° (E) 400 ml/min, θ = 3° (F) 1000 ml/min, θ = 3°

(G) 100 ml/min, θ = 5° (H) 400 ml/min, θ = 5° (I) 1000 ml/min, θ = 5°

Fig. D.1 Stratified flow in a partially filled pipe at different flow rates, inclination angle and 0 RPM. Pipe ID: 54 mm; Pipe length: 1000 mm. (Flow direction is from right to left. Images A-I are captured at ψ = 0º) (Re'_f = 258 − 1958, $Fr\varphi$ = 0)

D.2 Pendant

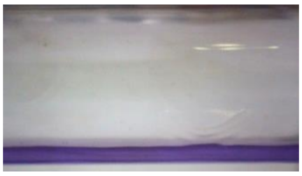

(A) 100 ml/min, 62 RPM, θ = 0°

(B) 100 ml/min, 62 RPM
θ = 3°

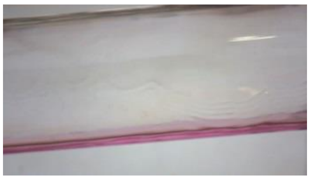

(C) 400 ml/min, 62 RPM
θ = 3°

(D) 1000 ml/min, 62 RPM
θ = 3°

(E) 100 ml/min, 62 RPM
θ = 5°

(F) 400 ml/min, 62 RPM
θ = 5°

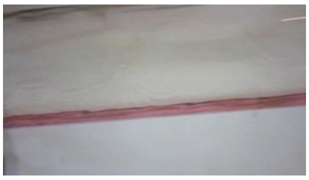

(G) 1000 ml/min, 62 RPM
θ = 5°

Fig. D.2 Pendants in a partially filled horizontal pipe at different flow rates. Pipe ID: 54 mm; Pipe length: 1000 mm. (Flow direction is from right to left. Images A-G are captured at ψ = 0º) ($Re'_f = 258 - 3808$, $Fr\varphi$ = 0.06 – 0.64)

D.3 Smooth Tooth

(A) 100 ml/min, 300 RPM

θ = 0.8°

(B) 400 ml/min, 395 RPM

θ = 0.8°

(C) 1000 ml/min, 546 RPM

θ = 0.8°

(D) 100 ml/min, 181 RPM

θ = 2°

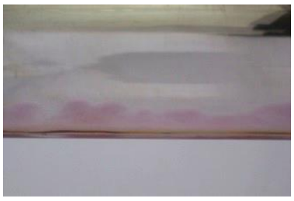

(E) 400 ml/min, 300 RPM

θ = 3°

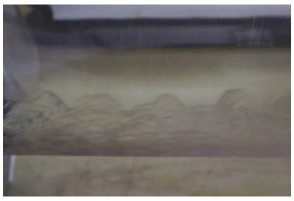

(F) 600 ml/min, 401 RPM

θ = 2°

(G) 100 ml/min, 175 RPM

θ = 5°

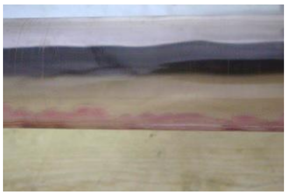

(H) 400 ml/min, 229 RPM

θ = 5°

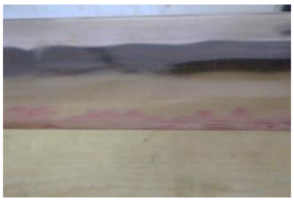

(I) 1000 ml/min, 358 RPM

θ = 5°

Fig. D.3 Smooth tooth flow pattern in a partially filled pipe at different flow rates and inclination angles. Pipe ID: 54 mm; Pipe length: 1000 mm. (Flow direction is from right to left. Images A-G are captured at ψ = 45º) (Re'_f = 258 − 3808, $Fr\varphi$ = 0.6 – 7.82)

D.4 Shark Tooth

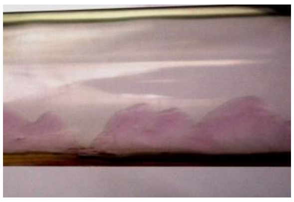

(A) 400 ml/min, 500 RPM

θ = 0.8°

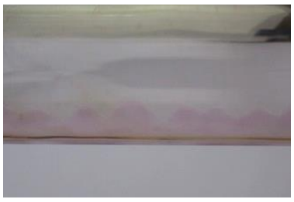

(B) 100 ml/min, 305 RPM

θ = 3°

(C) 200 ml/min, 370 RPM

θ = 3°

(D) 400 ml/min, 400 RPM

θ = 3°

(E) 100 ml/min, 220 RPM

θ = 4°

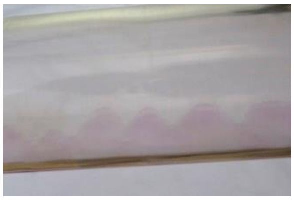

(F) 200 ml/min, 347 RPM

θ = 4°

(G) 100 ml/min, 267 RPM

θ = 5°

(H) 200 ml/min, 275 RPM

θ = 5°

(I) 1000 ml/min, 358 RPM

θ = 5°

Fig. D.4 Shark tooth flow pattern in a partially filled pipe at different flow rates and inclination angles. Pipe ID: 54 mm; Pipe length: 1000 mm. (Flow direction is from right to left. Images A-H are captured at ψ = 45º while Image I is captured at ψ = 0°)

(Re'_f = 258 − 3808, $Fr\varphi$ = 0.93 – 6.56)

D.5 Effect of heat flux

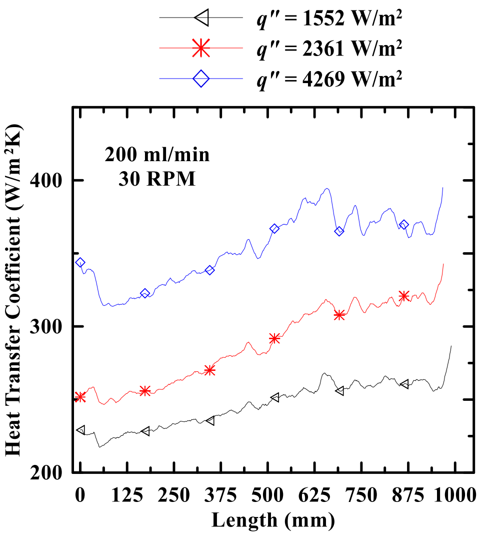

(A) 30 RPM, 200 ml/min

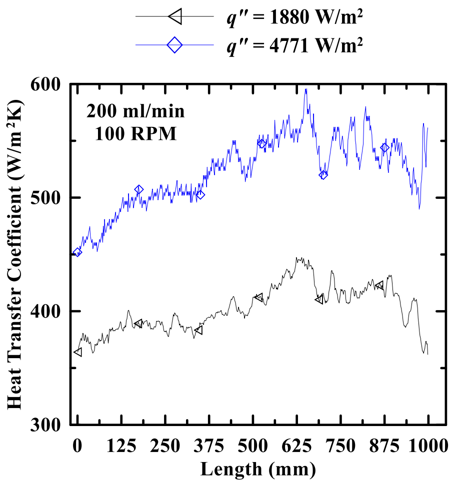

(B) 100 RPM, 200 ml/min

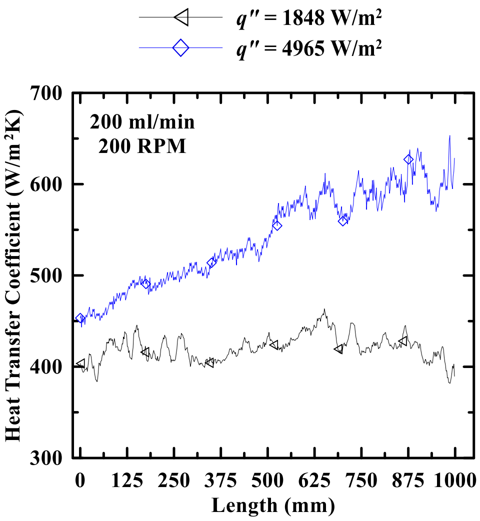

(C) 200 RPM, 200 ml/min

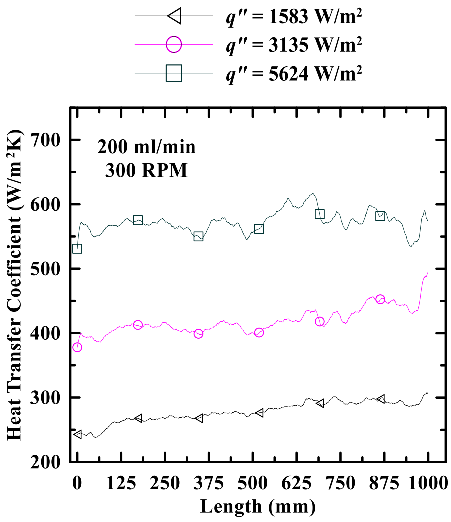

(D) 300 RPM, 200 ml/min

Fig. D.5 Effect of heat flux on heat transfer coefficient in a partially filled heated rotating pipe.

Pipe ID: 32.8 mm; Pipe length: 1000 mm (Re_f = 175, Re_ϕ = 1873 – 49902)

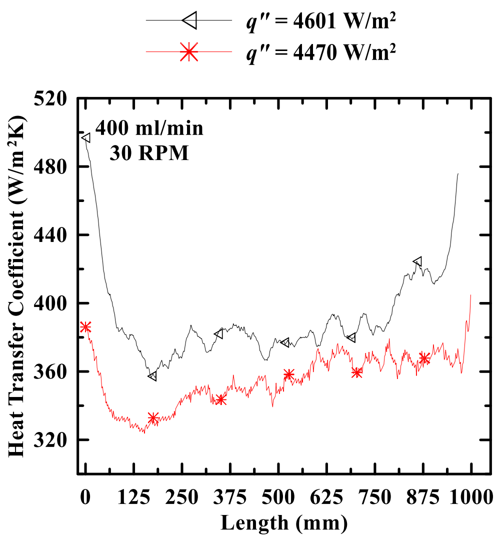

(E) 30 RPM, 400 ml/min

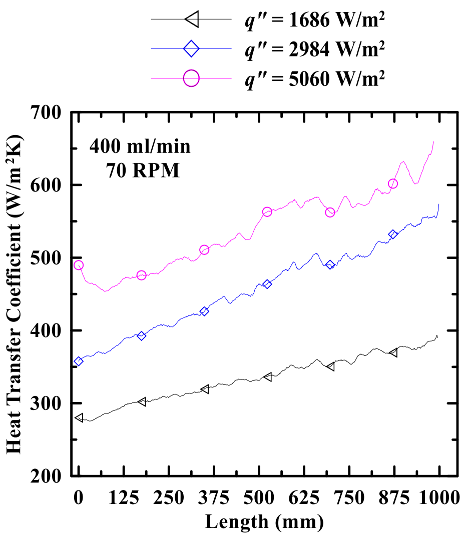

(F) 70 RPM, 400 ml/min

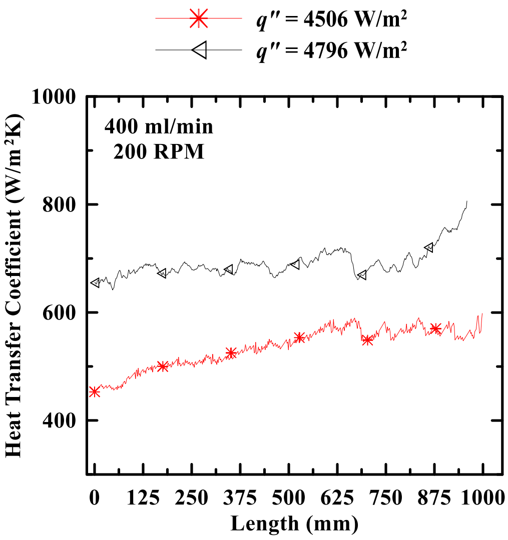

(G) 200 RPM, 400 ml/min

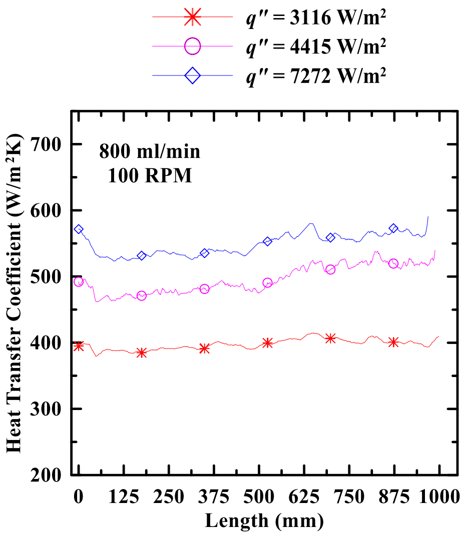

(H) 100 RPM, 800 ml/min

Fig. D.5 Effect of heat flux on heat transfer coefficient in a partially filled heated rotating pipe.

Pipe ID: 32.8 mm; Pipe length: 1000 mm (Re_f = 352, Re_ϕ = 4979 – 30882)

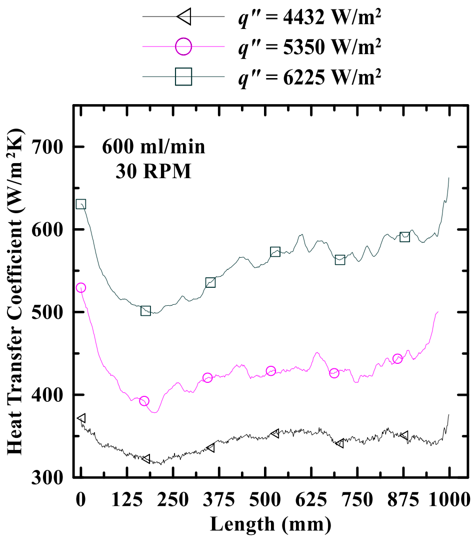

(I) 30 RPM, 600 ml/min

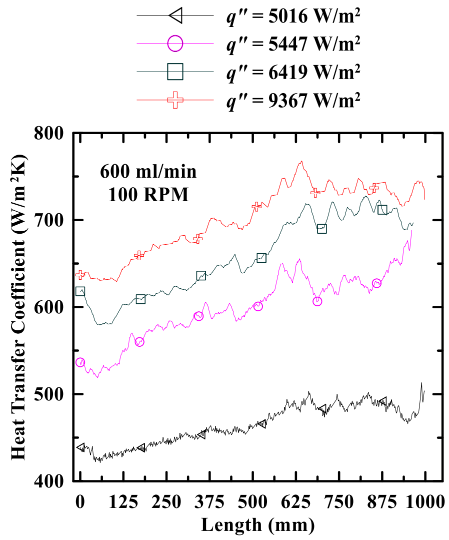

(J) 100 RPM, 600 ml/min

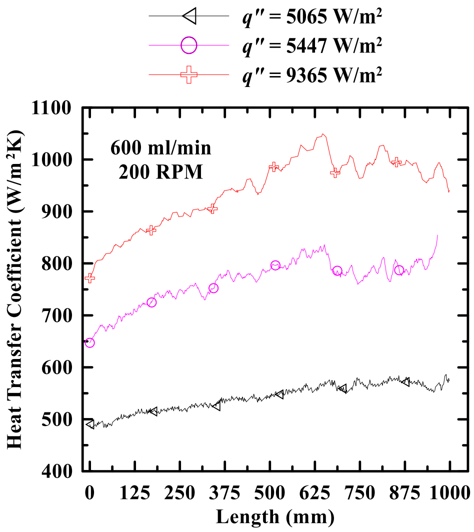

(K) 200 RPM, 600 ml/min

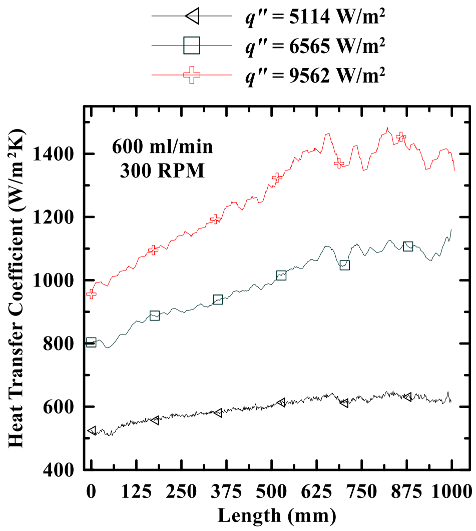

(L) 300 RPM, 600 ml/min

Fig. D.5 Effect of heat flux on heat transfer coefficient in a partially filled heated rotating pipe.

Pipe ID: 32.8 mm; Pipe length: 1000 mm (Re_f = 536, Re_ϕ = 5062 – 45245)

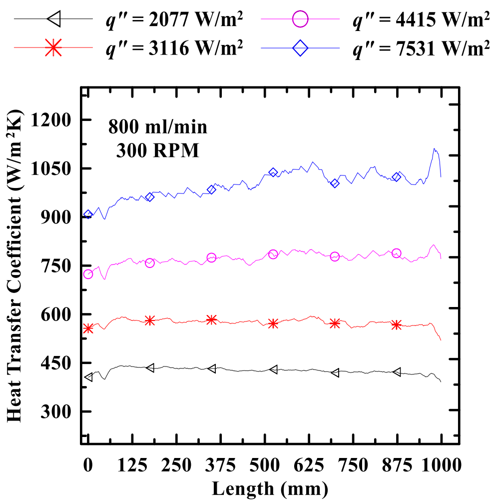

(M) 300 RPM, 800 ml/min

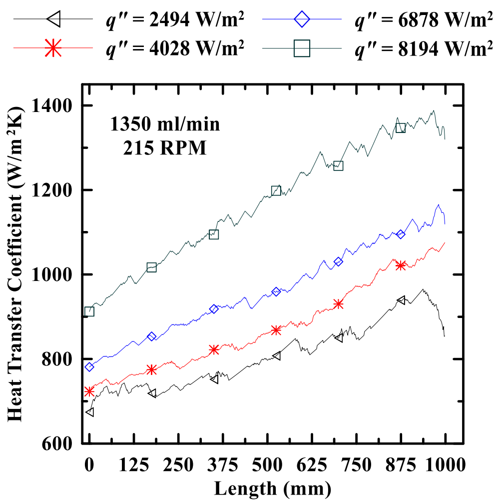

(N) 215 RPM, 1350 ml/min

Fig. D.5 Effect of heat flux on heat transfer coefficient in a partially filled heated rotating pipe.

Pipe ID: 32.8 mm; Pipe length: 1000 mm (Re_f = 536, Re_ϕ = 5062 – 45245)

D.6 Effect of flow rate

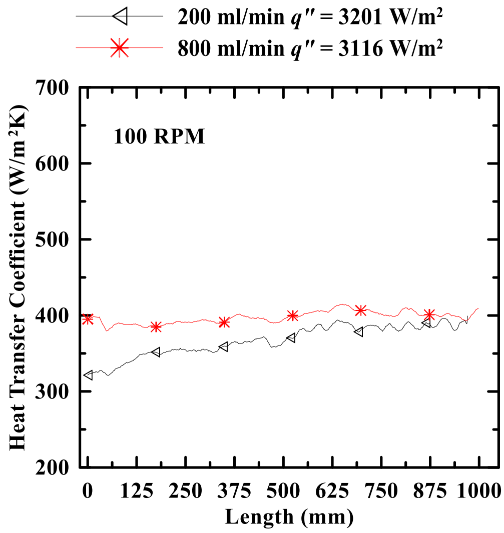

(A) 100 RPM

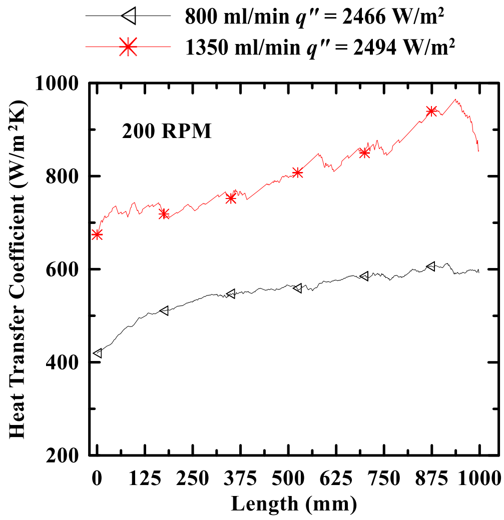

(B) 200 RPM

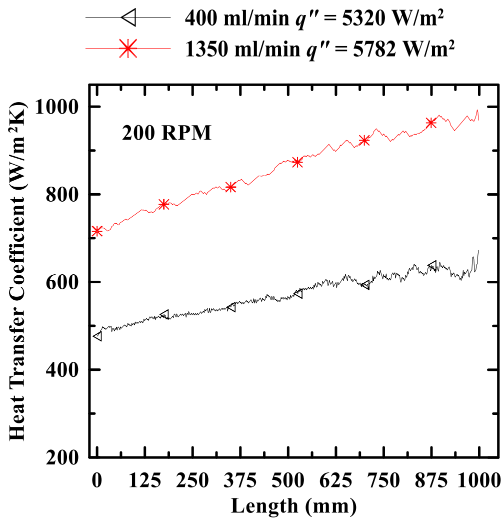

(C) 200 RPM

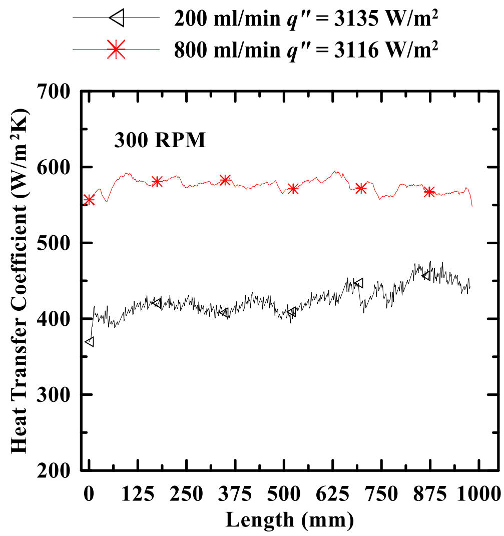

(D) 300 RPM

Fig. D.6 Effect of flow rate on heat transfer coefficient in a partially filled heated rotating pipe.

Pipe ID: 32.8 mm; Pipe length: 1000 mm (Re_f = 183 - 741, Re_ϕ = 16402 – 46555)

D.7 Effect of rotation rate

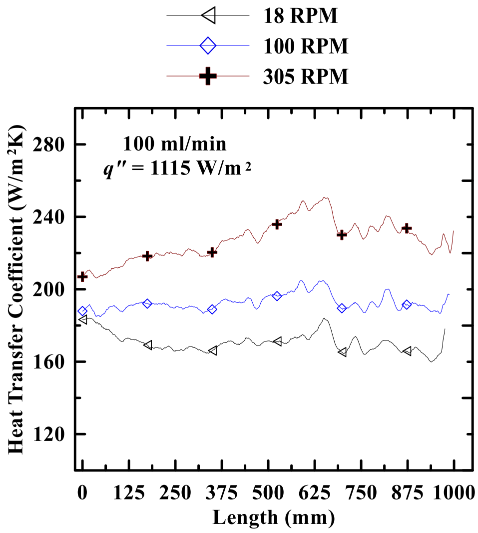

(A) 100 ml/min, $q'' = 1115$ W/m^2

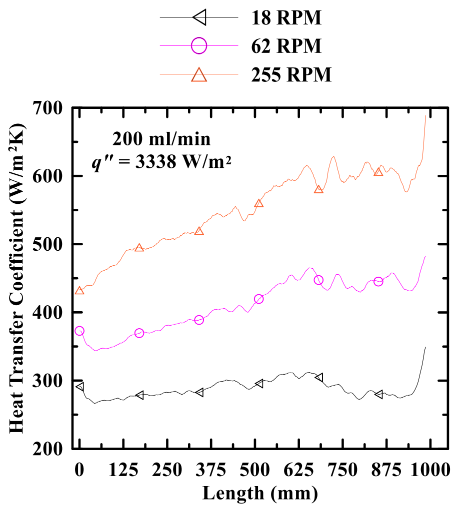

(B) 200 ml/min, $q'' = 3338$ W/m^2

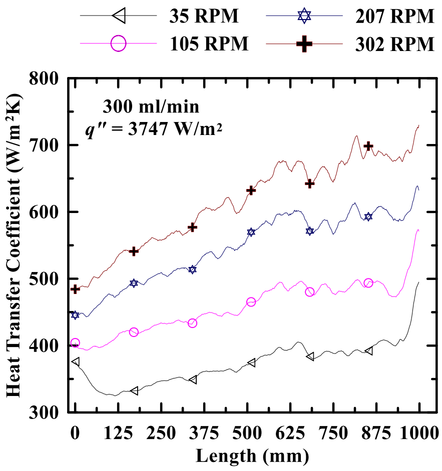

(C) 300 ml/min, $q'' = 3747$ W/m^2

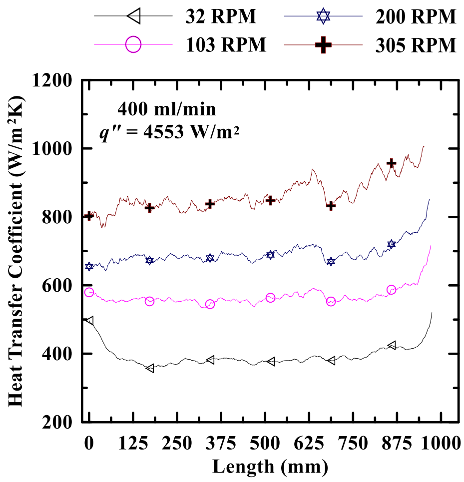

(D) 400 ml/min, $q'' = 4553$ W/m^2

Fig. D.7 Effect of rotation rate on heat transfer coefficient in a partially filled heated rotating pipe.

Pipe ID: 32.8 mm; Pipe length: 1000 mm (Re_f = 87 - 355, Re_ϕ = 4573 – 49902)

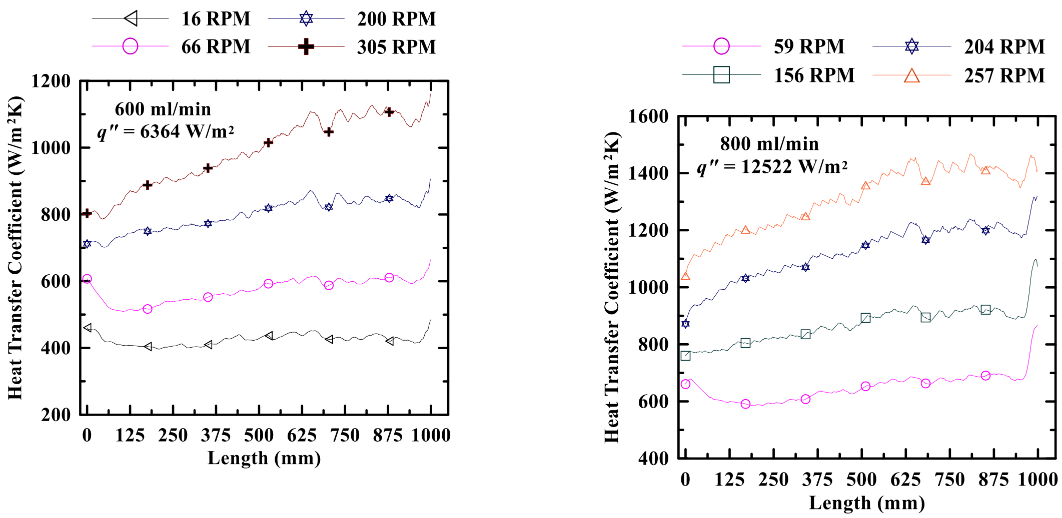

(E) 600 ml/min, $q'' = 6364$ W/m^2 (F) 800 ml/min, $q'' = 12522$ W/m^2

Fig. D.7 Effect of rotation rate on heat transfer coefficient in a partially filled heated rotating pipe.

Pipe ID: 32.8 mm; Pipe length: 1000 mm (Re_f = 87 - 355, Re_ϕ = 4573 – 49902)

D.8 Effect of Inclination

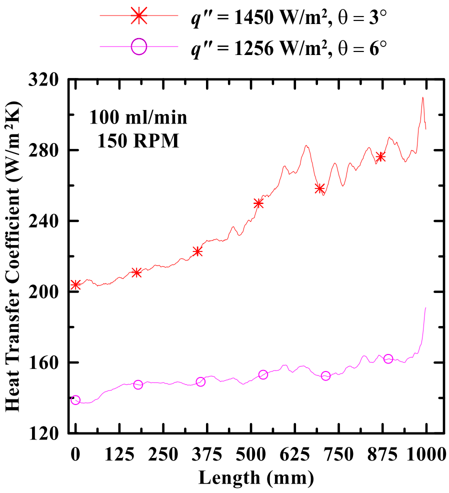

(A) 150 RPM, 100 ml/min

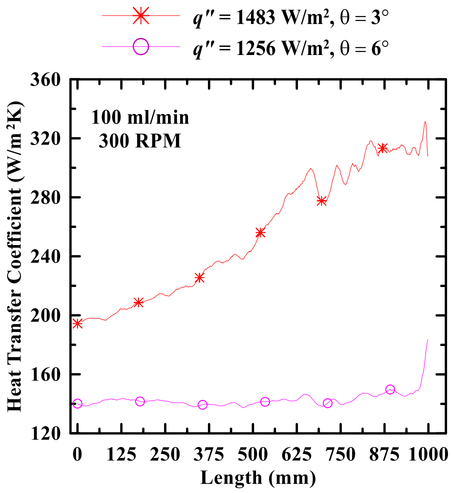

(B) 300 RPM, 100 ml/min

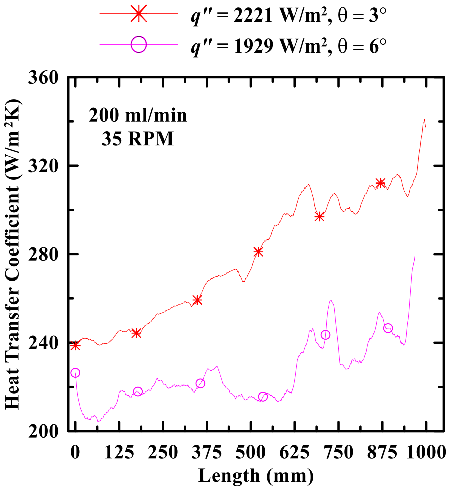

(C) 35 RPM, 200 ml/min

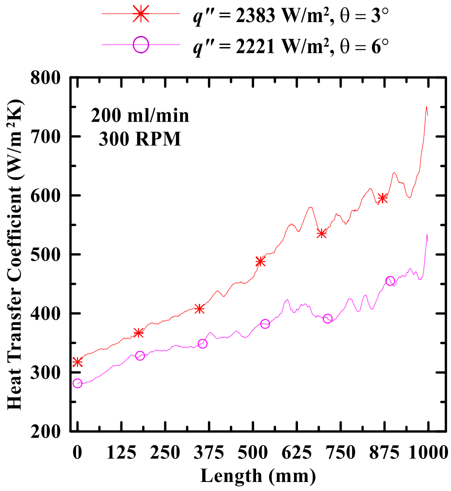

(D) 300 RPM, 200 ml/min

Fig. D.8 Effect of pipe inclination on the heat transfer coefficient in a partially filled heated rotating pipe at constant rotation rate, flow rate and comparable wall heat flux.

Pipe ID: 32.8 mm; Pipe length: 1000 mm

(Re_f = 86 - 516, Fr = 1.67 – 44.6 × 10^{-4}, Re_ϕ = 4573 – 45415)

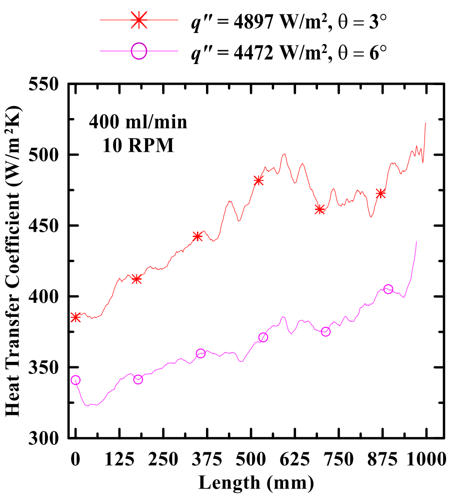

(E) 10 RPM, 400 ml/min

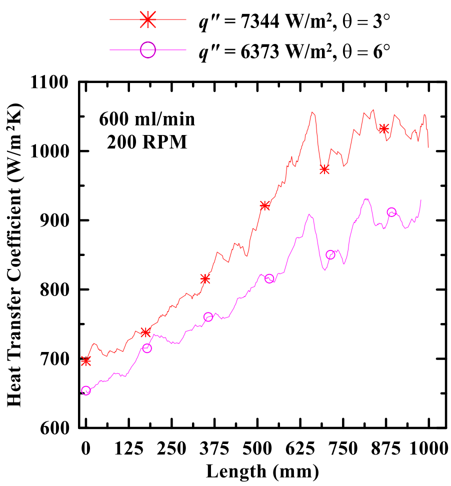

(F) 200 RPM, 600 ml/min

Fig. D.8 Effect of pipe inclination on the heat transfer coefficient in a partially filled heated rotating pipe at constant rotation rate, flow rate and comparable wall heat flux.

Pipe ID: 32.8 mm; Pipe length: 1000 mm

(Re_f = 86 - 516, Fr = 1.67 – 44.6 × 10^{-4}, Re_ϕ = 4573 – 45415)

D.9 Effect of heat flux in inclined system

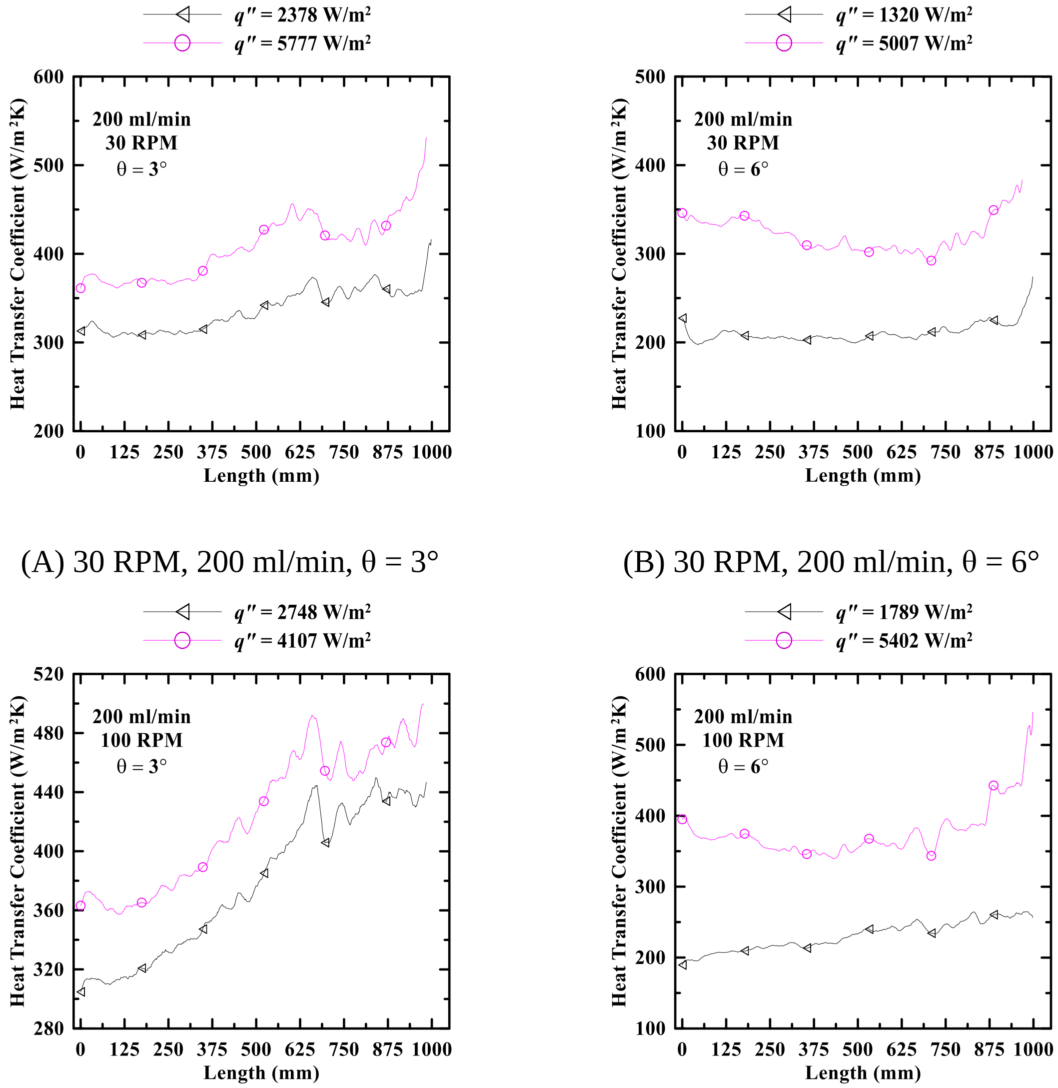

(A) 30 RPM, 200 ml/min, θ = 3°

(B) 30 RPM, 200 ml/min, θ = 6°

(C) 100 RPM, 200 ml/min, θ = 3°

(D) 100 RPM, 200 ml/min, θ = 6°

Fig. D.9 Effect of heat flux on heat transfer coefficient in a partially filled heated rotating pipe.

Pipe ID: 32.8 mm; Pipe length: 1000 mm

(Re_f = 86 - 677, Fr = 8.41 – 85.5 × 10^{-4}, Re_ϕ = 4753 – 44994)

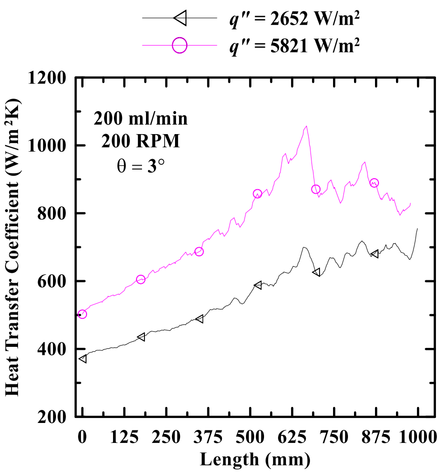

(E) 200 RPM, 200 ml/min, θ = 3°

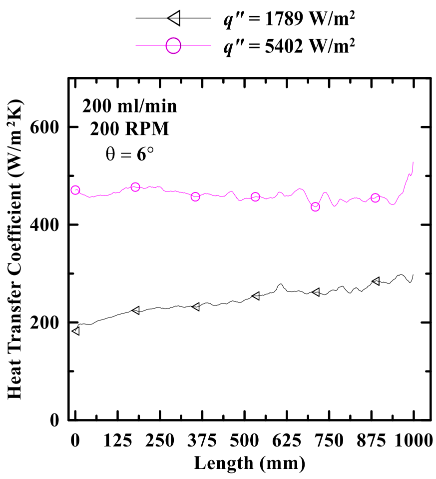

(F) 200 RPM, 200 ml/min, θ = 6°

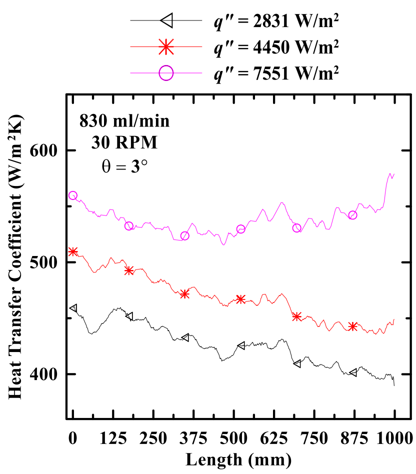

(G) 30 RPM, 830 ml/min, θ = 3°

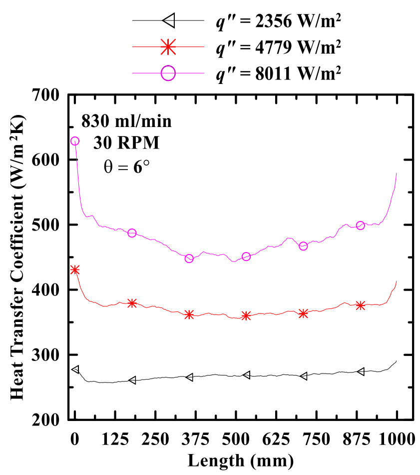

(H) 30 RPM, 830 ml/min, θ = 6°

Fig. D.9 Effect of heat flux on heat transfer coefficient in a partially filled heated rotating pipe.

Pipe ID: 32.8 mm; Pipe length: 1000 mm

(Re_f = 86 - 677, Fr = 8.41 – 85.5 × 10^{-4}, Re_ϕ = 4753 – 44994)

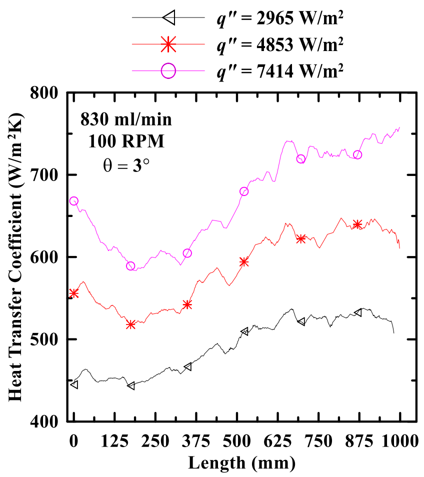

(I) 100 RPM, 830 ml/min, θ = 3°

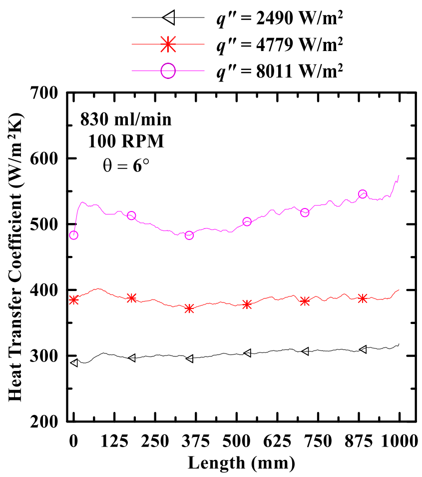

(J) 100 RPM, 830 ml/min, θ = 6°

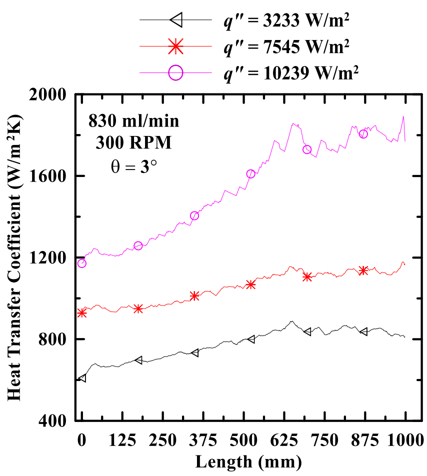

(K) 300 RPM, 830 ml/min, θ = 3°

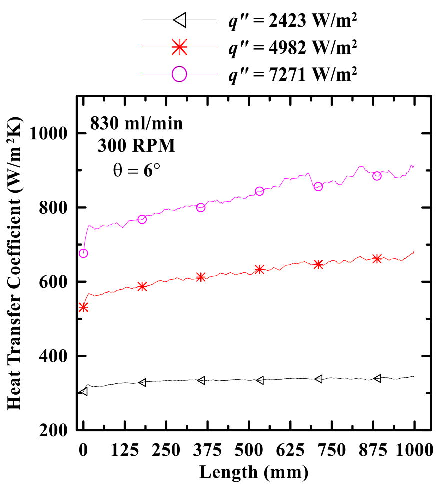

(L) 300 RPM, 830 ml/min, θ = 6°

Fig. D.9 Effect of heat flux on heat transfer coefficient in a partially filled heated rotating pipe.

Pipe ID: 32.8 mm; Pipe length: 1000 mm

(Re_f = 86 - 677, Fr = 8.41 – 85.5 × 10^{-4}, Re_ϕ = 4753 – 44994)

D.10 Effect of flow rate in inclined system

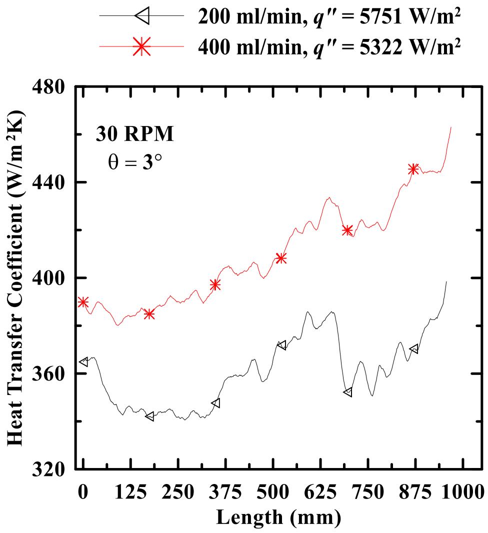

(A) 30 RPM, θ = 3°

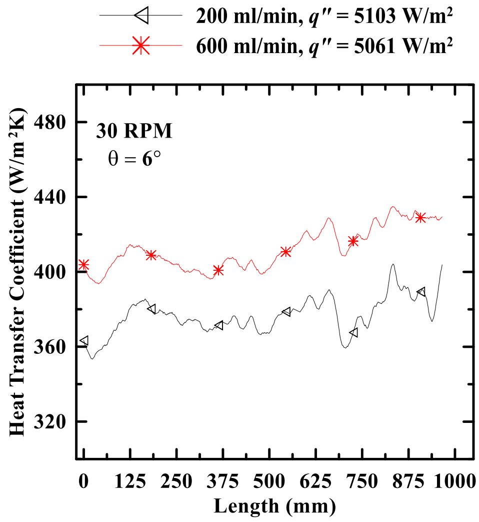

(B) 30 RPM, θ = 6°

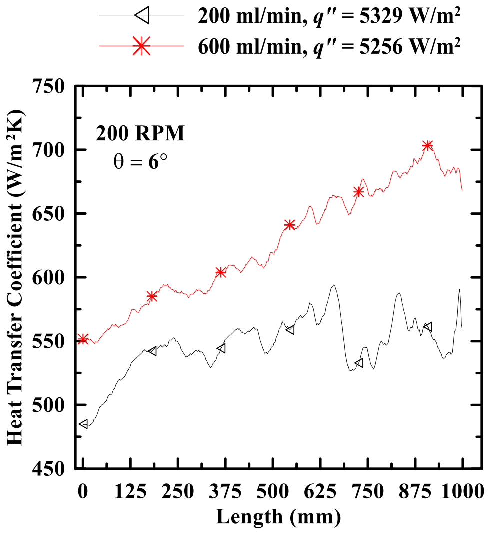

(C) 200 RPM, θ = 6°

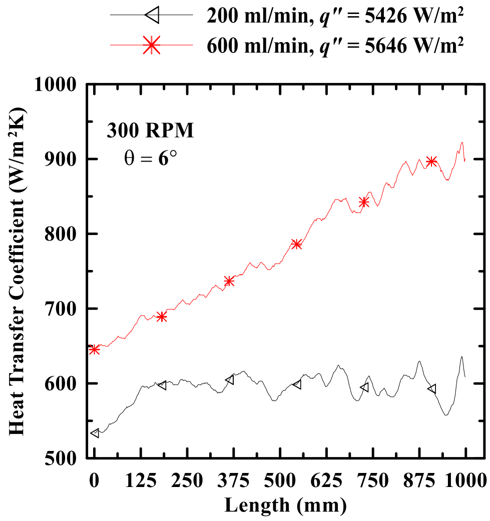

(D) 300 RPM, θ = 6°

Fig. D.10 Effect of flow rate on heat transfer coefficient in a partially filled heated rotating pipe.

Pipe ID: 32.8 mm; Pipe length: 1000 mm

(Re_f = 171 - 351, Fr = 8.41 – 19.8 × 10^{-4}, Re_ϕ = 4753 – 44994)

D.11 Effect of rotation rate in inclined system

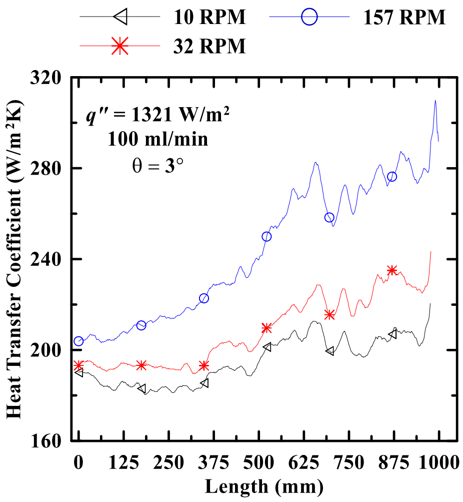

(A) 100 ml/min, $q'' = 1321$ W/m^2, θ = 3°

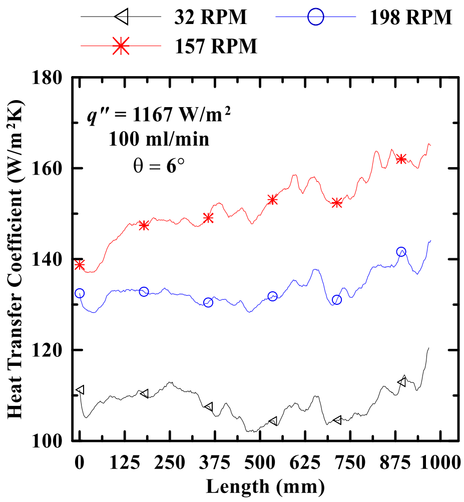

(B) 100 ml/min, $q'' = 1167$ W/m^2, θ = 6°

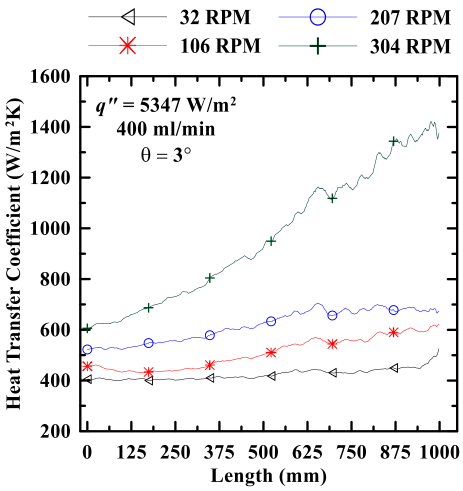

(C) 400 ml/min, $q'' = 5347$ W/m^2, θ = 3°

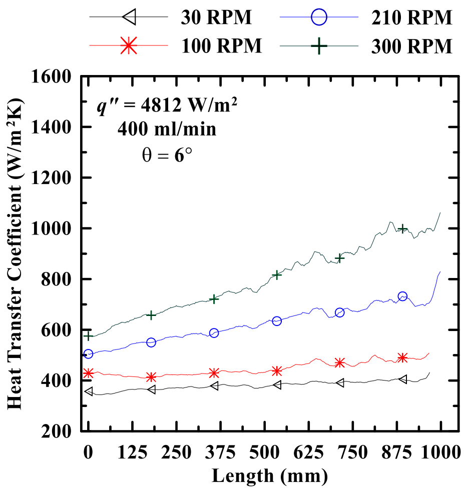

(D) 400 ml/min, $q'' = 4812$ W/m^2, θ = 6°

Fig. D.11 Effect of rotation rate on heat transfer coefficient in a partially filled heated rotating pipe.

Pipe ID: 32.8 mm; Pipe length: 1000 mm

(Re_f = 86 - 511, Fr = 1.67 – 44.6 × 10^{-4}, Re_ϕ = 4608 – 41225)

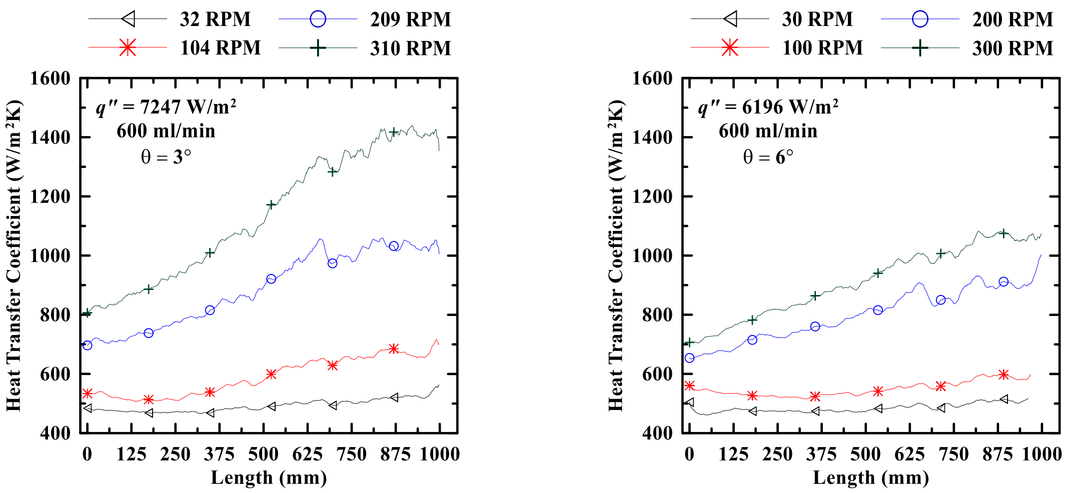

(E) 600 ml/min, q'' = 7247 W/m^2, θ = 3° (F) 600 ml/min, q'' = 6196 W/m^2, θ = 6°

Fig. D.11 Effect of rotation rate on heat transfer coefficient in a partially filled heated rotating pipe.

Pipe ID: 32.8 mm; Pipe length: 1000 mm

(Re_f = 86 - 511, Fr = 1.67 – 44.6 × 10^{-4}, Re_ϕ = 4608 – 41225)

D.12 Effect of Inclination

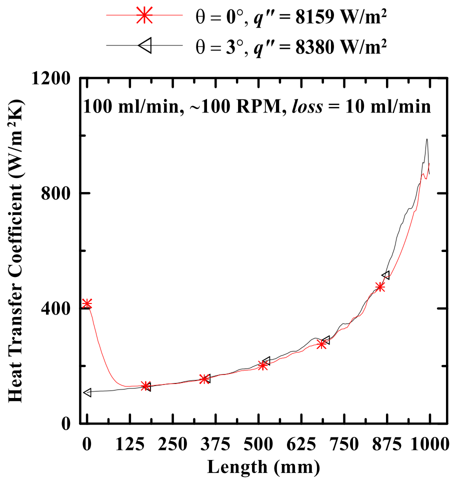

(A) 100 RPM, 100 ml/min

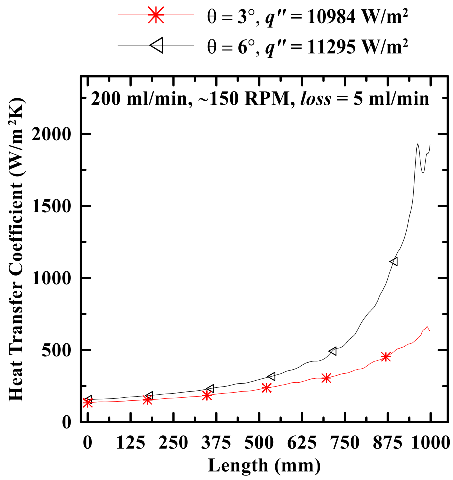

(B) 150 RPM, 200 ml/min

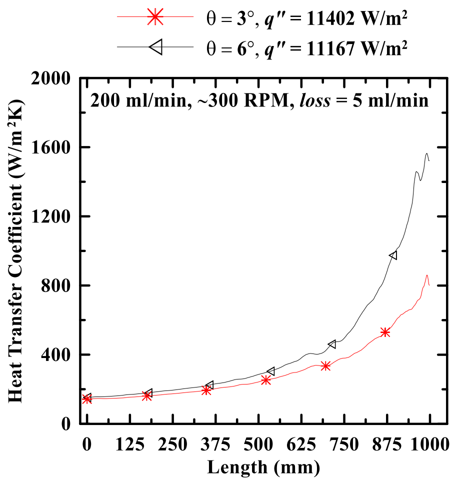

(C) 300 RPM, 200 ml/min

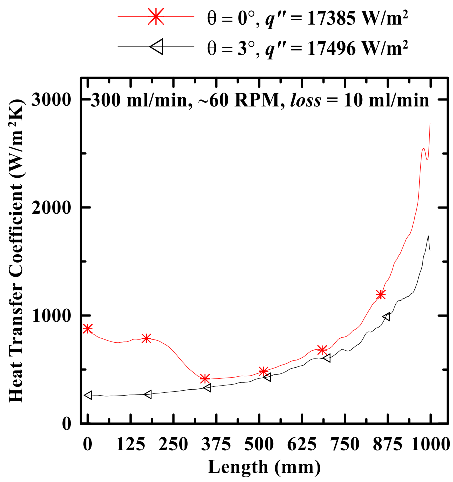

(D) 60 RPM, 300 ml/min

Fig. D.12 Effect of pipe inclination on the heat transfer coefficient in a partially filled rotating evaporator at constant rotation rate, flow rate and comparable wall heat flux.

Pipe ID: 32.8 mm; Pipe length: 1000 mm (Re_f = 104 - 425)

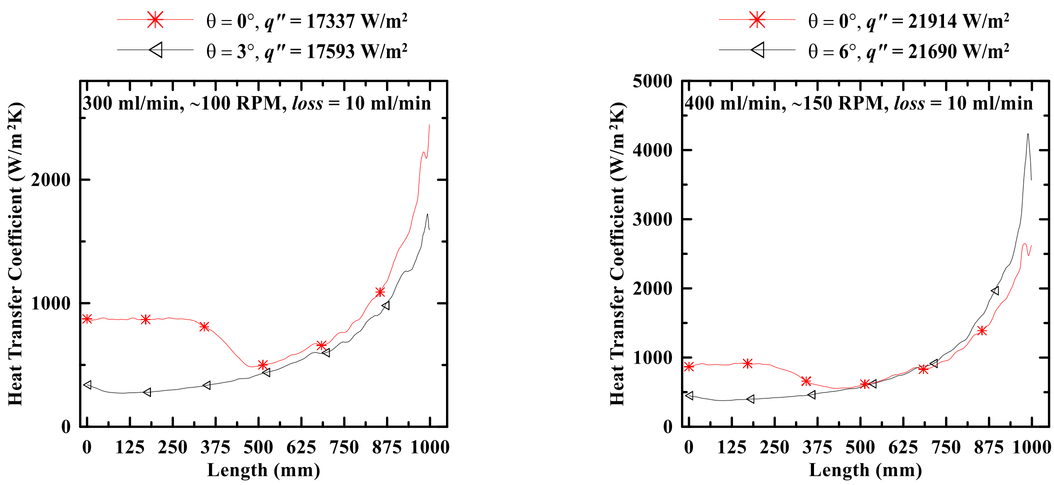

(E) 100 RPM, 300 ml/min

(F) 150 RPM, 400 ml/min

Fig. D.12 Effect of pipe inclination on the heat transfer coefficient in a partially filled rotating evaporator at constant rotation rate, flow rate and comparable wall heat flux.

Pipe ID: 32.8 mm; Pipe length: 1000 mm (Re_f = 104 - 425)

D.13 Effect of Heat flux

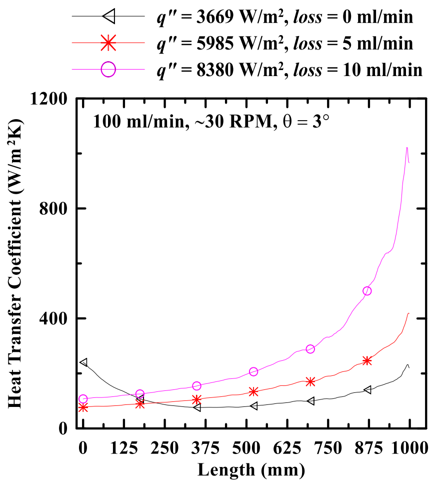

(A) 30 RPM, 100 ml/min, θ = 3°

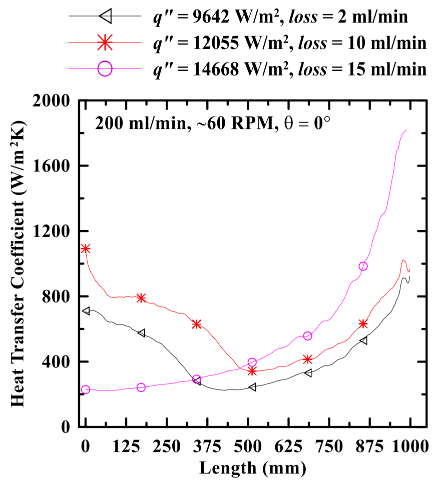

(B) 60 RPM, 200 ml/min, θ = 0°

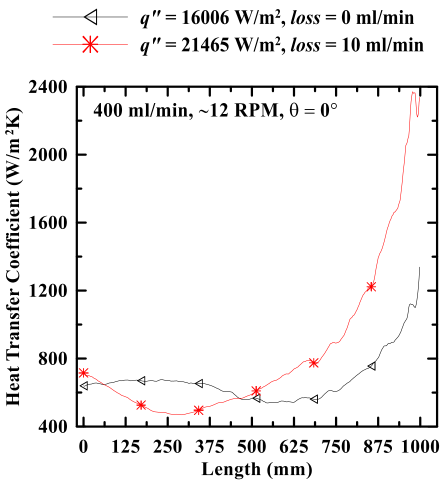

(C) 12 RPM, 400 ml/min, θ = 0°

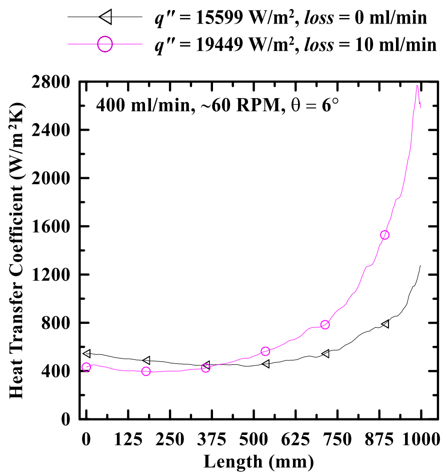

(D) 60 RPM, 400 ml/min, θ = 6°

Fig. D.13 Effect of wall heat flux on the heat transfer coefficient in a partially filled rotating evaporator at constant rotation rate, flow rate and inclination.

Pipe ID: 32.8 mm; Pipe length: 1000 mm (Re_f = 104 - 421)

D.14 Effect of Flow rate

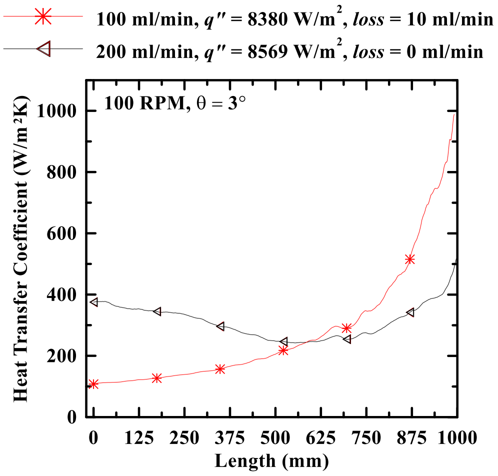

(A) 100 RPM, θ = 3°

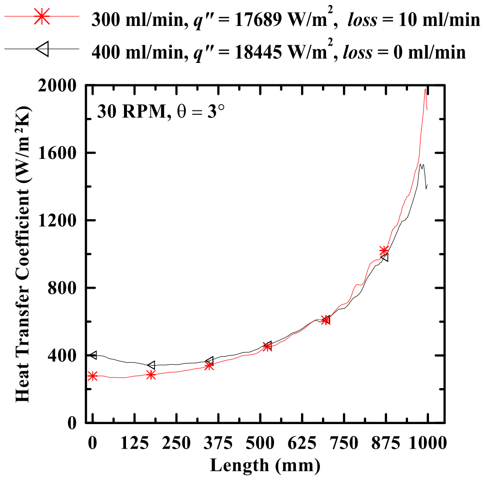

(B) 30 RPM, θ = 3°

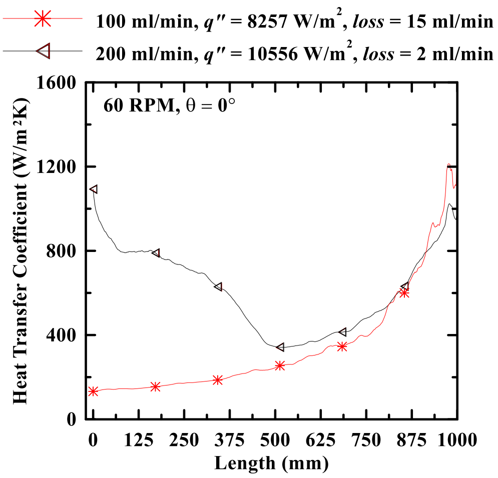

(C) 60 RPM, θ = 0°

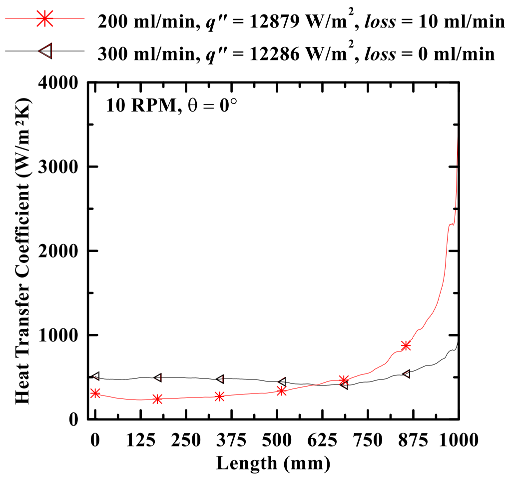

(D) 10 RPM, θ = 0°

Fig. D.14 Effect of liquid volume flow rate on the heat transfer coefficient in a partially filled rotating evaporator at constant rotation rate, wall heat flux and inclination.

Pipe ID: 32.8 mm; Pipe length: 1000 mm (Re_f = 106 - 425)

D.15 Effect of Rotation rate

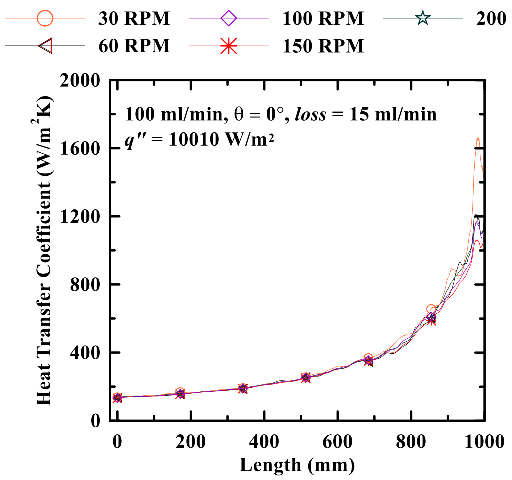

(A) 100 ml/min, θ = 0°

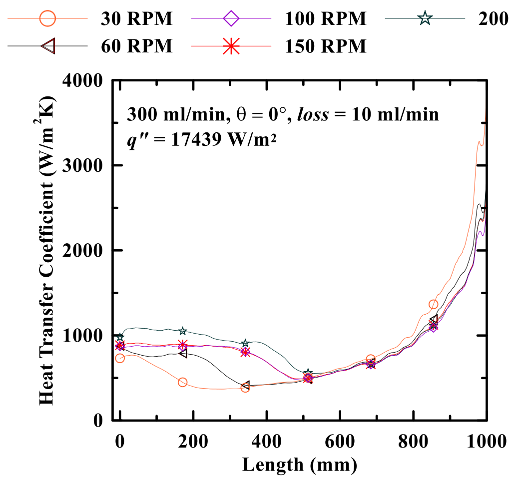

(B) 300 ml/min, θ = 0°

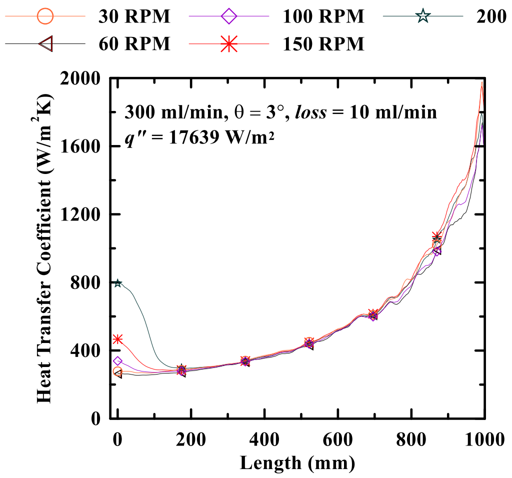

(C) 300 ml/min, θ = 3°

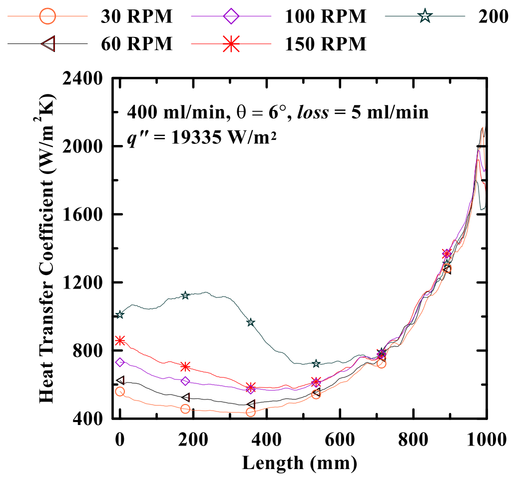

(D) 400 ml/min, θ = 6°

Fig. D.15 Effect of rotation rate flow rate on the heat transfer coefficient in a partially filled rotating evaporator at constant liquid volume flow rate, wall heat flux and inclination.

Pipe ID: 32.8 mm; Pipe length: 1000 mm (Re_f = 104 - 418)

REFERENCES

Ashmore, J., Hosoi, A.E. and Stone, H.A., 2003. The effect of surface tension on rimming flows in a partially filled rotating cylinder. Journal of Fluid mechanics, 479, pp.65-98.

Baburajan, P.K., Bisht, G.S., Gupta, S.K. and Prabhu, S.V., 2013. Measurement of subcooled boiling pressure drop and local heat transfer coefficient in horizontal tube under LPLF conditions. Nuclear Engineering and Design, 255, pp.169-179.

Baker, J., Oliver, T., Lin, L., Ponnapan, R. and Leland, J., 2001. Correlations of critical Froude number for annular-rimming flow in rotating heat pipes. Journal of fluids engineering, 123(4), pp.909-913.

Barnea, E., Kovalivker, E., Mizrahi, J. and Yacoub, N., 1972. The flow of thin films inside rotating cylindrical tubes. The Canadian Journal of Chemical Engineering, 50(6), pp.685-689.

Beckman, J.R., Campagnolo, J.F. and Kratzke, K., 1998. Rotating drum heat exchanger. Chemical Engineering Communications, 168(1), pp.1-11.

Benilov, E.S. and Lapin, V.N., 2013. Inertial instability of flows on the inside or outside of a rotating horizontal cylinder. Journal of Fluid Mechanics, 736, pp.107-129.

Boote, O.A.M. and Thomas, P.J., 1999. Effects of granular additives on transition boundaries between flow states of rimming flows. Physics of Fluids, 11(8), pp.2020-2029.

Bergles, A.E. and Rohsenow, W.M., 1964. The determination of forced-convection surface-boiling heat transfer. Journal of Heat Transfer, 86(3), pp.365-372.

Bergman, T. L. and Incropera, F. P., 2006. Fundamentals of heat and mass transfer. John Wiley & Sons

Borisov, G.B., Kascheev, V.A., Mityanin, A.S., Oshurko, V.B. and Podymova, T.V., 2011. Optimisation of processes in a two-stage installation for liquid radioactive waste immobilisation. International Journal of Nuclear Energy Science and Technology, 6(2), pp.121-126.

Buflovak, P.K, Hebeler Process Solutions (2018), http://www.buflovak.com

Cannon, J.N. and Kays, W.M., 1969. Heat transfer to a fluid flowing inside a pipe rotating about its longitudinal axis. Journal of Heat Transfer, 91(1), pp.135-139.

Chen, J.C., 1966. Correlation for boiling heat transfer to saturated fluids in convective flow. Industrial & engineering chemistry process design and development, 5(3), pp.322-329.

Chen, P.J., Tsai, Y.T., Liu, T.J. and Wu, P.Y., 2007. Low volume fraction rimming flow in a rotating horizontal cylinder. Physics of Fluids, 19(12), p.128107.

Chicharro, R., Vazquez, A. and Manasseh, R., 2011. Characterization of patterns in rimming flow. Experimental Thermal and Fluid Science, 35(6), pp.1184-1192.

Chun, K.R. and Seban, R.A., 1971. Heat transfer to evaporating liquid films. Journal of Heat Transfer, 93(4), pp.391-396.

Collier, J.G. and Thome, J.R., 1981. Convective boiling and condensation. McGraw-Hill

Cowen, G., Norton-Berry, P. and Steel, M.L., Imperial Chemical Industries Ltd, 1982. Chemical process on the surface of a rotating body. U.S. Patent 4,311,570.

Davis, E.J. and Anderson, G.H., 1966. The incipience of nucleate boiling in forced convection flow. AIChE Journal, 12(4), pp.774-780.

Dropkin, D. and Carmi, A., 1956. Natural convection heat transfer from a horizontal cylinder rotating in air. Transactions of the ASME, 79, pp.741-749.

Duffy, B.R. and Wilson, S.K., 2009. Large-Biot-number non-isothermal flow of a thin film on a stationary or rotating cylinder. The European Physical Journal Special Topics, 166(1), pp.147-150.

Fujita, T. and Ueda, T., 1978. Heat transfer to falling liquid films and film breakdown—I: Subcooled liquid films. International Journal of Heat and Mass Transfer, 21(2), pp.97-108.

Fukasawa, T., Inagaki, Y., Arima, T. and Sato, S., 2016. Flexible Waste Management to Increase the Effectiveness of Minor Actinide P&T Technology. Procedia Chemistry, 21, pp.365-370.

Gray, V.H., 1969. The rotating heat pipe-A wickless, hollow shaft for transferring high heat fluxes. Proceedings of ASME/AIChE Heat Transfer Conference, Minneapolis, pp. 1–5.

Gungor, K.E. and Winterton, R.H.S., 1986. A general correlation for flow boiling in tubes and annuli. International Journal of Heat and Mass Transfer, 29(3), pp.351-358.

Hardik, B.K. and Prabhu, S.V., 2016. Boiling pressure drop and local heat transfer distribution of water in horizontal straight tubes at low pressure. International Journal of Thermal Sciences, 110, pp.65-82.

Haji-Sheikh, A., Lakshimanarayanan, R., Lou, D.Y. and Ryan, P.J., 1984. Confined flow in a partially-filled rotating horizontal cylinder. Journal of fluids engineering, 106(3), pp.270-278.

Hosoi, A.E. and Mahadevan, L., 1999. Axial instability of a free-surface front in a partially filled horizontal rotating cylinder. Physics of Fluids, 11(1), pp.97-106.

Johnson, R.E., 1988. Steady-state coating flows inside a rotating horizontal cylinder. Journal of Fluid Mechanics, 190, pp.321-342.

Kandlikar, S.G., 1991. Development of a flow boiling map for subcooled and saturated flow boiling of different fluids inside circular tubes. Journal of Heat Transfer, 113(1), pp.190-200.

Kandlikar, S.G., 1998. Heat transfer characteristics in partial boiling, fully developed boiling, and significant void flow regions of subcooled flow boiling. Journal of Heat Transfer, 120(2), pp.395-401.

Karweit, M.J. and Corrsin, S., 1975. Observation of cellular patterns in a partly filled, horizontal, rotating cylinder. The Physics of Fluids, 18(1), pp.111-112.

Kascheev, V.A. and Podymova, T.V., 2012. Modeling of the behavior of liquid radwastes in a rotary calcination furnace. Atomic Energy, 113(2), pp.106-111.

Khetni, M., 2018. Design, construction and evaluation of a vacuum evaporation system for the concentration of aqueous whey protein solutions (Doctoral dissertation, Stellenbosch: Stellenbosch University).

Kreith, F., 1969. Convection heat transfer in rotating systems. In Advances in heat transfer (Vol. 5, pp. 129-251). Elsevier.

Krivosheev, B.N., Kukharskii, M.P. and Portnov, V.D., 1979. Heat transfer in the evaporator section of a rotating heat pipe at low rotational speeds. Journal of Engineering Physics and Thermophysics, 37(1), pp.773-778.

Kuo, C., Iida, H.T., Taylor, J.H. and Kreith, F., 1960. Heat transfer in flow through rotating ducts. Journal of Heat Transfer, 82(2), pp.139-151.

Lennemann, W.L., 1978. The management of high-level radioactive wastes. IAEA Bull, 21(4), pp.1-16.

Lin, L. and Faghri, A., 1997. Heat transfer analysis of stratified flow in rotating heat pipes with cylindrical and stepped walls. International journal of heat and mass transfer, 40(18), pp.4393-4404.

Lin, L. and Faghri, A., 1999. Heat transfer in micro region of a rotating miniature heat pipe. International Journal of Heat and Mass Transfer, 42(8), pp.1363-1369.

Lin, L. and Groll, M., 1996. Critical conditions for collapse of annular flow in a rotating heat pipe with a cylindrical wall. Heat transfer engineering, 17(3), pp.29-34.

Lioumbas, J.S., Paras, S.V. and Karabelas, A.J., 2005. Co-current stratified gas–liquid downflow—Influence of the liquid flow field on interfacial structure. International Journal of Multiphase Flow, 31(8), pp.869-896.

Liu, Z. and Winterton, R.H.S., 1991. A general correlation for saturated and subcooled flow boiling in tubes and annuli, based on a nucleate pool boiling equation. International journal of heat and mass transfer, 34(11), pp.2759-2766.

Ilmanen, P., 2017. Modeling of thin film evaporator for ionic liquid recycling.

Lopez-Toledo, J., 2006. Heat and mass transfer characteristics of a wiped film evaporator (Doctoral dissertation).

Marsden, D., McGowan, B., Garth, B., Skillen, N., Scott, S., Guerif, H.N., Guillois, E., Flament, T., Sartelet, S., Prod'homme, A. and Pereira-Mendes, F., 2010. Vitrification Assistance Program: International Cooperation on Vitrification Technology (Part II)-10157. Waste Management Symposia, Phoenix, AZ, pp. 1-5.

Marsh, W.J. and Mudawar, I., 1989. Predicting the onset of nucleate boiling in wavy free-falling turbulent liquid films. International journal of heat and mass transfer, 32(2), pp.361-378.

Melo, F., 1993. Localized states in a film-dragging experiment. Physical Review E, 48(4), p.2704.

Moffatt, H.K., 1977. Behaviour of a viscous film on the outer surface of a rotating cylinder. Journal de mécanique, 16, pp.651-673.

Murakami, M. and Kikuyama, K., 1980. Turbulent flow in axially rotating pipes. Journal of Fluids Engineering, 102(1), pp.97-103.

Murray, P., Bailly, F., Strachan, D., Senentz, G. and Veyer, C., 2009. Qualification of a Vitrified High Level Waste Product to Support Used Nuclear Fuel Recycling in the US-9474. Waste Management Symposia, Phoenix, AZ, pp. 1-5.

Mutzenburg, A.B., 1965. Agitated Thin-Film Evaporators. Part 1. Thin-Film Technology. Chem. Eng.(New York), 72(19), pp.175-178.

National Institute of Standards and Technology, Thermophysical Properties of Fluid Systems, (2016), http://webbook.nist.gov/chemistry/fluid

Navidi, W.C., 2008. Statistics for engineers and scientists . McGraw-Hill.

Orr, F.M. and Scriven, L.E., 1978. Rimming flow: numerical simulation of steady, viscous, free-surface flow with surface tension. Journal of Fluid Mechanics, 84(1), pp.145-165.

Patel, V.C. and Mavani, A., 2012. Design of Wiped Film Evaporator (WFE) System With Recovery of Working Fluid For Herbal Products. MIT International Journal of Mechanical Engineering, 2, pp.105-08.

Pattenden, R.F., 1964. Heat transfer from a rotating tube with controlled fluid flow. Journal of Mechanical Engineering Science, 6(2), pp.144-149.

Patton, E. and Feagan, Jr, R., 1941. Method of Installing Tube-Wall Thermocouples. Industrial & Engineering Chemistry Analytical Edition, 13(11), pp.823-824.

Petitjean, V., De Vera, R., Hollebecque, J.F., Tronche, E., Flament, T., Pereira Mendes, F. and Prod'homme, A., 2006. La Hague continuous improvement program: Enhancement of the vitrification throughput". Waste Management Symposia, Phoenix, AZ, pp. 1-5.

Phillips, O.M., 1960. Centrifugal waves. Journal of Fluid Mechanics, 7(3), pp.340-352.

Reich, G. and Beer, H., 1989. Fluid flow and heat transfer in an axially rotating pipe—I. Effect of rotation on turbulent pipe flow. International journal of heat and mass transfer, 32(3), pp.551-562.

Reich, G., Weigand, B. and Beer, H., 1989. Fluid flow and heat transfer in an axially roatating pipe—II. Effect of rotation on laminar pipe flow. International journal of heat and mass transfer, 32(3), pp.563-574.

Sato, T. and Matsumura, H., 1964. On the conditions of incipient subcooled-boiling with forced convection. Bulletin of JSME, 7(26), pp.392-398.

Shah, M.M., 1976, January. General correlation for heat-transfer during subcooled boiling in pipes. In ASHRAE Journal-American Society of Heating Refrigerating and Air-Conditioning Engineers(Vol. 18, No. 12, pp. 41-42). 1791 Tullie circle NE, Atlanta, GA 30329: American Society Heat Refrigeration Air-conditioning ENG. INC.

Shevchuk, I.V., 2009. Convective heat and mass transfer in rotating disk systems. Berlin: Springer.

Shevchuk, I.V. and Khalatov, A.A., 1997. Heat transfer and hydrodynamics in channels rotating about their axis. Journal of engineering physics and thermophysics, 70(3), p.511.

Shmerler, J.A. and Mudawwar, I., 1988a. Local heat transfer coefficient in wavy free-falling turbulent liquid films undergoing uniform sensible heating. International journal of heat and mass transfer, 31(1), pp.67-77.

Shmerler, J.A. and Mudawwar, I., 1988b. Local evaporative heat transfer coefficient in turbulent free-falling liquid films. International journal of heat and mass transfer, 31(4), pp.731-742.

Standiford, F.C., 2000. Evaporation. Kirk-Othmer Encyclopedia of Chemical Technology.

Suppiah Singaram, S., Lodha, H. and Jachuck, R.J., 2014. Experimental investigation of continuous single-phase rimming flow in a horizontal rotating cylinder. AIChE Journal, 60(11), pp.3939-3950.

Suzuki, A., Inagaki, Y., Matsumura, T., Muroya, Y. and Fukasawa, T., 2018. Practical Research on Flexible HLW Management System for MA Recovery. Transactions of the American Nuclear Society, Vol. 119, pp. 293-296.

Thoroddsen, S.T. and Mahadevan, L., 1997. Experimental study of coating flows in a partially-filled horizontally rotating cylinder. Experiments in fluids, 23(1), pp.1-13.

Tirumkudulu, M. and Acrivos, A., 2001. Coating flows within a rotating horizontal cylinder: Lubrication analysis, numerical computations, and experimental measurements. Physics of Fluids, 13(1), pp.14-19.

White, A., 1964. Flow of a fluid in an axially rotating pipe. Journal of Mechanical Engineering Science, 6(1), pp.47-52.

Wilson, S.K., Hunt, R. and Duffy, B.R., 2002. On the critical solutions in coating and rimming flow on a uniformly rotating horizontal cylinder. The Quarterly Journal of Mechanics and Applied Mathematics, 55(3), pp.357-383.

Yan, J., Bi, Q., Liu, Z., Zhu, G. and Cai, L., 2015. Subcooled flow boiling heat transfer of water in a circular tube under high heat fluxes and high mass fluxes. Fusion Engineering and Design, 100, pp.406-418.